12-2016

Soil Moduli Obtained from a Back Pressure Constant Rate of Strain Bender Element Consolidation Apparatus

Yi Zhao
University of Arkansas, Fayetteville

Soil Moduli Obtained from a Back Pressure Constant Rate of Strain Bender Element Consolidation Apparatus

A dissertation submitted in partial fulfillment
of the requirements for the degree of
Doctor of Philosophy in Engineering

by

Yi Zhao
Chengdu University of Technology
Bachelor of Science in Civil Engineering, 2007
Southwest Jiaotong University
Master of Science in Bridge and Tunneling Engineering, 2010

December 2016
University of Arkansas

This dissertation is approved for recommendation to the Graduate Council.

_____
Richard A. Coffman, Ph.D., P.E., P.L.S.
Dissertation Director

_____
Michelle Bernhardt, Ph.D.
Committee Member

_____
Norman D. Dennis, Ph.D.
Committee Member

_____
Christopher Liner, Ph.D.
Committee Member

ABSTRACT

A back-pressure saturated, constant-rate-of-strain consolidation device was modified to incorporate bender elements (BP-CRS-BE) and thus allowed for shear wave measurements during consolidation tests. This newly fabricated system has many advantages over other previous or current devices: 1) it can be utilized not only for laboratory prepared soil samples but also for field sampled soils such as Shelby tube samples, and 2) continuous compression curves, and continuous values of vertical hydraulic conductivity and coefficient of consolidation can be acquired with a significant reduction in testing time. Soil modulus values such as shear modulus and constrained modulus are also able to be accurately determined through a given test.

This proposed research included three phases: 1) fabrication of the BP-CRS-BE device and verification of system compliance, 2) input signal sensitivity analysis for the bender element tests, and 3) performance tests on soil samples. Specifically, a brass sample and kaolinite soil samples were utilized to perform the verification. The obtained soil properties such as compression index (c_c), recompression index (c_r), swell index (c_s), compression ratio (R_c), recompression ratio (R_r), swell ratio (R_s) and consolidation coefficient (c_v) as collected using the BP-CRS and BP-CRS-BE devices were compared. For the BP-CRS-BE tests on soil, Kaolinite and Illite soil type were utilized to investigate the following relationships: 1) the shear modulus as a function of the void ratio, the amount of axial strain, and/or the amount of stress; 2) the relationship between the shear modulus and the constrained modulus of the soil; and 3) the effects of anisotropic properties on the behavior of the soil.

In addition, the methodology and systematic procedures that were utilized to obtain constrained modulus (M), small strain shear modulus (G_{max}), drained Poisson's ratio values (ν), effective stress values in the horizontal direction ($\sigma_h^{'}$), coefficient of lateral earth pressure (K_0),

and drained friction angle values (ϕ') were discussed. Besides acquiring accurate soil parameters for the geotechnical design, the results obtained from the BP-CRS-BE tests will also enable soil parameters to be obtained to establish a constitutive model for any given soil.

ACKNOWLEDGEMENTS

I would like to express my gratitude to my academic advisor and committee chair, Dr. Richard Coffman. I have been so blessed to be able to study under Dr. Coffman's supervision, not only because I received financial support to complete this program, but also because he taught me an active attitude in life and a hard-working spirit, and together we cultivated creative thinking abilities. Dr. Coffman is dedicated and highly responsible for his team, and he is always available to provide help to students whenever and wherever we need his advice. Without his guidance, support and encouragement, this dissertation would not have been accomplished. Thus I would like to thank him sincerely.

I also would like to thank Dr. Norman Dennis for his dedication and valuable guidance. His knowledge in geotechnical practice and his professional character have truly inspired me. Some of those challenges turned out to be immeasurably valuable for a professional engineer. I would like to thank Dr. Michelle Bernhardt for serving as a role model in my efforts to become a professor. I also owe a lot of thanks to Dr. Christopher Liner, who provided me with great advice and help in understanding the shear wave measurement and soil materials from the geophysical field, which greatly enriched my understanding in this topic.

I would like to thank the civil engineering department to provide the assistantship through my study. I also thank all the faculty and staff in the department of civil engineering at the University of Arkansas. Those who shared the technical knowledge and encouragement are not limited to Dr. Clint Wood, Dr. Wen Zhang, Dr. Micah Hale, Dr. Selvam, and Dr. Kevin Hall. It has been a great experience to learn from them.

I also would like to thank all my coworkers and friends for their support and encouragement. Great thanks to Sean Salazar for the laboratory device fabrication, to Nabeel

Mahmood for providing triaxial testing data. Special thanks to Dr. Cyrus Garner, Dr. Morgan Race, Sarah Bey, Elvis Ishimwe, and Johnathan Blanchard for their partnership, understanding, and enormous support. I thank Robert Haslam from the Quality Writing Center for great help during final version revision of this document. I also should give thanks to Mekkes Lee, Edith Lee, Bill Moeller, Karilyn Moeller and other friends from church who provided blessed support and encouragement in my spiritual life and the life-long friendship that have changed the way I think and helped me go through a "difficult dessert".

I would like to thank my brothers Dr. Yun Zhao and Jiang Zhao for their support and love. Special thanks go to my brothers for growing up with me and sharing their personal opinion during the PhD study.

I would like to show my great gratitude to my parents, Mr. Jinhu Zhao and Ms. Qiuping Gao, for their unreserved love and unconditional support. Without their encouragement and love, this dissertation would not have been finished. I would like to thank both of them for teaching me the wisdom of life and providing me the strength to face difficulties in life.

Finally, I would like to thank my wife Haixia Wang and my daughters Ella Jing Zhao and Grace Tongtong Zhao. I am so blessed to have you all in my life. Special thanks to my wife for the companion, encouragement and decision-making during difficulties. Special thanks to my mother-in-law Fengzhen Shi and my mom for their taking care of my daughters in the United States. This dissertation is dedicated to my family.

TABLE OF CONTENTS

LIST OF FIGURES

LIST OF TABLES

LIST OF PUBLISHED OR SUBMITTED PAPERS

Chapter 3: Coffman, R.A., Salazar, S.E., Zhao, Y., "Discusson of Measurement of Stiffness Anisotropy in Kaolinite Using Bender Element Tests in Floating Wall Consolidometer by X. Kang, G-C Kang, and B. Bate." *Geotechnical Testing Journal*. Vol. 37, No. 6, 2014, pp. 1-4.

Chapter 4: Zhao, Y., Coffman, R.A., "Back-Pressure Saturated Constant-Rate-of-Strain Consolidation Device with Bender Elements: Verification of System Compliance." *Journal of Testing and Evaluation*, Vol. 44, No. 6, 2016, pp. 1–12, doi:10.1520/JTE20140291.

Chapter 5: Zhao, Y., Mahmood, N. S., Coffman, R.A., "Small-Strain and Large-Strain Modulus Measurements with a Consolidation Device." *Journal of Testing and Evaluation*, Under review, Manuscript Number: JTE-2016-0331, 2016.

Chapter 6: Zhao, Y., Mahmood, N., and Coffman, R. A., "Soil Fabric and Anisotropy as Observed Using Bender Elements during Consolidation," *Clays and Clay Minerals*, Under Review, Manuscript Number: CCM-1143, 2016.

CHAPTER 1: Introduction

1.1. Chapter Overview

The methodology and procedures that were utilized to accurately determine the soil properties (static and dynamic) that are required for geotechnical design and constitutive model creation are introduced in this document. Specifically, the soil parameters that were obtained, and that are described in this document, include compression index (c_c), recompression index (c_r), swell index (c_s), coefficient of consolidation (c_v), compression ratio (R_c), recompression ratio (R_r), swell ratio (R_s), shear wave velocity (V_s), shear modulus (G), constrained modulus (M), Poisson's ratio (v), and friction angle (ϕ). To achieve the goal of obtaining the aforementioned soil parameters, a back-pressure saturated constant-rate-of-strain consolidation testing device with bender elements measurements (BP-CRS-BE) was designed, fabricated, and evaluated. This chapter is divided into the following sections: 1) an overview of the research project is presented in Section 1.2, 2) the benefits of this proposed research to the geotechnical engineering community are presented in Section 1.3, and 3) the organization of the dissertation is presented in Section 1.4.

1.2. Project Description

The hypothesis of this research is that *the newly fabricated BP-CRS-BE device can be utilized to obtain the soil properties required for geotechnical design and application, including shear modulus, constrained modulus, Poisson's ratio and friction angle, all of which can be accurately determined (90% confidence interval).*

The goal of this research was to 1) examine the relationship between shear modulus (or shear wave velocity), as obtained from the bender element (BE) measurements, and changing levels of stress during consolidation tests, and to 2) examine the effects of soil anisotropy on the

soil behavior during consolidation tests. To accomplish this goal, the shear wave velocity was measured by using the BEs that were incorporated into a BP-CRS device; the measured shear wave velocity values were then utilized to calculate the shear modulus. To ensure the results were meaningful, a verification of system compliance was conducted following the fabrication of the BP-CRS-BE device. This verification was completed by comparing the performance of the existing BP-CRS device with the newly created BP-CRS-BE device. After the amount of system compliance of the newly designed BP-CRS-BE device was determined, a sensitivity analysis was also performed by using the BE equipment to determine the optimal parameters for measurement of the shear wave velocity values. The validation of the testing system was then evaluated through a comparison of the shear modulus values, which were obtained from the BE tests, and the shear modulus values, which were obtained from the CRS tests by using BP-CRS-BE device and correlations. Furthermore, the procedures for obtaining the soil parameters such as shear modulus (G), constrained modulus (M), Poisson's ratio (v), and friction angle (ϕ) were developed. Finally, the effects of soil anisotropy on the soil behavior during various consolidation tests were evaluated. A flow chart of the proposed research plan is presented in Figure 1.1

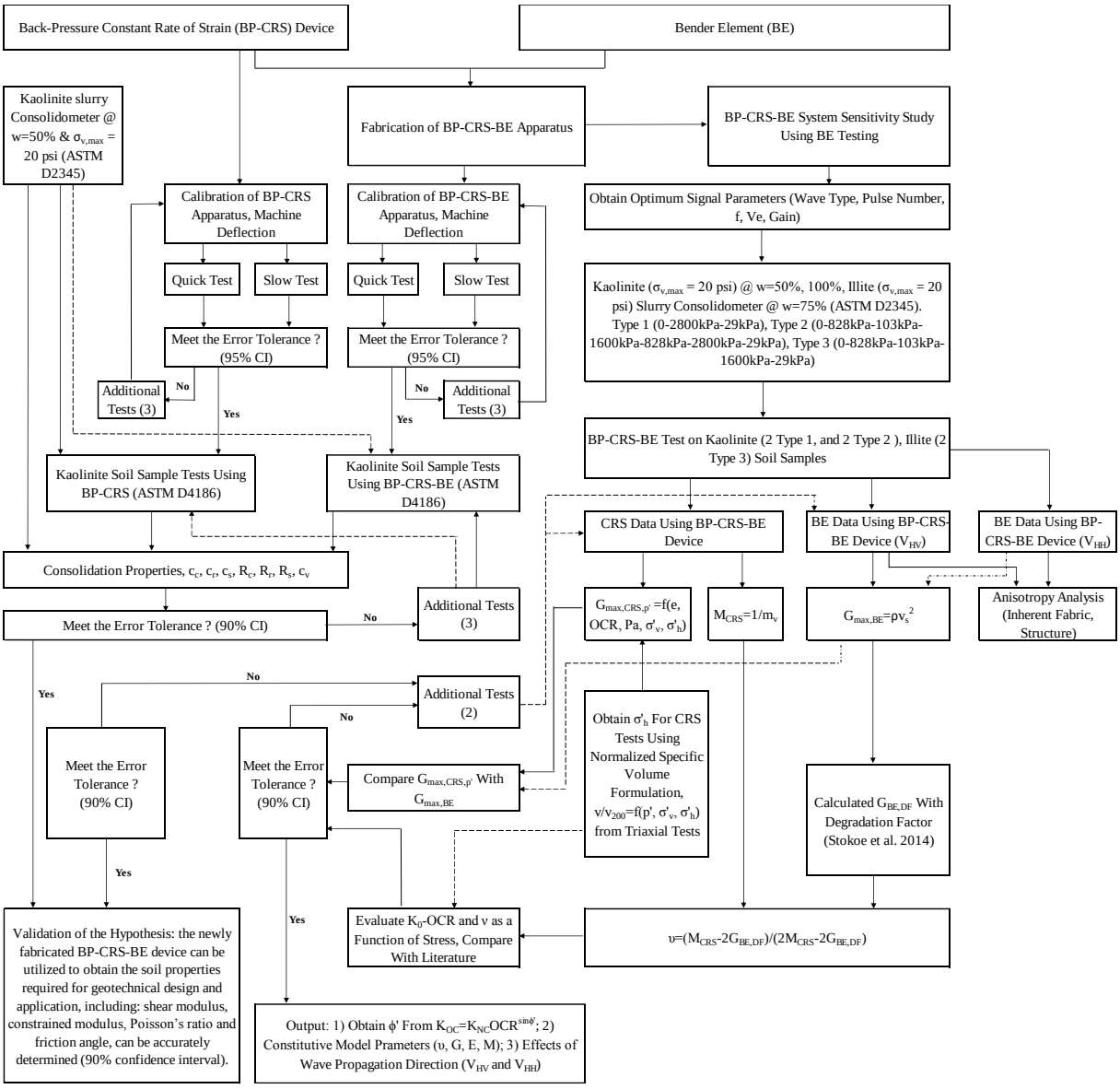

Figure 1.1. Flow chart of the proposed research.

1.3. Benefits to Geotechnical Engineering Community

By incorporating the capability of measuring shear waves during a CRS consolidation test, the use of BEs offers a potential cost benefit by allowing the soil modulus values to be measured at various stress levels without destruction to the various soil samples. Moreover, the results obtained from BEs tests, during this study have been shown to provide an accurate estimation of the soil modulus and other design parameters (coefficient of lateral earth pressure,

friction angle, and Poisson's ratio). Specifically, the benefits from this research include the following items.

- The ability to conduct BP-CRS-BE tests on field sampled Shelby tube samples to identify accurate static and dynamic soil properties.
- The ability to examine the shear modulus as a function of the void ratio, the amount of axial strain, and/or the amount of stress.
- The ability to establish a relationship between the shear modulus and the constrained modulus of the soil.
- The ability to provide the procedures for obtaining comprehensive stress information in three directions through a BP-CRS-BE test and a triaxial test.
- The ability to investigate the anisotropic properties of soil.
- The ability to provide soil parameters for the establishment of constitutive models.

1.4. Dissertation Organization

The following objectives were completed to prove that the aforementioned soil properties were obtained by using the BP-CRS-BE device.

1) Fabrication and calibration of the BP-CRS-BE device.
2) Determination of the shear wave velocity (V_s) and the corollary small strain shear modulus from the bender elements ($G_{\max,BE}$) during the consolidation process, while using the BP-CRS-BE device.
3) Determination of the large strain constrained modulus (M) and the correlated shear modulus ($G_{\max,CRS,p'}$) from the consolidation test measurements, by using the BP-CRS-BE device.

4) Determination of Poisson's ratio (ν) from 1) the measured small-strain shear modulus ($G_{\max .BE}$) obtained by using the BE data, and from 2) the measured large-strain constrained modulus (M) obtained by using the CRS data.
5) Quantification and correlation of the small-strain and large-strain soil moduli to other parameters including void ratio (e), specific volume (v), over-consolidation ratio (OCR), coefficient of lateral earth pressure (K_0), effective stress ($\sigma_v' \; and \; \sigma_h'$), and drained friction angle (ϕ').
6) Evaluation and verification of the developed shear modulus by comparing the measured small-strain shear modulus values ($G_{\max .BE}$) that were obtained from the BE test measurements with the predicted shear modulus values ($G_{\max,CRS,p'}$) that are determined from existing empirical equations that utilize soil parameters ($e, PI, OCR, \sigma_v', and \; \sigma_h'$) that are obtained from the CRS test measurements.
7) Examination and formulation of the coefficient of lateral earth pressure (K_0) as a function of OCR. Determination the effective friction angle (ϕ') of the soil by using the formulated equations from the CRS data when plotted in the OCR-K_0 space.
8) Investigation of the effects of the shear wave propagation direction ($V_{s,HV} \; and \; V_{s,HH}$) and soil anisotropy on the testing results.

Specifically, this research was conducted to achieve the goal of accurate determination of soil properties for geotechnical design and for the establishment of a constitutive model. The results from this research will be described within seven chapters of this dissertation. A summary of related literature review is included in Chapter 2. The contents of Chapters 3 through 6 have been published or have been submitted for publication. These chapters include consideration of

machine deflection on the BP-CRS-BE device (Chapter 3), verification of the BP-CRS-BE system compliance (Chapter 4), small-strain and large-strain soil modulus measurements (Chapter 5), and soil anisotropy observed during consolidation using bender elements within the consolidation device (Chapter 6). A summary of the research findings that were discussed in this dissertation and recommendations for additional research are presented in Chapter 7.

Specifically, the discussion of the advantages of the BP-CRS-BE device over a floating wall consolidometer for measuring soil properties and shear wave velocity are described in Chapter 3. This discussion was published within the *Geotechnical Testing Journal*. The full reference is Coffman, R.A., Salazar, S.E., Zhao, Y., "Discussion of Measurement of Stiffness Anisotropy in Kaolinite Using Bender Element Tests in a Floating Wall Consolidometer by X. Kang, G.-C. Kang, B. Bate" *Geotechnical Testing Journal*. Vol. 37, No. 6, 2014, pp. 1-5. doi:10.1520/GTJ20140162.

A technical paper about the determination of the system compliance of the newly fabricated BP-CRS-BE device, which included shear wave measurements, is described in Chapter 4. This paper was published in the *Journal of Testing and Evaluation*. The full reference is Zhao, Y. and Coffman, R. A., "Back-Pressure Saturated Constant-Rate-of-Strain Consolidation Device With Bender Elements: Verification of System Compliance," *Journal of Testing and Evaluation*, Vol. 44, No. 6, 2016, pp. 1–12, doi:10.1520/JTE20140291. ISSN 0090-3973.

Another technical paper about the principles and the procedures that were utilized for the determination of small-strain and large-strain soil modulus values, by using the BP-CRS-BE device, is presented in Chapter 5. The paper was submitted to the *Journal of Testing and Evaluation*. The full reference is Zhao, Y., Mahmood, N., and Coffman, R. A., "Small-Strain and

Large-Strain Modulus Measurements with a Consolidation Device," *Journal of Testing and Evaluation*, Under Review, Manuscript Number: JTE-2016-0331, 2016.

The effects of soil anisotropy on the soil behavior were investigated and quantified by using the BP-CRS-BE device. The results from this investigation were included in a technical paper which is presented in Chapter 6. This paper was submitted to *Clay and Clay Minerals*. The full reference is Zhao, Y., Mahmood, N., and Coffman, R. A., "Soil Fabric and Anisotropy as Observed Using Bender Elements during Consolidation," *Clay and Clay Minerals*, Under Review, Manuscript Number: CCM-1143, 2016.

A summary of the results and recommendations throughout this dissertation is described in Chapter 7, but not limited to, 1) the importance of accounting for machine deflection in any given consolidation device, 2) the procedures of obtaining the static and dynamic soil parameters and their relationships, and 3) the effects of soil anisotropy on the soil behavior during a consolidation test. Recommendations for future testing are also included in Chapter 7.

1.5. References

Coffman, R.A., Salazar, S.E., Zhao, Y., "Discussion of Measurement of Stiffness Anisotropy in Kaolinite Using Bender Element Tests in Floating Wall Consolidometer by X. Kang, G-C Kang, and B. Bate." *Geotechnical Testing Journal*. Vol. 37, No. 6, 2014, pp. 1-4.

Zhao, Y. and Coffman, R. A., "Back-Pressure Saturated Constant-Rate-of-Strain Consolidation Device With Bender Elements: Verification of System Compliance," *Journal of Testing and Evaluation*, Vol. 44, No. 6, 2016, pp. 1–12, doi:10.1520/JTE20140291. ISSN 0090-3973.

Zhao, Y., Mahmood, N., and Coffman, R. A., "Small-Strain and Large-Strain Modulus Measurements with a Consolidation Device," *Journal of Testing and Evaluation*, Under Review, Manuscript Number: JTE-2016-0331, 2016.

Zhao, Y., Mahmood, N., and Coffman, R. A., "Soil Fabric and Anisotropy as Observed Using Bender Elements during Consolidation," *Clays and Clay Minerals*, Under Review, Manuscript Number: CCM-1143, 2016.

CHAPTER 2: Literature Review

2.1. Chapter Overview

A review of the literature is presented within this chapter. Specifically, an overview of the constant-rate-of-strain (CRS) consolidation test procedures and an introduction of the dynamic approaches that have been used within the consolidation tests are presented in Section 2.2. The theory of bender elements (BE), the application of bender elements within consolidation tests, and the technical problems associated with bender elements are described in Section 2.3. In Section 2.4, the near-field effects caused by the design of the testing equipment and/or the soil sample size are presented. The soil moduli obtained from BE measurements within the small-strain range and the corresponding correlations, predicted shear modulus values, and empirical equations that have been utilized to estimate the effective friction angle of soil are presented in Section 2.5. The empirical equations for determining the coefficient of lateral earth pressure, as a function of friction angle of soil, are presented in Section 2.6. Information regarding soil anisotropy and the associated soil behavior is presented in Section 2.7. Shear wave velocity and shear modulus due to soil anisotropy are presented in Section 2.8 and Section 2.9, respectively. The soil compression and swelling equations, in terms of specific volume and mean effective stress, are presented in Section 2.10. Finally, the relationship between axial strain and shear strain is presented in Section 2.11.

2.2. Constant-Rate-of-Strain Consolidation Tests

Constant-rate-of-strain consolidation tests, hereinafter defined as CRS tests, were first proposed by Smith and Wahls (1969) and Wissa et al. (1971). Compared to incremental load tests, the advantages of CRS consolidation tests include 1) continuous compression curves in terms of load and displacement (or stress and void ratio, or stress and strain), 2) continuous values of vertical hydraulic conductivity and consolidation coefficient, and 3) cost efficiency in

terms of time (Ladd and DeGroot 2003). To determine the consolidation properties for any soil type, several different types of devices have been developed to perform CRS tests under specific conditions. These devices have consisted of the 1) conventional, stand-alone, closed CRS consolidometer, 2) triaxial insert, closed CRS consolidometer, 3) open CRS consolidometer, and 4) open CRS consolidometer with shear wave velocity measurement capability.

The aforementioned original conventional, stand-alone, closed CRS consolidometer allowed for back pressure saturation and thus allowed for the effective stress to be obtained during the consolidation tests (Smith and Wahls 1969, Wissa et al. 1971). The procedures proposed by Wissa et al. (1971) for performing CRS tests were the foundation for the American Society for Testing and Materials (ASTM) method D4186 (ASTM D4186 2014). The triaxial insert device is similar to the conventional device but was included into a triaxial cell to provide multi-use equipment instead of stand-alone equipment. The open CRS consolidometer is like the open incremental load consolidometer described in ASTM D2435 (2014) but also includes pore pressure measurement capability at the bottom of the sample to enable constant rate of loading. As reported in Landon and DeGroot (2006), Landon et al. (2007), Landon (2007), dynamic soil properties such as shear wave velocity have been previously incorporated within a Trautwein/GEOTAC acrylic open CRS consolidometer. Based on a review of the literature, the measurement of shear wave has not been incorporated into a closed, back-pressure saturated, CRS consolidometer. Landon (2007) installed the BEs within the base plate and top plate of the open CRS consolidometer, and thus the shear waves were vertically propagated and horizontally polarized (VH); the shear wave velocity was then obtained from these measured waves (Figure 2.1). The drawback of this open CRS consolidometer is that back pressure saturation was not achieved and that the travel path between the BEs was short.

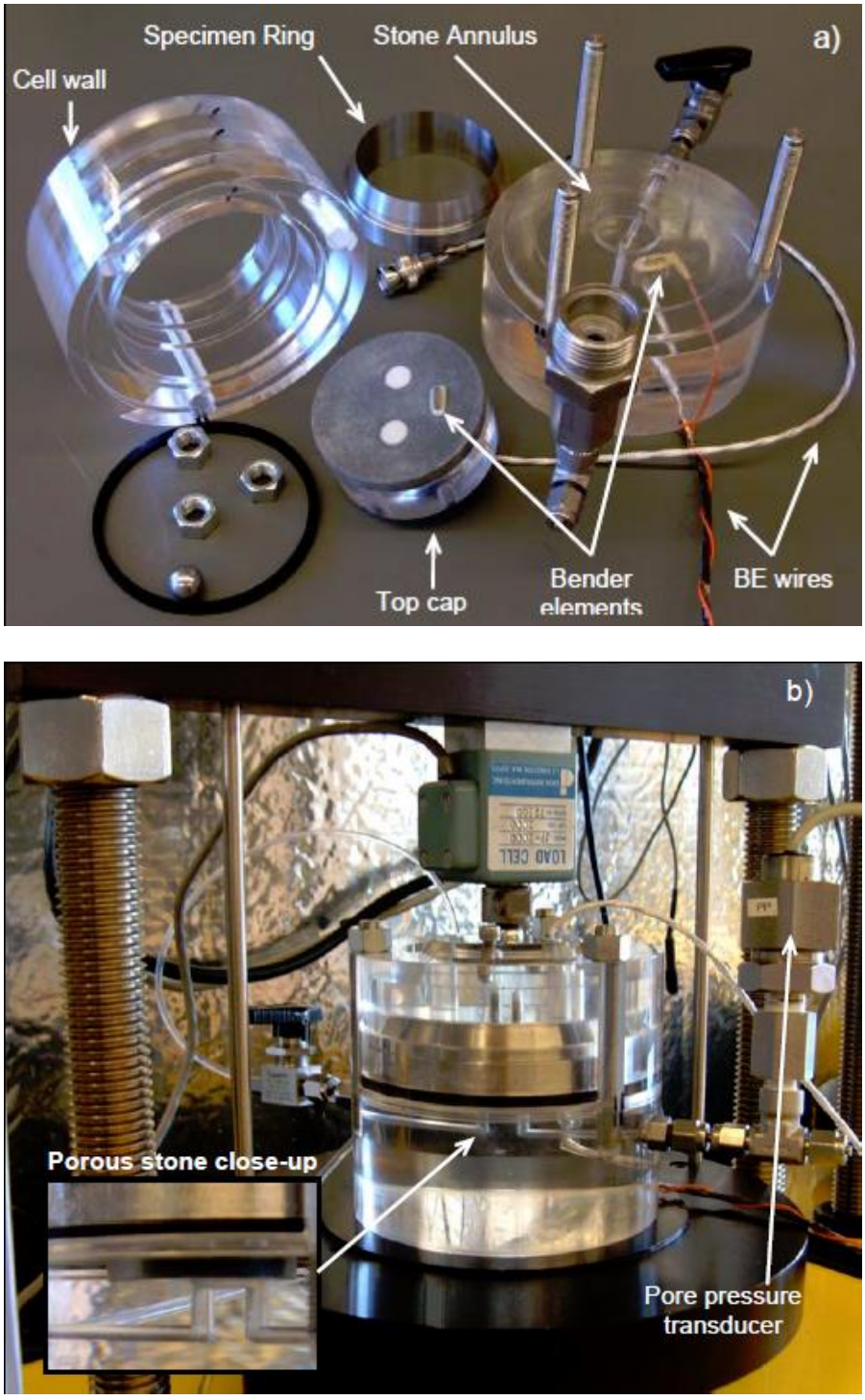

Figure 2.1. Bender elements in an open cell shear wave measurement CRS device: a) apparatus and b) a setup of device for a test (from Landon et al. 2007).

2.3. Bender Elements

As a non-destructive testing method, piezoelectric transducers were introduced by Shirley and Hampton (1978) to measure soil properties. These bender elements (BEs) were originally used as an acoustical measurement tool to determine the physical properties of soil material. Specifically, two ceramic plates were used to generate a specified amount of displacement for a given excitation, as presented in Figure 2.2. Inversely, an incoming excitation voltage was generated when the bender element moved due to the incoming wave.

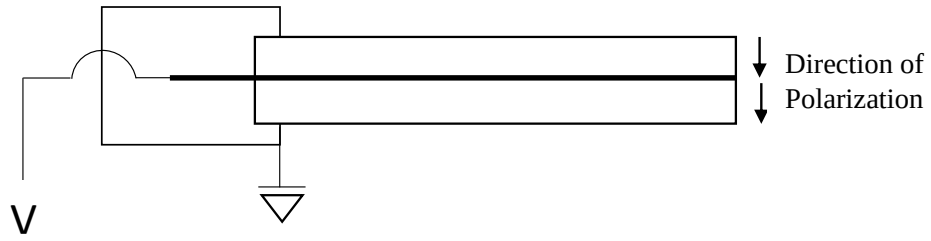

Figure 2.2. Ceramic bender elements (after Lee and Santamarina 2005).

BEs have been used extensively to measure soil properties within the fields of agriculture and civil engineering during the past several decades (i.e., Fam and Santamarina 1995, Brignoli et al. 1996, Landon et al. 2007, Montoya et al. 2011). The wave propagation has been used to examine soil properties through the use of the shear wave and the amount of attenuation. Noticing that a shear wave only propagates through the soil matrix and does not propagate through fluid, shear wave velocity measurements has thus been commonly utilized to measure the soil properties of saturated soil (Fam and Santamarina 1995). BEs have typically been previously installed in the vertical direction, within the top plate and base plate of an open oedometer, to examine the characteristics of a given geomaterial during consolidation, chemical diffusion, and cementation (Fam and Santamarina 1995, Fam and Santamarina 1997, Jovicic and Coop 1998, Landon 2007, Kang et al. 2014).

Another attempt of incorporating bender elements into a back pressure standard consolidometer (air used as confining fluid) was performed by Shibuya et al. (1998). Shibuya et al. (1998) placed the bender elements within the top plate and base plate in order to acquire VH-polarized shear waves during consolidation of soil sample. However, as observed by Shibuya et al. (1998), the near-field effects were too significant, due to the short length of soil samples and the resulting short travel distance for the shear waves.

BEs have also been used to analyze the anisotropic characteristics of soil during consolidation tests. Specifically, a floating wall consolidometer was recently developed by Kang et al. (2014) to measure anisotropy while also eliminating the detrimental bending moment of the BEs as a result of soil sample deformation in a traditional fixed wall setup. However, as mentioned in Coffman et al. (2014), there are four main disadvantages of this design: 1) discontinuous data due to incremental load, 2) only maintaining the degree of saturation rather than allowing unsaturated soil samples to become saturated, 3) only allowing slurry consolidated samples to be tested, and 4) excess deformation as associated with the use of cable ties to prevent the BEs from being pushed out due to the lateral load.

Recently, health monitoring of the BEs themselves during complicated testing situations, has been drawing attention. Specifically, the effects of electromagnetic crosstalk in "aggressive soil environment" was investigated by Montoya et al. (2011). The degradation of waterproofing of BEs due to the "aggressive soil environment" resulted in electromagnetic connections that distorted the received signals and resulted in inaccurate shear wave velocity measurements. To solve this problem, Montoya et al. (2011) proposed practical guidelines for the fabrication, operation, and health monitoring of bender elements, to ensure high quality testing results.

As per Montoya et al. (2011), the quality of the shear wave measurements was also affected by the waveform, wave excitation frequency, amplitude of the excitation signal, filtering, and stacking of the receiving signal. An example of crosstalk due to inappropriate shielding is presented in Figure 2.3. The red dashed highlights caused by crosstalk in Figure 2.3 prevent the acquisition of the received signals from BEs. Waveforms commonly utilized to generate shear waves using BEs have included the impulse wave (Lee and Santamarina 2005), the sine wave (Viggiani and Atkinson 1995, Brignoli et al. 1996), and the square wave (Dyvik and Madshus 1986, Montoya et al. 2011). Montoya et al. (2011) indicated that utilization of square waves to excite the source BE generated a distinct shear wave as compared to sine waves. The research performed by Salazar and Coffman (2014) justified that the square wave excited the BEs at the natural frequency and thus larger amounts of displacement were produced and strong signals were acquired.

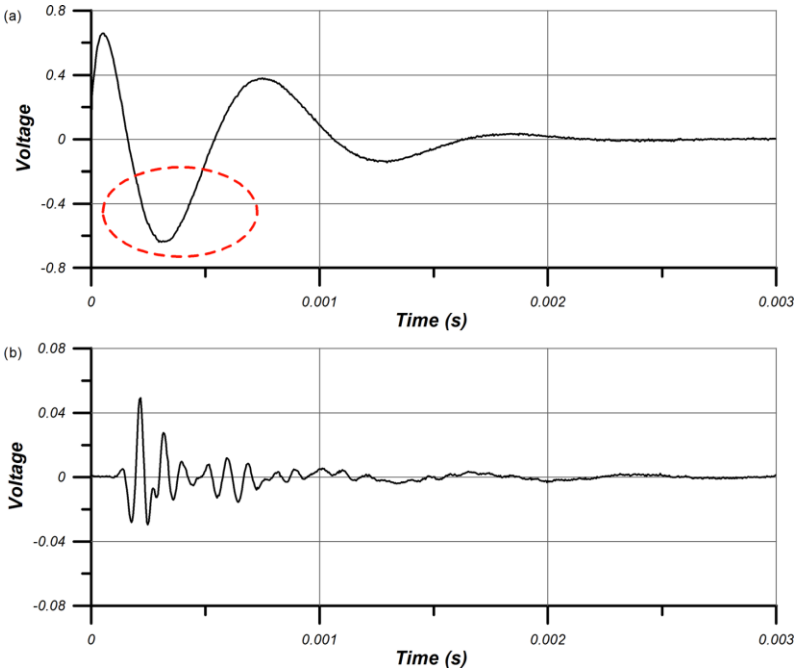

Figure 2.3. Bender element measurement in the soil tests for: a) electromagnetic crosstalk with inappropriate shielding and b) correct signal with proper shielding (from Montoya et al. 2011).

As for the frequency of the excitation wave, Lee and Santamarina (2005) reported that the most efficient approach of transmitting signals from a BE was at the resonant frequency of the BE; by exciting the BEs at the resonant frequency, the most energy was transmitted to the source BE. Because the amplitude of the transmitted waves affected the quality of the shear wave velocity measurement within the soil, guidelines for acquiring the resonant frequency using sine wave signals for the BEs were proposed by Viana da Fonesca et al. (2009). Specifically, at high voltages, soil sample disturbance was observed to occur due to the increased amplitude of the BEs and thus inaccurate shear wave velocity measurements were reported. Therefore, it was recommended that a sensitivity study be conducted for the testing system (Montoya et al. 2011).

Stacking techniques have also been used extensively in the BE testing. The transmitted signal was commonly repeated multiple times, which allowed for the recorded signal to be stacked. As a result, stacking has been shown to increase the signal-to-noise ratio and thus improve the quality of the received signal. Liner (2004) has indicated that the ratio of signal-to-noise is commonly improved by the square root of the number of traces that are summed in a given stack.

Multiple arrivals of waves from BEs have also been investigated to interpret ambiguous arrival times of the shear waves (Marjanovic and Germaine 2013). The multiple waves have been determined to be a combination of direct waves and reflected waves that have resulted from the testing device boundaries around the soil specimen. Johnson (2011) and Marjanovic and Germaine (2013) performed a ray path analysis to examine the discrepancies of the velocity results and concluded that side traveling P-waves and directly traveling P-waves had significant effects on the interpretation of the velocity results. Moreover, the filter paper that is commonly

located between the soil and the porous stones prevented the reflected waves from occurring and prevented a change in the polarity of the wave.

2.4. Near-Field Effect

The near-field effect is a detrimental phenomenon for seismic measurement because it violates one of the assumptions in seismic analysis (the assumption that only far-field waves should be measured). The near-field effect was shown to be caused by the coupling of primary waves and secondary waves at a short distance from the excitation source. Specifically, for transverse wave motion, the shear (S) wave is the main wave (far-field effect), and compression (P) wave only occurs as the near-field effect (Sanchez-Salinero et al. 1986). Compression waves decay much faster than shear waves and thus the greater the distance from the source, the smaller the near-field effect. The near-field effect has been determined to have significant detrimental effects on the quality of the signal and the determination of shear wave velocity measurements (Sanchez-Salinero et al. 1986, Arroyo et al. 2003, Lee and Santamarina 2005). Therefore, approaches have been proposed to eliminate the near-field effect based on the ratio of the wave travel distance (d) to the wavelength (λ). As proposed by Sanchez-Salinero et al. (1986), limiting the d/λ ratio to a value of two may eliminate the near-field effect.

Moreover, based on the equation provided by Sanchez-Salinero et al. (1986), either increasing d or decreasing λ (or the frequency of waves) can prevent the near-field effect. Specifically, during laboratory tests, either modifications to the testing apparatus or adjustment of soil sample size would enable the ratio requirement to be met (Equation 2.1). However, as for BEs in consolidation tests, the near-field effect has not been previously eliminated due to restrictions of the testing devices (Shibuya et al. 1998, Landon 2007).

$2<d/\lambda$ (after Sanchez-Salinero et al. 1986) Equation 2.1

2.5. Soil Modulus

Soil modulus is a critical parameter that governs the behavior of the soil and affects geotechnical design. As discussed in Atkinson (2007), four commonly used soil moduli include Young's modulus (E), bulk modulus (K), shear modulus (G), and constrained modulus (M). Based on elastic theory, the four soil moduli may be correlated to one another. For formulation of elastic constitutive equations, the major assumption is that the material is elastic. However, for a material consisting of solid particles, such as soil particles, the stress-strain behavior is commonly non-linear and thus, non-elastic. But, according to Drnevich (1985), Sadda (1988), Brignoli et al. (1996), the elasticity assumption may be true for the linear portion of the stress-strain relationship (at small strain levels on the order of 0.0001 to 0.001 percent). Moreover, small strain measurements on the order of 0.001 percent were considered to be small strain for seismic tests in the field (Sanchez-Salinero et al. 1986, Landon 2007). However, small strain measurements on the order of 0.0001 percent, have been utilized in the laboratory (Shibuya et al. 1998).

2.5.1. *Measured Soil Modulus from Shear Wave Measurements*

Hardin and Blandford (1989) considered two ways to determine the elastic modulus of particulate materials. These included 1) applying a small incremental cyclic shear stress to measure the elastic shear modulus (Equation 2.2), and 2) applying a small incremental cyclic compressive strain to measure the elastic constrained modulus (Equation 2.3). Alternately, and more conveniently, elastic moduli have been determined by using shear wave propagation (obtained from resonant column shear tests) or compression wave propagation through particulate materials. Likewise, by utilizing the density of the soil (ρ), Hardin and Blandford

(1989) obtained elastic shear modulus (G) from shear wave velocity (V_s) and elastic constrained modulus (M) from compression wave velocity (V_p).

$$G = \rho V_s^2 \quad \text{(after Hardin and Blandford 1989)} \quad \text{Equation 2.2}$$

$$M = \rho V_p^2 \quad \text{(after Hardin and Blandford 1989)} \quad \text{Equation 2.3}$$

2.5.2. *Measured Soil Modulus from Consolidation Tests*

Large-strain constrained modulus values are commonly obtained from CRS consolidation tests. Specifically, as reported in Smith and Wahls (1969) as presented as Equation 2.4, these moduli values (as obtained at various stress levels) have been obtained by utilizing the consolidation theory developed by Terzaghi (1943). Wissa et al. (1971) also proposed a linear solution to obtain the coefficient of volume compressibility (m_v) from a CRS test through the change of strain and the change of stress level. However, a non-linear solution (Equation 2.5), in which a constant compression index (C_c) is assumed, is most commonly employed. Both of these solutions (linear and nonlinear) are included within the ASTM D4186 (2014) standard. According to the standard, the constrained modulus can be calculated using Equation 2.6 for both the linear and nonlinear solution. The Poisson's ratio value (ν) can then be determined from the G and the M by using Equation 2.7.

$$m_v = \frac{\Delta\varepsilon}{\Delta\sigma_v} = r\left(\frac{\Delta t}{\Delta\sigma_v}\right) \quad \text{(after Smith and Wahls 1969)} \quad \text{Equation 2.4}$$

$$m_v = \frac{\Delta\varepsilon}{\Delta(\log\sigma_v)} = r\left(\frac{\Delta t}{\Delta(\log\sigma_v)}\right) \quad \text{(after Wissa et al. 1971)} \quad \text{Equation 2.5}$$

$$M = 1/m_v \quad \text{(after Duncan and Bursey 2013)} \quad \text{Equation 2.6}$$

$$\nu = \frac{M - 2G}{2(M - G)}$$ (after Duncan and Bursey 2013) Equation 2.7

Within Equations 2.4 and 2.5, $\Delta\varepsilon$ is the change in strain over a time interval Δt; $\Delta\sigma_v$ is the change in total stress over a time interval Δt; and *r* is the strain rate.

2.5.3. *Shear Modulus Degradation Curve*

Decreasing values of shear modulus with increasing values of strain have been observed and examined through dynamic tests on soils (Seed and Idriss 1970, Seed et al. 1986, Vucetic and Dobry 1991, Ishibashi 1992, Darendeli 2001, and Stokoe et al. 2004). A modulus degradation factor G/G_{max} was developed for clay soils with various plastic index (PI) values over a range in shear strain values from 0.00001 percent to 1 percent, as shown in Figure 2.4 (Darendeli 2001, Stokoe et al. 2004). Furthermore, the modulus degradation factors that were presented in Duncan and Bursey (2013) provided a convenient but limited way to obtain shear modulus values at large strain values.

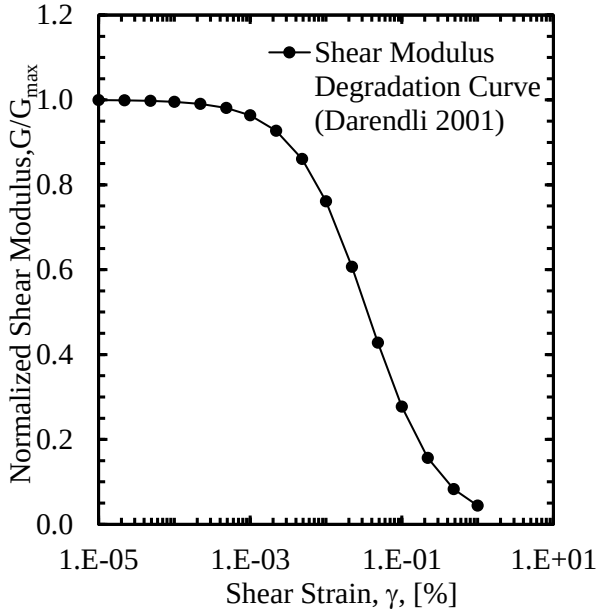

Figure 2.4. **Normalized shear modulus as a function of shear strain (modified from Darendli 2001).**

2.5.4. *Empirical Soil Modulus Equations*

To address the inherent soil properties attributed to depositional environment, extensive research was conducted by previous researchers (i.e., Hardin and Blandford 1989, Landon 2007) to formulate values of shear modulus as a function of the state of stress, over-consolidation ratio (OCR), and void ratio (e). Equation 2.8 was proposed by Hardin and Blandford (1989) based on the results of small-amplitude cyclic simple shear tests. Lo Presti et al. (1993) and Landon (2007) also developed methods based on the results obtained from oedometer tests to predict the shear modulus, as presented in Equation 2.9 and Equation 2.10, respectively. The correlation between shear modulus (G) and constrained modulus (M) was documented by Smith and Wahls (1969).

$$G_{\max} = \frac{S \cdot OCR^{k}}{F(e)} P_a^{1-n} (p')^{n} \qquad \text{(after Hardin and Blandford 1989)} \qquad \text{Equation 2.8}$$

$$G_{\max} = \frac{S}{F(e)} P_a^{1-n} (\overline{\sigma_v} \cdot \overline{\sigma_h})^{\frac{n}{2}} \qquad \text{(after Lo Presti et al. 1993)} \qquad \text{Equation 2.9}$$

$$G_{\max} = S \cdot F(e) P_a^{1-2n} (\sigma_v' \sigma_h')^{\frac{n}{2}} \qquad \text{(after Landon 2007)} \qquad \text{Equation 2.10}$$

$$G = \frac{M(1-2v)}{2(1-v)} \qquad \text{(after Smith and Wahls 1969)} \qquad \text{Equation 2.11}$$

Within Equations through 2.8 to 2.11, $G_{\max}$ is the small strain shear modulus of soil; n=0.5 is the elastic constant; k is the empirical exponent which depends on the plasticity index (PI) of the soil; P_a is the atmospheric pressure; $F(e)$, the function of void ratio (e), typically, $F(e) = 0.3 + 0.7e^2$ for Equation 2.8, and $F(e) = e^{1.3}$ for Equation 2.9; σ_v' is the vertical effective stress; σ_h' is the horizontal effective stress.

2.6. Lateral Earth Pressure and Friction Angle

To estimate the coefficient of lateral pressure (K_0), Jaky (1944) proposed an equation (Equation 2.12) that had been utilized to estimate the effective friction angle (ϕ') for normally consolidated soils. Mayne and Kulhaway (1982) also investigated the influence of OCR on K_0 for overconsolidated soils, and the Mayne and Kulhaway (1982) equation is presented as Equation 2.13.

$$K_0 = 1 - \sin\phi' \quad \text{(after Jaky 1944)} \quad \text{Equation 2.12}$$

$$K_0 = (1 - \sin\phi')(OCR)^{\sin\phi'} \quad \text{(after Mayne and Kulhaway 1982)} \quad \text{Equation 2.13}$$

2.7. Soil Anisotropy

Two types of soil anisotropy dominate and affect soil behavior. These types include 1) stress induced anisotropy and 2) inherent, fabric or structural anisotropy (Jovicic and Coop 1998, Kang et al. 2014). It had been found that the stress induced anisotropy played a very small role in the effect on the soil behavior under the axi-symmetric loading conditions (Jovicic and Coop 1998). In contrast, the inherent anisotropy was found to significantly affect soil behavior and was found to be one of the factors that induced plastic strain within the soil (Jovicic and Coop 1998; Kang et al. 2014). For soil within a consolidation test, the change in strain due to the dissipation of the excess pore water pressure typically causes the soil particles to compact and rearrange and thus results in fabric anisotropy. In fact, the change in strain during consolidation has been attributed to the applied stress on the soil, and thus, some researchers termed this situation as stress induced fabric anisotropy (Kang et al. 2014), which should be distinguished from the aforementioned stress induced anisotropy. Additionally, the inherent anisotropy was caused by different factors (depositional fabric and strain induced fabric), and depended upon the soil type.

For sand, the inherent anisotropy was mainly caused by the soil depositional fabric. However, for clay, the inherent anisotropy was mainly caused by the change in strain as a result of large deformation (Jovicic and Coop 1998).

2.8. Shear Wave Velocity Due to Soil Anisotropy

Soil anisotropy has been investigated by the shear wave velocity measurement in different propagation directions. Jovicic and Coop (1998) measured the vertically propagated horizontally polarized (VH) shear wave and the horizontally propagated vertically polarized (HV) shear wave on two Kaolinite soil samples, respectively, through a triaxial device. The two testing soil samples were required to be cut along the major and minor principal stress directions, respectively. As reported in Pennington et al. (1997), Nash et al. (1999), Ling et al. (2000), Yamashita et al. (2000), Pennington et al. (2001), Yimsiri and Soga (2002), Yamashita et al. (2005), Piriyakul (2006), instead of conducting the BE tests on two samples, triaxial devices have also been modified to allow the assembly of three pairs of BEs into the soil samples from three directions to measure the HV shear waves, VH shear waves, and HH shear. A schematic illustration of the shear wave measurements from different directions is presented in Figure 2.5. Zeng and Ni (1999) investigated the soil anisotropy through multiple directions by inserting the BEs from vertical and horizontal directions into soil samples within an oedometer device, and shear wave velocities from multiple directions were obtained. Kang et al. (2014) fabricated a consolidation device with bender elements enabled to measure HV shear waves, VH shear waves, and HH shear waves.

Pennington et al. (1997) reported that for Gault clay, the $V_{s,HH}$ value was greater than $V_{s,HV}$ value, that the $V_{s,HV}$ value was greater than $V_{s,VH}$ value, and that the $V_{s,HH}$ / $V_{s,HV}$ ratio was around 1.20, while the $V_{s,HV}$ / $V_{s,VH}$ ratio was around 1.17. Yamashita et al. (2000) found that for

Toyoura sand and Kusshаro sand, the shear wave velocity values ($V_{s,HH}$) were greater than $V_{s,HV}$ values, and the $V_{s,HH}$ / $V_{s,HV}$ ratio was between 1.05 and 1.13, respectively. Yamashita et al. (2000) also reported that there was no significant difference between the $V_{s,HV}$ values and $V_{s,VH}$ values for these sand materials. However, for laboratory prepared Kaolinite soil with sodium concentrations in the confining fluid, Kang et al. (2014) found that the $V_{s,HH}$ values were greater than the $V_{s,HV}$ values, while the $V_{s,HV}$ values were greater than the $V_{s,VH}$ values. The $V_{s,HH}$ / $V_{s,HV}$ ratio was around 1.20, while the $V_{s,HV}$ / $V_{s,VH}$ ratio was around 1.14. In fact, the fabric anisotropy dominated the soil anisotropy, and the degree of fabric anisotropy changed during the loading-unloading process during consolidation. Also, the anisotropy of the soil behaved differently during loading and unloading which was associated with the amount of applied load. It was found that the amount of soil anisotropy for Kaolinite, infused with sodium solution increased when the applied effective stress values were greater than 50-100 kPa (Kang et al. 2014).

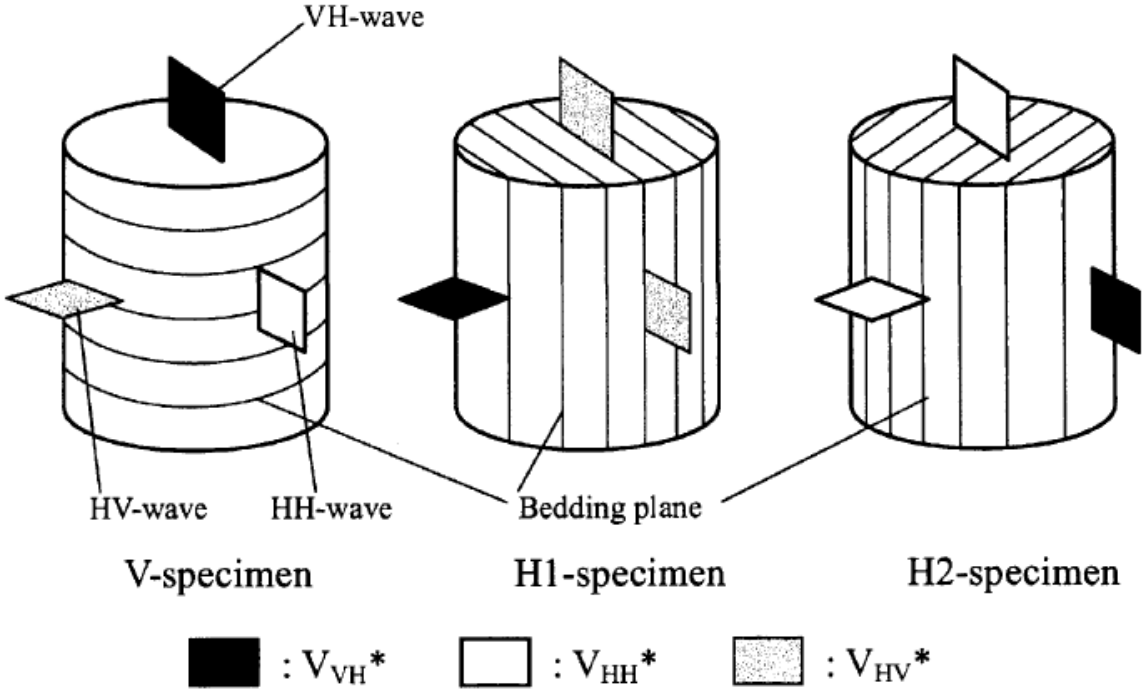

Figure 2.5. Schematic illustration of HV shear wave, VH shear wave, and HH shear measurements using bender elements (from Yamashita et al., 2000).

2.9. Shear Modulus Due to Soil Anisotropy

Pennington et al. (1997) reported that the shear modulus was inherently anisotropic due to the depositional fabric of clay, and it was found that the degree of anisotropy for a natural soil was significantly greater than for a reconstituted soil. For reconstituted Gault clay, the shear modulus values $G_{max,HH}$ (calculated from $V_{s,HH}$) were greater than $G_{max,HV}$ (calculated from $V_{s,HV}$), and the $G_{max,HH}$ / $G_{max,HV}$ ratio was around 1.5, while the $G_{max,HH}$ / $G_{max,HV}$ ratio was around 1.0 (Pennington et al. 1997). Jovicic and Coop (1998) found that for natural London clay, the shear modulus values $G_{max,HH}$ were greater than $G_{max,HV}$, and the $G_{max,HH}$ / $G_{max,HV}$ ratio was between 1.5 to 1.7, while the $G_{max,HH}$ / $G_{max,HV}$ ratio was between 1.24 to 1.33 for the reconstituted London clay. Additionally, Nash et al. (1999) conducted a soil anisotropy investigation on Gault clay, in a triaxial cell device, and concluded that the strain induced anisotropy dominated soil anisotropy. Nash et al. (1999) also found that the $G_{max,HH}$ / $G_{max,HV}$ ratio was a function of 1) void ratio and 2) the state of stress and stress path to which the sample was subjected. For an anisotropically consolidated stress condition, the $G_{max,HH}$ / $G_{max,HV}$ ratio varied from 1.5 to 1.9 when the void ratio decreased from 1.35 to 0.85; however, for an isotropically consolidated stress condition, the $G_{max,HH}$ / $G_{max,HV}$ ratio varied from 1.45 to 1.52 when the void ratio decreased from 1.3 to 0.98 (Nash et al. 1999).

The shear modulus or shear wave velocity has been shown to be affected by the direction of wave propagation. It was found that G_{HH} was about 70 percent greater than G_{VH} and G_{HV} for the consolidation tests on natural soil by using HH, VH, and HV shear waves (Jovicic and Coop 1998). The stress-induced fabric anisotropy of kaolinite was found, and the shear wave velocities from this test had the order: $V_{HH} > V_{HV} > V_{VH}$ (Roesler 1979, Pennington et al. 1997, Kang et al.

2014). Additionally, for higher applied stress levels on the soil, higher values of V_s were observed (Lee et al. 2008, Kang et al. 2014).

2.10. Compression and Swelling Equations

Previous researchers put efforts to quantify the soil behavior when subjected to loading and unloading. Roscoe et al. (1958) reported a nonlinear solution to accurately approximate the behavior of soils subjected to loading and unloading. The schematic illustration is presented in Figure 2.6. Specifically, equations were proposed to determine the specific volume (Equation 2.14) as a function of mean effective stress, during compression (Equation 2.15) and swelling (Equation 2.16), respectively. Equation 2.15 has proven to be suitable for normally consolidated soil and Equation 2.16 has proven to be suitable for overconsolidated soil.

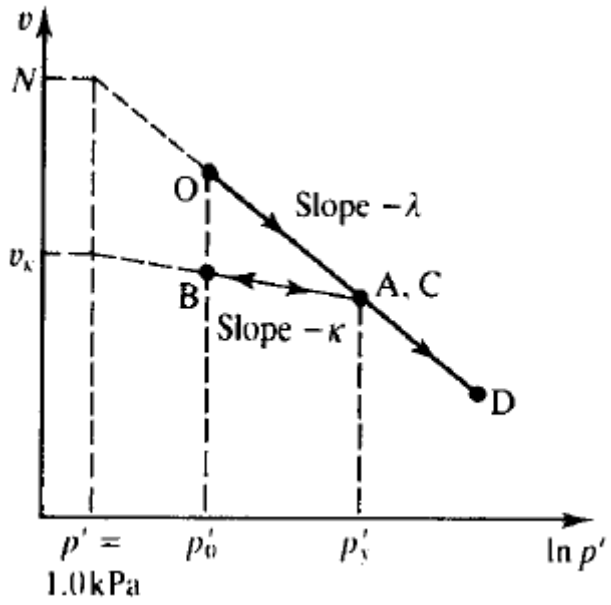

Figure 2.6. Isotropic compression and swelling model (from Atkinson 2007).

$v = 1 + e$	(after Roscoe et al. 1958)	Equation 2.14
$v = N - \lambda \cdot \ln(p')$	(after Roscoe et al. 1958)	Equation 2.15
$v = v_\kappa - \kappa \cdot \ln(p')$	(after Roscoe et al. 1958)	Equation 2.16

Within Equations 2.14 through 2.16, v is the specific volume, N and v_κ are the values of v at $p' = 1kPa$ for the compression and swell line, respectively, λ is the gradient for the normal consolidation line, κ is the gradient of the swelling line, p' is the mean effective stress, and e is the void ratio.

2.11. Relationship between Shear Strain and Axial Strain

Different models were utilized to establish the relationship between shear strain and axial strain. Vecchio and Collins (1986) proposed a method to establish the relationship between shear strain and axial strain by utilizing a "cracked element" model, as presented in Figure 2.7. By utilizing the Mohr's circle method as presented in Figure 2.7(b), the shear strain (γ_{xy}) was found to be a function of the strain values ε_x and ε_2 that are defined in Figure 2.7(a), and the equation is presented in Equation 2.17.

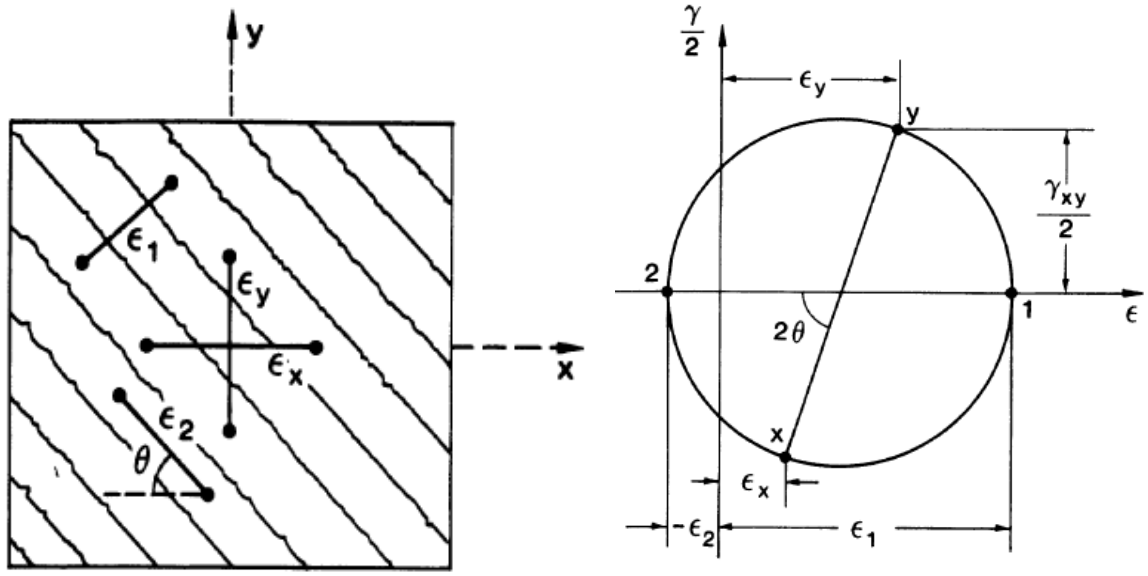

(a) **(b)**

Figure 2.7. A cracked element model for a) average strains in cracked element, and b) Mohr's circle for average strains (from Vecchio and Collins 1986).

$$\gamma_{xy} = \frac{2(\varepsilon_x - \varepsilon_2)}{\tan\theta}$$ (from Vecchio and Collins 1986) Equation 2.17

As presented in Equation 2.18, and described within Sharma and Fahey (2003) and Atkinson (2007), the relationship between shear strain (γ), axial strain (ε_1), and radial strain ($\varepsilon_{2,3}$) was defined by utilizing strain compatibility, using the "Cambridge method." The shear strain (γ) was defined by Poisson's ratio (ν) and the axial strain (ε_1), as documented in Equation 2.19.

$$\gamma = \frac{2}{3}(\varepsilon_1 - \varepsilon_3)$$ (after Sharma and Fahey 2003, Atkinson 2007) Equation 2.18

$$\gamma = (1+\nu)\varepsilon_1$$ (after Yasuhara et al. 2003) Equation 2.19

Schanz et al. (1999) defined the plastic shear strain (γ^p) as a function of plastic axial strain (ε_1^p) as presented in Equation 2.20, by utilizing a "hardening" model. For hard soils, the plastic volume (ε_v^p) changes are very small and thus can be neglected, and thus the plastic shear strain will be approximately twice the plastic axial strain.

$$\gamma^p = 2\varepsilon_1^p - \varepsilon_v^p \approx 2\varepsilon_1^p$$ (from Schanz et al. 1999) Equation 2.20

Multiple, interrelated concepts and soil parameters were introduced within this chapter. As discussed in the next chapter, these interrelated parameters (CRS, BE, near-field effects, soil modulus, over-consolidated ratio, mean effective stress, coefficient of lateral earth pressure, friction angle, and Poisson's ratio) will be investigated to develop constitutive relationships for various soils. A lack of previous research has led to the need to perform the research that is described in this document.

2.12. References

American Society for Testing and Materials, "Standard Test Method for One-Dimensional Consolidation Properties of Soils Using Incremental Loading," *Annual Book of ASTM Standards*, Designation *D 2345*, ASTM, West Conshohocken, PA, 2014.

American Society for Testing and Materials, "Standard Test Method for One-Dimensional Consolidation Properties of Saturated Cohesive Soils Using Controlled-Strain Loading," *Annual Book of ASTM Standards, Designation D 4186*, ASTM, West Conshohocken, PA, 2014.

Arroyo, M., Muir Wood, D., and Greening, P. D., "Source Near-field Effects and Pulse Tests in Soil Samples," *Geotechnique*, Vol. 53, No. 3, 2003, pp. 337–345.

Atkinson, John, "The Mechanics of Soils and Foundations," Taylor & Francis, 2007.

Brignoli, E.G.M., M. Gotti, and K.H. Stokoe, "Measurement of Shear Waves in Laboratory Specimens by Means of Piezoelectric Transducers", *Geotechnical Testing Journal*, 19(4), 1996, pp.384-397.

Coffman, R.A., Salazar, S.E., Zhao, Y., "Discussion of Measurement of Stiffness Anisotropy in Kaolinite Using Bender Element Tests in Floating Wall Consolidometer by X. Kang, G-C Kang, and B. Bate." *Geotechnical Testing Journal*. Vol. 37, No. 6, 2014, pp. 1-4.

Darendeli, M.B., "Development of a New Family of Normalized Modulus Reduction and Material Damping Curves." Doctoral dissertation, University of Texas, Austin, TX, 2001.

Duncan, J. and Bursey, A., "Soil Modulus Correlations." *Foundation Engineering in the Face of Uncertainty*, 2013, pp. 321-336. doi: 10.1061/9780784412763.026.

Drnevich, V.P., "Recent Developments in Resonant Column Testing." Richart Commemorative Lectures, Proceedings, ASCE Specialty Session, Detroit, 1985, pp.79-107.

Dyvik, R., and Madshus, C., "Lab Measurements of G_{max} Using Bender Elements," Proceedings of the ASCE Convention on Advances in the Art of Testing Soils under Cyclic Conditions, 1986, pp. 186–196.

Fam, M., and Santamarina, J. C., "Study of Geoprocesses with Complementary Mechanical and Electromagnetic Wave Measurements in an Oedometer," *Journal* of Geotechnical *Engineering*, Vol. 18, No. 3, 1995, pp. 307–314.

Fam, M., and Santamarina, J. C., "A Study of Consolidation Using Mechanical and Electromagnetic Waves," *Geotechnique*, Vol. 47, No. 2, 1997, pp. 203–219.

Hardin, B. O., "The Nature of Stress-Strain Behavior for Soils." *Proceedings of the geotechnical division speciality conference on earthquake engineering and soil dynamics*, ASCE, Pasadena, 1978, pp. 3-90.

Hardin, B.O. and Blandford, G.E., "Elasticity of Particulate Material." *Journal* of Geotechnical *Engineering*, Vol. 115, No. 6, 1989, pp.788–805.

Ishibashi, I., "Effect of Soil Plasticity on Cyclic Response (Discussion)." *Journal* of *Geotechnical Engineering*, Vol. 118, No. 5, 1992, pp.830-832.

Jaky, J., "The Coefficient of Earth Pressure at Rest," *J. Soc. Hung. Architects Engineers*, Vol. 7, 1944, pp. 355-358.

Johnson, S. M., "Modeling a Bender Element Test Using Abaqus Finite Element Program." *Master's thesis*, Massachusetts Institute of Technology, Cambridge, MA, 2001.

Jovicic, V., and Coop, M. R., "The Measurement of Stiffness Anisotropy in Clays with Bender Element Tests in the Triaxial Apparatus." *Geotechnical Testing Journal*, ASTM, Vol. 21, No.1, 1998, pp. 3-10.

Kang, X., Kang, G.-C., and Bate, B., "Measurement of Stiffness Anisotropy of Kaolinite Using Bender Element Tests in a Floating Wall Consolidometer". *Geotechnical Testing Journal*. ASTM. Vol. 37, No.5. 2014, pp. 1-16.

Ladd, C.C. and DeGroot, D.J., Invited Paper: "Recommended Practice for Soft Ground Site Characterization," The Arthur Casagrande Lecture, *Proceedings of the 12th Panamerican Conference on Soil Mechanics and Geotechnical Engineering*, Boston, MA, 2003, pp.3-57.

Landon, M. M., and DeGroot, D. J., "Measurement of Small Strain Shear Modulus Anisotropy on Unconfined Clay Samples Using Bender Elements," *Proceedings of GeoCongress 2006*, ASCE, 2006.

Landon, M. M., DeGroot, D. J., and Sheahan, T. C., "Nondestructive Sample Quality Assessment of a Soft Clay Using Shear Wave Velocity," *J. Geotech. Geoenviron. Eng.*, Vol. 133, No. 4, 2007, pp. 424–432.

Landon, M. M., "Development of a Non-destructive Sample Quality Assessment Method of Soft Clays," *Ph.D. dissertation*, University of Massachusetts, Amherst, MA, 2007.

Lee, J.-S., and Santamarina, J. C., "Bender Elements: Performance and Signal Interpretation," *J. Geotech. Geoenviron. Eng*., 2005, pp. 1063–1070.

Lee, C., Lee, J.-S., Lee, W., and Cho, T.-H., "Experiment Setup for Shear Wave and Electrical Resistance Measurements in an Oedometer," *Geotech. Test. J.*, Vol. 31, No. 2, 2008, pp. 149–156.

Liner, Christopher, "Elements of 3-D Seismology," Pennwell, 2nd edition, 2004.

Lings, M. L., Pennington, D. S., and Nash, D. F. T., "Anisotropic Stiffness Parameters and their Measurement in a Stiff Natural Clay," *Géotechnique*, Vol. 50, No. 2, 2000, pp. 109–125.

Lo Presti D.C.F., Jamiolkowski M., Lancellotta R. and Vercelli L., "Maximum shear modulus measurement using bender elements in oedometer tests", *Rivista Italiana de Geotechnica*, Vol.(XXVII), No. 1, 1993, pp. 5-9.

Marjanovic, J., and Germaine, J.T., "Experimental Study Investigating the Effects of Setup Conditions on Bender Element Velocity Results." *Geotechnical Testing Journal*, Vol. 36, 2013, p. 11, doi: DOI: 10.1520/GTJ20120131.

Mayne, P. W. and Kulhawy, F. H., "K_0-OCR Relationships in Soil," *Journal of the Geotechnical Engineering Division*, Vol. 108, No. GT6, 1982, pp. 851-872.

Montoya, B.M., Gerhard, R., DeJong, J.T., Weil, M.H., Martinez, B.C., and Pederson, L., "Fabrication, Operation, and Health Monitoring of Bender Elements in Aggressive Environments," *Geotechnical Testing Journal*, Vol.35, No. 5, 2011, pp. 1-15.

Nash, D.F.T., Lings, M.L., and Pennington, D.S., "The Dependence of Anisotropy G0 Shear Moduli on Void Ratio and Stress State for Reconstituted Gault Clay." *Proc., 2nd Int. Symp. on Pre-Failure Deformation Characteristics of Geomaterials*, Torino, 1999, pp. 229-238.

Pennington, D. S., Nash, D. F. T., and Lings, M. L., "Anisotropy of G_0 Shear Stiffness in Gault Clay," *Geotechnique*, ol. 47, No. 3, 1997, pp. 391–398.

Pennington, D.S., Nash, D.F.T., and Lings, M.L., "Horizontally Mounted Bender Elements for Measuring Anisotropic Shear Moduli in Triaxial Clay Specimens." *Geotechnical Testing Journal*, Vol. 24, No. 2, 2001, pp.133-144.

Piriyakul, K., "Anisotropic Stress-Strain Behavior of Belgian Boom Clay in the Small Strain Region." Ph.D., Ghent University, 2006.

Roesler, S. K., "Anisotropic Shear Modulus due to Stress Anisotropy," *J. Geotech. Eng. Div.*, Vol. 105, No. 7, 1979, pp. 871–880.

Roscoe, K. H., Schofield, A., & Wroth, C. P., "On the yielding of soils." *Geotechnique*, Vol. 8, No. 1, 1958, pp.22-53.

Sadda, A. S., "Hollow Cylinder Torsional Devices: Their Advantages and Limitation," *Advanced Triaxial Testing of Soil and Rock, ASTM STP 997*, Philadelphia, PA. 1988, pp.766-779.

Salazar, S.E., Coffman, R.A., "Design and Fabrication of End Platens for Acquisition of Small-Strain Piezoelectric Measurements during Large-Strain Triaxial Extension and Triaxial Compression Testing." *Geotechnical Testing Journal*, Vol. 37, No. 6, 2014, pp. 1-12. doi:10.1520/GTJ20140057.

Sanchez-Salinero, I., Roesset, J. M., and Stokoe, K. H., II, "Analytical Studies of Body Wave Propagation and Attenuation," *Geotechnical Engineering GR86-15*, University of Texas at Austin, September, 1986.

Schanz, T., Vermeer, P.A. and Bonnier, P.G., "The Hardening Soil Model: Formulation and Verification." *Beyond 2000 in computational geotechnics*, 1999, pp.281-296.

Seed, H.B. & Idriss, I.M., "Soil Moduli and Damping Factors for Dynamic Response Analyses." Report EERC-70-10, Earthquake Engineering Research Center, University of California, Berkeley, CA, 1970.

Seed, H.B., Wong, R.T., Idriss, I.M. & Tokimatsu, K., "Moduli and damping factors for dynamic analyses of cohesionless soils". *Journal of Geotechnical Engineering*, ASCE. Vol. 112, No. 11, 1986, pp.1016-1032.

Sharma, S. and Fahey, M., "Degradation of Stiffness of Cemented Calcareous Soil in Cyclic Triaxial Tests." *J. Geotech. Geoenviron. Eng*., Vol. 129, No. 7, 2003, pp. 619-629.

Shibuya, S., Hwang, S. C., & Mitachi, T., "Elastic Shear Modulus of Soft Clays from Shear Wave Velocity Measurement." *Geotechnique*, Vol. 47, No. 3, 1998, pp: 593-601.

Shirley, D.J. & Hampton, L.D., "Shear-Wave Measurements in Laboratory Sediments", *Journal of Acoustics Soc. Am*., Vol. 63, No.2, 1978, pp. 607-613.

Smith, R., and Wahls, H., "Consolidation under Constant Rates of Strain," *Journal of the Soil Mechanics and Foundations Division*, Vol. 95, No. SM2, 1969, pp. 519–539.

Stokoe, K.H., II, Joh, S.H. & Woods, R.D., "Some Contributions of In Situ Geophysical Measurements to Solving Geotechnical Engineering Problems." *2nd International Conference on Site Characterization (ISC-2)*, Porto, Portugal, September, 2004.

Terzaghi, K., "Theoretical soil mechanics." New York: J. Wiley and Sons, Inc, 1943.

Vecchio, F.J. and Collins, M.P., "The Modified Compression-Field Theory for Reinforced Concrete Elements Subjected to Shear." *ACI J.*, Vol. 83, No. 2, 1986, pp.219-231.

Viana da Fonseca, A., Ferreira, C., and Fahey, M., "A Framework Interpreting Bender Element Tests, Combining Time-domain and Frequency-domain Methods," *Geotech. Test. J*., Vol. 32, No. 2, 2009.

Viggiani, G. and Atkinson, J. H., "Interpretation of bender element tests." *Geotechnique*, Vol. 45, No. 1, 1995, pp. 149-154.

Vucetic, M. & Dobry, R., "Effect of Soil Plasticity on Cyclic Response." *J. Geotech. Eng*., Vol. 117, No. 1, 1991, pp.89-107.

Wissa, A., Christain, J., Davis, H., and Heiberg, S., "Consolidation at Constant Rate of Strain," *Journal of the Soil Mechanics and Foundations Division*, Vol. 97, No. SM10, 1971, pp. 1391–1413.

Yamashita,S., Jamiolkowski,M., and Presti,D.C.F., "Stiffness Nonlinearity of Three Sands". *Journal of Geotechnical and Geoenvironmental Engineering*, Vol. 126, No.10, pp. 929-938.

Yamashita, S., Hori, T., and Suzuki, T., "Effects of Initial and Induced Anisotropy on Initial Stiffness of Sand by Triaxial and Bender Elements Tests." *Geomechanics*: 2005, pp. 350-369. doi: 10.1061/40797(172)20

Yasuhara, K., Murakami, S., Song, B., Yokokawa, S., and Hyde, A., "Postcyclic Degradation of Strength and Stiffness for Low Plasticity Silt." *J. Geotech. Geoenviron. Eng*., 10.1061/(ASCE)1090-0241(2003)129:8(756), 2003, pp. 756-769.

Yimsiri, S., Soga, K., "Application of Micromechanics Model to Study Anisotropy of Soils at Small Strain." *Soil and Foundations*, Vol. 42, 2002, pp. 15-26.

Zeng, X. and Ni, B., "Stress-Induced Anisotropic G_{max} of Sands and Its Measurements." ASCE *Journal of Geotechnical and Geoenvironmental Engineering*, Vol. 125, No. 9, 1999, pp.741-749.

CHAPTER 3: Consideration of Machine Deflection on a BP-CRS-BE Device

3.1. Chapter Overview

For the purpose of performing shear wave velocity measurement within soil samples that are subjected to a consolidation process, bender elements (BE) were introduced into two consolidation devices. The two consolidation devices were identified as: (1) the floating wall consolidometer with bender element measurement (FW-BE) from the Missouri University of Science and Technology (Kang et al. 2014), and (2) the back-pressure saturated, constant-rate-of-strain consolidation device with bender elements measurement (BP-CRS-BE) from the University of Arkansas. The two types of consolidation devices with the incorporation of the bender elements (BE) were compared in terms of design of the device of facilitating the BE, the soil samples preparation methods, the compliance of the devices during consolidation, the measurements of the shear wave velocities, and the methods of identifying the shear wave velocities. The BP-CRS-BE device had many advantages over the FW-BE because: (1) it can be utilized in both of the laboratory prepared soil samples and the field sampled soils, (2) continuous compression curve, continuous values of vertical hydraulic conductivity and coefficient of consolidation, and significant reduction in testing time. Furthermore, it was recommended that additional tests (machine deflection tests) should be conducted for the FW-BE tests to obtain accurate soil properties. Moreover, the system lag due to shear waves traveling through the testing system was required to be determined for the accuracy of shear wave velocity. Finally, it was recommended to identify the compression waves besides the shear waves for the further calculation of the constrained modulus and Poisson's ratio.

The paper enclosed in this chapter has been published within the *Geotechnical Testing Journal*. The full reference is: Coffman, R.A., Salazar, S.E., Zhao, Y., "Discussion of Measurement of Stiffness Anisotropy in Kaolinite Using Bender Element Tests in a Floating

Wall Consolidometer by X. Kang, G.-C. Kang, B. Bate" *Geotechnical Testing Journal*. Vol. 37, No. 6, 2014, pp. 1-5. doi:10.1520/GTJ20140162.

3.2. Additional Results

This chapter focuses on the feasibility and advantages of selecting the CRS device to incorporate the bender elements to perform the shear wave velocity measurement during a consolidation process. The advantages of the BP-CRS-BE tests over the FW-BE tests or the incremental loading tests were covered in the following paper. The shear wave velocity measurement in the BP-CRS-BE tests, the procedures of determination of the shear wave velocity will not be presented herein, but will be described in Chapter 4.

For completeness, additional results of the machine deflection and the load-deflection obtained from the tests conducted by using BP-CRS-BE are presented here. Specifically, the machine deflection results (Figure 3.1) were obtained from five "quick method" tests performed on the BP-CRS-BE by using a dummy brass sample which was assumed to be incompressible. The five tests were identical and the averaged deflection values were utilized to represent the machine deflection at corresponding loads. In addition, load-deflection results (Figure 3.2) were obtained from five tests performed on kaolinite soil samples by using the BP-CRS-BE device. It is shown that the influence of the machine deflection on the soil deflection is significant and cannot be neglected.

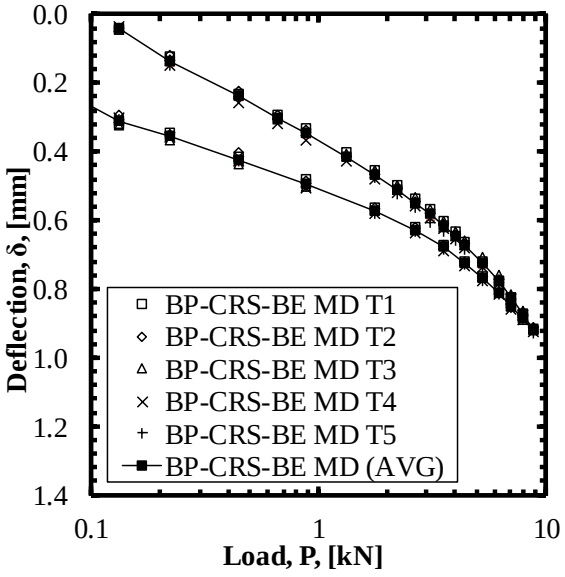

Figure 3.1. Machine deflection obtained from the "quick method" by using BP-CRS-BE device on a dummy sample.

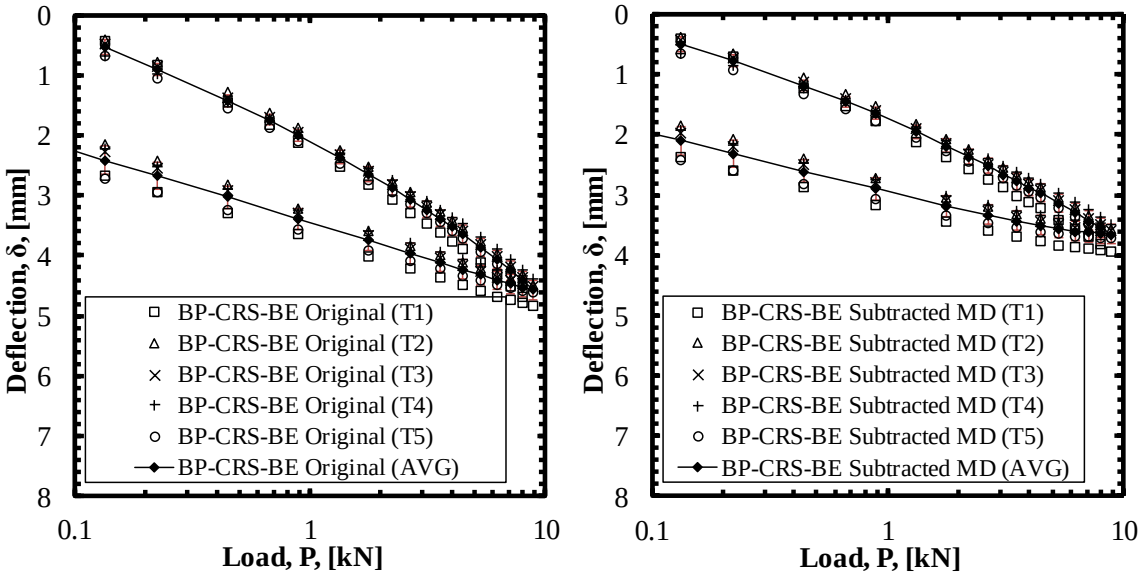

(a) (b)

Figure 3.2. Soil deflection obtained from the tests on kaolinite soil by using BP-CRS-BE device for: a) original soil deflection, and b) original soil deflection subtracting machine deflection.

Discussion of "Measurement of Stiffness Anisotropy in Kaolinite Using Bender Element Tests in a Floating Wall Consolidometer" by X. Kang, G.-C. Kang, and B. Bate

Richard A. Coffman PhD PE PLS [1], Sean E. Salazar EIT[2], Yi Zhao[2]

3.3. Abstract

The procedures utilized and results obtained from a newly designed floating wall consolidation device are compared with those obtained from a modified triaxial insert, traditional fixed wall, back-pressure saturated, constant-rate-of-strain consolidation device that incorporated bender elements (BP-CRS-BE). Specifically, the need for additional measurements within the floating wall consolidation device including machine deflection and tip-to-tip measurements are highlighted and discussed. The procedures that were utilized to collect and reduce the measured shear wave and compression wave data, as collected using the newly designed floating wall consolidation device, are also questioned.

3.4. Discussion

The Kang et al. (2014), in the paper entitled "Measurement of Stiffness Anisotropy Using Bender Element Test in a Floating Wall Consolidometer," presented a new consolidation device to enable the use of bender elements to measure soil stiffness. Specifically, a floating wall design was developed by Kang et al. (2014) to eliminate detrimental bending moment that may develop upon horizontally installed bender elements as a result of soil settlement, during consolidation, in a traditional fixed wall setup. Moreover, Kang et al. (2014) presented incremental load consolidation (using a load ratio equal to two) and shear wave velocity data that were obtained using the newly created floating wall consolidation cell.

Recently, as presented in Figure 3.3, a triaxial insert, traditional fixed wall, back-pressure saturated, constant-rate-of-strain consolidation device was modified by researchers at the

University of Arkansas to incorporate bender elements (BP-CRS-BE). Kaolinite samples that were 25.4mm tall by 63.5mm in diameter were tested within the BP-CRS-BE device. This soil sample size enabled a reduction in near-field effects while also allowing for: 1) samples obtained from conventional Shelby tubes to be tested, 2) rapid consolidation times, and 3) higher applied confining stresses (up to 2800kPa as tested using a traditional GeoJac load frame with a prescribed maximum load of 8.9kN), as compared to the 100mm tall by 114mm diameter soil samples reported in Kang et al. (2014). Horizontally propagating shear waves with vertical particle motion (HV) were transmitted and received within the BP-CRS-BE device (as the device was currently fabricated). However, the BP-CRS-BE device can also be further modified to enable generation of other wave and particle motions but was not, at this time, because of the potential for near-field effects (specifically for VH waves). Unlike other fixed wall devices in which near-field effects may have been present within the collected VH shear wave velocity data (Landon 2007) or in which the bender elements were damaged (Bate et al. 2013), the bender elements in the BP-CRS-BE were allowed to move with the sample while the sample consolidated. Specifically, Delrin® slide bars and Delrin® guides were used to reduce the amount of friction in the movement of the slide bars (that contained the bender elements) during the consolidation test, thereby preventing detrimental bending moments to develop on the bender elements.

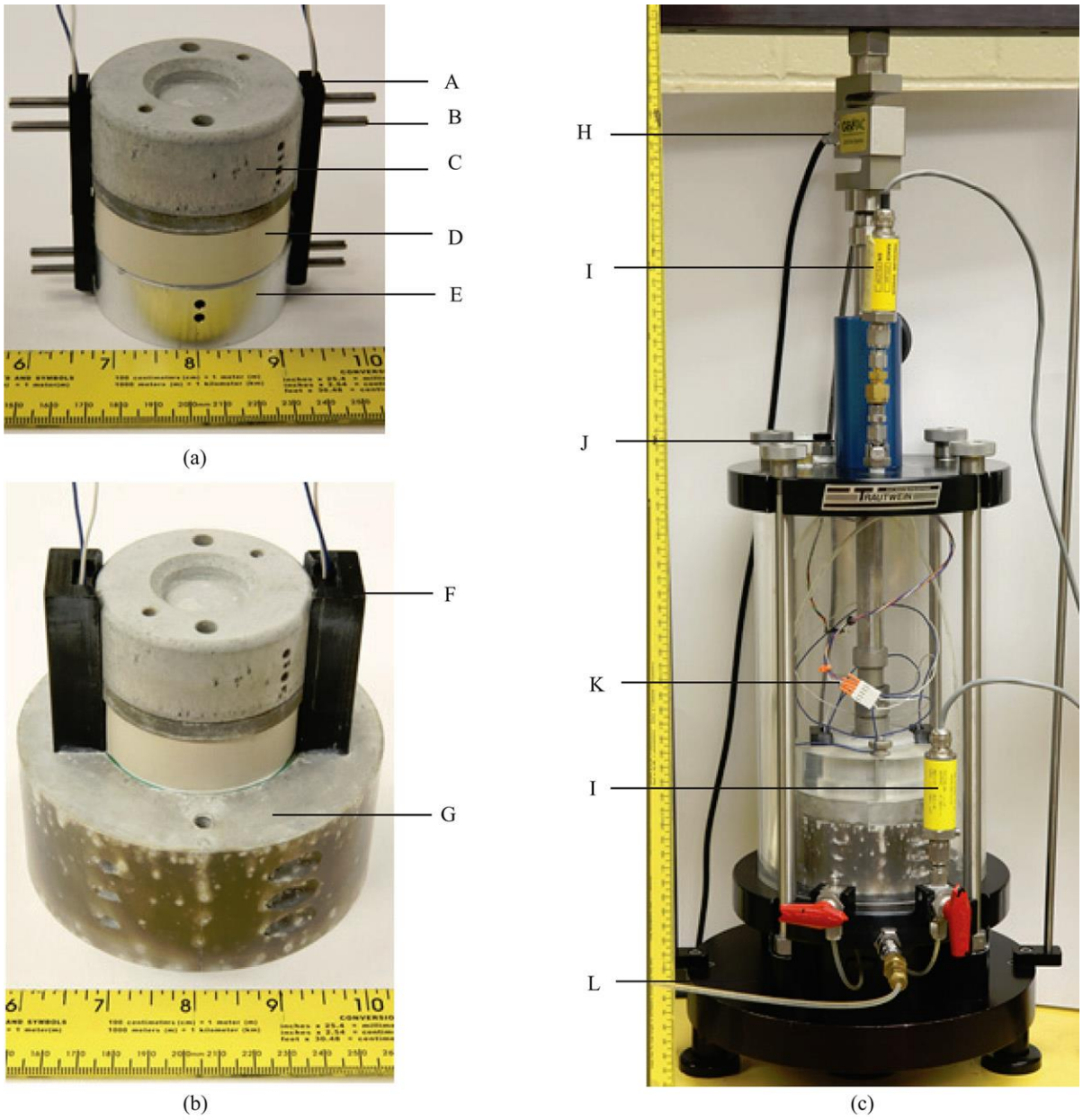

A. Delrin® slide bar. B. Dowel. C. Alumimum loading cap. D. Soil sample. E. Jig. F. Delrin® guide. G. Alumimum base pedestal. H. Load cell. I. Pressure transducer. J. Nine-pin-feed-through connector. K. Wire harness. L. Base plate.

Figure 3.3. Photographs of the BP–CRS–BE consolidometer: (a) insertion of bender elements into the sample using a jig, (b) sample prior to ring placement around sample, (c) sample within the BP–CRS–BE insert within triaxial chamber.

In Ladd and DeGroot (2003), the advantages of the constant-rate-of-strain consolidation test (continuous compression curve, continuous values of vertical hydraulic conductivity and

coefficient of consolidation, significant reduction in testing time) over the incremental load test are presented. Because of these advantages, the BP-CRS-BE device was developed as a constant-rate-of-strain test instead of as an incremental load test like the incremental load floating-wall consolidometer device that was reported in Kang et al. (2014). Specifically, the BP-CRS-BE device was developed as a constant-rate-of-strain device because Ladd and DeGroot (2003) identified that "doubling the load is too high to properly define the compression curve." Furthermore, the back-pressure saturation component of the BP-CRS-BE device allowed for unsaturated soil samples to become saturated, through the use of a pressurized triaxial chamber, instead of for the saturation to be "maintained" in the water chamber as reported in Kang et al. (2014).

Laboratory prepared (slurry consolidated) kaolinite samples (albeit different sources of kaolinite and different salt concentrations in the pore fluid) were tested within the BP-CRS-BE device and within the Kang et al. (2014) device. There are several benefits to utilizing laboratory prepared samples, including a priori knowledge of the: maximum vertical effective stress, level of saturation, and material properties. The soil tested in the BP-CRS-BE device was also tested in a conventional fixed ring consolidometer (BP-CRS) without bender elements to compare the amount of machine deflection (MD) and the consolidation parameters obtained from the devices with bender elements (BP-CRS-BE) and without bender elements (BP-CRS).

Although the amount of wall-soil interface friction was obtained for the Kang et al. (2014) device, no comparison tests were performed to determine the amount of machine deflection or if the consolidation parameters obtained from the floating cell wall with bender elements device matched parameters obtained from tests conducted using a conventional fixed ring. The use of "cable ties to keep the bender elements from being pushed out by the lateral

earth pressure when the vertical load increased," as described in the Kang et al. (2014), may lead to additional deformation, as compared to a conventional fixed ring test. Furthermore, the amount of machine deflection may lead to a reduction in the consolidation indices (recompression index [C_r], compression index [C_c], and swell index [C_s]) of up 15, 20, and 26 percent, respectively (Figure 3.4, Table 3.1). The amount of machine deflection may be even more critical in the Kang et al. (2014) device than in the BP-CRS-BE device because a compressible geosynthetic was used as a drainage material instead of an incompressible corundum porous stone (like the stone that was used in the BP-CRS-BE device). Therefore, it is recommended that additional tests be conducted in the Kang et al. (2014) device to determine 1) the amount of machine deflection (by using a brass "dummy" sample) and 2) if additional deformation is observed within the kaolinite samples when the bender elements are present (by using kaolinite and a floating cell wall without holes for the bender elements).

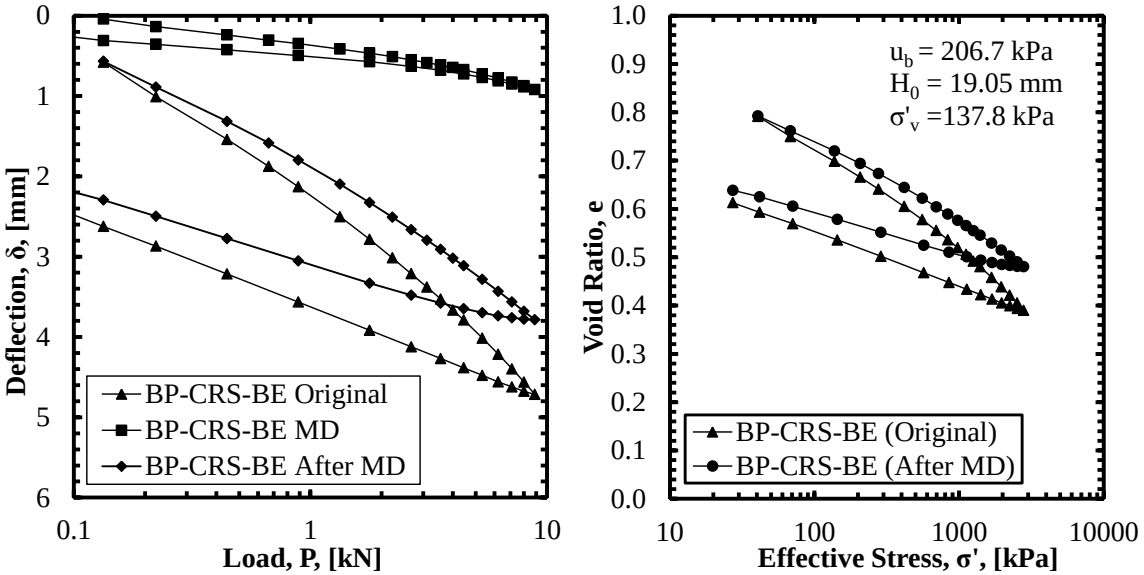

(a) (b)

Figure 3.4. Influence of machine deflection obtained for the BP-CRS-BE device in terms of a) load-deformation and b) effective stress-void ratio.

Table 3.1. **Summary of soil consolidation indices.**

Test	C_r	C_c	C_s
BP-CRS-BE (pre-MD)	0.17	0.27	0.11
BP-CRS-BE (post-MD)	0.14	0.22	0.08
Difference (%)	15.16	20.70	26.12

The shear wave velocity measurements that were obtained using the Kang et al. (2014) device were obtained by manually selecting the first zero-crossing of the first major peak. According to Kang et al. (2014), "the average shear wave velocity of Georgia RP-2 kaolinite was less than published values." Furthermore, Kang et al. (2014) state "the smaller particle size makes shear waves transmit through longer and more tortuous force chains (chains of particle contacts), which was postulated to yield reduced stiffness." Instead, it should have been postulated that the shear wave velocity values were less than the published values because of improper selection of the travel times. Specifically, as reported in Salazar and Coffman (2014), the use of time domain selection of travel times should not be utilized for determination of shear wave velocity because the obtained values of shear wave velocity are only approximate. Furthermore, although Kang et al. (2014) mentioned that the tip-to-tip distance was selected as the shear wave propagation distance; the shear waves and travel times that were obtained from a calibration tip-to-tip test (conducted outside of the floating cell wall) were not reported. As discussed in Salazar and Coffman (2014), the results obtained from a tip-to-tip test are necessary to determine the signal polarity of the generated and received waves and to calculate the time correction associated with the system time delay (system lag). The polarity and lag are crucial for identifying the correct travel time. Therefore, it is recommended that tip-to-tip testing be conducted, using the Kang et al. (2014) bender elements, to determine the signal polarity and that

signal cross correlation methods (Viggiani and Atkinson 1995) be employed to determine the shear wave travel times.

Kang et al. (2014) negated the importance of the compression wave in an attempt to enhance the shear wave response by changing the excitation frequency and reducing the near-field effect. For instance, no compression waves are observed in the signal presented in Figures 4 or 8 of the Kang et al. (2014) article. However, as discussed in Salazar and Coffman (2014), proper identification of the first arrival of the compression wave and the shear wave may lead to the determination of Poisson's ratio values and constrained modulus values. Thus, both compression and shear waves should be collected and analyzed.

3.5. References

Bate, B., Choo, H., Burns, S., "Dynamic Properties of Fine-grained Soils Engineering with a Controlled Organic Phase," *Soil Dynamics Earthquake Engineering*, Vol. 53, 2013, pp. 176-186.

Kang, X., Kang, G.-C., and Bate, B., "Measurement of Stiffness Anisotropy in Kaolinite Using Bender Element Tests in a Floating Wall Consolidometer," *Geotechnical Testing Journal*, Vol. 37, No. 5, 2014, pp. 1-15, doi:10.1520/GTJ20120205. ISSN 0149-6115.

Ladd, C.C., DeGroot, D.J., "Recommended Practice for Soft Ground Site Characterization: Arthur Casagrande Lecture." *Proceedings of the 12th Pan American Conference on Soil Mechanics and Geotechnical Engineering*, Massachusetts Institute of Technology, Cambridge, Massachusetts, 2003.

Landon, M.M., "Development of a Non-destructive Sample Quality Assessment Method for Soft Clays," *Ph.D. Dissertation. University of Massachusetts*, Amherst, MA, 2007.

Salazar, S.E., Coffman, R.A., "Design and Fabrication of End Platens for Acquisition of Small-Strain Piezoelectric Measurements during Large-Strain Triaxial Extension and Triaxial Compression Testing." *Geotechnical Testing Journal*, Vol. 43, No. 2, 2014, pp. 1-11. doi:10.1520/GTJ20140057.

CHAPTER 4: BP-CRS-BE: Verification of System Compliance

4.1. Chapter Overview

A newly designed triaxial insert, back-pressure saturated, constant rate-of-strain consolidation device was modified for the inclusion of bender elements (BP-CRS-BE) that generate and acquire horizontally propagated, vertically polarized waves (HV wave). The amount of system compliance of the BP-CRS-BE was determined through a series of laboratory tests conducted on a dummy brass sample and on kaolinite soil samples. The same tests were also conducted by using the BP-CRS device. The testing results from the BP-CRS-BE and the BP-CRS were compared and similar outcomes were observed. Specifically, the obtained results from the two devices included: the machine deflection, recompression index (c_r), compression index (c_c), swell index (c_s), and the coefficient of consolidation (c_v). Furthermore, the optimum parameters (number of sending wave, sending wave type, excitation voltage, and gain) that were used in the bender element tests were determined by a series of tests. Finally, the method of identifying the shear wave velocity from the bender element test was introduced.

The paper enclosed in this chapter has been published in the *Journal of Testing and Evaluation*. The full reference is: Zhao, Y. and Coffman, R. A., "Back-Pressure Saturated Constant-Rate-of-Strain Consolidation Device With Bender Elements: Verification of System Compliance," *Journal of Testing and Evaluation*, Vol. 44, No. 6, 2016, pp. 1–12, doi:10.1520/JTE20140291. ISSN 0090-3973.

4.2. Additional Results

Determination of the Optimum Excitation Signal Parameters

The excitation signal parameters for a bender element testing include: waveforms (sine, square), the types of signals (single-pulse, dual-pulse, four-pulse), excitation voltage (1V, 2V, 4V, 8V), and excitation frequency (10 kHz – 30 kHz). To obtain a high quality received signal, a

series of sensitive studies was performed on a kaolinite soil sample. High quality received signal has the character of high signal to noise ratio (SNR). In other words, high amplitude in soil signals but low amplitude in noise signals are expected for a good received signal.

The generated and acquired signals for BP-CRS-BE tests on kaolinite for single-pulse sine wave and square wave are presented in Figure 4.1. The same received waves were obtained regardless of the type of source wave. However, the sine wave had the advantage in identifying the excitation time of the source wave over the square wave, as shown in Figure 4.1. Thus the sine wave was selected as the source wave to eliminate the ambiguity of travel time identification of the shear wave.

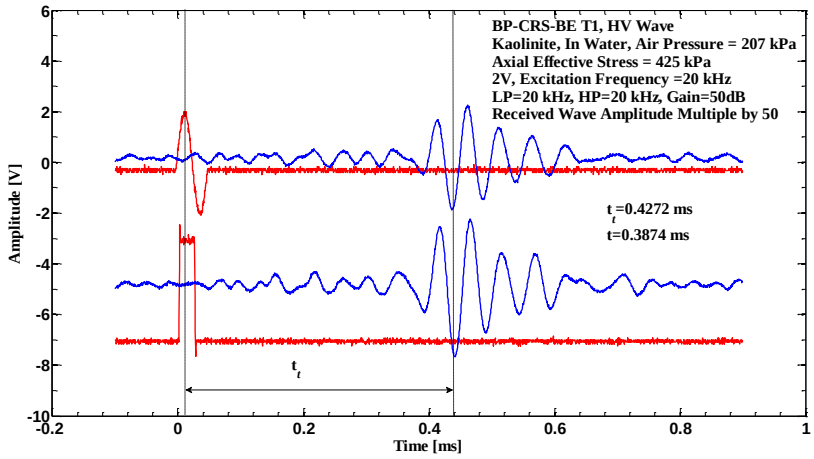

Figure 4.1. Generated and acquired signals for BP-CRS-BE tests on kaolinite for single-pulse sine wave and square wave.

The generated and acquired signals for BP-CRS-BE tests on kaolinite soil sample for single-pulse, dual-pulse, and four-pulse are presented in Figure 4.2. All three types of source signals resulted in the same arrival time for received signals. The single-pulse was selected as the source wave due to: 1) simplicity, and 2) less interference with the shear wave from the top cap.

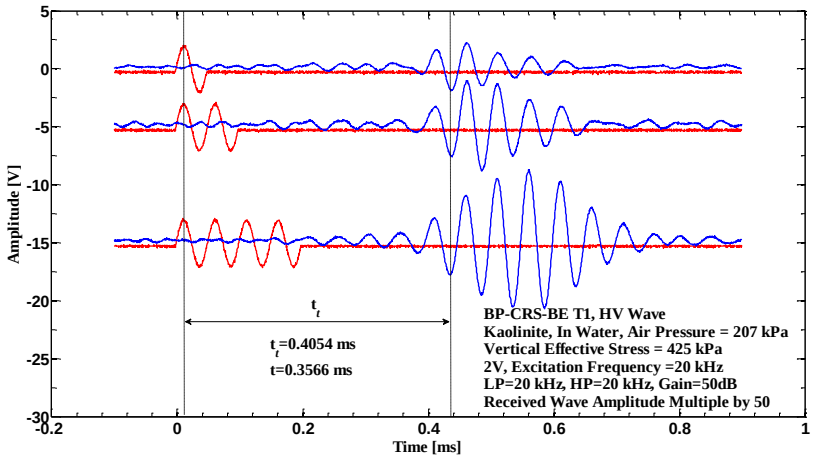

Figure 4.2. Generated and acquired signals for BP-CRS-BE tests on kaolinite for single-pulse, dual-pulse, and four-pulse.

The excitation voltage of the source wave ranges from 1V to 8V based on the ability of the Quattro system or the National Instruments. It should be noted that the bender elements may be damaged by the high voltage of the excitation wave. The bender elements were found damaged or de-functionalization in the utilization of 8V in the BP-CRS-BE test. It was also found that the increase of the excitation voltage of the source wave did not significantly improve the quality of the received signals. Although the amplitude of the received soil wave increased with the increasing of the excitation voltage, the amplitude of the received noise signal also increased proportionally. Thus the excitation voltage of the source wave was limited to either 2V or 4V.

Generally, the excitation frequency ranges from 10 kHz to 30 kHz in the BP-CRS-BE test. The optimum excitation frequency depends upon the stiffness of the soil sample. In other words, the optimum excitation frequency varies with the applied vertical stress on the soil samples, and the best excitation frequency should be determined when performing bender elements testing during consolidation. It is recommended that at least three different frequencies be utilized in every applied vertical stress level.

Back-Pressure Saturated Constant-Rate-of-Strain Consolidation Device With Bender Elements: Verification of System Compliance

Yi Zhao[1], Richard A. Coffman, PhD, PE, PLS[2]

4.3. Abstract

A back-pressure saturated, constant-rate-of-strain (BP-CRS) consolidation device was modified to incorporate bender elements (BE). A series of laboratory tests were conducted on a dummy brass sample and on kaolinite soil samples, using the BP-CRS and BP-CRS-BE devices, to determine the amount of system compliance for the BP-CRS-BE device, as compared to the BP-CRS device. The amount of machine deflection was determined for both the BP-CRS-BE device and BP-CRS device. Two approaches (quick and slow) were evaluated for determining the machine deflection. The machine deflection results, as obtained from both methods, were comparable; therefore, the use of the quick method is recommended. The respective average amount of maximum machine deflection (brass sample) and maximum corrected vertical deformation (kaolinite sample) for the BP-CRS and BP-CRS-BE devices were 0.78 mm and 0.88 mm (machine deflection) and 3.15 mm and 3.43 mm (soil deformation), respectively.

Consolidation parameters were determined by subtracting the amount of respective machine deflection from the amount of vertical deformation that was measured during tests that were performed on kaolinite soil samples. The consolidation parameters, as obtained from both devices, were also comparable. The average values of recompression index (c_r), compression index (c_c), swell index (c_s), and coefficient of consolidation (c_v) for the kaolinite samples that were tested in the BP-CRS and BP-CRS-BE devices were 0.07 and 0.08, 0.19 and 0.21, 0.08 and 0.07, and 9.3E-8 m^2/s and 9.6E-7 m^2/s, respectively. Because similar values were obtained for the consolidation parameters, as obtained by using either the BP-CRS device or the BP-CRS-BE device, the use of the newly designed BP-CRS-BE device is advocated because the BP-CRS-BE

device also enabled collection of shear wave velocity measurements while the sample was being subjected to various stress levels.

Keywords: system compliance, constant-rate-of-strain, consolidation, shear wave velocity

4.4. Introduction

Constant-rate-of-strain (CRS) consolidation testing began being utilized within geotechnical engineering in the late 1960s and early 1970s when Smith and Wahls (1969) and Wissa et al. (1971) introduced the topic. In the four decades since the inception of the testing apparatus, several types of devices have been developed to perform the CRS test. These devices consist of the conventional, stand-alone, closed CRS consolidometer (ASTM D4186 2012), the triaxial insert, closed CRS consolidometer (Trautwein 2014), and the standard, stand-alone, open incremental load consolidometer or CRS consolidometer (Landon 2007, Trautwein 2014). The aforementioned closed devices allow for backpressure saturation while the open device does not allow for backpressure saturation. Within the past 10 years, researchers have also been utilizing bender elements (BE), within CRS testing devices, to determine the small-stain shear modulus of the soil through the use of correlations with measured shear wave velocity (Landon 2007, Kang et al. 2014). However, as discussed in Coffman et al. (2014), the BE were installed within an open device and generated vertically propagating waves that were horizontally polarized or on samples that must be slurry consolidated (Landon 2007, Kang et al. 2014). Because CRS samples are typically very thin (approximately 25.4mm), near-field effects may have been present within the collected shear wave velocity data (making it difficult to decipher the amount of travel time for first shear wave) (Landon 2007). To overcome the near-field effects and to enable anisotropic measurements of small-strain shear modulus for slurry consolidated or Shelby tube obtained samples, a triaxial insert, closed CRS consolidometer was modified at the

University of Arkansas (UofA) to enable BE testing using horizontally propagating waves, that were vertically polarized, across a 6.35cm diameter sample during CRS testing.

Two series of tests were performed, utilizing two different devices, in an effort to verify the large-strain consolidation parameters and shear wave signals that were obtained from the modified device (the device that includes BE inserts and is hereafter identified as the BP-CRS-BE), and the non-modified device (the device that does not include BE inserts and is hereafter identified as the BP-CRS). One series of tests involved conducting tests on a brass sample while the other series of tests involved conducting tests on laboratory prepared, slurry consolidated, kaolinite samples. An overview of the BP-CRS and BP-CRS-BE devices is presented herein followed by the testing procedures and data reduction methods that were utilized to validate the BP-CRS-BE device. Furthermore, a comparison of the obtained results (BP-CRS and BP-CRS-BE) is then presented and a discussion is provided to outline the justification for use of the BP-CRS-BE device.

4.5. Fabrication of Apparatus

To facilitate the incorporation of BE into the CRS device, the design for the single-drainage CRS consolidometer was modified to include Delrin® slide bars, attached to the top cap, that housed the BE (Figure 4.3). Although the BE are presented within the Delrin® slide bars (as shown in the left-hand portion of Figure 4.3), the BE slide bars were only used during testing on the kaolinite soil samples; dummy Delrin® slide bars (slide bars without bender elements, as shown in the right-hand portion of Figure 4.3) were utilized during the machine deflection testing on the brass dummy sample. Furthermore, Delrin® guides were utilized to surround the slide bars to enable the slide bars (and therefore the BE) to move in the vertical direction, with the center of the soil sample, as the soil sample consolidated. This was

accomplished by rigidly attaching the top of the Delrin® slide bars to the aluminum top cap of the consolidometer insert. The stainless steel confining ring was also modified to facilitate the vertical movement of the aforementioned Delrin® slide bar within the aforementioned Delrin® guides (Figure 4.4).

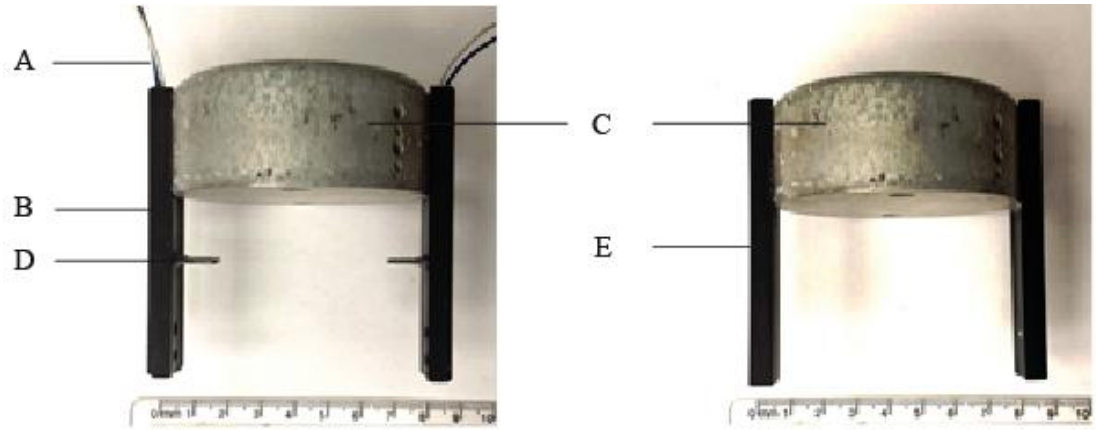

(a) (b)

A. Wires (+/-). B. Delrin® slide bars with BE.
C. Aluminum loading cap. D. Bender element.
E. Delrin® slide bard without BE.

Figure 4.3. Photograph of a) BE within the fabricated Delrin® slide bars and b) dummy fabricated Delrin® slide bars that were used in the BP-CRS-BE device.

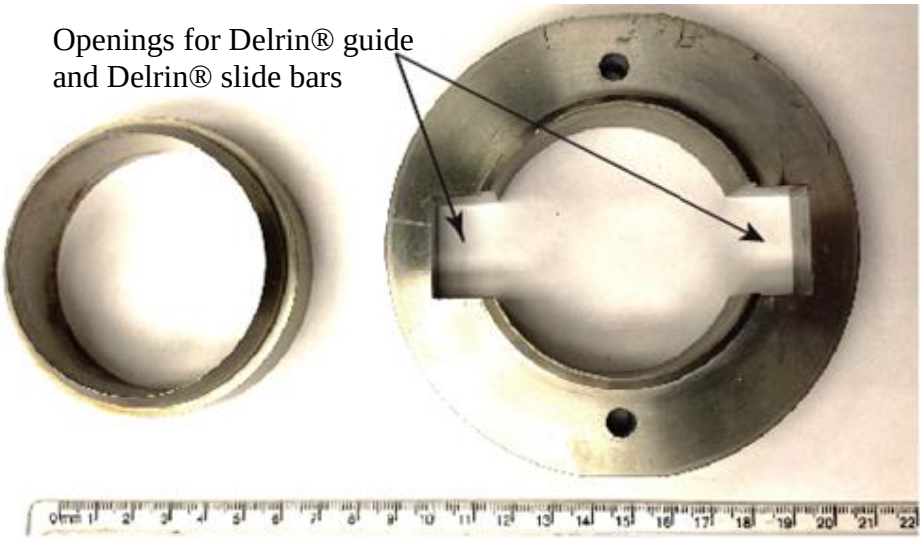

(a) (b)

Figure 4.4. Photograph of the stainless metal confining ring for a) BP-CRS and b) BP-CRS-BE devices.

Other fabrication differences between the BP-CRS and the BP-CRS-BE devices included 1) the aluminum base pedestals of the inserts, 2) the acrylic confining rings, 3) the o-ring gaskets and 4) the throughput electronics (Figure 4.5). Because of the aforementioned inclusion of the slide bars within the BP-CRS-BE device, the outside diameter of the stainless steel confining ring was increased for the BP-CRS-BE device. This increase in size resulted in a need for a larger triaxial cell (14cm inside diameter instead of the typical 11.4cm inside diameter cell). However, the same triaxial cell (14cm inside diameter) was utilized to conduct tests using both the BP-CRS consolidometer insert and the BP-CRS-BE consolidometer insert. To accommodate for the increase in size of the BP-CRS-BE stainless steel confining ring (10.16cm outside diameter), the outside diameters of the BP-CRS-BE aluminum base pedestal and the BP-CRS-BE acrylic confining ring were both increased from 10.16cm to 11.43cm.

The slide bars and guides prevented the use of the typical 3.2mm thick, 6.7 cm diameter round o-ring gasket (located within a circular groove cut into the base pedestal insert and placed underneath the stainless steel confining ring in the BP-CRS device). The purpose of this o-ring was to separate the excess pore pressure at the bottom of the sample from the confining pressure in the cell chamber for the BP-CRS-BE device. Therefore, to enable pressure separation within the BP-CRS-BE device, a 6.35 mm thick Viton® gasket was used in place of the o-ring. The outside diameter of the Viton® gasket was the same as the inside diameter of the stainless steel confining ring (6.35cm) and the inside diameter of the gasket was the same as the outside diameter of the porous stone that was located below the bottom of the sample (5.08cm). Although there was some friction between the gasket and the slide bars, this gasket allowed for 1) the slide bars to advance past the bottom of the sample, 2) confinement of the excess pore pressure at the bottom of the sample, and 3) a smaller diameter porous stone to be used within

the BP-CRS-BE device (5.08cm) than the stone that was used within the BP-CRS device (6.35cm).

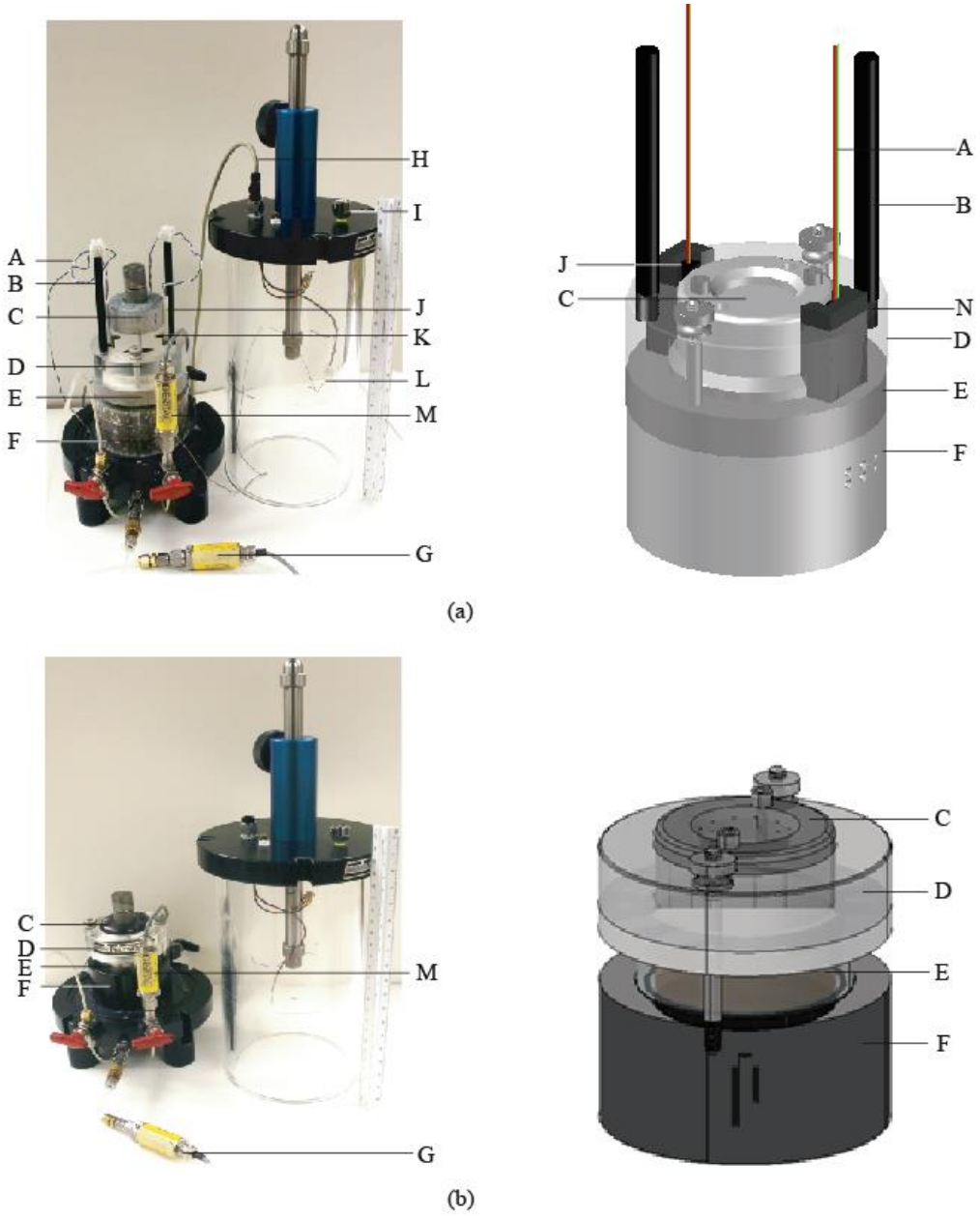

A. BE wires (+/-). B. Wire harness and post. C. Top cap (aluminum). D. Confining ring (acrylic). E. Confining ring (stainless steel). F. Base pedestal (aluminum). G. Cell pressure transducer. H. Grounding cable (Faraday cage). I. Cell pressure application port. J. Delrin® slide bar. K. Bender element. L. Grounding wire connection (nine-pin). M. Pore pressure transducer. N. Delrin® slide guide.

Figure 4.5. Photographs and schematic of the a) BP-CRS-BE and b) BP-CRS triaxial insert CRS consolidometers (as modified from Coffman et al. [2014]).

As presented in Figure 4.6, in a similar fashion to Coffman et al. 2014 and Salazar and Coffman (2014), the electronic signals for the bender elements were generated and acquired from a National Instruments Labview® waveform generation and acquisition program that utilized a 18-bit M Series (NI PCI-6281) card and a E-Series Input/Output connector block (NI SCB-68). A multi-channel filter (Krohn-Hite 3362) and a digital oscilloscope (Tektronix TDS 2012 B) were also used to: filter (high pass and low pass filters were applied), gain (typical gain of 50dB), monitor, and record the generated and acquired signals. Unlike the electronic signal data that were generated and acquired without electrical interference or cross-talk, as presented in Salazar and Coffman (2014), it was discovered that shielding conduit and grounding wires were required to prevent the electrical interference and the cross-talk between the generated and acquired signals.

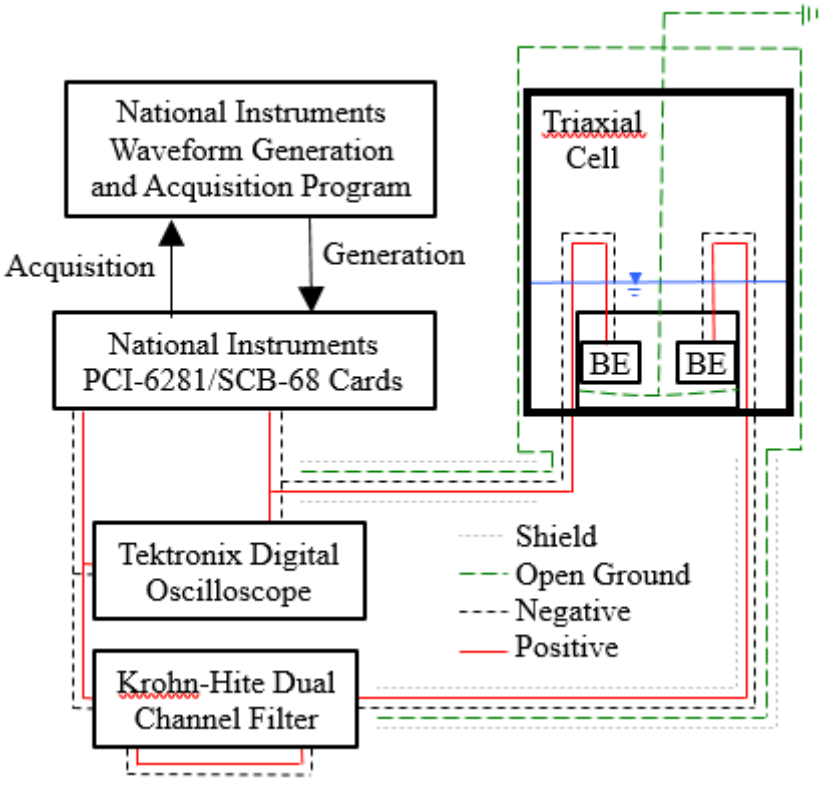

Figure 4.6. Equipment and wire schematic utilized for BP-CRS-BE device.

Therefore, the cabling (positive, negative, and open ground wires) between the connector block and the triaxial cell were fed through the two drainage line ports (the drainage lines within these ports are typically connected to the acrylic top platen of the triaxial sample during a triaxial test but were not required for a CRS test). The positive and negative wires carrying the generated signals went through one drainage line port and the positive and negative wires carrying the acquired went through the other drainage line port. After the wires exited from the bottom of the triaxial cell, the wires were placed within separate stainless steel conduits (stainless steel water hoses). Each of the conduits contained an open grounding wire, to prevent the interference between the generated and acquired signals. Specifically, the generated signals were transmitted by using the positive and negative wires that were located within one conduit and the acquired signals were transmitted by using positive and negative wires that were located within the other conduit. Furthermore, to avoid damage to the sensitive electronics, air was utilized in place of water within the top half of the triaxial chamber and the wiring harnesses for the electronic connections were located on posts within the air. However, water was still utilized to surround the sample to ensure saturation. To prevent cross-talk, an additional grounding wire was fed into the triaxial cell through a nine-pin connector that was located within the top cap of the triaxial cell and was wrapped around the aluminum base pedestal within the water (like a Faraday cage) to prevent cross-talk.

4.6. Testing Procedure

The testing procedure was separated into two stages. The first stage included tests being conducted on a brass ‘dummy’ sample to determine the deflection of the respective device under given loading increments. The second stage included conducting tests utilizing laboratory prepared kaolinite samples to determine the consolidation properties from both devices and the

shear modulus from the BP-CRS-BE device. Tests were performed using both devices (BP-CRS and BP-CRS-BE), during both stages, in an effort to determine the similarities and differences between the devices. A 44.5kN load capacity, 7.62cm stroke limit servo-mechanical load frame and a 1035kPa air regulated panel board were utilized to perform all of the tests. Although these capacities were available, the tests were performed to a maximum load of 8.9kN, under a back-pressure of 206.7kPa. The procedures utilized to perform the testing during Stage 1 and Stage 2 are outlined herein.

4.6.1. *Machine Deflection as Determined using Brass 'Dummy' Sample*

While performing the machine deflection testing, a 25.4mm tall brass 'dummy' sample was inserted into the respective stainless steel confining ring and the apparatus was assembled around the brass sample. The only differences between the 'dummy' brass sample and the 'actual' kaolinite soil samples were the material properties of the samples and the heights of the samples. Although several tests were performed on 25.4mm tall kaolinite samples from the laboratory prepared samples (Samples K1-K4), the height of the kaolinite samples was reduced to 19.05mm due to extrusion of the kaolinite around the top of the confining ring for the 25.4mm tall samples. Therefore, only laboratory prepared samples numbered K5-K11 were utilized for the testing that is documented herein.

Two testing procedures were utilized to perform the machine deflection testing. The procedures consisted of a 'quick' testing technique (3 hours) and a 'slow' testing technique (20 hours). The 'quick' testing technique consisted of utilizing a "machine deflection" sub-routine within the Trautwein GeoTAC Sigma-1 CRS-SI program that caused the loading platen of the device to move, resulting in 1) an increase in the amount of applied load to the maximum prescribed value of load (8.9kN) and then 2) a decrease in the amount of applied load until no

load was on the sample. The ‘quick’ type of test was only used to determine, and can only be used to determine, the machine deflection values for a load-unload type of test and not for a load-unload-reload-unload type of test. The deformation values (and corresponding load values) from the ‘quick’ test were recorded at 18 points during the loading cycle and at 13 points during the unloading cycle. These values were stored in the initialization file (.ini) of the program.

The ‘slow’ testing technique consisted of performing tests following the same procedures that were utilized to conduct the tests on the actual soil samples. Using this technique the strain rate and consolidation schedule (maximum or minimum strain or stress level at which to unload or reload) were prescribed (Table 4.1). Although the same testing sequence was prescribed for the brass and kaolinite samples, the tests performed on the brass samples were completed more quickly than the tests completed on the kaolinite samples because of a more rapid pore pressure dissipation rate for the tests using the brass sample. All of the data were stored as voltage values. Therefore, during post-processing of the data, the data were converted from voltage values to values in engineering units by utilizing: 1) the voltage values that corresponded to zero load/pressure/displacement/volume, 2) the corresponding calibration factor values, and 3) the corresponding excitation voltage values. Although all of the aforementioned load/pressure/displacement/volume data were collected from the load frame, only the load/displacement data were utilized to determine the amount of machine deflection. Significantly more data were collected during the ‘slow’ tests; however, in an effort to compare the ‘quick’ tests and the ‘slow’ tests the values from the ‘quick’ data were interpolated to include the same load values that were obtained during the ‘slow’ tests.

Table 4.1. CRS testing strain rate and consolidation schedule.

Step	Strain Rate (%/hour)	Uncorrected Limit Strain (%)	Uncorrected Limit Stress (kPa)
Loading	0.5	30	2800
Unloading	0.5	0	29

4.6.2. *Laboratory Prepared Kaolinite Samples*

Multiple kaolinite slurry soil samples were prepared using KaoWhite S kaolinite (obtained from Thiele Kaolin Company in Sandersville, GA). The 50-percent water content kaolinite slurry samples were 1) placed into a 6.35cm diameter dead-weight slurry consolidometer, 2) subjected to a prescribed stress level of 137.8 kPa (by subjecting the 6.35cm diameter sample to 0.44 kN of applied load), and 3) allowed to consolidate. Following the end of primary consolidation, individual sub-samples were removed from the slurry consolidometer and tested in either the BP-CRS or BP-CRS-BE device. The samples were laboratory prepared, using the slurry consolidometer, to ensure that the consolidation properties of the samples (specifically the pre-consolidation pressure) were identical (Figure 4.7). Time-rate consolidation properties including the coefficient of consolidation (c_v) values were also obtained for the various laboratory prepared samples (Samples K5-K11) following the procedures outlined in Casagrande (1936).

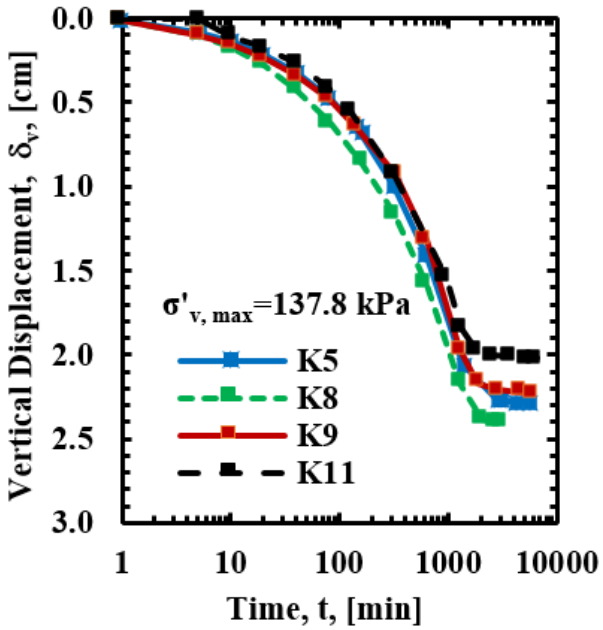

Figure 4.7. Time-rate consolidation curves for the samples that were consolidated from slurry, in the slurry consolidometer, prior to CRS testing (laboratory prepared samples).

4.6.3. *BP-CRS and BP-CRS-BE Testing on Laboratory Prepared Kaolinite Soil Sample*

The testing procedures utilized to perform the tests using the BP-CRS and BP-CRS-BE were identical. However, although the machine deflection values stored in the .ini files do not affect the results obtained from the respective tests, the corresponding average values of machine deflection, as obtained from the respective 'quick' tests, were contained within the corresponding .ini files for the BP-CRS and BP-CRS-BE devices. The height of the soil samples, the back-pressure saturation sequence, the rate at which the tests were performed, and the termination criteria were identical for all tests performed using both devices. Specifically, 19.08mm tall sub-samples were obtained from the slurry consolidometer samples by extruding the consolidated samples from the slurry consolidometer into a 19.08mm tall confining ring and using the ring as a mold to trim the samples to the height of the ring. The aforementioned trimmings were utilized to determine the initial water content of the sample.

Following trimming, the samples were extruded, weighed, and then inserted into the 25.4mm tall stainless steel confining ring for the BP-CRS or the 25.4mm tall stainless steel confining ring for the BP-CRS-BE device. After the combined sample and ring were placed into the respective device, the triaxial chamber was assembled around the triaxial insert. The triaxial chamber was then placed into the load frame, the chamber was partially filled with water, and the drainage lines that were connected to the bottom of the sample were purged of air by using water. The kaolinite sample, located within the triaxial insert, inside of the triaxial chamber, was then allowed to back-pressure saturate under a 206.7kPa back-pressure for 30 minutes prior to beginning the consolidation phase of the test. This back-pressure was also maintained during the consolidation phase of the test.

The uncorrected (disregarding piston uplift) stress termination criterion for the loading portion of the consolidation phase of the test was 2800kPa (corresponding to 8.9kN of measured force). Because the test can be either stress or strain terminated, the allowable strain was increased to 30 percent to ensure that the stress limit was reached before the strain limit. After reaching an uncorrected stress level of 2800kPa, the respective samples were unloaded to an uncorrected stress level of 29kPa or a strain level of zero percent. Again, the stress level termination criterion was reached prior to the strain level termination criterion. Upon reaching the unloading termination criteria, the sample was removed from the triaxial insert, and a water content test was performed on the entire sample by placing the ring and soil sample into a tin and then placing the tin into an oven.

4.6.4. *Verification of the Electronic Signals Obtained from the Bender Elements*

Shear wave velocity testing was also performed on the kaolinite samples within the BP-CRS-BE device. Signals were generated and received, every one-half to two hours during the

CRS test, at various stress levels. At each stress level, at least five signals were generated and acquired; the acquired signals were stacked to increase the signal to noise ratio. Furthermore, different types of signals (single pulse, dual pulse, tri pulse) were generated using different waveforms (sine, square) to aid in the identification of the shear wave(s) that traveled through the soil. Moreover, to aid in the identification of the shear wave(s) that traveled through the soil, the bender elements were also tested within the triaxial cell when the BP-CRS-BE device was assembled with no soil sample present; instead, water or air were located in the place of the kaolinite soil sample.

As reported by others (Montoya et al. 2012, Marjanovic and Gremaine 2013), even though the bender elements were waterproofed by following the procedures discussed in Montoya et al. (2012), electrical interference and cross-talk were evident within the signals that were received through the soil sample. The cause of the electrical interference and cross-talk was worrisome because these effects were not previously observed when the same National Instruments Labview® waveform generation and acquisition program, NI PCI-6281 card, NI SCB-68, Krohn-Hite 3362, and Tektronix TDS 2012 B were utilized (Coffman et al. 2014, Salazar and Coffman 2014). The difference between the system reported in Salazar and Coffman (2014) for triaxial testing and the system, as shown previously in Figure 4.5 for CRS testing, was the way in which the wires (connected to the bender elements) were arranged. The generated signals in Salazar and Coffman (2014) were transmitted through a nine-pin wiring harness that was located within the top cap of the triaxial cell to the acrylic top platen; the wires that were utilized to control the bender element that generated the signal included a positive wire, a negative wire, and a grounding wire. The acquired signals in Salazar and Coffman (2014) were transmitted through wires that passed through a nylon screw that was used to connect the acrylic

bottom platen to the bottom plate of the triaxial device; the wires that were utilized to control the bender element that acquired the signal included a positive wire, a negative wire, and a grounding wire that was connected to the other grounding wire outside of the triaxial cell. Therefore, because the wires that exited the triaxial cell went through a nylon screw, these wires were not in contact with any portion of the metallic cell. Furthermore, because the results in Salazar and Coffman (2014) were obtained from a triaxial test, there was no direct metallic contact between the wires that transmitted the generated and acquired signals (the soil specimen within the triaxial test was surrounded by a flexible rubber membrane and capped with acrylic platens instead of the specimen in the CRS test being surrounded by a metallic ring and capped with metallic caps).

4.7. Results and Discussion

The results obtained from the aforementioned testing procedures include: 1) proper wiring techniques to remove electrical interference and cross-talk, 2) machine deflection relationships for the BP-CRS and BP-CRS-BE devices, as obtained from the 'quick' and 'slow' testing procedures, 3) force – deformation relationships, as obtained from the tests performed on the kaolinite soil samples, using the BP-CRS and BP-CRS-BE devices, 4) void ratio – effective stress relationships, as obtained from the tests performed on the kaolinite soil samples, using the BP-CRS and BP-CRS-BE devices, 5) effective stress – axial strain relationships, as obtained from the tests performed on the kaolinite soil samples, using the BP-CRS and BP-CRS-BE devices, and 6) the consolidation properties of the kaolinite, as obtained from the tests performed on the kaolinite soil samples, using the BP-CRS and BP-CRS-BE devices and the slurry consolidometer. In addition to these relationships, the methods used to reduce the data are presented because these methods were observed to influence the obtained results.

4.7.1. *Proper Wiring Techniques*

As presented in Figure 4.8, the time required for the generated signal to travel through the soil (t) was determined by subtracting the time required for the signal to travel through the system in a tip-to-tip arrangement (t_d) from the time required for the signal to travel through the system in the arrangement in which the BP-CRS-BE tests were performed (t_t). Furthermore, as presented in Figure 4.8, the signals that were associated with the electrical interference and cross-talk ($t_{crosstalk}$) were removed by using the wiring techniques that were previously presented in Figures 4.5 and 4.6 (grounding and shielding). Although these electrical features did not have to be removed because there was a time delay between the cross-talk and shear wave signals, the cross-talk was removed to aid in the data interpretation (Marjanovic and Germaine 2013). However, signals from another shear wave were problematic. Specifically, the shear wave that traveled from the bender element that generated the signal, through the Delrin ® slide bar, through the aluminum top cap, and through the opposite Delrin ® slide bar to the bender element that acquired the signal typically possessed a larger amplitude and always traveled faster (t_{topcap}) than the shear wave that traveled directly through the soil (t_t). As the soil consolidated and the soil became stiffer, the relative amplitude of the shear wave that traveled through the top cap diminished due to the stiffness contrast between the soil and the aluminum top cap decreasing. During unloading of the soil, the stiffness contrast between the soil and the aluminum top cap again increased, resulting in larger amplitudes of the signals that were associated with the shear wave that that traveled through the top cap.

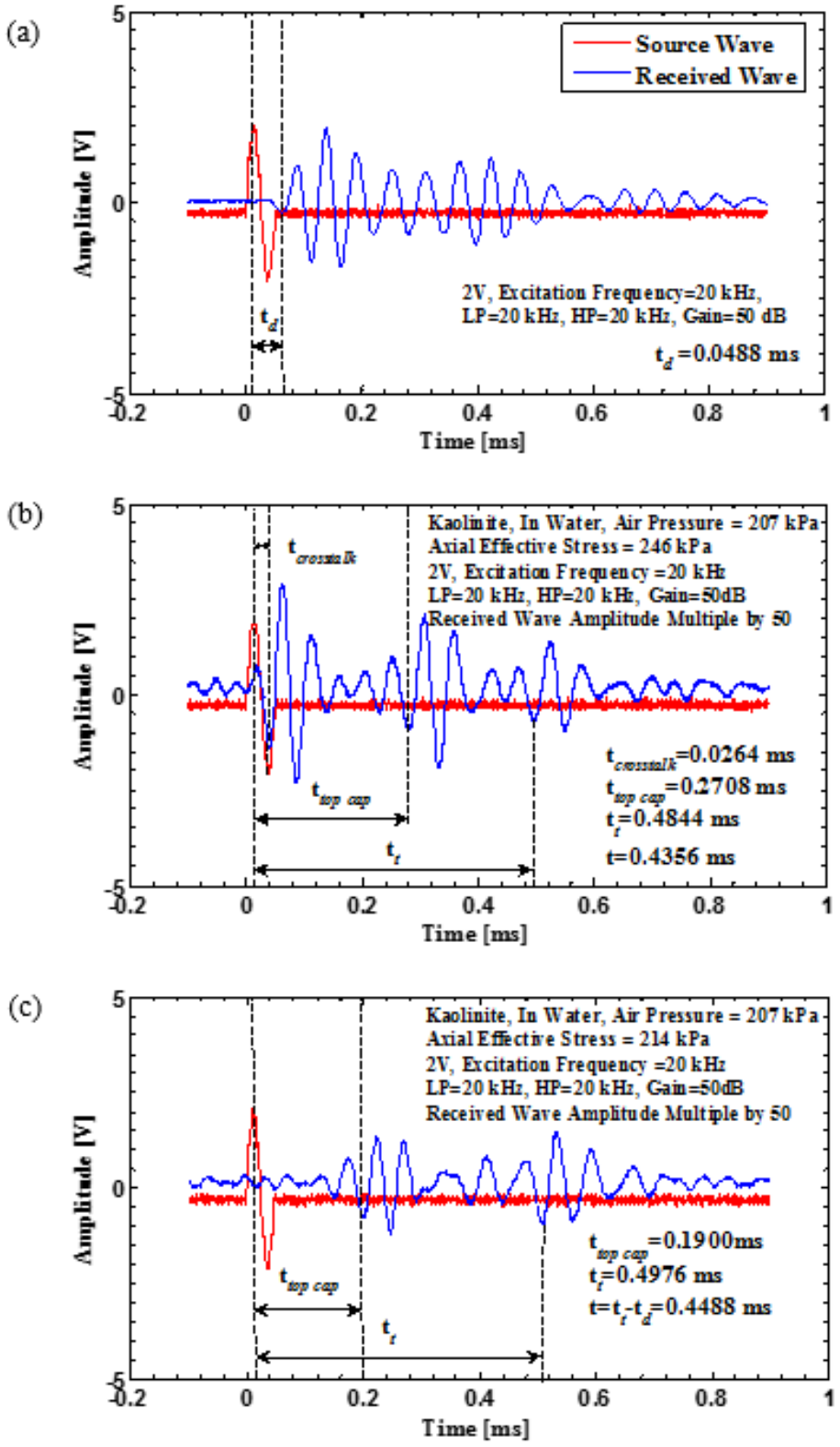

Figure 4.8. Generated and acquired signals for: a) tip to tip test, b) BP-CRS-BE test on kaolinite including cross-talk and top cap shear waves, and c) BP-CRS-BE test on kaolinite including top cap shear waves.

4.7.2. *Machine Deflection*

As presented in Figures 4.9 and 4.10, the average amounts of machine deflection, at a maximum force of 8.9kN, for the 'quick' and 'slow' tests, as conducted in the BP-CRS and BP-CRS–BE devices, were 0.782mm and 0.759mm for the BP-CRS device and 0.883mm and 0.816mm for the BP-CRS-BE device. The shapes of the curves were similar with a rounded shape observed during the loading and unloading cycles. However, the initial slope of the BP-CRS-BE curves was steeper than the slope observed for the curves obtained from the BP-CRS device. Although plastic deformation was observed following the loading and unloading cycles, the amount of plastic deformation at corresponding force levels was consistent for multiple tests. Moreover, the amount of plastic deformation that was observed following the completion of all tests was consistent (approximately 0.24mm for both of the devices regardless of the testing time). Thereby, the amount of plastic deformation (machine deflection), at corresponding levels of force, may be subtracted from the measured amount of deformation observed for soil samples to determine the amount of soil deformation.

Based on the obtained results, the 'quick' or the 'slow' test may be used to determine the amount of machine deflection. Although the 'quick' test takes less time than the 'slow' test, the 'quick' test may only be utilized if the test is performed as a load-unload cycle. If the test is performed as a load-unload-reload-unload cycle, then a 'slow' test must be performed to determine the amount of machine deflection. Because the tests can be strain or stress terminated it is also best to wait to perform the machine deflection test until after the tests are conducted on the soil samples so that the same loading cycle conditions that were utilized for the soil testing can be utilized for the machine deflection testing.

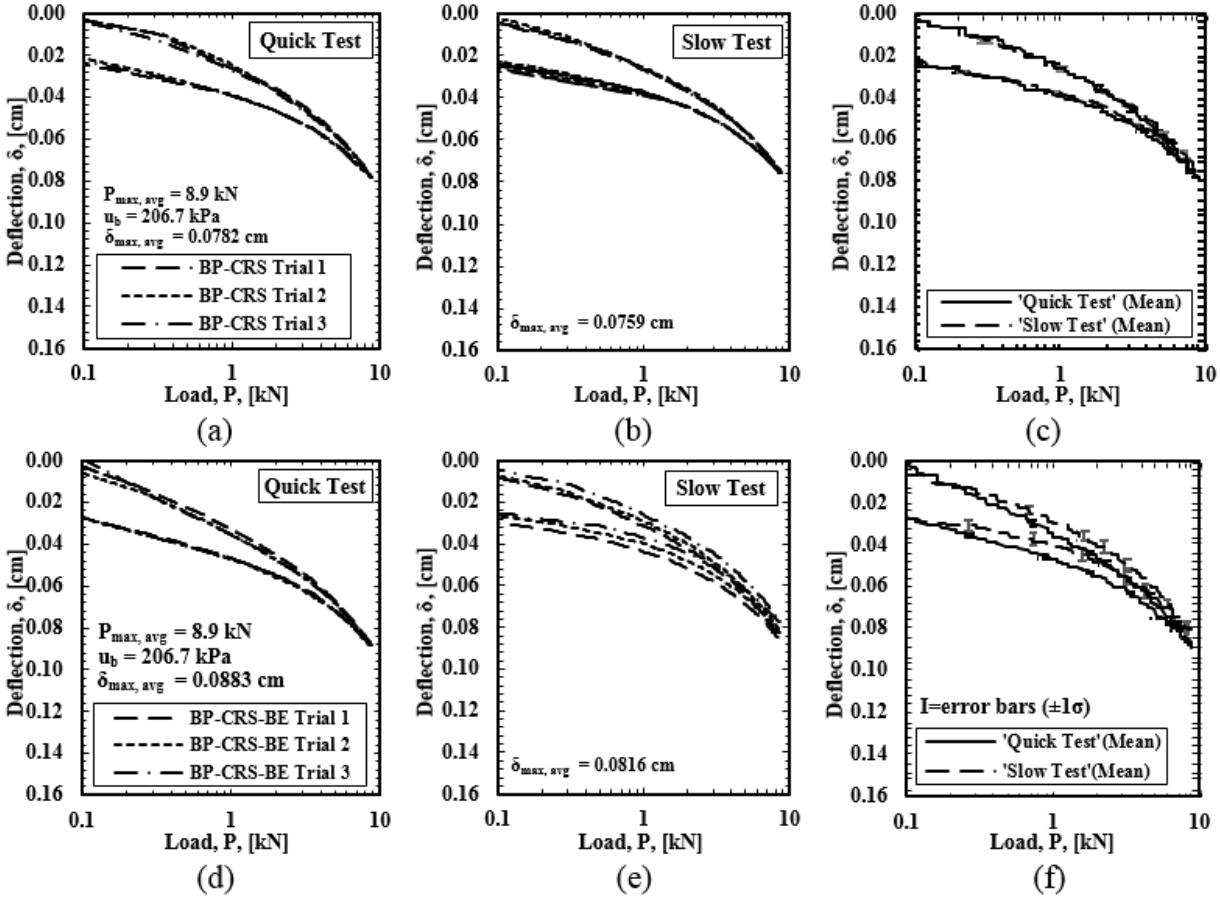

Figure 4.9. Machine deflection results obtained from the: a) 'quick', b) 'slow', and c) mean of the 'quick' and 'slow' tests for the BP-CRS device and the d) 'quick', e) 'slow', and f) mean of the 'quick' and 'slow' tests for the BP-CRS-BE device.

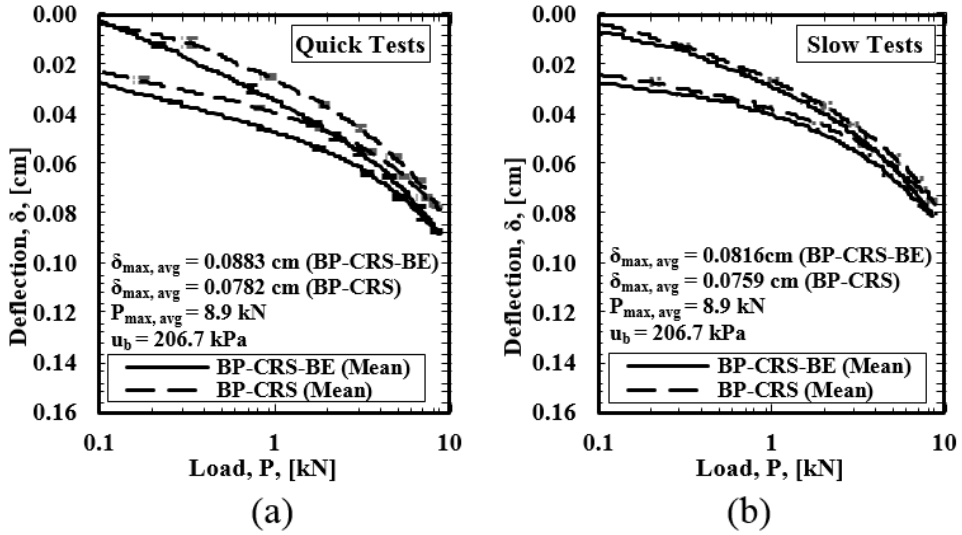

Figure 4.10. Comparison of the machine deflection results obtained from the BP-CRS and BP-CRS-BE devices.

The increased amount of movement (approximately 0.10mm at the maximum force) that was observed for the BP-CRS-BE device (Figure 4.10) is believed to be associated with the Delrin® slide bars and the Viton® gasket. Although the Delrin® slide bars were fabricated to ensure a frictional fit within the Delrin® guide, the fabrication tolerance associated with this modification reduced the stiffness of the confining ring, by allowing a slight amount of lateral deformation at the locations of the two slide bars. Moreover, the reduction in stiffness that resulted from a portion of the sample resting on the Viton® gasket, instead of the porous stone, may have resulted in more apparent vertical displacement in the BP-CRS-BE device than in the BP-CRS device.

Although the determination of the amount of machine deflection is outlined in the ASTM D4186 standard (2012), and the amount of machine deflection is commonly obtained following the "machine deflection" subroutine in the Trautwein GeoTAC CRS-SI software, many users are unaware that the values of machine deflection are not automatically subtracted from the recorded data as collected during tests on soil samples. Therefore, post-processing is required to subtract the amount of machine deflection from the measured values after the measured data have been converted from voltage values into values in engineering units.

4.7.3. *Force - Deformation Relationship*

The force – deformation relationships, as observed prior to and following correction for machine deflection, are presented in Figure 4.11 (Figure 4.11a and 4.11b for the BP-CRS and Figure 4.11d and 4.11e for the BP-CRS-BE). Only three tests were performed using the BP-CRS and BP-CRS-BE devices because of the reproducibility of the force – deformation relationship using the devices. The reason why the results obtained from the BP-CRS-BE were slightly less repeatable than the BP-CRS results may be attributed to a number of factors. These factors

include 1) the aforementioned increase in vertical deformation associated with the use of Delrin® and Vitron® in the BP-CRS-BE device, and/or 2) improper seating of the axial piston into the top cap prior to beginning the consolidation stage. Furthermore, possible variations in the material properties of the laboratory prepared samples may have also contributed to the lack of reproducibility within the BP-CRS-BE device; however, this contribution has been neglected because the amount of uncertainty in the laboratory prepared samples is similar for the samples tested in both the BP-CRS and the BP-CRS-BE devices. Specifically, this similarity is shown in the tables presented in Figures 4.11c and 4.11f for each of the sub-samples (S), obtained from the different laboratory prepared material (M) samples, based on the initial void ratio and the initial moisture content.

To overcome the variability associated with the data obtained from the BP-CRS-BE device, two data reduction techniques were considered. These two techniques include 1) correcting all of the curves to the curve with the minimum amount of deformation (at the maximum force value) in the force – deformation relationship or 2) correcting all of the curves to the curve with the highest void ratio (at the maximum force value) in the void ratio – deformation relationship. The corrected deformation curves are presented in Figure 4.11c and 4.11f for the BP-CRS and BP-CRS-BE devices, respectively. The corrected curves, based on the void ratio – effective stress relationships and based on the axial strain – effective stress relationships, are discussed and presented in the next two sections, respectively.

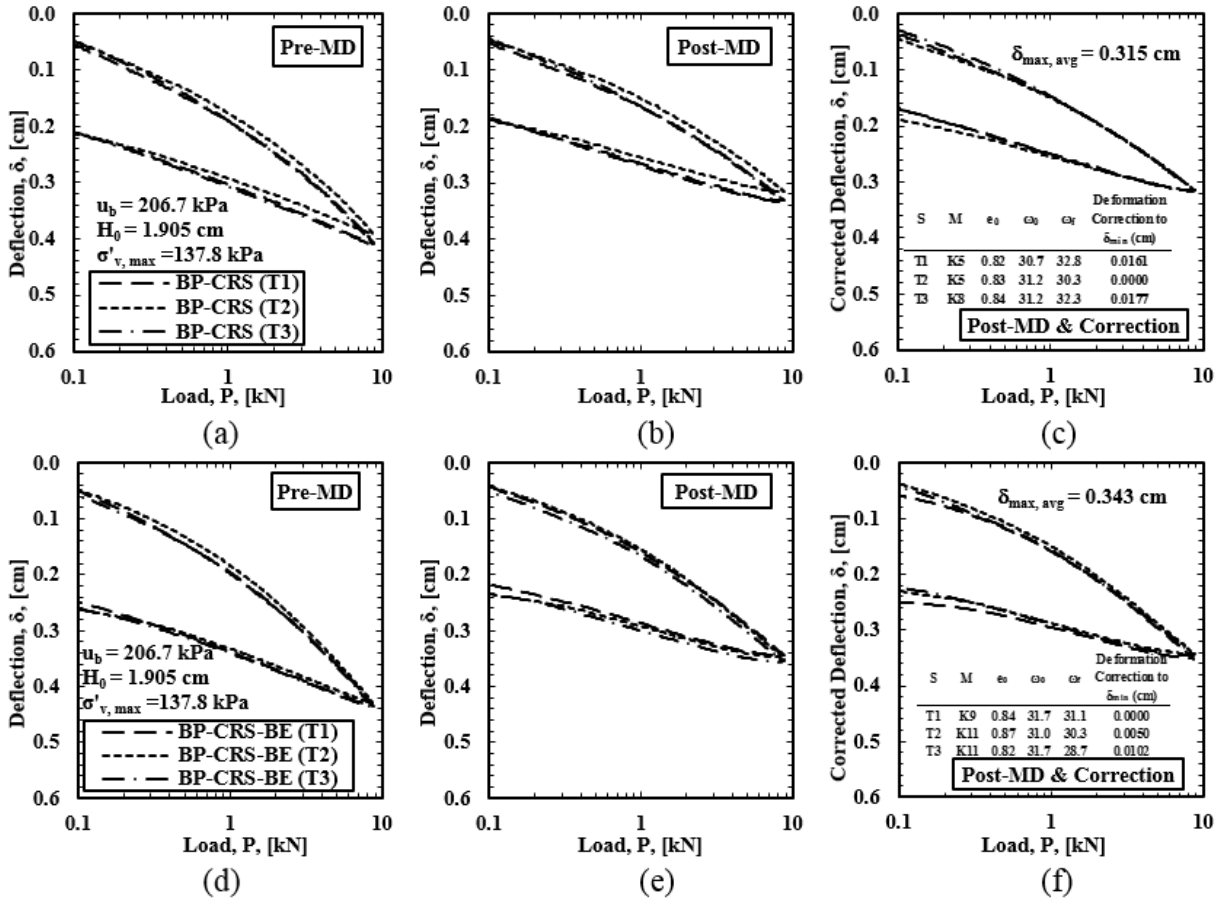

Figure 4.11. Pre- and post-machine deflection and post-machine deflection/post-deformation correction results for tests conducted on kaolinite samples in the BP-CRS (a, b, c) and BP-CRS-BE device (d, e, f), respectively (as modified from Coffman et al. [2014]).

4.7.4. *Void Ratio – Effective Stress Relationship*

Consolidation properties including the preconsolidation stress $[\sigma'_p]$ and the consolidation indices (recompression index $[c_r]$, compression index $[c_c]$, and swell index $[c_s]$) are typically obtained using the void ratio – effective stress relationship. Therefore, the void ratio – effective stress relationships, as presented in Figures 4.12a and 4.12c, were developed from the corrected force and deformation data that were used to generate the previously presented post-machine deflection, deflection corrected, force – deformation curves (Figure 4.11). In a similar fashion to the way in which the deformation correction was performed, a void ratio correction was instead applied to the data by correcting (shifting along the y-axis) all of the curves to the curve with the

highest void ratio (at the maximum force value) in the void ratio – deformation relationship (Figure 4.12b and 4.12d). This correction reduced the amount of variation within the data when presented in the void ratio – effective stress space. Like with the deformation correction, the void ratio correction was used to alleviate the variation associated with the vertical deformation caused by the use of Delrin® and Vitron® and caused by improper seating.

4.7.5. *Axial Strain – Effective Stress Relationship*

Commonly, it is more simple to obtain and utilize consolidation ratios (recompression ratio $[R_r]$, compression ratio $[R_c]$, and swell ratio $[R_s]$) using the axial strain – effective stress relationship than it is to obtain and utilize consolidation indices. Therefore, the axial strain – effective stress relationships are presented in Figure 4.13. Specifically, the axial strain – effective stress relationships, as obtained by correcting the data to the curve with the minimum deformation (Figure 4.13a and 4.13c) or maximum void ratio (Figure 4.13b and 4.13d), are presented. Regardless of the method used to correct the data (deformation or void ratio), the curves exhibit the same shape (same slope for the various consolidation properties); the curves are just shifted to align with the curve that possessed the minimum amount of deformation or the curve that possessed the maximum void ratio. It is recommended that the void ratio correction be applied when determining the compression indices and the deformation correction be applied when determining the compression ratios.

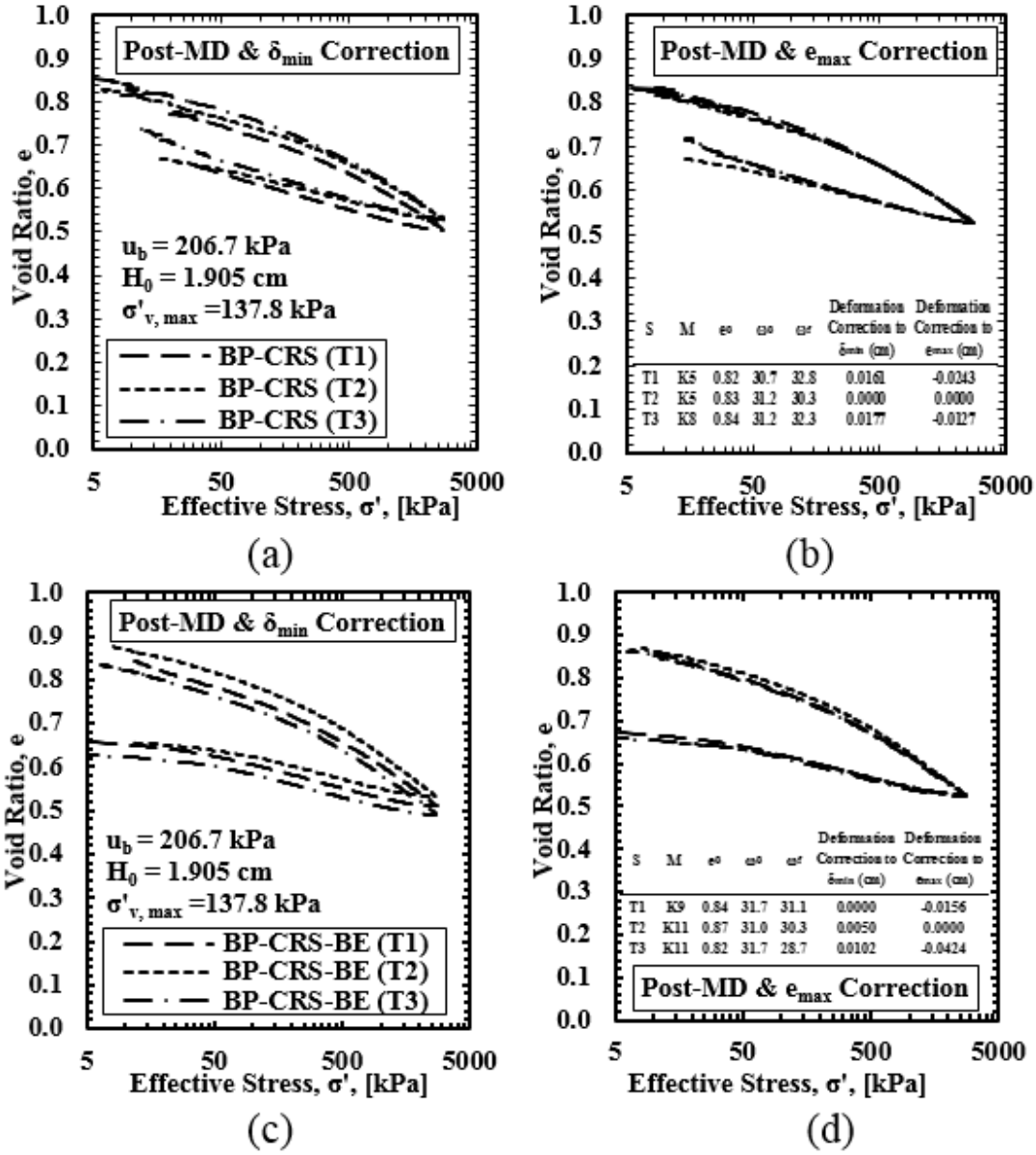

Figure 4.12. Post-machine deflection/post-correction results for the tests conducted on kaolinite samples based on deformation correction (a, c) and void ratio correction (b, d) for the BP-CRS and BP-CRS-BE devices, respectively, in void ratio – effective stress space.

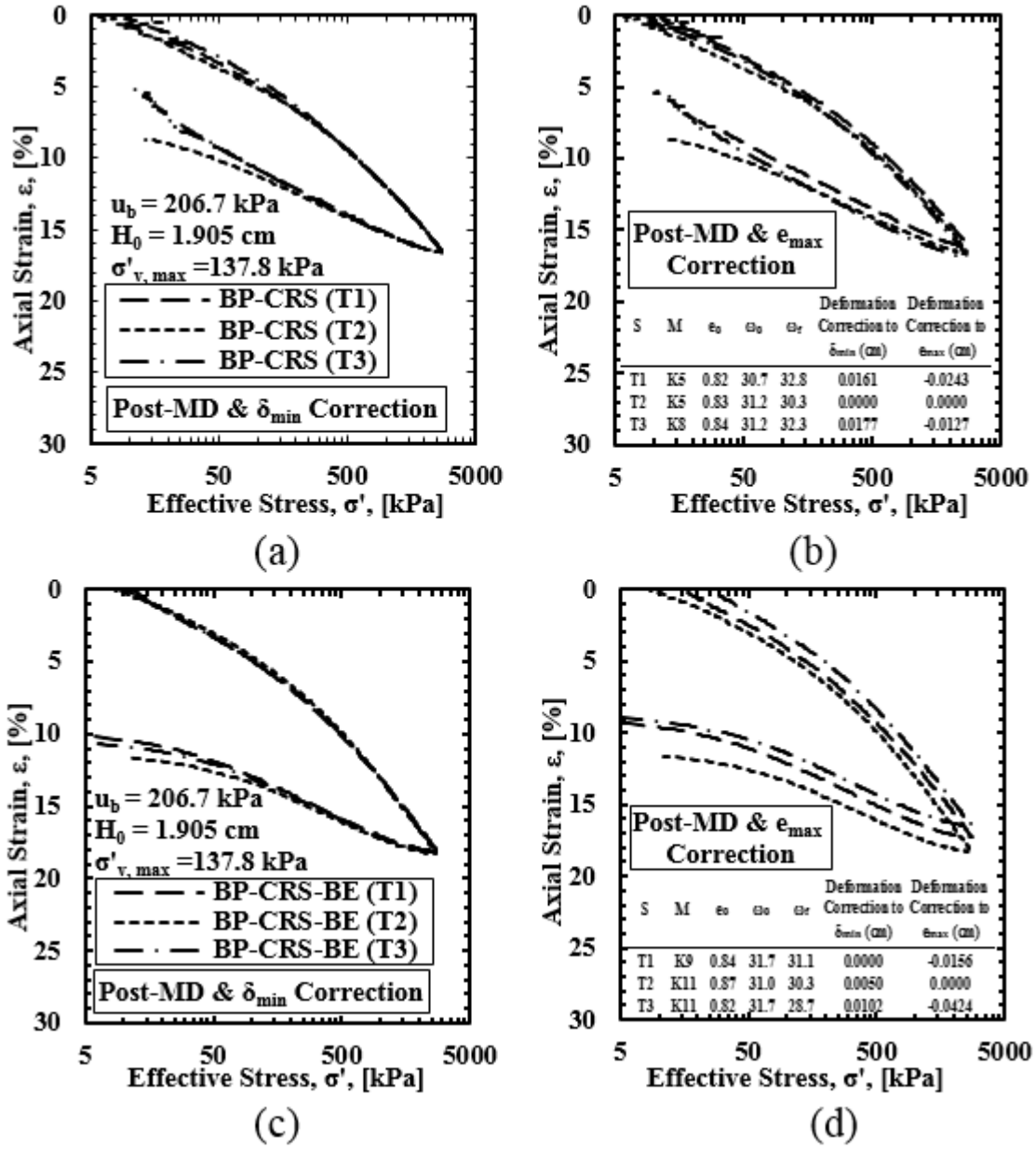

Figure 4.13. Post-machine deflection/post-correction results for the tests conducted on kaolinite samples based on deformation correction (a, c) and void ratio correction (b, d) for the BP-CRS and BP-CRS-BE devices, respectively, in axial strain – effective stress space.

4.7.6. *Measured Consolidation Properties*

The measured preconsolidation pressure values were obtained by utilizing the techniques described in Casagrande (1936) and Becker et al. (1987) and are presented in Table 4.2. The consolidation coefficients (indices and ratios) were obtained by determining the slope of the

recompression, compression, and swell lines that were presented in the void ratio – effective stress and axial strain – effective stress relationships, respectively, and the values are recorded in Table 4.2. The coefficient of consolidation values were obtained by utilizing the techniques described in Terzaghi and Fröhlich (1936) and in the ASTM D4186 standard (2012) for the slurry consolidometer tests and for the CRS tests, respectively, and are presented in Table 4.3.

Table 4.2. Consolidation properties obtained from the CRS tests (as modified from Coffman et al. [2014]).

Device Type	Tests	Cr	Cc	Cs	Rr	Rc	Rs	σ_p', [kPa]	
								Casagrande (1936)	Becker et al. (1987)
BP-CRS	T1	0.07	0.19	0.08	0.04	0.10	0.04	178.3	136.8
	T2	0.08	0.19	0.07	0.04	0.10	0.04	196.1	143.4
	T3	0.07	0.18	0.09	0.04	0.10	0.05	151.6	126.2
BP-CRS-BE	T1	0.09	0.20	0.07	0.05	0.11	0.04	140.7	141.2
	T2	0.07	0.22	0.07	0.04	0.12	0.04	141.7	141.8
	T3	0.08	0.21	0.07	0.04	0.11	0.04	136.4	137.0

Table 4.3. Properties of laboratory prepared kaolinite samples as obtained from the slurry consolidometer data and the CRS consolidation data.

Device Type	Test	Sample Batch	σ_p', [kPa]	C_v, (m^2/sec.)	
				Consolidometer	CRS tests
BP-CRS	T1	K5	137.8	1.7E-08	8.4E-08
	T2	K5	137.8	1.7E-08	1.1E-07
	T3	K8	137.8	2.3E-08	8.8E-08
BP-CRS-BE	T1	K9	137.8	2.2E-08	2.5E-07
	T2	K11	137.8	2.0E-08	2.4E-06
	T3	K11	137.8	2.0E-08	2.0E-07

Because the samples that were utilized for the CRS testing were laboratory prepared from slurry, the preconsolidation pressure (137.8 kPa) was established by utilizing the static weight slurry consolidometer. Therefore, the σ_p' values that were measured during the CRS test (Table 4.2) should match the σ_p' values that were established following consolidation of the laboratory

prepared, slurry consolidated, samples. The average σ_p' values, as obtained for the BP-CRS device utilizing the Casagrande (1936) and Becker et al. (1987) techniques, were 175.3 and 135.5 kPa, respectively. Likewise, the average σ_p' values, as obtained for the BP-CRS-BE device utilizing the Casagrande (1936) and Becker et al. (1987) techniques, were 139.6 and 140.0 kPa, respectively. Although the closest measured average value of σ_p', to the actual σ_p' value, was obtained using the BP-CRS device (as determined from the data analyzed using the Becker et al. [1987] technique), the average value obtained from the BP-CRS-BE device was approximately one percent above the actual value.

The average values of c_r, c_c, c_s for the kaolinite samples that were tested in the BP-CRS-BE and BP-CRS devices were 0.08 and 0.07 (c_r), 0.21 and 0.19 (c_c), and 0.07 and 0.08 (c_s), respectively. The deviation in the c_r values is of little importance because the c_s values are commonly utilized in place of the c_r values when determining the amount of consolidation settlement by use of the Schmertmann (1955) field reconstruction technique. The 11 percent difference in the calculated c_c values corresponded to the aforementioned increase in vertical deformation that was associated with the use of Delrin® and Vitron® within the BP-CRS-BE device. The higher average value of c_c, as obtained from the BP-CRS-BE device, may produce settlement estimates that are more representative of field conditions as the amount of settlement is commonly under predicted based on BP-CRS data (Coffman and Bowders [2009]).

The average values for the coefficient of consolidation (c_v), at the same effective stress that was utilized to consolidate the laboratory prepared samples (137.8 kPa), as obtained from the BP-CRS-BE and BP-CRS devices were 9.6E-7 m^2/sec and 9.3E-8 m^2/sec (c_v), respectively. The difference in these c_v values was counter intuitive, as the average c_c value obtained using the BP-CRS-BE device was higher than the average c_c value obtained using the BP-CRS device.

Typically, higher values of c_c correspond to lower values of c_v. These average values were approximately one order of magnitude (5 to 48 times for the BP-CRS and BP-CRS-BE devices, respectively) higher than the average c_v value (2.0E-8 m^2/sec) that was calculated from the time-rate data that were collected during consolidation of the laboratory prepared samples (i.e. collected while consolidating the laboratory prepared samples from a slurry). Like with the higher average value of c_c, the higher average value of c_v, as obtained from the BP-CRS-BE device, may also produce settlement estimates that are more representative of field conditions (Coffman and Bowders 2009).

Due to the well-known relationship between the value of c_v and the value of hydraulic conductivity (k), the value of k that was obtained from the BP-CRS-BE was higher than the value of k obtained from the BP-CRS (Figure 4.14). This difference was expected because the previously mentioned average value of c_v that was obtained from the BP-CRS-BE was higher than the average value of c_v that was obtained from the BP-CRS. As presented in Figure 4.14, although the values of k that were obtained from the BP-CRS-BE and from the BP-CRS were within the same order of magnitude, for a given void ratio value, the values of k that were obtained from the BP-CRS-BE were always higher than the values obtained from the BP-CRS. Furthermore, there was more uncertainty within the values of k, as obtained from the tests performed using the BP-CRS-BE device, than the amount of uncertainty that was obtained from tests that were performed using the BP-CRS device. The increase in the amount of uncertainty was associated with the variable amounts of dissipation of excess pore water pressure at the interface between the Delrin® guide and the Delrin® slide bar.

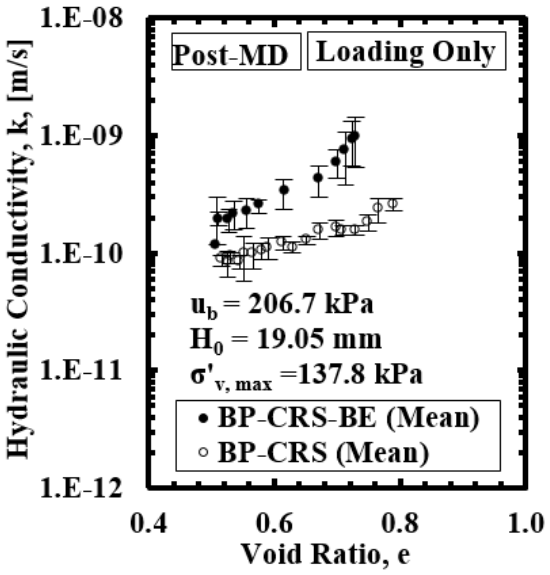

Figure 4.14. Comparison of the hydraulic conductivity results, as a function of void ratio, as obtained from the BP-CRS-BE and the BP-CRS.

4.8. Conclusions

A triaxial insert, back-pressure saturated, constant rate-of-strain, consolidation device was modified for the inclusion of bender elements that generate and acquire horizontally propagated, vertically polarized waves. The device was fabricated to allow for the bender elements to move with the soil as the soil consolidates by using sliding bars that were made from Delrin®. The use of Delrin® within the BP-CRS-BE resulted in an increase in the average values of compression index and coefficient of consolidation as compared to the BP-CRS device. The increase in the c_c values and the c_v values that were observed for the BP-CRS-BE device are more representative of the field conditions. Therefore, the use of the BP-CRS-BE triaxial insert is recommended for determining the consolidation properties of soils, because accurate consolidation properties were obtained and because shear wave velocity measurements were also determined using the device.

4.9. References

American Society for Testing and Materials, "Standard Test Method for One-Dimensional Consolidation Properties of Saturated Cohesive Soils Using Controlled-Strain Loading." *Annual Book of ASTM Standards*, Designation D4186, Vol. 4.09, ASTM International, West Conshohocken, PA. 2012.

Becker, D.E., Crooks, J.H.A., Been, K., Jefferies, M.G., "Work as a Criterion for Determining In situ and Yield Stresses in Clays". *Canadian Geotechnical Journal*, Volume 24, 1987, pp. 549-564.

Casagrande, A., "The Determination of Pre-consolidation Load and its Practical Significance". *Proceedings Soil Mechanics and Foundation Engineering*, Volume 3, 1936, pp. 60-64.

Coffman, R.A., Bowders, J.J., Summary of Laboratory Testing Results, Grand Forks, ND. *University of Missouri Institute for Interdisciplinary Geotechnics Final Report*. Client: Burns and McDonnell Engineering, Inc., January, 2009.

Coffman, R.A., Salazar, S.E., Zhao, Y., "Discussion of Measurement of Stiffness Anisotropy in Kaolinite Using Bender Element Tests in a Floating Wall Consolidometer by X. Kang, G.-C. Kang, B. Bate." *Geotechnical Testing Journal*. Vol. 37, No. 6, 2014, pp. 1-5. doi:10.1520/GTJ20140162.

Kang, X., Kang, G.-C., Bate, B. "Measurement of Stiffness Anisotropy in Kaolinite Using Bender Elements in a Floating Wall Consolidometer." *Geotechnical Testing Journal*. Vol. 37, No. 5, 2014, pp. 1-15.

Landon, M. M., "Development of a Non-destructive Sample Quality Assessment Method of Soft Clays," *Ph.D. Dissertation*, University of Massachusetts, Amherst, MA, 2007.

Montoya, B.M., Gerhard, R., DeJong, J.T., Wilson, D.W., Weil, M.H., Martinez, B.C., and Pederson, L., "Fabrication, Operation, and Health Monitoring of Bender Elements for Aggressive Environments". *Geotechnical Testing Journal*. Vol. 35, No. 5, 2012, pp. 1-15. doi:10.1520/GTJ103300.

Marjanovic, J., Germaine, J.T., "Experimental Study Investigating the Effects of Setup Conditions on Bender Element Velocity Results". *Geotechnical Testing Journal*. Vol. 36, No. 2, 2012, pp. 1-11. doi:10.1520/GTJ20120131.

Salazar, S.E., Coffman, R.A., "Design and Fabrication of End Platens for Acquisition of Small-Strain Piezoelectric Measurements during Large-Strain Triaxial Extension and Triaxial Compression Testing." *Geotechnical Testing Journal*, Vol. 37, No. 6, 2014, pp. 1-12. doi:10.1520/GTJ20140057.

Schmentmann, J.H., "The Undisturbed Consolidation Behavior of Clay". *ASCE Transactions*, Volume 120, 1955, pp. 1201-1227.

Smith, R., and Wahls, H., "Consolidation Under Constant Rates of Strain," *Journal of the Soil Mechanics and Foundations Division*, Volume 95, No. SM2, 1969, pp. 519-539.

Terzaghi, K. T. and O. K. Frohlich, "Theorie der Setzung von Tonschichten," FranzDeuticke, Leipzig, 1936.

Trautwein, Stephen, "FW: CRS brochures". *Personal Electronic Mail Communication to Richard Coffman*, July 3, 2014.

Wissa, A., Christain, J., Davis, H., and Heiberg, S., "Consolidation at Constant Rate of Strain," *Journal of the Soil Mechanics and Foundations Division*, Volume 97, No. SM10, 1971, pp. 1391-1413.

CHAPTER 5: Small-Strain and Large-Strain Modulus Measurements

5.1. Chapter Overview

Three BP-CRS-BE tests were performed on Kaolinite soil samples to obtain small-strain and large-strain modulus. Specifically, small-strain shear modulus values (G_{max}) were obtained from the bender element measurements. In these tests, horizontal bender elements were utilized to generate the horizontally propagate and vertically polarized shear wave (HV). Large-strain constrained modulus values (*M*) were obtained from the constant-rate-of-strain consolidation (*CRS*) tests. To bridge from small-strain modulus (G_{max}) to large-strain modulus values (*G*), a shear modulus degradation curve was utilized. By using the aforementioned *G* and *M* values, the drained Poisson's ratio values (ν) were then calculated for the soil samples. Additionally, a group of normalized specific volume functions were developed to determine the horizontal effective stress values during loading and unloading stages. The values of coefficient of lateral earth pressure were acquired by using the previously obtained horizontal effective stress and the vertical effective stress. The drained friction angle values for the soil then were determined from the $K_0 - OCR$ function. Finally, the methodology and the procedure that were utilized to obtain the aforementioned values (M, G_{max}, G, v, $\overline{S_h}$, ν, K_0, ϕ') were presented and discussed. It is to be noted that the triaxial testing data, which were utilized to formulate the specific volume functions, were provided by Nabeel S. Mahmood.

The paper enclosed in this chapter has been submitted within the *Journal of Testing and Evaluation*. The full reference is: Zhao, Y., Mahmood, N., and Coffman, R. A., "Small-Strain and Large-Strain Modulus Measurements with a Consolidation Device," *Journal of Testing and Evaluation*, Submitted for Review, Manuscript Number: JTE-2016-0331, 2016.

5.2. Additional Results

The additional results obtained from the BP-CRS-BE T1, T2, and T3 tests, which were not covered in the submitted paper, included three items: 1) waterfall plots for BP-CRS-BE T2 and T3, 2) drained Poisson's ratio-overconsolidation ratio relationship, and 3) pore water pressure-overconslidation ratio relationship.

5.2.1. *Waterfall Plots*

The waterfall plots for the BP-CRS-BE T2 and T3 tests are presented in Figure 5.1 and 5.2. Horizontal bender elements were utilized in these tests and thus HV shear waves were generated. There was a desire to utilize Quattro equipment to collect received signal data rather than oscilloscope equipment because the Quattro equipment will generate and store the source signals and received signals automatically, while the oscilloscope requires manual collection of the received signals. The oscilloscope was utilized to collect the received shear wave signal data for the BP-CRS-BE T1 and T2 tests, while the Quattro was utilized to collect the received shear wave signal data for the BP-CRS-BE T3 test. The quality of received signal data obtained from the oscilloscope (BP-CRS-BE T2 test, as shown in Figure 5.1) was better than the Quattro (BP-CRS-BE T3 tests, as presented in Figure 5.2) because of higher resolution for oscilloscope equipment. Thus, the oscilloscope was preferred to be utilized to collect received shear wave signals for all additional of the tests. Furthermore, although great caution was taken when assembling the sample and conducting the test, minor crosstalk was observed in BP-CRS-BE T2 tests, as shown in Figure 5.1. This crosstalk did not affect the identification of the shear wave velocity in this case. However, special care should be taken when connecting the wires within the BP-CRS-BE system, and proper grounding and shielding should be checked frequently during the test.

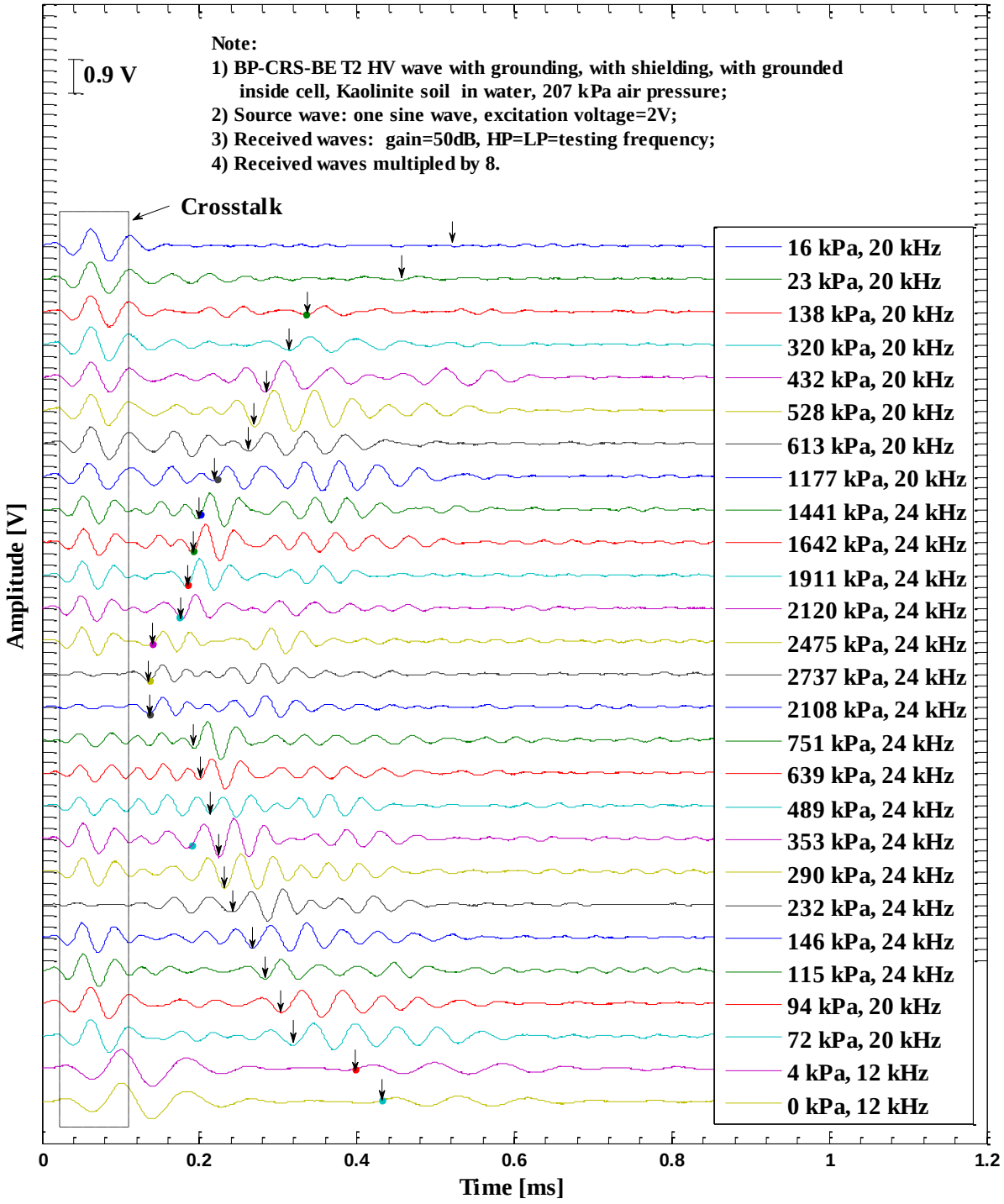

Figure 5.1. Waterfall plot of collected shear wave signals of BP-CRS-BE T2 on kaolinite soil for determination of V_s (HV) during consolidation tests (oscilloscope collected shear wave signals).

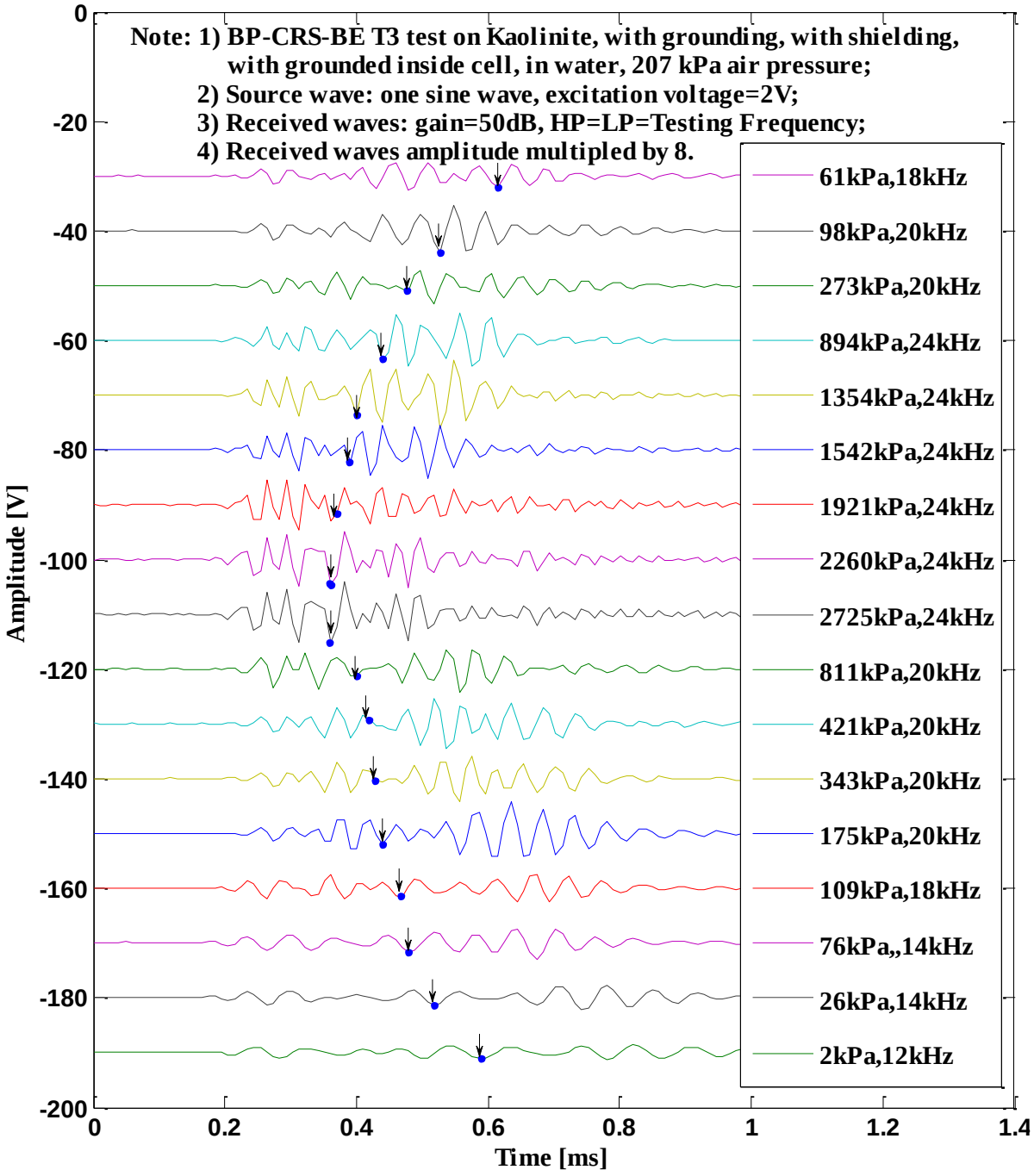

Figure 5.2. Waterfall plot of collected shear wave signals of BP-CRS-BE T3 on kaolinite soil for determination of V_s (HV) during consolidation tests (quattro collected shear wave signals).

5.2.2. *Drained Poisson's Ratio as a Function of OCR*

The drained Poisson's ratio - overconsolidation relationship, which were developed from the three tests that were performed by using a BP-CRS-BE device on kaolinite soil, are presented in Figure 5.3. The results from the three tests are similar and once again validated the repeatability of the BP-CRS-BE tests. The reduction in the Poisson's ratio values was associated with the decreasing of pore water pressure within the soil samples under drained conditions. In other words, the pore water pressure decreased with the increase of the overconsolidation ratio during the unloading stage, as presented in Figure 5.4.

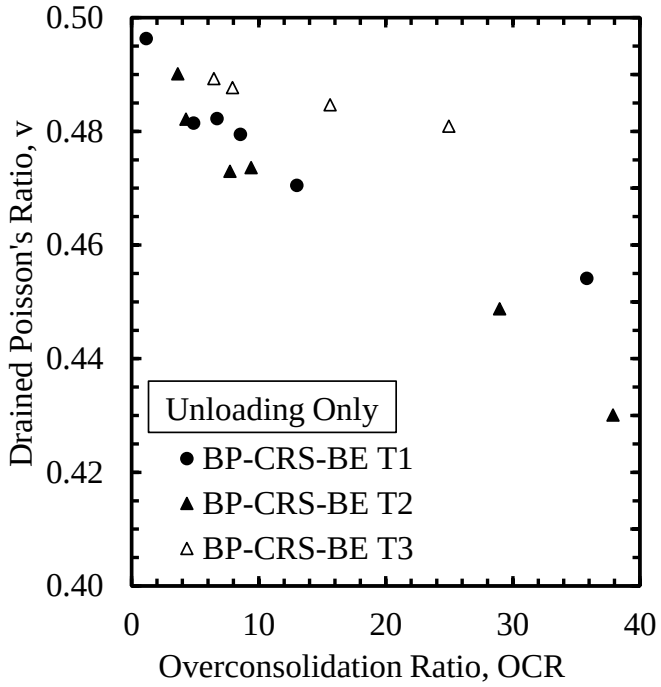

Figure 5.3. Drained Poisson's ratio as a function of overconsolidation ratio.

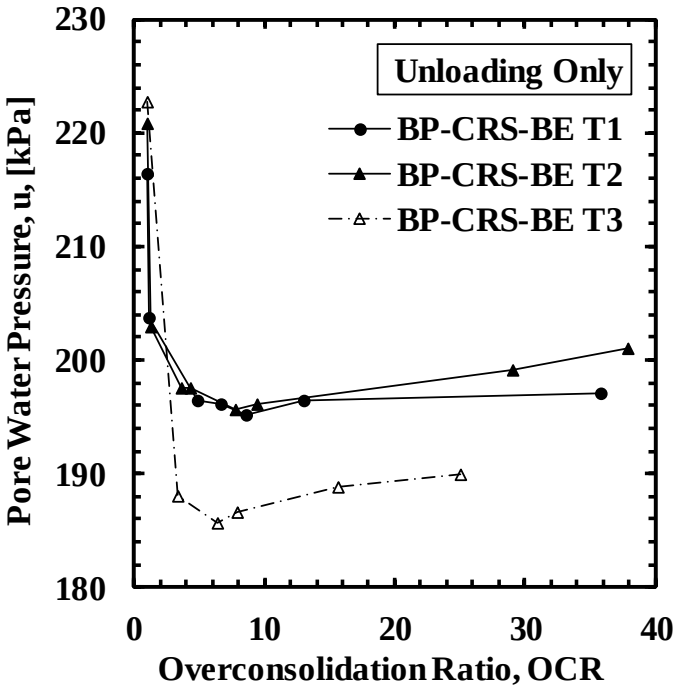

Figure 5.4. Pore water pressure as a function of overconsolidation ratio.

Small-Strain and Large-Strain Modulus Measurements with a Consolidation Device

Yi Zhao[1], Nabeel S. Mahmood[2], Richard A. Coffman[3]

5.3. Abstract

By using the back-pressure saturated, constant rate-of-strain, consolidation device with bender elements (BP-CRS-BE), values of large-strain constrained modulus (*M*) and small-strain shear modulus (G_{max}) were obtained from tests performed on kaolinite soil specimens. To span from G_{max} to the large-strain shear modulus values (*G*), a shear modulus degradation curve was utilized. Drained Poisson's ratio values (ν) were then calculated for the soil by utilizing the aforementioned *M* and *G* values. Moreover, effective stress values in the horizontal direction ($\overline{\sigma_h}$), within the BP-CRS-BE device, were obtained by utilizing the measured 1) vertical effective

stress ($\overline{\sigma_v}$) data, 2) normalized specific volume (v) functions, and 3) supplementary triaxial testing data; these normalized functions were developed for both the loading and unloading stages of the tests. For the unloading stages, values of the coefficient of lateral earth pressure (K_0) were also calculated by using the aforementioned horizontal and vertical stresses. Furthermore, drained friction angle values (ϕ') for the soil were obtained by using the BP-CRS-BE device. The methodology and procedures that were utilized to obtain all of the aforementioned values (M, G_{max}, G, v, $\overline{\sigma}_h$, $\overline{\sigma}_v$, v, K_0, ϕ') are discussed herein.

The following five observations were made. 1) The G_{max} values increased with increasing values of vertical effective stress ($\overline{\sigma}_v$) and decreased with increasing values of OCR. 2) The G_{max} values that were obtained by utilizing the large-strain BP-CRS-BE device ($G_{\max,CRS,p'}$), that were back-calculated by considering the modulus reduction, matched the G_{max} values that were obtained from the bender element measurements within the BP-CRS-BE device ($G_{\max,BE}$). 3) The v values increased with $\overline{\sigma}_v$ values but decreased with the increasing void ratio (e) values. 4) The K_0 values increased with increasing OCR values. 5) The ϕ' values that were calculated for the soil that was tested within the BP-CRS-BE device, by using the $K_0 - OCR$ data that was obtained from the BP-CRS-BE device (21.2, 16.0, 24.7 degrees) were in agreement with the ϕ' values that was obtained from modified Mohr-Coulomb diagram from a triaxial test on the same soil (20.7 degrees).

Keywords: small-strain, large-strain, bender element, constant rate-of-strain consolidation, constrained modulus, shear modulus, shear wave velocity, over-consolidation ratio, drained Poisson's ratio, drained friction angle

5.4. Introduction

Piezoelectric transducers have been extensively utilized, within the soil mechanics laboratory or in the field, because of 1) the non-destructive testing aspect associated with the implementation of this transducer type, while and 2) enabling the measurement of shear wave velocity. When compared to traditional soil testing methods, the use of bender elements offers a potential cost/benefit advantage by allowing soil moduli values to be measured without destruction to the soil (Dyvik and Olsen 1989, Shibuya et al. 1998, Pennington et al. 2001, Lee and Santamarina 2005, Landon and DeGroot 2006, Montoya et al. 2011, Salazar and Coffman 2014). To make use of advantage, a back-pressure saturated, constant rate-of-strain, consolidation device with bender elements (BP-CRS-BE) was developed and fabricated at the University of Arkansas (Coffman et al. 2014, Zhao and Coffman 2016). As documented in Coffman et al. (2014) and Zhao and Coffman (2016), the machine deflection of the apparatus, the uplift and friction forces on the piston, and the friction forces on the slide bars, were taken into account so that the BP-CRS-BE device could be utilized to preform tests on either the laboratory prepared soil specimens or the field obtained Shelby tube soil samples. The results obtained from the bender elements, within the BP-CRS-BE apparatus, and from the BP-CRS-BE device itself allowed for accurate estimation of 1) the large-strain and small-strain soil modulus values and 2) for other design parameters (coefficient of lateral earth pressure, drained friction angle, and drained Poisson's ratio).

By incorporating bender elements into the BP-CRS-BE device, the following relationships were developed and are discussed herein. 1) The relationship between shear wave velocity and the vertical effective stress. 2) The relationship between shear wave velocity and void ratio. 3) The relationship between the large-strain constrained modulus and the small-strain

shear modulus, as a function of axial strain. 4) The relationship between the drained Poisson's ratio and the vertical effective stress. 5) The relationship between the drained Poisson's ratio and void ratio. 6) The relationship between the coefficient of lateral earth pressure and the over-consolidation ratio.

A method to bridge from small-strain shear modulus values to large-strain shear modulus values, through the utilization of the shear modulus degradation curve, was also developed and is discussed herein. For completeness, 1) the background for modulus determination and CRS testing is presented, 2) the procedures for obtaining the horizontal stress values and other parameters for the BP-CRS-BE tests on kaolinite soil, by utilizing supplementary triaxial test data, are presented, and 3) the various results that were obtained by utilizing the BP-CRS-BE are documented.

5.5. Background

Small-strain shear modulus values have historically been determined by utilizing field tests or within laboratory tests. For example, torsional shear tests have been performed to obtain the small-strain (10^{-4} to 10^{-1} percent) shear modulus and damping parameters (Hardin and Black 1968, Hardin and Drnervich 1972a, Hardin and Drnervich 1972b, Drnevich et al. 1978, Hardin 1978, Iwasaki et al. 1978, Isenhower and Stokoe 1979, Drnevich 1985, Darendeli 2001, Youn et al. 2008). Also, resonant column tests have been utilized to measure small-strain (10^{-5} to 1 percent) shear modulus values (Drnevich et al. 1978, Isenhower and Stokoe 1979, Darendeli 2001, Youn et al. 2008, Sasanakul 2005). Moreover, cyclic triaxial tests have been utilized to determine the small-strain (10^{-2} to 5 percent) shear modulus degradation as a function of shear strain (Kokusho 1980, Georgiannou et al. 1991, Sharma 2003, Zekkoset al. 2008, El Mohtar et al. 2013). In the aforementioned measurement methods, the relationship of small-strain shear

modulus, as a function of shear strain, was the main point of interest. Specifically, shear modulus degradation curves were developed and the dynamic properties were determined within the small-strain range. However, these methods are limited by complexity of 1) the testing procedures and 2) data processing.

Bender elements have also been used to measure small-strain (less than 10^{-3} percent) shear modulus of soil materials. Moreover, these instruments have been incorporated into existing equipment to measure the shear wave velocity of soil during other soil tests (Shirley and Hampton1978, Strassburger 1982, Dyvik and Madshus 1985, Dyvik 1989, Viggiani and Atkinson 1995, Brignoli et al. 1996, Jovicic et al. 1996, Pennington et al. 1997, Brocanelli and Rinaldi 1998, Arulnathan et al. 1998, Fioravante and Capoferri 2001, Kawaguchi et al. 2001, Mohsin and Airey 2003, Lee and Santamarina 2005, Salem 2006, Valle-Molina 2006, Landon 2007, Viana da Fonseca et al. 2009, Ghayoomi 2011, Montoya et al. 2011, Valle-Molina and Stokoe 2012, Kang et al. 2014, Salazar and Coffman 2014, Zhao and Coffman 2016). The limitation, of the aforementioned small-strain shear modulus testing devices, is that no soil modulus values were obtained for large-strain scenarios (greater than 5 percent).

Historically, large-strain soil modulus values were obtained from CRS consolidation tests. Specifically, as reported in (Smith and Wahls 1969), these moduli values were obtained by utilizing the consolidation theory developed by (Terzaghi 1943). As described within Wissa et al. (1971) and ASTM D4186 (2014), a linear solution was proposed to obtain the coefficient of volume compressibility (m_v) from CRS tests, by utilizing the ratio of the change of strain level to the change of stress level. According to ASTM D4186 (2014), the constrained modulus (M) is typically calculated by taking the reciprocal of m_v. The large-strain shear modulus values can then be calculated from the elastic relationships between the constrained modulus and Poisson's

ratio values. The axial strain range for the CRS tests is typically around 20-30 percent. Recently, Zhao and Coffman (2016) fabricated a modified CRS device that incorporated bender elements to bridge the gap between small-strain shear modulus measurements and large-strain shear modulus measurements. One of the main challenges that had to be overcome to bridge this gap was that axial strain values were measured in the CRS test while shear strain values were measured in the traditional (torsional shear, resonant column, and cyclic triaxial) tests. However, the relationship between shear strain (γ), axial strain (ε_1), and radial strain ($\varepsilon_{2,3}$) was defined by utilizing strain compatibility, using the "Cambridge method", as presented in Sharma and Fahey (2003) and Atkinson (2007).

In addition to the aforementioned shear modulus degradation behavior, Hardin (1978) and Lo Presti et al. (1993), and others (Iwasaki et al. 1978, Jovicic et al. 1996, Pennington et al. 1997, Shibuya et al. 1998, Darendeli 2001, Landon and DeGroot 2006, Landon 2007, Kang et al. 2014) have also examined the effects of soil parameters such as vertical effective stress ($\bar{\sigma}_v$), horizontal effective stress ($\bar{\sigma}_h$), mean effective stress (p'), over-consolidation ratio (*OCR*), and void ratio (*e*) on the small-strain shear modulus. Specifically, empirical methods have been proposed to predict small-strain shear modulus from the various soil parameters.

5.6. Materials and Methods

As shown in the flowchart presented in Figure 5.5, the following five items were completed and are discussed within this section. 1) Information regarding the kaolinite soil specimens that were prepared for the BP-CRS-BE and triaxial tests. 2) The methods that were utilized to perform the BP-CRS-BE tests and the triaxial tests. 3) The equations that were utilized during data reduction. 4) The procedures that were utilized to determine the horizontal stress in

the BP-CRS-BE, as related to the triaxial data. 5) The procedures that were utilized to determine design values from the BP-CRS-BE.

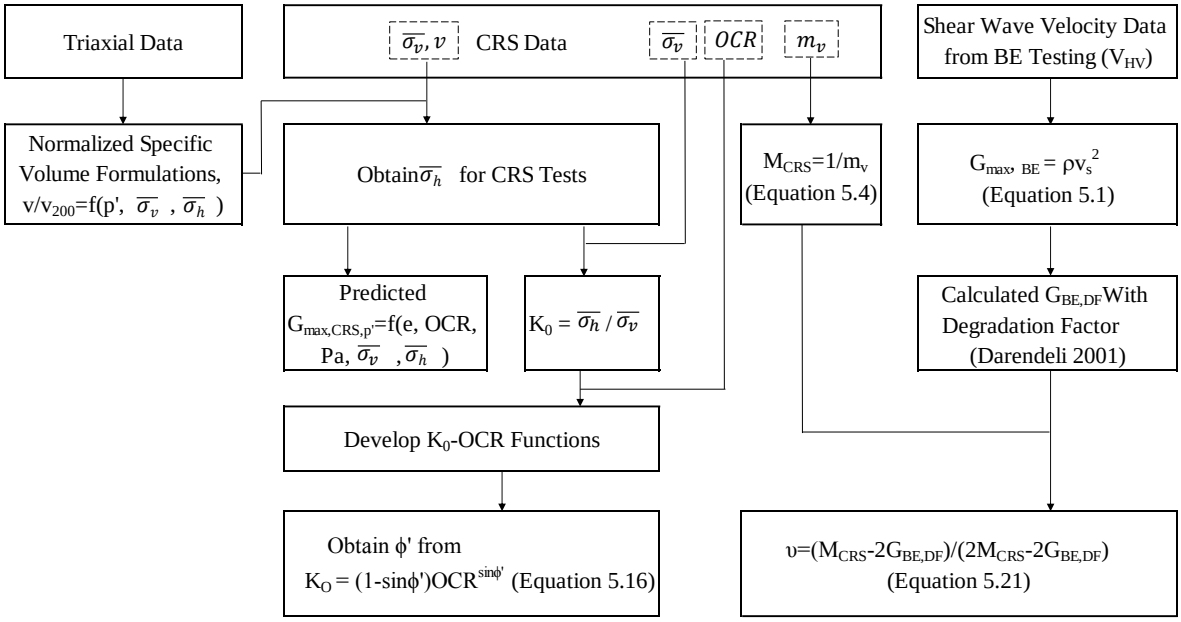

Figure 5.5. **Flowchart that was followed to determine soil parameters by using the BP-CRS-BE.**

5.6.1. *Sample Preparation*

Kaolinite soil (KaoWhite-S product), that was obtained from Thiele Kaolin in Sandersville, Georgia, was mixed with de-ionized, de-aired, water to form a 50-percent water content slurry. The slurry was then poured into a 3.81-cm diameter (triaxial specimens) or a 6.35-cm diameter (BP-CRS-BE specimens) slurry consolidometer and subjected to a vertical effective stress of 137.8kPa.

Triaxial tests were performed on specimens with a nominal length to diameter ratio of two. Prior to triaxial testing but following completion of the pre-consolidation process under the aforementioned 137.8kPa preconsolidation stress, these specimens were extruded from the slurry consolidometer. Like with the slurry consolidated BP-CRS-BE specimens that were reported in

Zhao and Coffman (2016), the time required to reach 100-percent average degree of consolidation was determined by following the procedures prescribed in Casagrande (1936).

After trimming a given specimen from the slurry consolidometer, the trimmings were collected for water content confirmation and each of the specimens was then: 1) measured (mass, length, diameter), 2) placed in between pieces of filter paper that were located in between porous stones that were located in between acrylic platens, 3) encased within membrane, 4) surrounded by the triaxial cell wall, and 5) connected to the loading piston by using a vacuum attachment. As shown in Salazar and Coffman (2014) and Race and Coffman (2011), the loading pistons that were utilized in the various cells also each contained an internal load cell. Therefore, after connecting the top platen to the loading piston, silicon oil (5cSt), instead of water, was utilized as the confining fluid. The use of silicone oil helped to prevent damage to the internal electronics (load cell) while also supplying the required confining stress. All of the triaxial chambers that were utilized for the triaxial testing were identical to the triaxial chamber that was shown in Salazar and Coffman (2014).

5.6.2. *Testing Methods*

The specimen-transfer procedures and the BP-CRS-BE testing procedures followed the procedures and devices that were utilized by and previously reported in Zhao and Coffman (2016). The procedures that were utilized for the triaxial testing are described herein. Each triaxial specimen was back-pressure saturated and consolidated prior to shearing the specimen following a triaxial compression or a triaxial extension mode of failure. Back-pressure saturation was completed by utilizing two servo-controlled flow pumps, each with a regulated capacity of 2068kPa. One of the pumps was filled with silicone oil and supplied the pressure that was required for the confining stress (cell pressure). The other pump was filled with deionized,

deaired, water and supplied the pressure that was required for the pore water pressure (back pressure).

During consolidation, the area of the specimen was not allowed to change (K_0-condition) while the vertical and radial effective stresses were increased (consolidation) and then decreased (over-consolidation). Specifically, during the servo-controlled K_0 -consolidation process, water was pulled from (consolidation) or pushed into (over-consolidation) the specimen at a given flow rate that was a function of the strain rate at which the piston moved to apply the axial stress. The pressure within the pump that controlled the confining stress was then increased or decreased to maintain the prescribed pore water pressure within the specimen. Although the K_0 -consolidation process was implemented by using the GeoTAC-Trautwein TruePath testing program (Trautwein 2014), that controlled the 8.9-kN capacity GeoTAC-Trautwein GeoJac load frame and the two 150-mL, 2068kPa capacity, GeoTAC-Trautwein DigiFlow pumps, the procedure mimicked the K_0-consolidation procedure that was described in Menzies (1988). The K_0-consolidation process was completed when the desired value of vertical effective stress was reached. Commencement of the shearing process immediately followed the completion of the K_0-consolidation process.

Dearing shearing, the valves (top and bottom) located at the triaxial cell, which were used to connect the internal tubing to the servo-controlled pore pressure pump, were closed. However, the valve that was located at the triaxial cell, and was connected to the pore pressure transducer was kept open. Therefore, consolidated-undrained ($\overline{CU}$) tests, with pore pressure measurements, were performed by closing the valves to the pore water pump during shearing. Effective stress values were determined by subtracting the pore pressure (as obtained from the pore pressure transducer) from the total stress measurements. Although numerous parameters were obtained during the triaxial testing, the parameters of interest that were measured, during

the various triaxial tests, included the: phase relationship (specimen height, specimen area, specimen volume, water content, void ratio, specific volume), pump volumes, pump pressures, deviator stress, total and effective principal stresses, and axial deformation. Specifically, as described in the next section, the values for the specific volume, vertical effective stress, and mean effective stress were important in comparing the data collected from the triaxial device with the data collected from the BP-CRS-BE device.

Multiple triaxial tests were performed at various over-consolidation ratio levels and following various stress paths (conventional triaxial compression [CTC] and reduced triaxial extension [RTE]). Specifically, the soil specimen were initially reconsolidated past the previous maximum of 137.8 kPa to vertical effective stress values of 310kPa, 413kPa, or 827 kPa. For the normally consolidated specimens, the specimens were tested immediately upon reaching these stress levels. For the over-consolidated specimens, the specimens were initially consolidated to the aforementioned levels but were then over-consolidated, by reducing the axial stress, (while maintaining constant area) until the respective soil specimen was subjected to an over-consolidation ratio value of two, four, or eight. The consolidation/over-consolidation methodology is presented in Table 5.1.

Table 5.1. Triaxial testing consolidation and over-consolidation process.

Maximum Consolidation Stress ($\overline{\sigma}_{max}$)	Pre-Shear Vertical Effective Stress ($\overline{\sigma}_{vc}$)			
	OCR=1	OCR=2	OCR=4	OCR=8
[kPa]	[kPa]	[kPa]	[kPa]	[kPa]
310	310	155	78	39
414	414	207	103	52
828	828	414	207	103

5.6.3. *Equations Utilized for Data Reduction*

Several equations that are available within the literature helped to facilitate the data reduction for the BP-CRS-BE tests. As documented in Hardin and Blandford (1989), the equation for determining shear moduli by using shear wave propagation through particulate materials is presented in Equation 5.1. Specifically, by utilizing the density of the soil (ρ), and the measured shear wave velocity (V_s) from the bender element data, the small-strain shear modulus ($G_{\max,BE}$) was obtained. As previously mentioned, the relationship between the shear strain (γ), the axial strain (ε_1) and the radial strain ($\varepsilon_{2,3}$) was defined by following strain compatibility, using the "Cambridge method" as presented in Equation 5.2 (Sharma and Fahey 2003, Atkinson 2007). The shear strain (γ) was equal to two thirds of ε_1, for the BP-CRS-BE tests, because the values $\varepsilon_{2,3}$ were neglebible due to the stiffness of the constrained ring. Also, as previously mentioned, the large-strain constrained modulus (M_{CRS}) equations were proposed by Smith and Wahls (1969), based on the consolidation theory that was developed by Terzaghi (1943). These equations were also documented within the ASTM D4186 standard, and are presented herein as Equations 5.3 and 5.4.

$$G_{\max,BE} = \rho V_s^2 \qquad \text{(after Jaky [1944])} \qquad \text{Equation 5.1}$$

$$\gamma = \frac{2}{3}(\varepsilon_1 - \varepsilon_3) \qquad \text{(after Casagrande [1943])} \qquad \text{Equation 5.2}$$

$$m_v = \frac{\Delta\varepsilon_a}{\Delta\sigma_v} = r\left(\frac{\Delta t}{\Delta\sigma_v}\right) \qquad \text{(after Wissa et al. [1971], Lo Presti [1993])} \qquad \text{Equation 5.3}$$

$$M_{CRS} = \frac{1}{m_v} \qquad \text{(from Duncan, J. and Bursey [2013])} \qquad \text{Equation 5.4}$$

Within Equation 5.3, $\Delta\varepsilon_a$ is the change in axial strain over a time interval (Δt); $\Delta\sigma_v$ is the change in total stress over Δt; and r is the strain rate.

The equations proposed by Hardin (1978) and Lo Presti et al. (1993), presented as Equations 5.5 and 5.6, respectively, were utilized to find the small strain shear modulus ($G_{\max,CRS,P'}$), using data obtained from the CRS device and knowledge about the mean effective stress (p'). These obtained values ($G_{\max,CRS,P'}$) were compared with the aforementioned $G_{\max,BE}$ that were obtained from the bender element tests.

$$G_{\max,CRS,P'} = \frac{S \cdot OCR^k}{F(e)} P_a^{1-n} (p')^n \qquad \text{(after Hardin [1978])} \qquad \text{Equation 5.5}$$

$$G_{\max} = \frac{S}{F(e)} P_a^{1-n} (\overline{\sigma_v} \cdot \overline{\sigma_h})^{\frac{n}{2}} \qquad \text{(after Lo Presti et al. [1993])} \qquad \text{Equation 5.6}$$

Within Equations 5.5 through 5.6, the previously undefined variables include: S, the stiffness coefficient; n=0.5, the elastic constant; k, the empirical exponent that depends on the plasticity index (PI) of the soil; P_a, the atmospheric pressure; F(e), the function of void ratio (e), typically, $F(e) = 0.3 + e^2$ for Equation 5.5, and $F(e) = e^{1.3}$ for Equation 5.6.

5.6.4. *Procedures for Obtaining Horizontal Stress Values for BP-CRS-BE Device*

The specific volume (*v*) values were calculated by utilizing Equation 5.7. Specifically, values for void ratio (*e*) were determined by following the ASTM D4186 standard (2014); the respective *v* values were then obtained by adding a value of unity to each of the *e* values. Axial deformation, the initial height, and the final water content measurements, on the respective on the whole specimen, were utilized, along with phase relationships, to determine the specific volume measurements.

Because K_0-consolidation was performed on the triaxial specimens, the horizontal stress level on all of the soil specimens, within the BP-CRS-BE device, should have been similar to the horizontal stress level on the soil specimens with the triaxial device when the specimens were at

the same vertical effective stress. Although the various specimens were consolidated to different values of vertical effective stress and then over-consolidated to different values of vertical effective stress, the slope of the respective normalized consolidation lines or the respective normalized over-consolidation lines should have been similar. Due to certain specimens being subjected to additional plastic deformation when loaded to higher stress states, the specific volume value that was used for each normalization process was selected on the consolidation curve (Figure 5.6a) or the over-consolidation curve (Figure 5.6b), to obtain the consolidation behavior or over-consolidation behavior, respectively. The value of 200 kPa was selected because it was greater than the previous consolidation pressure within the slurry consolidometer, but less than the imposed maximum consolidation stress that the specimen would sustain within the BP-CRS-BE. Therefore, the curves at this point were straight lines (virgin compression or swell). The curves were required to be normalized due to slight differences in the initial void ratio of the soil specimens or due to the soil specimens, within the BP-CRS-BE device, being loaded to higher values of vertical effective stress than the soil specimens within triaxial device.

After the curves were normalized, the normalized specific volume data, from the triaxial device, were also plotted as a function of the natural log of the mean effective stress (Figure 5.7). The general patterns of the data were determined by utilizing log-normal trend lines in the arithmetic-natural logarithmic plots. Equations, of the same form (Equations 5.7 through 5.9) as those developed by Roscoe et al. (1958), were developed for these aforementioned trend lines. Specifically, Equation 5.10 was developed for the normally consolidated (loading) trend line (Figure 5.7a) and Equation 5.11 was developed for the over-consolidated (swelling, unloading) trend line (Figure 5.7b). Equations 5.10 and 5.11 were then rearranged to allow for determination of the mean effective stress. Furthermore, this value of mean effective stress was

then equated to the Cambridge definition of mean effective stress for the normally consolidated (loading) trend line (Equation 5.12) and for the over-consolidated (swelling, unloading) trend line (Equation 5.13). The Cambridge definition of mean effective stress was selected because the parameters obtained or derived from this method can be further utilized to establish numerical models (i.e. Cam-Clay model). Therefore, the horizontal state of stress was determined, at various levels of the vertical state of stress within the BP- CRS-BE device, by using Equations 5.4 and 5.15.

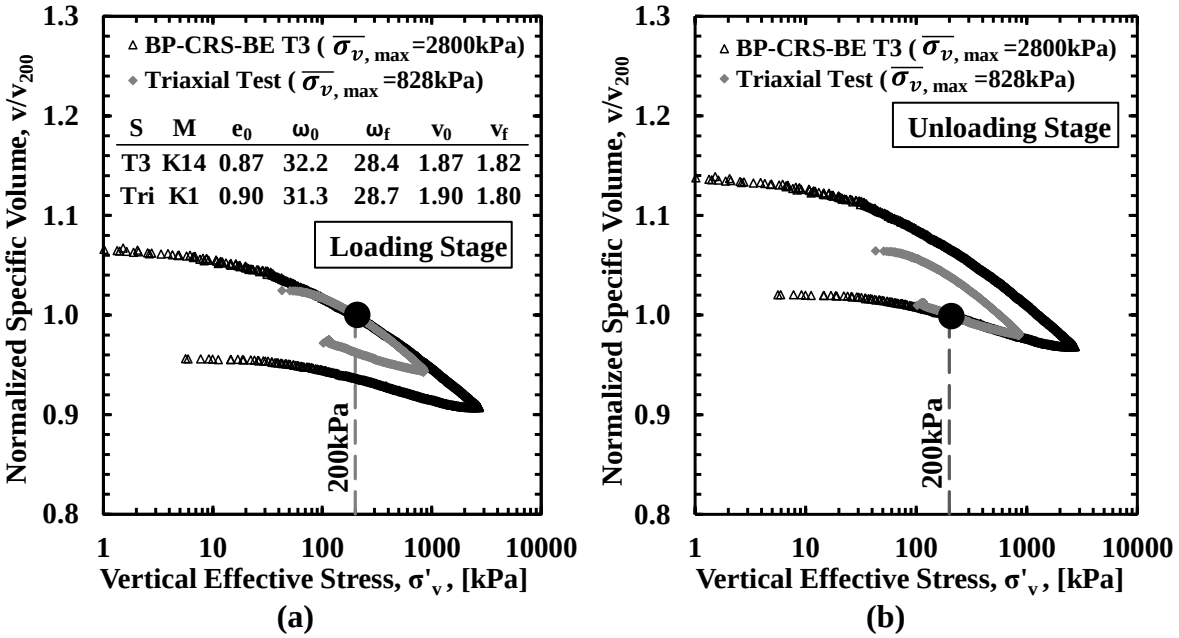

Figure 5.6. **Normalized specific volume, as a function of vertical effective stress, for the 2800kPa, OCR=466, BP-CRS-BE T3 test and the 828kPa, OCR=8, triaxial test for a) consolidation and b) over-consolidation.**

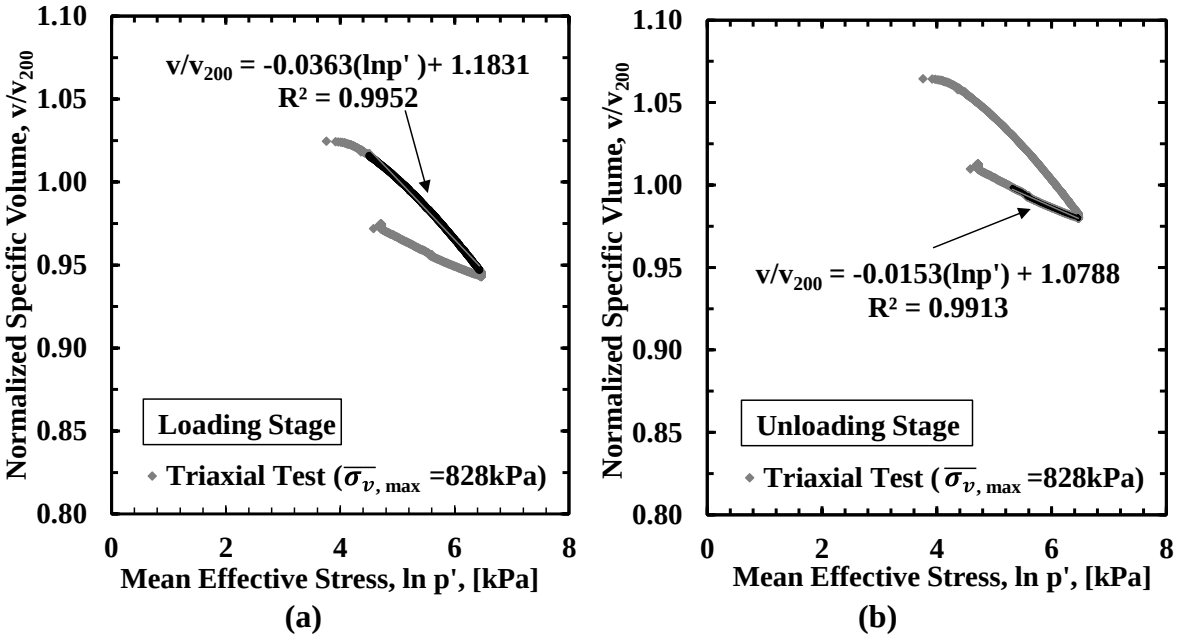

Figure 5.7. Log-normal regression formula of the normalized specific volume as a function of mean effective stress for (a) loading and (b) unloading during the triaxial test.

$$v = 1 + e$$ (after Roscoe et al. [1958]) Equation 5.7

$$v = N - \lambda \cdot \ln(p')$$ (after Roscoe et al. [1958]) Equation 5.8

$$v = v_{\kappa} - \kappa \cdot \ln(p')$$ (after Roscoe et al. [1958]) Equation 5.9

$$\frac{v}{v_{200}} = A - B \cdot \ln(p')$$ (after Roscoe et al. [1958], normalized, loading) Equation 5.10

$$\frac{v}{v_{200}} = C - D \cdot \ln(p')$$ (after Roscoe et al. [1958], normalized, unloading) Equation 5.11

$$e^{\left(\frac{A-\frac{v}{v_{200}}}{B}\right)} = p' = \frac{\overline{\sigma_1} + 2\overline{\sigma_3}}{3}$$ For Loading Only Equation 5.12

$$e^{\left(\frac{C-\frac{v}{v_{200}}}{D}\right)} = p' = \frac{\overline{\sigma_1} + 2\overline{\sigma_3}}{3}$$ For Unloading Only Equation 5.13

$$\overline{\sigma_{h\,(BP-CRS-BE)}} = 3 \cdot e^{\left(\frac{A-\frac{v}{v_{200}}}{B}\right)} - \overline{\sigma_v}$$ For Loading Only Equation 5.14

$$\overline{\sigma_{h\,(BP-CRS-BE)}} = 3 \cdot e^{\left(\frac{C-\frac{v}{v_{200}}}{D}\right)} - \overline{\sigma_v}$$ For Unloading Only Equation 5.15

Within Equations 5. 7 through 5. 15, $\frac{v}{v_{200}}$ is the normalized specific volume (normalized to the specific volume value at a stress of 200 kPa); A and C are similar to N and v_κ and are the values of $\frac{v}{v_{200}}$ at p'=1.0 kPa for the virgin compression and swell trendline, respectively; B is similar to λ and is the gradient for the normal consolidation trendline; D is similar to κ and is the gradient of the swelling trendline; $\overline{\sigma_1}$ is the major principal stress; and $\overline{\sigma_3}$ is the minor principal stress.

5.6.5. *Procedures for Determining Soil Parameters (K_0, OCR, ϕ', v, G_{max}, G, ν)*

After the horizontal effective stress values were calculated, following the procedure that was described in the previous section, values for the coefficient of lateral earth pressure (K_0) were obtained, at various stress and strain levels. These K_0 values were obtained by dividing a respective value of the horizontal effective stress within the BP-CRS-BE by the corresponding value of the vertical effective stress within the BP-CRS-BE.

Due to slight amounts of specimen disturbance that developed while 1) removing the specimen from the slurry consolidometer and 2) placing the specimen into the BP-CRS-BE, the over-consolidation ratio (OCR) values for the specimens were unknown until the previous

maximum past pressure (the pre-consolidation stress within the slurry consolidometer) had been reached within the BP-CRS-BE device. After the previous maximum past pressure had been reached, the OCR value, for a given amount value of vertical effective stress, was equal to the new maximum vertical effective stress value divided by the said vertical effective stress value. Because creep within the soil specimens and the BP-CRS-BE device were found when the OCR values were less than two along the unloading line, only OCR values greater than two (those on the unloading or swell line) were analyzed. Semi-logarithmic $K_0 - OCR$ curves were then developed by utilizing the previous mentioned values that were obtained for K_0 and the OCR values. The general pattern of the data was determined by utilizing an exponential decay trend line within this semi-logarithmic $K_0 - OCR$ plot. An equation, of the same form as the equation that originally developed by Jaky (1944) and Mayne and Kulhawy (1982) and presented in Equation 5.16, was developed for the trend line that was generated for each test. Because the equations were of the same form, the coefficient and the exponent within the equations (*Y* and *Z* in Equation 5.17) were proportional to the drained friction angle (ϕ'). Therefore, various values of ϕ' were obtained by utilizing this methodology (Equations 5.18 and 5.19).

$$K_0 = (1 - \sin\phi')(OCR)^{\sin\phi'} \quad \text{(after Mayne and Kulhawy [1982])} \qquad \text{Equation 5.16}$$

$$K_0 = Y \cdot OCR^Z \qquad \text{Equation 5.17}$$

$$Y = 1 - \sin\phi' \qquad \text{Equation 5.18}$$

$$Z = \sin\phi' \qquad \text{Equation 5.19}$$

Within Equations 5.16 through 5.19, K_0 is the at-rest coefficient of lateral earth pressure, OCR is the over-consolidation ratio, Y is the coefficient, Z is the exponent, and ϕ' is the drained friction angle.

Measured values for the small-strain shear modulus ($G_{max,BE}$) and large-strain shear modulus ($G_{BE,DF}$) were determined from the shear wave velocity measurements that were obtained from the bender elements (utilizing Equation 5.1, as previously presented). The shear wave velocity measurements were acquired following the procedures described in Coffman et al. (2014) and described in Zhao and Coffman (2016). Values for the density of the soil, at various levels of axial strain, were determined from phase diagram relationships. Specifically, the density was determined by dividing the mass of the specimen, at a given time, by the volume of the specimen at the same time. Because the specimen was back-pressure saturated, the values for the volume of the specimen and the mass of the specimen both 1) proportionally decreased during loading (as water was expelled from the specimen) and 2) proportionally increased during unloading (as water was imbibed by the specimen).

A waterfall plot (Figure 5.8) was generated for each of the BP-CRS-BE tests. These plots aided in determining of the amount of time that was required for a given shear wave to travel through the soil. Specifically, the travel time decreased as the specimen was loaded and increased as the specimen was unloaded. As discussed in Salazar and Coffman (2014), Coffman et al. (2014), and Zhao and Coffman (2016), the amount of time that was required for the shear wave to travel through the data acquisition system (tip-to-tip) was subtracted from the amount of time that was required for the shear wave to travel through the soil and acquisition system. In addition to the corrections with regard to the travel time data, the vertical effective stresses were also corrected by subtracting the amount of static friction from the applied load. Specifically, the amount of load 1) between the slide bars and the slide bar housings and 2) between the piston and the piston housing, when movement commenced, was subtracted. To evaluate the

repeatability of the measurements, shear wave velocity measurements were collected during three tests that were performed on kaolinite soils using the BP-CRS-BE device.

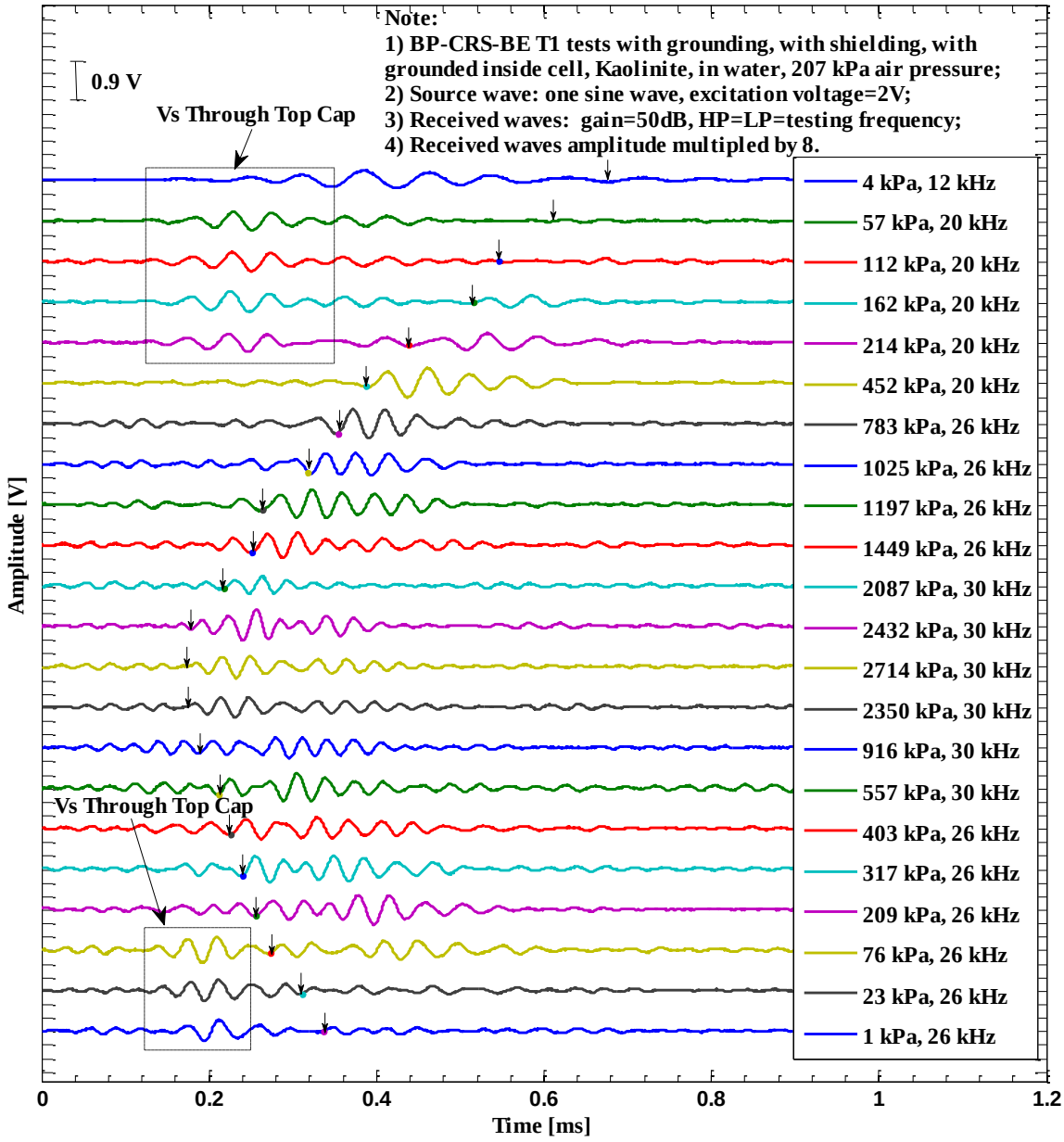

Figure 5.8. Waterfall plot of collected shear wave signals of BP-CRS-BE T1 on kaolinite soil for determination of Vs (HV) during consolidation tests (Oscilloscope collected shear wave signals).

To transfer from small-strain shear modulus ($G_{max,BE}$) to large-strain shear modulus ($G_{BE,DF}$), a modified shear modulus degradation curve (Figure 5.9) was developed by utilizing the results from the aforementioned work that were reported in Darendeli (2001) and Stokoe et al. (2004). Specifically, the curve that was developed by Darendeli (2001) for clayey soils with moderate plasticity (PI=30) was utilized. As shown in Figure 5.9, the large-strain shear modulus was calculated by using an equation (Equation 5.20) that was developed by extrapolating the bottom portion of the curve developed by Darendeli (2001).

$$G_{BE,DF} = G_{max,BE} \cdot (0.0468 \cdot \gamma^{0.754}) \quad \text{(developed from Darendeli [2001])} \quad \text{Equation 5.20}$$

Within Equation 5.20, γ is the shear strain, $G_{max,BE}$ is the small-strain shear modulus obtained from the bender elements), and $G_{BE,DF}$ is the degradation factor applied, bender element obtained, large-strain shear modulus.

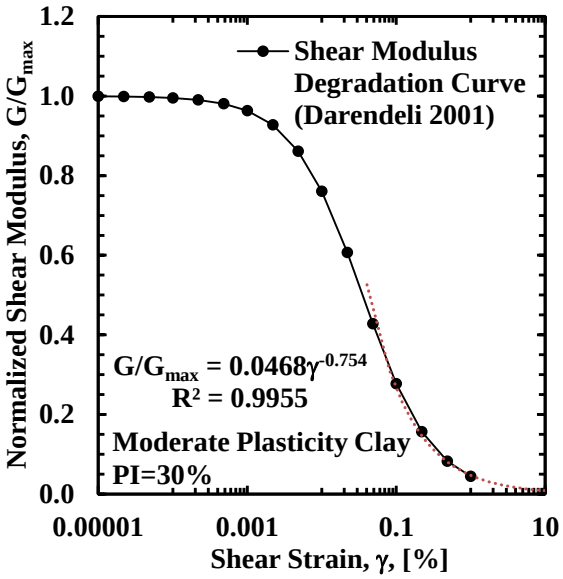

Figure 5.9. **Modified shear modulus degradation curve (after Darendli 2001).**

Drained Poisson's ratio values were determined by utilizing the aforementioned calculated values of constrained modulus and the degradation factor applied, bender element

obtained, large-strain shear modulus values. Specifically, these calculated values were obtained from Equation 5.21. The Young's modulus was then calculated from the constrained modulus and Poisson's ratio by using Equation 5.22.

$$\nu = \frac{M_{CRS} - 2G_{BE,DF}}{2(M_{CRS} - G_{BE,DF})} \qquad \text{Equation 5.21}$$

$$E = \frac{M_{CRS}(1+\nu)(1-2\nu)}{1-\nu} \qquad \text{Equation 5.22}$$

5.7. Results and Discussion

The results obtained by utilizing the aforementioned methods and procedures included the following five items. 1) The measured shear wave velocity-vertical effective stress relationships and shear wave velocity - void ratio relationships. 2) The measured large-strain constrained modulus-axial strain relationships and the measured small-strain shear modulus-axial strain relationship. 3) A comparison between the measured small-strain shear modulus and the predicted small-strain shear modulus. 4) Drained Poisson's ratio - vertical effective stress relationships and drained Poisson's ratio-normalized specific volume relationships, for the loading and unloading stages of the BP-CRS-BE tests on kaolinite soil. 5) A procedure for calculating the coefficient of lateral earth pressure and friction angle values for the kaolinite soil using the BP-CRS-BE device.

5.7.1. *Shear Wave Velocity*

The shear wave velocity-vertical effective stress relationship is shown in Figure 5.10a. When compared with the results that were reported in Kang et al. (2014), the shear wave velocity values that were obtained from the three tests, using BP-CRS-BE device, were greater than the shear wave velocity values that were obtained by Kang et al. (2014). Likewise, for comparison, the shear wave velocity - specific volume data from the three tests completed within the BP-

CRS-BE device and the Kang et al. (2014) data are presented in Figure 5.10b. Although the data did not appear to correlate, or to be reproducible within the shear wave velocity - vertical effective space, the data did correlate and were reproducible within the shear wave velocity - specific volume space. Therefore, the reason that the data did not correlate within the shear wave velocity - vertical effective stress was because the specimens possessed different amounts of voids (different specific volumes) while at the same level of vertical effective stress. Moreover, as previously reported in Coffman et al. (2014), higher levels of stress were achieved within the BP-CRS-BE device than within the device that was developed by Kang et al. (2014). In summary, the variability within the three tests conducted using BP-CRS-BE device was attributed to a number of factors. These factors included: 1) slight variations in the material properties of the laboratory prepared specimens, 2) improper seating of the loading piston to the loading cap as associated with piston friction and slide bar friction, and 3) possible improper grounding within the testing system due to corrosion of the grounding wire.

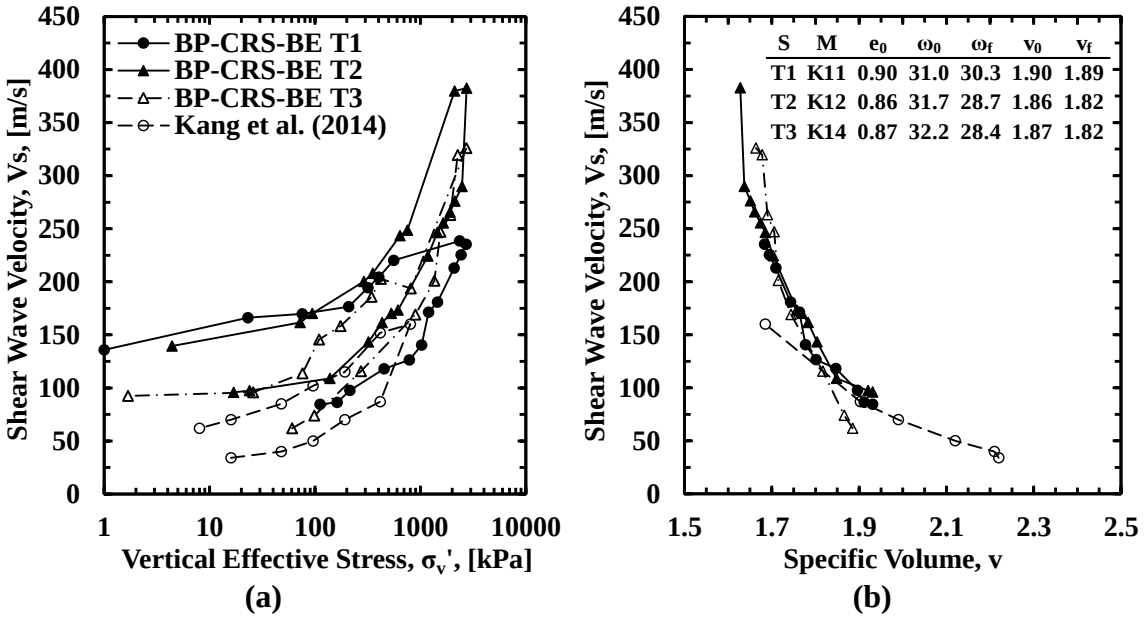

Figure 5.10. Shear wave velocity results obtained from the BP-CRS-BE device for (a) shear wave velocity - vertical effective stress relationship, and (b) shear wave velocity - void ratio relationship.

5.7.2. *Constrained Modulus and BE Measured Shear Modulus*

The constrained modulus - axial strain relationship and shear modulus - axial strain relationship, which were developed from the three tests that were performed using BP-CRS-BE device on kaolinite soil, are presented in Figures 5.11a and 5.11b, respectively. Based on the testing results, the testing procedure is repeatable in terms of constrained modulus–specific volume (Figure 5.11c) and shear modulus-specific volume (Figure 5.11d). However, variation does exist within the shear modulus-axial strain relationship. The reason why the results of shear modulus were less repeatable than constrained modulus was attributed to a number of factors. These factors included: 1) the small - strain shear wave measurements were more sensitive to the amount of strain within the soil specimen than large-strain consolidation data measurements, 2) variations in the structure of the laboratory prepared soil specimens as caused by variability of material properties or variability in stress history, and 3) possible improper grounding within the testing system due to corrosion of the grounding wire. Like with the shear wave velocity - specific volume plot (Figure 5.10b), the variability was shown to be associated with the differences in the amounts of voids (different specific volumes) while at the same level of vertical effective stress (vertical strain in this case).

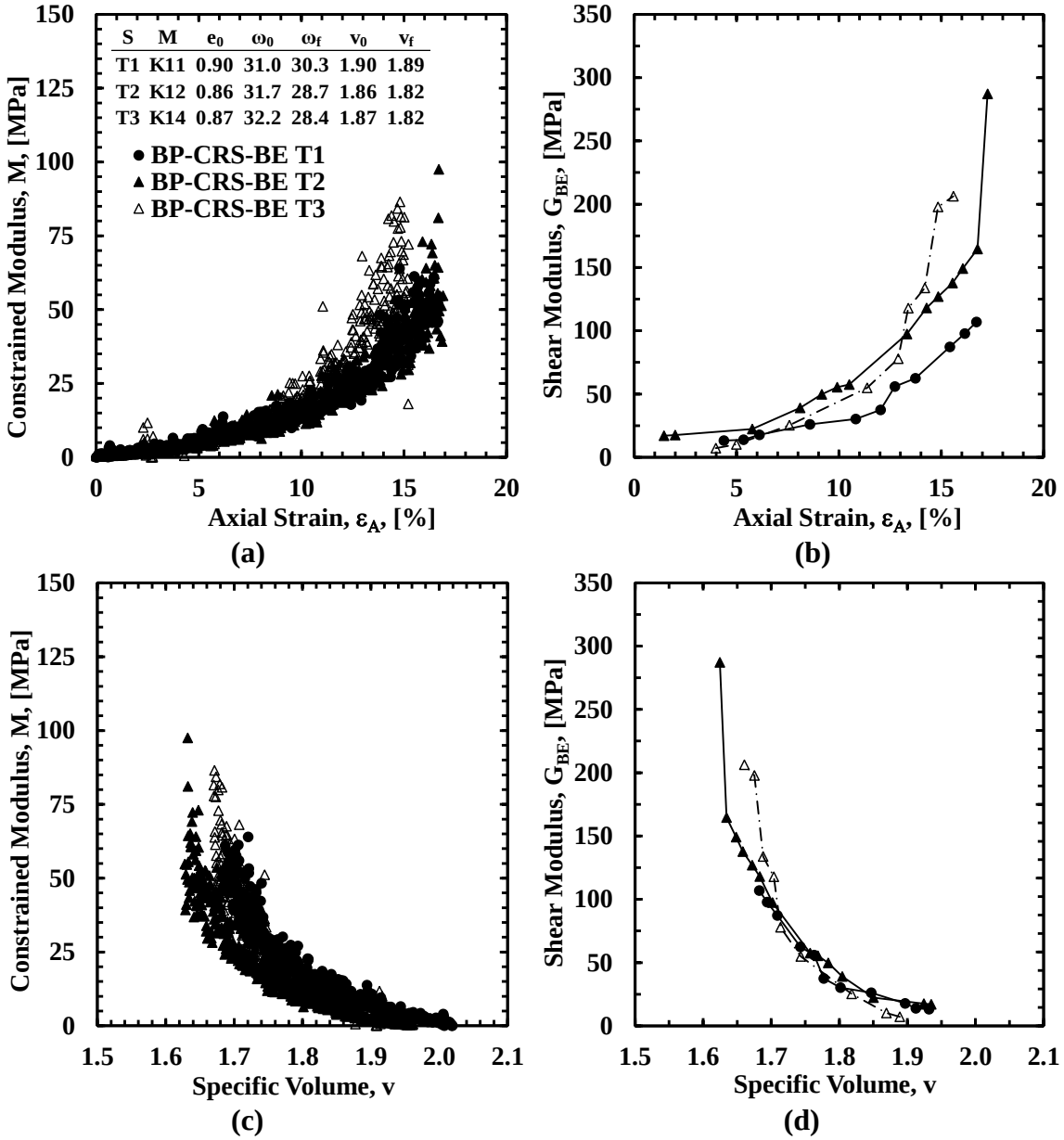

Figure 5.11. Soil modulus results obtained from the BP-CRS-BE device for (a) constrained modulus - axial strain relationship, (b) bender element measured shear modulus - axial strain relationship, (c) constrained modulus – specific volume relationship, and (d) bender element measured shear modulus – specific volume relationship.

5.7.3. *Shear Modulus from Empirical Equations*

The small-strain shear modulus - over-consolidation ratio relationships as obtained from BP-CRS-BE tests T1 through T3 are shown in Figure 5.12. The predicted shear modulus ($G_{max,CRS,p'}$) values that were calculated using the empirical Lo Presti equation were shown to be

in agreement with the shear modulus ($G_{max,BE}$) values that were obtained from the bender element measurements (Lo Presti et al. 1993). However, the variations in the small-strain shear moduli values, as obtained from empirical equations and from the bender element measurements, were attributed to two factors. 1) Different soil materials (cohesive clay by Hardin [1978] and Italian natural clay by Lo Presti et al. [1993]) were tested to develop the empirical equations rather than the kaolinite soil that was utilized in the BP-CRS-BE tests. 2) Different excitation shear waves (vertically propagating horizontally polarized [VH] and horizontally propagating horizontally polarized [HH] shear wave by Lo Presti et al. [1993], while horizontally propagating vertically polarized [HV] shear wave in the BP-CRS-BE tests) were utilized to obtain the shear modulus. Although variability does exists within the shear modulus values that were obtained from bender element measurements and the shear modulus values that were obtained from the empirical equations, the BP-CRS-BE measured shear modulus is recommended. Specifically, as discussed in Zhao and Coffman (2016), the BP-CRS-BE device is recommended because of the advantages associated with the use of the BP-CRS-BE device as compared with other devices (traditional oedometer, triaxial, cyclic triaxial, cyclic simple shear, resonant column torsional shear).

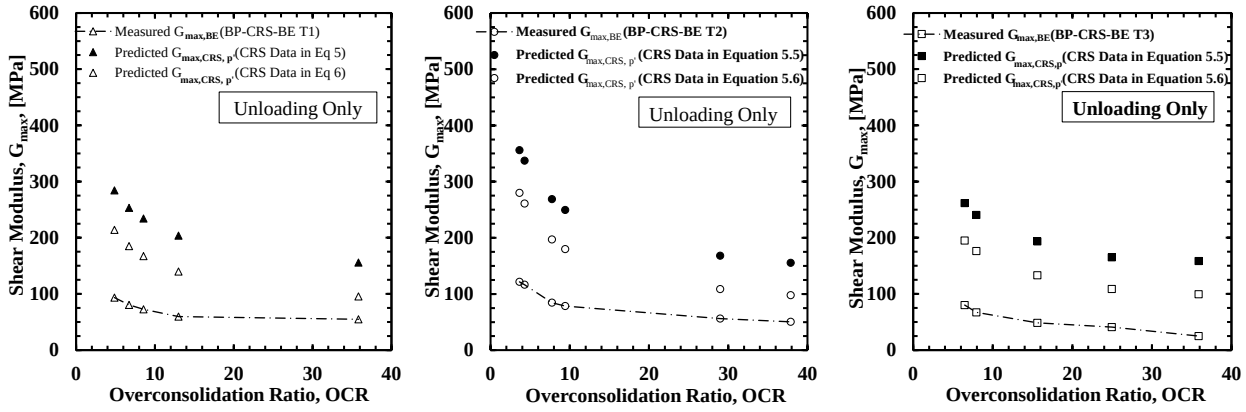

Figure 5.12. Measured and predicted small-strain shear modulus as a function of over-consolidation ratio for (a) BP-CRS-BE T1, (b) BP-CRS-BE T2, and (c) BP-CRS-BE T3.

5.7.4. *Comparison of Measured and Predicted Shear Modulus*

To better illustrate and verify the shear modulus values, the values that were obtained from the bender element measurements in the BP-CRS-BE device were compared with the values that were obtained from the empirical equations (Figure 5.13). For example (Figure 13a), it was determined that the $G_{\max .CRS,p'}$ and the $G_{\max,BE}$ values that were obtained from the loading stage for Test 3 were in agreement (1:1.2 and 1:1.3 for Lo Presti equation and Hardin equation, respectively). For the unloading data (Figure 5.13b), the values of $G_{\max .CRS,p'}$ from Lo Presti et al. (1993) were also in agreement (1:1) with the $G_{\max,BE}$ values. However, the values of $G_{\max .CRS,p'}$ from Hardin (1978) had some amount of variation (1:1.2) with an offset of 120 MPa. These results were surprising because the over-consolidation ratio was taken into account within the Hardin (1978) method but was not taken into account within the Lo Presti (1993) method. Although it was surprising, the Lo Presti (1993) method is recommended for verification purpose for future measured bender element data because it was shown to best match the measured shear modulus values. Moreover, based on these results, the predicted shear modulus values that were determined from the Lo Presti method may be utilized to approximate the Poisson's ratio for CRS data that were collected in a device that did not include bender elements.

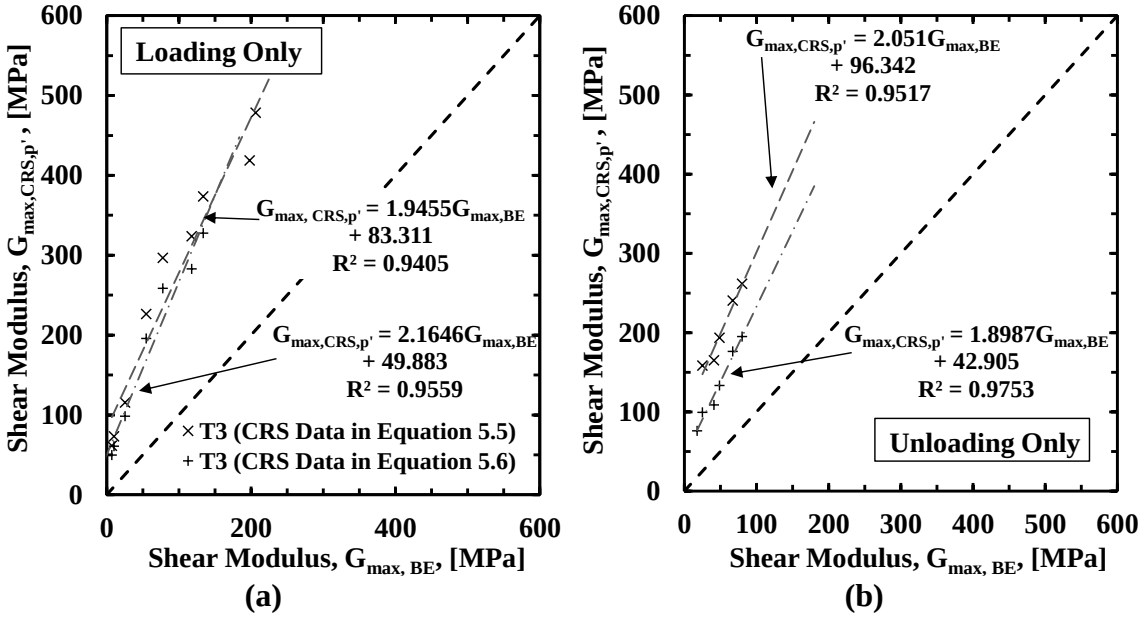

Figure 5.13. Soil modulus results obtained from the Test 3, as performed within the BP-CRS-BE device, for (a) constrained modulus-axial strain relationships for the loading stage, and (b) bender element measured shear modulus-axial strain relationships for the unloading stage.

5.7.5. *Drained Poisson's Ratio*

It was found that the values of drained Poisson's ratio increased with increasing values of vertical effective stress for both the loading and unloading stages for all the three tests (Figures 5.14a and 5.14b). The drained Poisson's ratio values for saturated soft clays (Poisson's ratio values from 0.4 to 0.5) that were recommended by Newcomb and Birgisson (1999) were validated by the BP-CRS-BE obtained values of drained Poisson's ratio. Unlike the typical value of 0.5 for the fully saturated, undrained, Poisson's ratio, the Poisson's ratio values for the saturated clay in a drained condition were less than 0.5. This reduction in the Poisson's ratio values was associated with a dissipation of pore pressure under drained conditions.

The drained Poisson's ratio - normalized specific volume relationships, for the loading and unloading stages of the three BP-CRS-BE tests, are presented in Figures 5.14c and 5.14d. A decrease in the drained Poisson's ratio value was observed with an increase in the specific

volume values. There was more variability in the Poisson's ratio values in the loading stage than these was in the unloading stage. The reason why the results obtained from the unloading stage had less variation than the results obtained from loading stage, for both drained Poisson's ratio - vertical effective stress relationships and the drained Poisson's ratio - normalized void ratio relationships, was attributed to a number of factors. These factors included: 1) higher degrees of saturation for the kaolinite soil during the unloading stage than the loading stage, and 2) less void space within the kaolinite soil specimens during the unloading stage than during the loading stage. These factors were confirmed by the shear wave velocity results that were previously presented in Figure 5.9a. Specifically, higher shear wave velocity values were obtained for the kaolinite soil during the unloading stage than during the loading stage, at the same stress level.

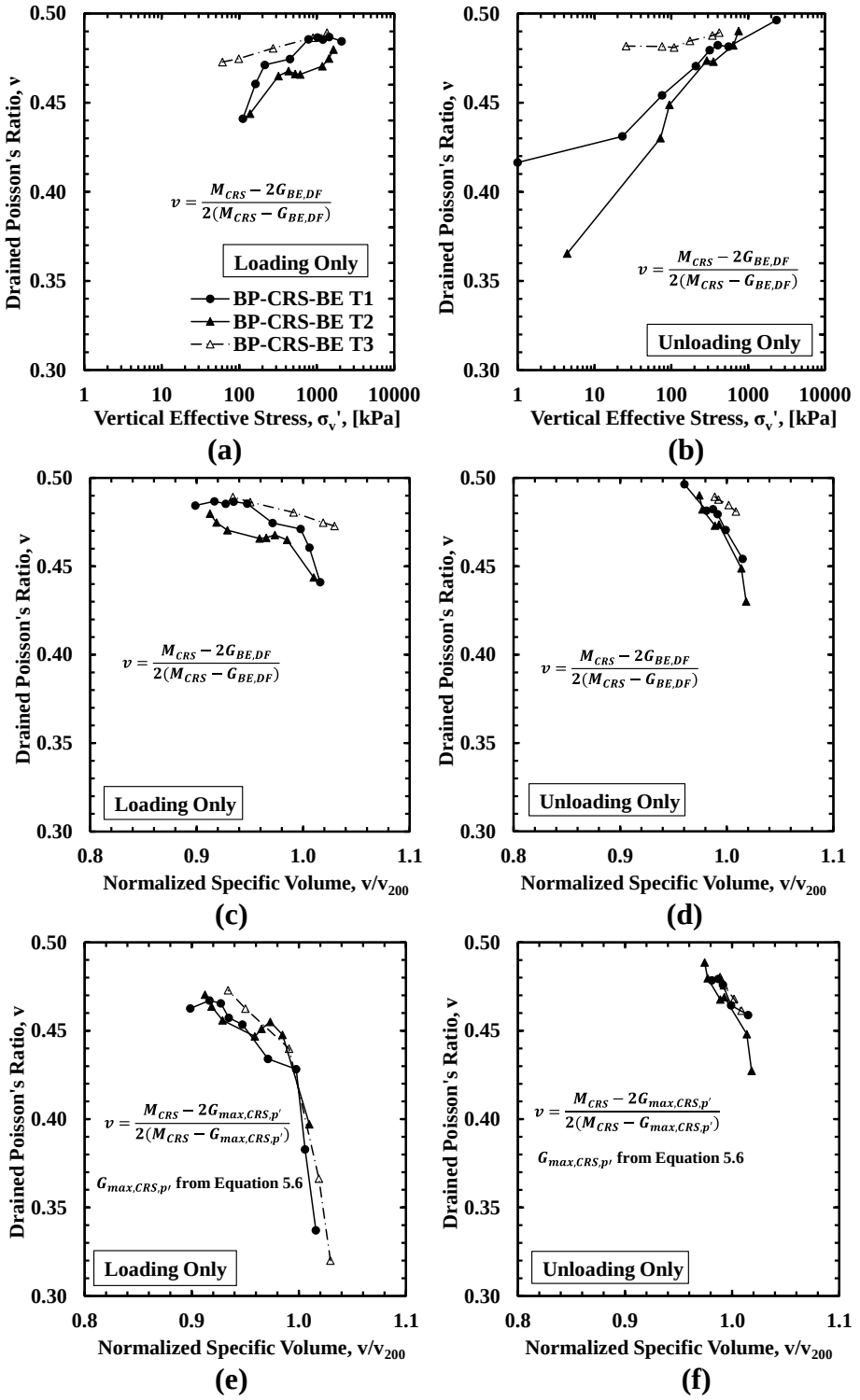

Figure 5.14. BP-CRS-BE testing results of Poisson's ratio-vertical effective stress relationship for (a) loading stage, (b) unloading stage; measured Poisson's ratio-normalized specific volume relationship for (c) loading stage and (d) unloading stage; and predicted Poisson's ratio-normalized specific volume relationship for (e) loading stage and (f) unloading stage.

5.7.6. *Coefficient of Lateral Earth Pressure and Friction Angle*

The coefficient of lateral earth pressure – over-consolidation ratio relationships, for the three BP-CRS-BE tests and the triaxial test, are shown in Figure 5.15. As presented in Table 2, it was determined that the drained friction angle (ϕ') values of the soil, as calculated using Equations 5.17 through 5.19, were similar. Specifically, the ϕ' values that were obtained from the BP-CRS-BE by using Equation 5.18 ($\phi' = 16.0^o$ to 24.7^o) were in agreement with the drained friction angle that was measured in the triaxial device ($\phi' = 13.8^o$ to 20.7^o), as discussed in the next section. The reason why the friction angle values that were calculated using the exponential part of the formula were smaller than the actual friction angle of soil was due to the use of large range of OCR values ($2 < OCR < 40$), rather than a small range of OCR values ($OCR < 8$) found in previous studies (Mayne and Kulhawy 1982, Landon and DeGroot 2006). The friction angle values that were obtained from the BP-CRS-BE tests were calculated based on the data that covered a larger range of OCR than the triaxial test data and thus provided a better approach to examine the K_0 - OCR relationships for soils. Furthermore, Equation 5.18 is recommended in the examination of the unloading of soils with large OCR values.

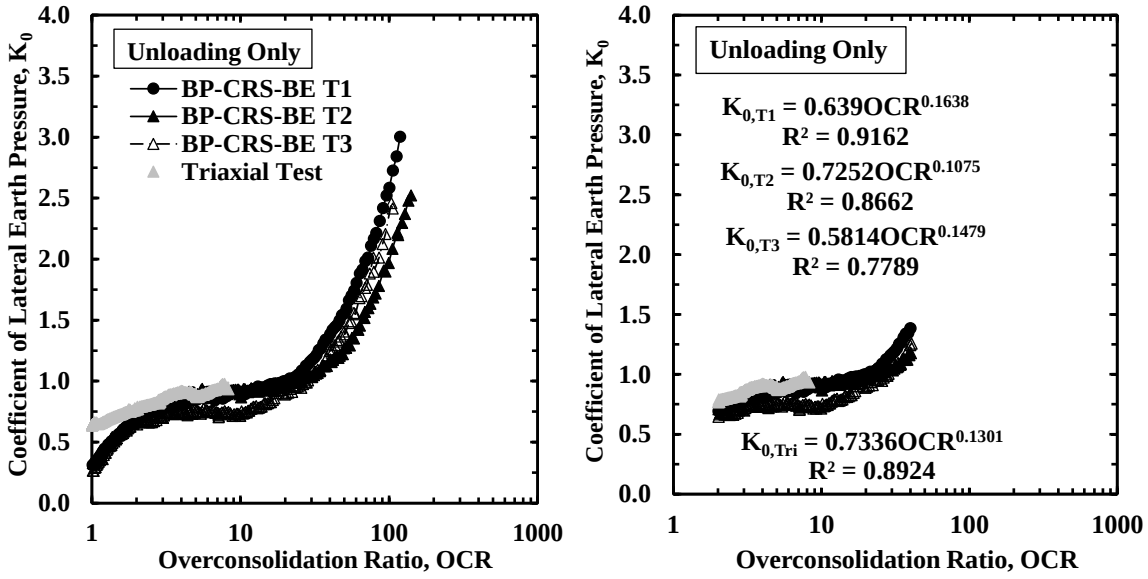

Figure 5.15. Coefficient of lateral earth pressure as a function of over-consolidation ratio for (a) all the data, and (b) selected data with *OCR* values between 2 and 40.

Table 5.2. Calculated drained friction angle for the BP-CRS-BE tests with *OCR* between 2 and 40.

Method	Test	Y, Z	ϕ'
Equation 5.18 (Y=1-sinϕ')	Triaxial RTE	Y= 0.7736	15.5
	BP-CRS-BE T1	Y= 0.6390	21.2
	BP-CRS-BE T2	Y= 0.7252	16.0
	BP-CRS-BE T3	Y= 0.5814	24.7
Equation 5.19 (Z=sinϕ')	Triaxial RTE	Z= 0.1301	7.5
	BP-CRS-BE T1	Z= 0.1638	9.4
	BP-CRS-BE T2	Z= 0.1075	6.2
	BP-CRS-BE T3	Z= 0.1479	8.5

5.7.7. *Comparisons between Triaxial and BP-CRS-BE Friction Angles*

The friction angle values for triaxial tests were obtained from the shearing stage for multiple tests. Specifically, the Cambridge representation of the deviatoric stress – mean effective stress relationships, for the triaxial tests, as shown in Figure 5.16, were utilized to determine the friction angle. Four sets of overconsolidation ratio (*OCR*) values were utilized, and three CTC and three RTE tests were performed for each *OCR* value. For each of the CTC

and RTE tests, the K_0 value was determined, as shown in the Figure 5.16. For each *OCR* test, one friction angle value was determined by using the trend line equation that plotted through the maximum deviatoric stress from the three tests.

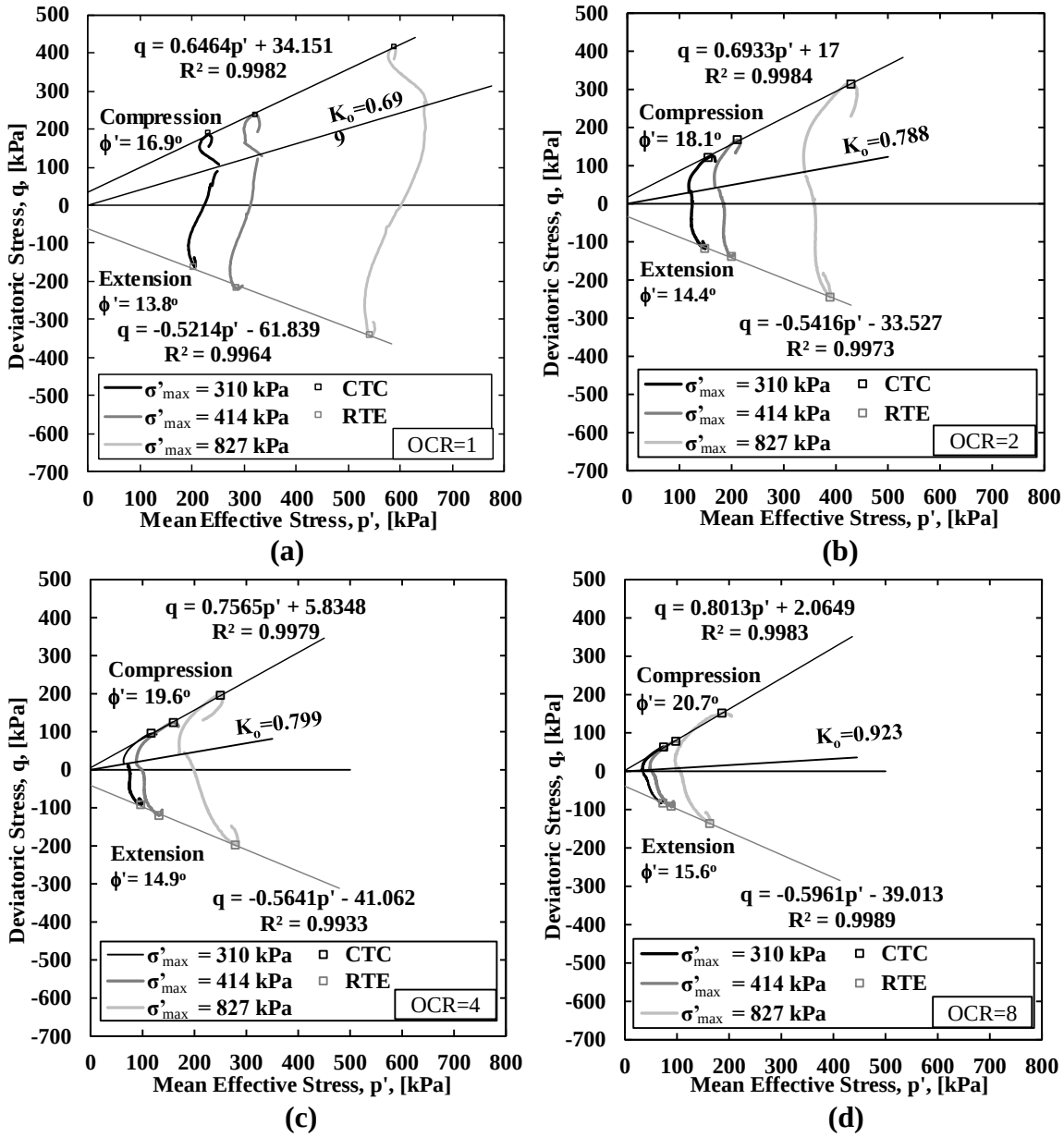

Figure 5.16. Cambridge representation of data from triaxial compression and extensions tests at (a) *OCR* =1 , (b) *OCR* =2, (c) *OCR* =4, and (d) *OCR* =8.

As shown in Figure 5.17, the measured friction angle values that were determined from the triaxial tests, were compared with the friction angle values that were determined by using the

BP-CRS-BE data within the aforementioned Equations 5.18 and 5.19. As previously mentioned, it was found that the measured friction angle values (ϕ') from the triaxial tests and the friction angle values (ϕ') from the BP-CRS-BE tests were in agreement. However, variations did exist within the values and the variations were associated with the stress path that was utilized to determine the friction angle. Because the BP-CRS-BE obtained friction angle value estimate was within the stress path dependent triaxial data, the predicted friction angle values, as determined by using Equation 5.18 ($Y = 1 - \sin\phi'$), as shown within Figure 5.17a, may be utilized to estimate the friction angle value obtained from the triaxial test.

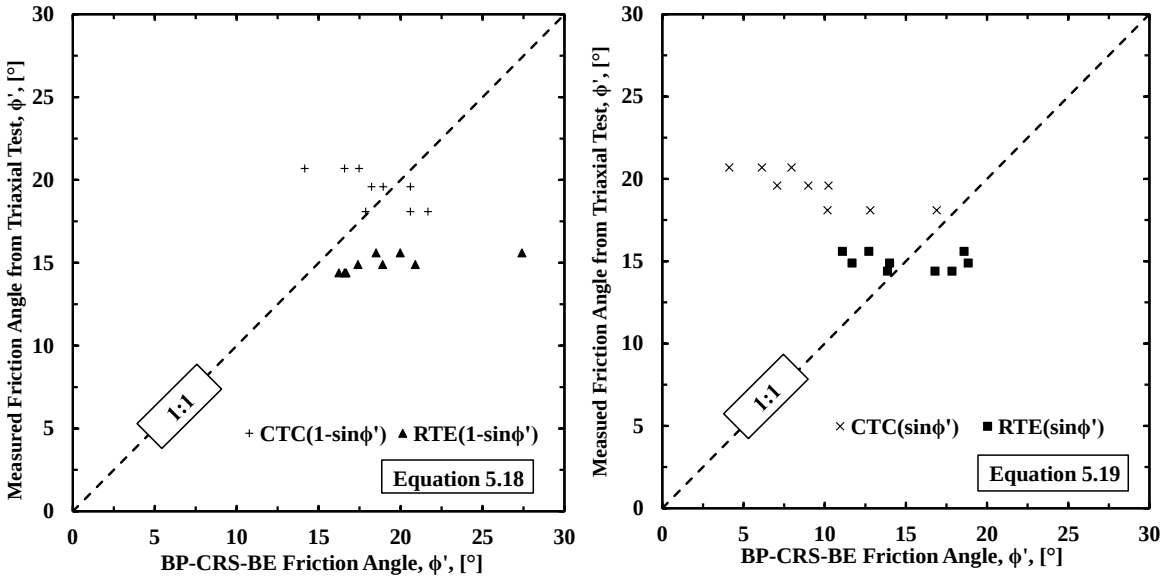

(a) (b)

Figure 5.17. Comparison of the friction angle from triaxial tests and the predicted friction angle by using (a) Equation 5.18, and (b) Equation 5.19.

5.7.8. *Comparisons between Triaxial and BP-CRS-BE Constrained and Young's Modulus*

The Young's modulus, as a function of overconsolidation ratio, for the BP-CRS-BE tests and the triaxial tests, are shown in Figure 5.18. For BP-CRS-BE tests, the Young's modulus values were calculated from the constrained modulus and Poisson's ratio by using Equation 5.22, as previously presented. The Young's modulus values for triaxial tests were obtained from the

stress-strain curve during the shearing stage. Specifically, the initial slope of the stress-strain curve was calculated by using the $d\sigma / d\varepsilon$ ratio, and this value was considered as Young's modulus. Generally, the Young's modulus values from the three BP-CRS-BE tests and the triaxial tests were in agreement.

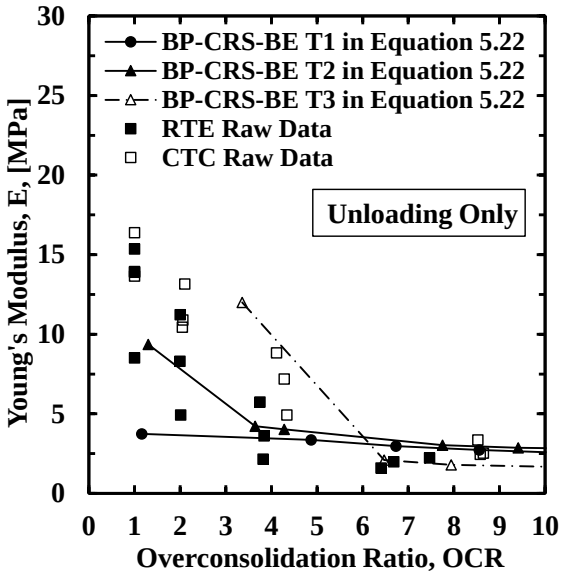

Figure 5.18. Young's modulus as a function of overconsolidation ratio.

5.8. Conclusions

Large-strain constrained modulus and small-strain shear modulus values were obtained from tests on kaolinite soil by using the back-pressure constant rate of strain consolidation bender elements (BP-CRS-BE) device. The procedures of obtaining horizontal stress for a BP-CRS-BE test, based on the results of a triaxial test and from a BP-CRS-BE test, were proposed. Values for the drained Poisson's ratio, the coefficient of lateral earth pressure, and the friction angle were obtained from the BP-CRS-BE tests on the kaolinite soil. Based on the findings, the use of the BP-CRS-BE device and the proposed techniques, was confirmed and verified. Thus the development of constitutive model parameters from the BP-CRS-BE testing applications is promising. The conclusions from this research are as follows:

1. The small strain shear modulus increased with the increasing of the vertical effective stress and decreased with the increasing of overconsolidation ratio.
2. The shear modulus may be predicted by only using soil properties such as: overconsolidation ratio, void ratio, horizontal and vertical effective stress and the atmosphere pressure. The predicted shear modulus values that were calculated by utilizing the Lo Presti method (1993) matched the measured shear modulus values that were obtained by using the bender element measurements.
3. The drained Poisson's ratio values increased with increasing amounts of vertical effective stress but decreased with increasing amounts of the void ratio. The drained Poisson's ratio values agreed with the values that were documented in the literature.
4. The coefficient of lateral earth pressure increased with the increase amounts of overconsolidation ratio. Using this relationship, drained friction angle values were determined by using the $K_0 - OCR$ relationship for the soil tested using the BP-CRS-BE device.
5. The drained friction angle values (ϕ') that were calculated for the soil tested within the BP-CRS-BE device were similar to the friction angle values that were obtained from the triaxial tests.

5.9. References

American Society for Testing and Materials, "Standard Test Method for One-Dimensional Consolidation Properties of Saturated Cohesive Soils Using Controlled-Strain Loading," *Annual Book of ASTM Standards, Designation D 4186*, ASTM, West Conshohocken, PA, 2014.

Arulnathan, R., Boulanger, R. W., and Riemer, M. F., "Analysis of Bender Element Tests," *Geotech. Test. J.*, Vol. 21, No. 2, 1998, pp. 120-131.

Atkinson John, "The Mechanics of Soils and Foundations." London: Taylor & Francis, 2007.

Brignoli, E.G.M., M. Gotti, and Stokoe, K.H., "Measurement of Shear Waves in Laboratory Specimens By Means of Piezoelectric Transducers", *Geotech. Test. J.*, Vol. 19, No. 4, 1996, pp. 384-397.

Brocanelli, D. and Rinaldi, V., "Measurement of Lowstrain Material Damping and Wave Velocity with Bender Elements in the Frequency Domain," *Can. Geotech. J.*, Vol. 35, No. 6, 1998, pp. 1032-1040.

Casagrande, A., "The Determination of Pre-Consolidation Load and Its Practical Significance," *Proc. Soil Mech. Found. Eng.*, Vol. 3, 1936, pp. 60-64.

Coffman, R.A., Salazar, S.E., Zhao, Y., "Discussion of Measurement of Stiffness Anisotropy in Kaolinite Using Bender Element Tests in Floating Wall Consolidometer by X. Kang, G-C Kang, and B. Bate." *Geotech. Test. J.*, Vol. 37, No. 6, 2014, pp. 1-4.

Darendeli, M.B., "Development of a New Family of Normalized Modulus Reduction and Material Damping Curves." *Doctoral Dissertation*, University of Texas, Austin, TX, 2001.

Drnevich, V.P., Hardin, B.O., and Shippy, D.J., "Modulus and Damping of Soils by the Resonant Column Method." *In Dynamic geotechnical testing*. Special Technical Publication 654, American Society for Testing and Materials (ASTM), West Conshohocken, Penn.1978, pp. 91–121.

Drnevich, V.P., "Recent Developments in Resonant Column Testing." *Richart Commemorative Lectures*, Proceedings, ASCE Specialty Session, Detroit, 1985, pp.79-107.

Duncan, J. and Bursey, A., "Soil Modulus Correlations." *Foundation Engineering in the Face of Uncertainty*. 2013, pp. 321-336.

Dyvik, R. and Madshus, C., "Lab Measurements of G_{max} Using Bender Elements," *Proceedings of Advances in the Art of Testing Soil Under Cyclic Conditions*, V. Khosla, Ed., ASCE, Reston, VA, 1985, pp. 186-196.

Dyvik, R. and Olsen, T. S., "G_{max} Measured in Oedometer and DSS Tests Using Bender Elements," *Proceedings, Twelfth International Conference on Soil Mechanics and Foundation Engineering, Rio de Janeiro*, Vol. 1, 1989, pp. 39-42.

El Mohtar, Chadi S., Drnevich, Vincent P., Santagata, Marika, and Bobet, Antonio, "Combined Resonant Column and Cyclic Triaxial Tests for Measuring Undrained Shear Modulus Reduction of Sand With Plastic Fines," *Geotechnical Testing Journal*, Vol. 36, No. 4, 2013, pp. 1-9.

Fioravante, V. and Capoferri, R., "On the Use of Multidirectional Piezoelectric Transducers in Triaxial Testing," *Geotech. Test. J.*, Vol. 24, No. 3, 2001, pp. 243-255.

Georgiannou, V. N., Hight, D. W., and Burland, J. B., "Behaviour of Clayey Sands under Undrained Cyclic Triaxial Loading," *Geotechnique*, Vol. 41, 1991, pp. 383-393.

Ghayoomi, M., "Seismically Induced Settlement of Partially-Saturated Sand," *Ph.D. Dissertation*, University of Colorado, Boulder, Boulder, CO, 2011.

Hardin, B.O. and Black, W.L., "Vibration Modulus of Normally Consolidated Clay." *ASCE Journal of the Soil Mechanics and Foundation Division*, Vol. 94, No. 2, 1968, pp.353-369.

Hardin, B.O., and Drnervich, V. P., "Shear Modulus and Damping in Soils: Design Equations and Curves." *J. Soil Mech. And Found. Div*., ASCE, Vol. 98, No. 7, 1972a, pp.667-692.

Hardin, B. O., and Drnervich, V. P., "Shear Modulus and Damping in Soils: Measurement and Parameter Effects." *J. Soil Mech. And Found*. Div., ASCE, Vol. 98, No. 6,1972b, pp. 603-624.

Hardin, B.O., "The Nature of Stress Stain Behavior of Soils." *Earthquake Engineering and Soil Dynamics*. ASCE, Vol.1, 1978, pp. 3–90.

Hardin, B.O. and Blandford, G.E., "Elasticity of Particulate Material." *Journal of Geotechnical Engineering*, Vol. 115, No. 6, 1989, pp. 788-805.

Isenhower W. M. and Stokoe K. H., "Strain-Rate Dependent Shear Modulus of San Francisco Bay Mud." *International Conferences on Recent Advances in Geotechnical Earthquake Engineering and Soil Dynamics*. Paper 15, 1979.

Iwasaki, T., Tatsuoka, F., and Takagi, Y., "Shear Moduli of Sands Under Cyclic Torsional Shear Loading." *Soils and Foundations*, Vol. 18, No. 1, 1978, pp. 39–56.

Jaky, J., "The Coefficient of Earth Pressure at Rest," *J. Soc. Hung. Architects Engineers*, Vol. 7, 1944, pp. 355-358.

Jovicic, V., Coop, M. R., and Simic, M., "Objective Criteria for Determining G_{max} from Bender Element Test," *Geotechnique*, Vol. 46, No. 2, 1996, pp. 357–362.

Kang, X., Kang, G.-C., and Bate, B., "Measurement of Stiffness Anisotropy of Kaolinite Using Bender Element Tests in a Floating Wall Consolidometer". *Geotech. Test. J.*, ASTM. Vol. 37, No. 5, 2014, pp. 1-16.

Kawaguchi, T., Mitachi, T., and Shibuya, S., "Evaluation of Shear Wave Travel Time in Laboratory Bender Element Test," *Proceedings of the 15th International Conference on Soil Mechanics and Geotechanics Engineering*, CRC Press, Boca Raton, FL, 2001, pp. 155-158.

Kokusho, T., "Cyclic Triaxial Test on Dynamic Soil Properties For Wide Strain Range." *Soils Found.*, Vol. 20, No.2, 1980, pp.45–60.

Landon, M. M., and DeGroot, D. J., "Measurement of Small-strain Shear Modulus Anisotropy on Unconfined Clay Samples Using Bender Elements," *Proceedings of GeoCongress 2006*, ASCE, 2006.

Landon, M. M., "Development of A Non-destructive Sample Quality Assessment Method of Soft Clays," *Ph.D. Dissertation*, University of Massachusetts, Amherst, MA, 2007.

Lee, J.-S., and Santamarina, J. C., "Bender Elements: Performance and Signal Interpretation," *Journal of Geotechnical and Geoenvironmental Engineering*, Vol. 131, No. 9, 2005, pp. 1063–1070.

Lo Presti D.C.F., Jamiolkowski M., Lancellotta R. and Vercelli L., "Maximum shear modulus measurement using bender elements in oedometer tests", *Rivista Italiana de Geotechnica*, Vol.(XXVII), No. 1, 1993, pp. 5-9.

Mayne, P. W. and Kulhawy, F. H., "Ko-OCR Relationships in Soil," *Journal of the Geotechnical Engineering Division*, Vol. 108, No. GT6, 1982, pp. 851-872.

Menzies, B.K., "A Computer Controlled Hydraulic Triaxial Testing System." *Advanced Triaxial Testing of Soil and Rock*, ASTM STP 977, Robert T. Donaghe, Ronald C. Chaney, and Marshall L. Silver, Eds., American Society for Testing Materials, Philadelphia, 1988, pp. 82-94.

Mohsin, A. K. M. and Airey, D. W., "Automating G_{max} Measurement in Triaxial Tests," *Proceedings of the 3rd International Symposium on the Deformation Characteristics of Geomaterials*, Lyon, France, Sept. 22–24, 2003, pp. 73-80.

Montoya, B.M., Gerhard, R., DeJong, J.T., Weil, M.H., Martinez, B.C., and Pederson, L., "Fabrication, Operation, and Health Monitoring of Bender Elements in Aggressive Environments," *Geotech. Test. J.*, Vol.35, No. 5, 2011, pp. 1-15.

Newcomb, D. E., and Birgisson B., "Measuring in Situ Mechanical Properties of Pavement Subgrade Soils." *Transportation Research Record*, Washington, DC: National Academy Press, 1999.

Pennington, D. S., Nash, D. F. T., and Lings, L. L., "Anisotropy of G_0 Shear Stiffness in Gault Clay," *Geotechnique*, Vol. 47, No. 3, 1997, pp. 391-398.

Pennington, D.S., Nash, D.F.T., and Lings, M.L., "Horizontally Mounted Bender Elements for Measuring Anisotropic Shear Moduli in Triaxial Clay Specimens." *Geotech. Test. J.*, Vol. 24, No. 2, 2001, pp. 133-144.

Race, M.L., Coffman, R.A., "Effects of Piston Uplift, Piston Friction, and Machine Deflection in Reduced Triaxial Extension Testing." ASCE Geotechnical Special Publication No. 211, Proc. GeoFrontiers 2011: Advances in Geotechnical Engineering, Dallas, Texas, March, 2011, pp. 2649-2658.

Roscoe, K. H., Schofield, A., and Wroth, C. P., "On the Yielding of Soils." *Geotechnique*, Vol. 8, No. 1, 1958, pp.22-53.

Salazar, S.E., Coffman, R.A., "Design and Fabrication of End Platens for Acquisition of Small-Strain Piezoelectric Measurements During Large-Strain Triaxial Extension and Triaxial Compression Testing." *Geotech. Test. J.*, Vol. 37, No. 6, 2014, pp. 1-12.

Salem, M. A., "Stiffness of Unsaturated Compacted Clays at Small Strains," *Ph.D. Dissertation*, Univeristy of Texas at Austin, Austin, TX, 2006.

Sasanakul, I., "Development Of An Electromagnetic And Mechanical Model For A Resonant Column And Torsional Testing Device For Soils." Ph.D. Dissertation, The Utah State University, Logan, Utah. 2005.

Sharma, S. and Fahey, M., "Degradation of Stiffness of Cemented Calcareous Soil in Cyclic Triaxial Tests." *J. Geotech. Geoenviron. Eng.*, Vol. 129, No. 7, 2003, pp. 619-629.

Shibuya, S., Hwang, S. C., and Mitachi, T., "Elastic Shear Modulus of Soft Clays From Shear Wave Velocity Measurement." *Geotechnique*, Vol. 47, No. 3, 1998, pp. 593-601.

Shirley, D. J. and Hampton, L. D., "Shear-Wave Measurement in Laboratory Sediments," *J. Acoust. Soc. Am.*, Vol. 63, No. 2, 1978, pp. 607–613.

Smith, R., and Wahls, H., "Consolidation under Constant Rates of Strain," *Journal of the Soil Mechanics and Foundations Division*, Vol. 95, No. SM2, 1969, pp. 519-539.

Stokoe, K.H., II, Joh, S.H. and Woods, R.D., "Some Contributions of In Situ Geophysical Measurements to Solving Geotechnical Engineering Problems." *2nd International Conference on Site Characterization (ISC-2)*, Porto, Portugal, September, 2004.

Strassburger, E., "Use of Piezoelectric Transducers for Stiffness and Density Measurements of Soils," *M.S. Report*, University of Texas at Austin, Austin, TX, 1982.

Terzaghi, K., "Theoretical Soil Mechanics." New York: J. Wiley and Sons, Inc, 1943.

Trautwein, S., "FW: True Path," Personal Communication, July 3, 2014.

Valle-Molina, C., "Measurements of V_p and V_s in Dry, Unsaturated, and Saturated Sand Specimens with Piezoelectric Transducers," *Ph.D. Dissertation*, University of Texas at Austin, Austin, TX, 2006.

Valle-Molina, C. and Stokoe, K. H., II, "Seismic Measurements in Sand Specimens with Varying Degrees of Saturation Using Piezoelectric Transducers," *Canadian Geotechnical Journal,* Vol. 49, No. 6, 2012, pp. 671–685.

Viana da Fonseca, A., Ferreira, C., and Fahey, M., "A Framework Interpreting Bender Element Tests, Combining Time-Domain and Frequency-Domain Methods," *Geotechnical Testing Journal*, Vol. 32, No. 2, 2009, pp. 91-107.

Viggiani, G. and Atkinson, J. H., "Interpretation of Bender Element Tests," *Geotechnique*, Vol. 45, No. 1, 1995, pp. 149-154.

Wissa, A., Christain, J., Davis, H., and Heiberg, S., "Consolidation at Constant Rate of Strain," *Journal of the Soil Mechanics and Foundations Division*, Vol. 97, No. SM10, 1971, pp. 1391-1413.

Youn, J. U., Choo, Y. W., & Kim, D. S., "Measurement of Small-Strain Shear Modulus G_{max} of Dry and Saturated Sands By Bender Element, Resonant Column, and Torsional Shear Tests." *Canadian Geotechnical Journal*, Vol. 45, No. 10, 2008, pp.1426-1438.

Zekkos, D., Bray, J. D., & Riemer, M. F., "Shear Modulus and Material Damping of Municipal Solid Waste Based on Large-Scale Cyclic Triaxial Testing." *Canadian Geotechnical Journal*, Vol. 45, No.1, 2008, pp. 45-58.

Zhao, Y., Coffman, R.A., "Back-Pressure Saturated Constant-Rate-of-Strain Consolidation Device with Bender Elements: Verification of System Compliance." *Journal of Testing and Evaluation*, Vol. 44, No. 6, 2016, pp. 1–12.

CHAPTER 6: Soil Fabric and Anisotropy as Observed Using BP-CRS-BE

6.1. Chapter Overview

To investigate and quantify the amount of soil anisotropy, two types of shear wave measurements were performed within the BP-CRS-BE consolidation device. Two sets of bender elements were fabricated to facilitate the horizontally propagated horizontally polarized (HH) and horizontally propagated vertically polarized (HV) shear wave measurements in the BP-CRS-BE device. The HH shear wave measurements were performed on one soil sample and the HV shear wave measurements were performed on an identical but different soil sample. Two different types of soil samples were utilized in the BP-CRS-BE tests. These soil types consisted of laboratory prepared Kaolinite soil slurry samples and Illite soil slurry samples. The behavior variation of soil properties due to water content was also examined, and the laboratory preparation method for the various soil samples, in terms of water content, was believed to induce variation in the soil fabric. Furthermore, the soil anisotropy observed during consolidation, by using bender elements, was investigated in terms of shear wave velocity and shear modulus. Moreover, the effects of soil type on the soil anisotropy were investigated.

The paper enclosed in this chapter has been submitted for publications within the *Clay and Clay Minerals Journal*. The full reference is: Zhao, Y., Mahmood, N., and Coffman, R. A., "Soil Fabric and Anisotropy as Observed Using Bender Elements during Consolidation," *Clay and Clay Minerals*, Under Review, Manuscript Number: CCM-1143, 2016.

6.2. Additional Results not Included in the Aforementioned Manuscript

The additional results obtained from the BP-CRS-BE HH and HV shear wave measurements, performed on Kaolinite soil and Illite soil samples, which were not covered in the submitted paper are presented herein. The results include: 1) a comparison of the amount of travel time observed in BP-CRS-BE tests (Figure 6.1 to 6.3), and 2) a comparison of the

Kaolinite and Illite soil in terms of: (a) void ratio as a function of vertical effective stress as obtained from CRS tests, (b) axial strain as a function of vertical effective stress as obtained from CRS tests, (c) void ratio as a function of vertical effective stress as obtained from triaxial tests, and (d) axial strain as a function of vertical effective stress as obtained from triaxial tests (Figure 6.4).

6.2.1. *Comparison of Travel Time Observed in BP-CRS-BE Tests*

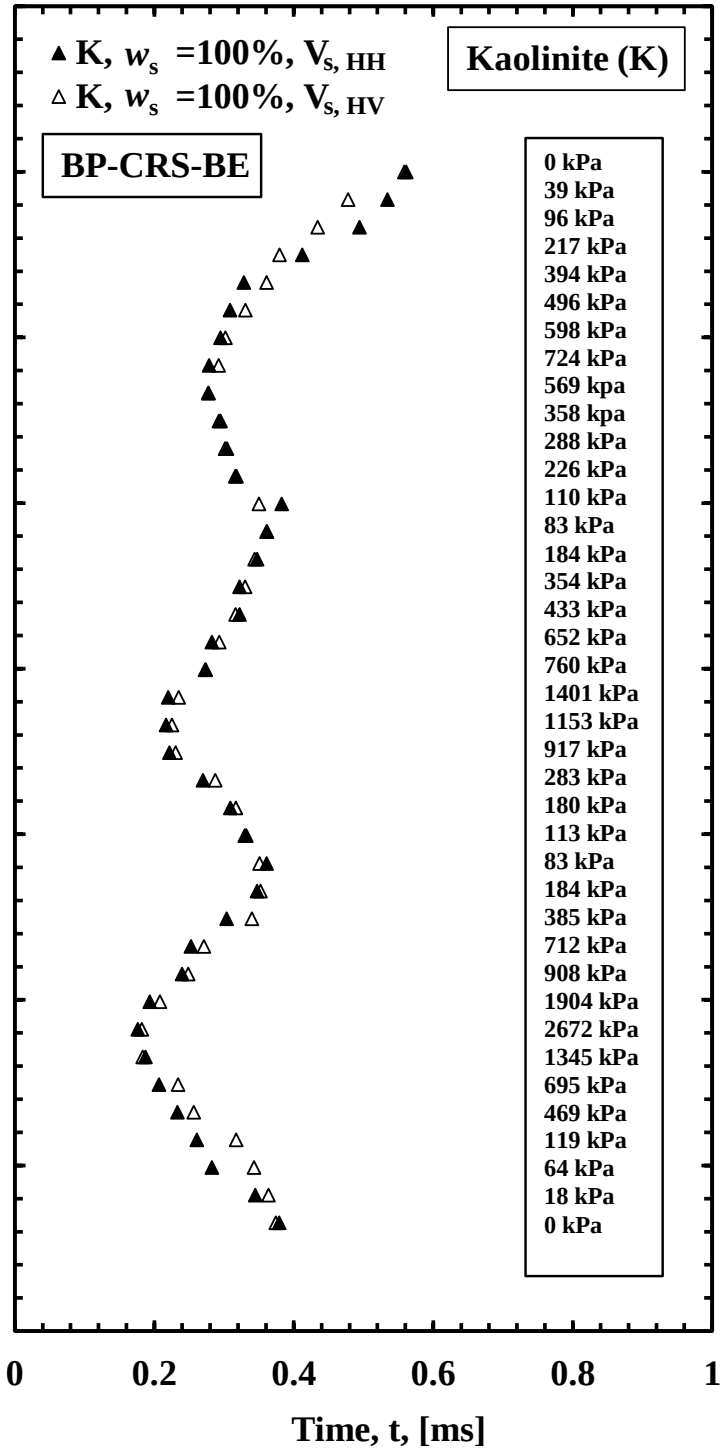

Figure 6.1. Comparison of the travel time (HH and HV) observed in BP-CRS-BE tests on Kaolinite soil prepared at an initial slurry water content of 100%.

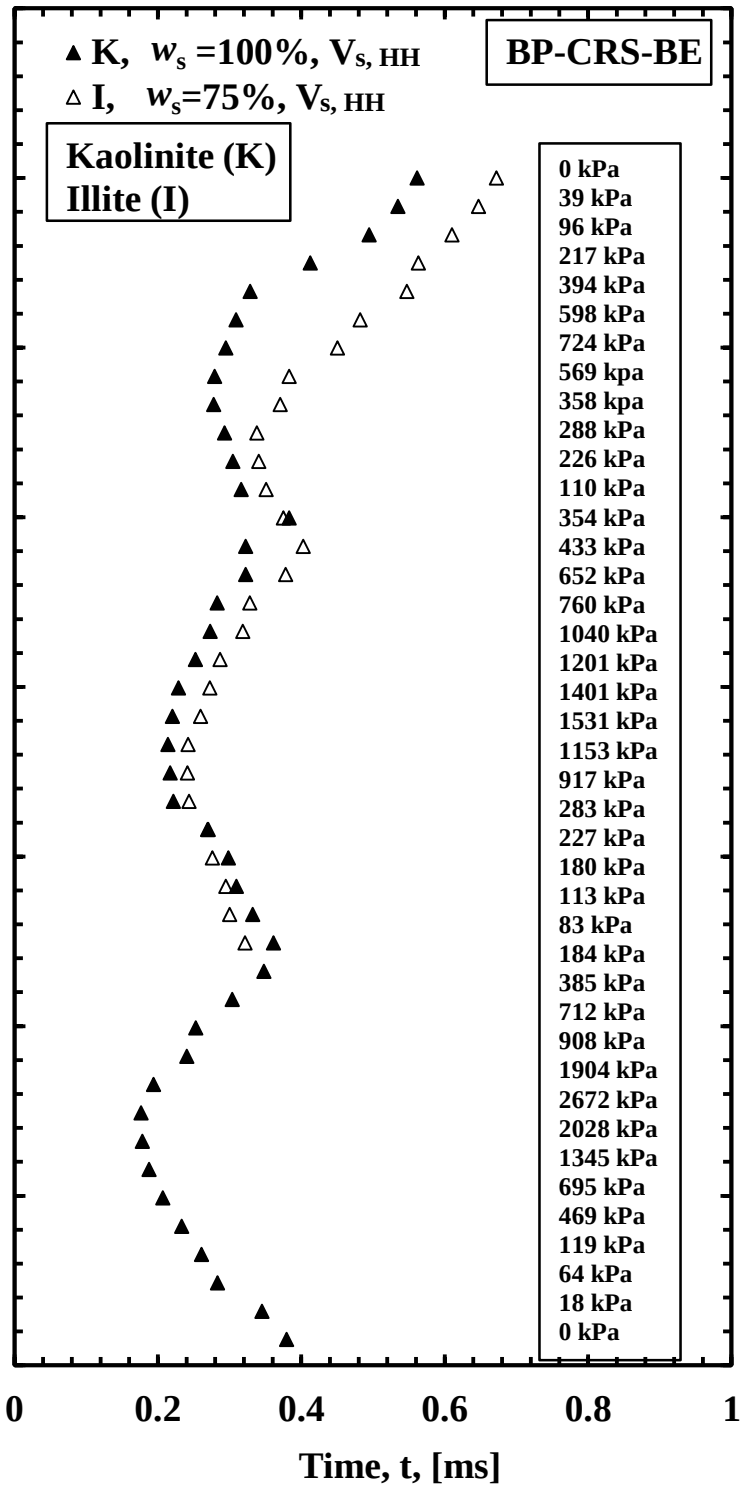

Figure 6.2. Comparison of the travel time (HH) observed in BP-CRS-BE tests on Kaolinite and Illite soil prepared at an initial slurry water content of 100% and 75%, respectively.

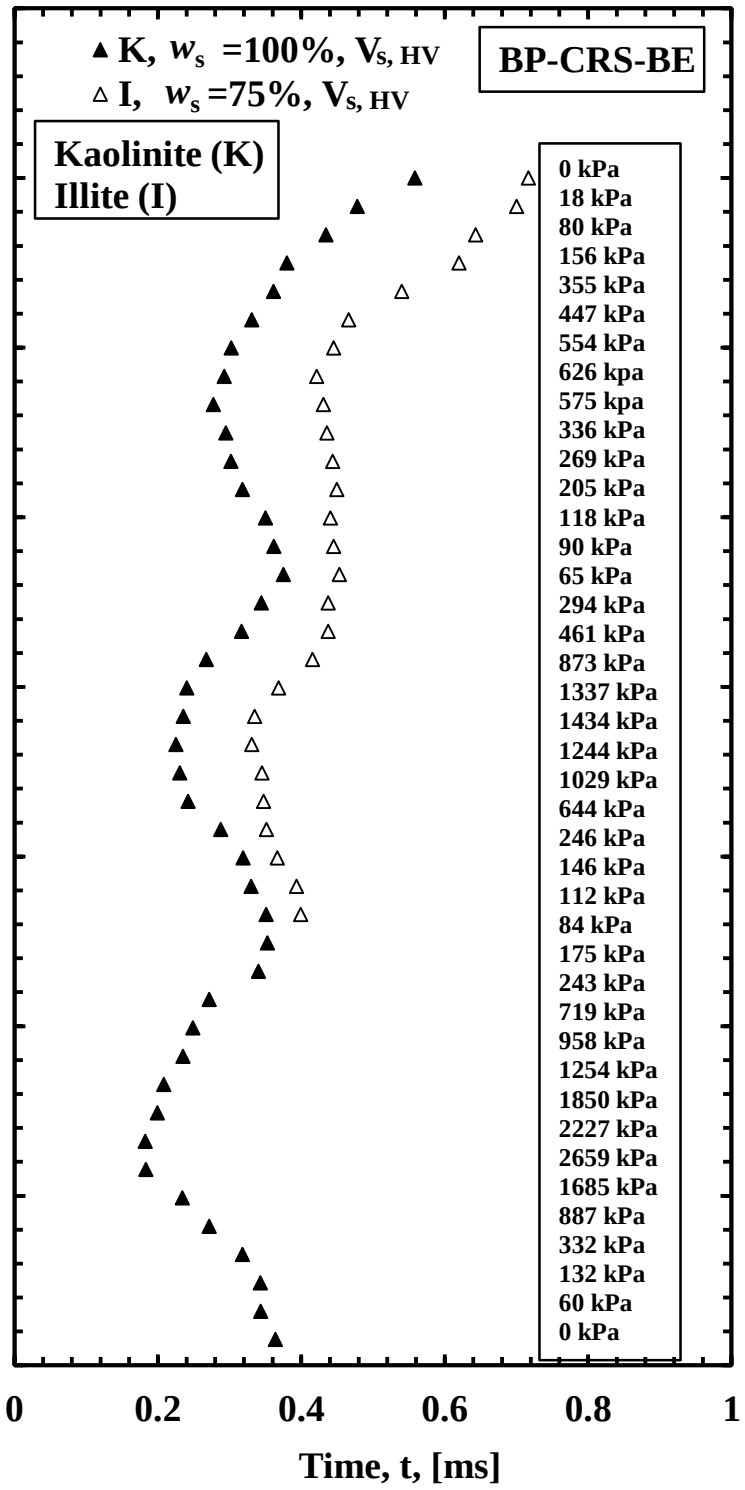

Figure 6.3. Comparison of the travel time (HV) observed in BP-CRS-BE tests on Kaolinite and Illite soil prepared at an initial slurry water content of 100% and 75%, respectively.

6.2.2. *Comparison of Kaolinite and Illite Soils during BP-CRS-BE and Tiaxial Tests*

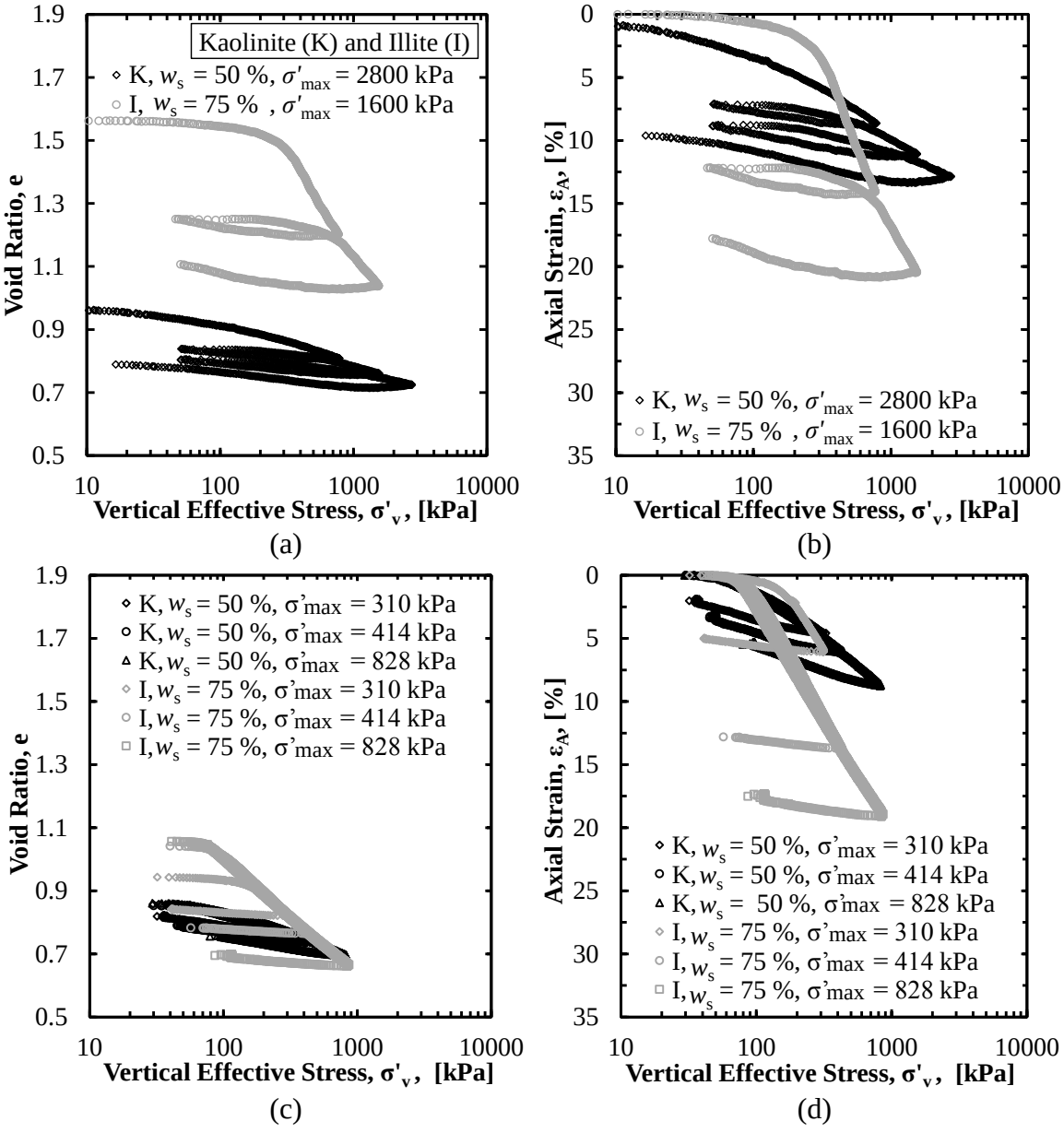

Figure 6.4. Comparison of the Kaolinite and Illite soil in terms of: (a) void ratio as a function of vertical effective stress as obtained from CRS tests, (b) axial strain as a function of vertical effective stress as obtained from CRS tests, (c) void ratio as a function of vertical effective stress as obtained from triaxial tests, and (d) axial strain as a function of vertical effective stress as obtained from triaxial tests.

Soil Fabric and Anisotropy as Observed Using Bender Elements during Consolidation

Yi Zhao[1], Nabeel Mahmood[2], Richard A. Coffman[3]

6.3. Abstract

By utilizing the back-pressure saturated, constant rate-of-strain, consolidation device, with bender elements (BP-CRS-BE), and by placing the bender elements, in the horizontal and vertical directions, the soil fabric and anisotropy of Kaolinite and Illite soil types were investigated. Specifically, two sets of bender elements were utilized to measure the shear wave velocity of soil samples. The two sets of bender elements enabled collection of two types of shear wave measurements, 1) horizontally propagated - vertically polarized shear waves (HV shear waves), and 2) horizontally propagated - horizontally polarized shear waves (HH shear waves).

For both the Kaolinite and Illite soil types, the measured HH shear wave velocity ($V_{s,HH}$) was higher than the measured HV shear wave velocity ($V_{s,HV}$) at corresponding applied stress levels. During the BP-CRS-BE tests, on the Kaolinite soil type, the fabric anisotropy (in terms of shear wave velocity) began when the vertical effective stress was larger than 400kPa; for the Illite soil type, the fabric anisotropy began at effective stress larger than 600kPa. The strain induced anisotropy dominated the soil behavior for both soil types; the rearrangement of soil particles within the soil structure resulted in plastic deformation. This phenomena was more pronounced for soil samples that were initially mixed at higher values of initial water content prior to pre-consolidation.

Keywords: soil anisotropy, strain induced fabric, bender elements, constant rate-of-strain consolidation, shear wave velocity, shear modulus

6.4. Introduction

The back-pressure saturated, constant rate-of-strain, consolidation device, with bender elements (BP-CRS-BE), that was described in Coffman et al. (2014) and Zhao and Coffman (2016), was utilized to investigate the effects of soil fabric and the amount of anisotropy for two soil types (Kaolinite and Illite). Specifically, a set of horizontally oriented bender elements and a set of vertically oriented bender elements were designed and installed into soil samples from the horizontal direction by using the BP-CRS-BE device. Therefore, HV and HH shear waves were measured, respectively. Multiple loading and unloading cycles were utilized to investigate the effects of loading history on the soil fabric and on the soil anisotropy.

The methods utilized to: 1) prepare soil samples, 2) collect the BP-CRS-BE data, and 3) determine and to compare the parameters from this BP-CRS-BE data, are described herein. The collected and evaluated parameters included: vertical displacement (δ_v), vertical effective stress ($\sigma_v^{'}$), deviatoric stress (q), mean effective stress (p'), void ratio (e), axial strain (ε_A), coefficient of volume compressibility (m_v), coefficient of consolidation (c_v), shear wave velocity (V_s), shear modulus (G), constrained modulus (M), and Young's modulus (E). From these parameters, comparisons between the Kaolinite soil samples, initially prepared with a water content of 50-percent or 100-percent, were performed to determine if different soil fabric was established under different slurry consolidation regimes. Likewise, as discussed herein, the parameters obtained from the Kaolinite soil samples were also compared with the parameters obtained from the Illite soil samples, that were prepared with an initial water content of 75-percent, to determine if the amount of anisotropy was different for different soil types. For comparison purposes, all of the aforementioned soil samples were pre-consolidated to 138 kPa, within the slurry consolidometer, prior to being placed into the BP-CRS-BE device.

6.5. Background

For geotechnical design, the assumption that the soil material is homogeneous and under isotropic conditions has been widely used (Terzaghi 1943, Terzaghi et al. 1996, Kaiser and Hewitt 1982). However, several case histories related to the failure of foundations, slopes, and levees led geotechnical engineers to question (Bauer 1984, Petroski, H. 1994, Stark and Eid 1998, Abdoun, T. and Dobry, R., 2002, Briaud et al. 2001, Briaud 2008, Tanaka et al. 2009). In particular, stress redistribution following changes in the internal or external conditions of a soil deposit, within or adjacent to given soil layers, may lead to failures (Lee and Rowe 1989, Sawangsuriya et al. 2007). In other words, the amount of soil anisotropy and the initial soil fabric have been shown to dominate the soil behavior and thus affect the geotechnical design (Meade, R. H., 1964, Gray and Al-Refeai 1986, Vucetic and Dobry 1991, Wheeler and Sivakumar 1995, Santamarina et al. 2001, Mitchell and Soga 2005). As discussed in Seed and Idriss (1970), Holzer (1981), Simpson et al. (1996), Gross and Kisslinger (1997), Belaedinelli et al. (1999), Ghayoomi (2011), the cause of soil anisotropy may be attributed to fluctuations in the ground water table level, excavation, tunneling, surcharge, or dynamic loading (earthquake impact or blast). Geotechnical design may not be effective without a full understanding of the amount of soil anisotropy, and without consideration of the effects of soil anisotropy on soil behavior.

Previous researchers have found two types of soil anisotropy that dominate and affect soil behavior. These two types include 1) stress induced anisotropy and 2) inherent, fabric, or structural anisotropy (Jovicic and Coop 1998, Yamashita et al. 2005, Kang et al. 2014). It has been found that the amount of stress induced anisotropy has played a very small role on the soil behavior under the axi-symmetric loading conditions (Jovicic and Coop 1998). In contrast, the inherent anisotropy has been found to significantly affect soil behavior and has been considered

to be one of the factors that has led to plastic strain within the tested soil (Jovicic and Coop 1998, Kang et al., 2014). In addition, the amount of inherent anisotropy has been caused by different factors (depositional fabric and strain induced fabric), and has depended upon the type of soil. For sand, the amount of inherent anisotropy was mainly attributed to the soil depositional fabric. However, for clay, the inherent anisotropy was mainly attributed to changes in the amount of strain as the result of large deformation (Jovicic and Coop 1998, Kuwano et al. 1999).

Historically, bender elements have been extensively utilized within the soil mechanics laboratory or for field studies to investigate the amount of soil anisotropy. Bender elements have been utilized due to the advantages of 1) non-destructive testing, 2) capability of shear wave velocity measurements, and 3) convenience of controlling the direction of shear wave propagation and polarization (Shirley and Hampton 1978, Dyvik and Olsen 1989, Lo Presti et al. 1993, Brignoli et al. 1996, Pennington et al. 1997, Shibuya et al. 1998, Zeng and Ni 1999, Pennington et al. 2001, Lee and Santamarina 2005, Yamashita et al. 2005, Landon and DeGroot 2006, Landon 2007, Montoya et al. 2011, Coffman et al. 2014, Kang et al. 2014, Salazar and Coffman 2014, Zhao and Coffman 2016, Zhao et al. 2016). Three types of bender element obtained shear wave measurements have been obtained by the previous researchers. These include: vertically propagated-horizontally polarized (VH) shear waves, horizontally propagated-vertically polarized (HV) shear waves, and horizontally propagated-horizontally polarized (HH) shear waves (Roesler 1979, Jovicic et al. 1996, Pennington et al. 1997, Jovicic and Coop 1998, Nash et al. 1999, Lings et al. 2000, Pennington et al. 2001, Yimsiri and Soga 2002, Yamashita et al. 2005, Piriyakul 2006, Kang et al. 2014). Therefore, the amount of soil anisotropy has been quantified by using the measured shear wave velocity or shear modulus for various soils.

It has been found that the shear modulus was inherently anisotropic due to the depositional fabric of clay, and it has also been found that the degree of anisotropy for natural soil was significantly greater than for reconstituted soil (Pennington et al. 1997, Jovicic and Coop 1998, Yamashita et al. 2005). Moreover, the $Vs_{,HH}$ shear wave velocity values have been found to be greater than the $Vs_{,HV}$ shear wave velocity values. However, no significant difference between the $Vs_{,HV}$ and $Vs_{,VH}$ shear wave velocity values has been previously observed (Yamashita et al. 2005, Kang et al. 2014).

Most of the previously mentioned researchers utilized laboratory prepared soil samples, although some of the investigations were performed using natural soils such as London Clay and Gault clay. Due to the limited capacity of the testing equipment, the tested soil was either 1) not subjected to high applied load, or 2) no field obtained soil sample was utilized in the tests. Therefore, a comprehensive understanding of the soil anisotropy behavior has not been demonstrated. Moreover, only measured shear wave velocity and shear modulus values have been utilized to investigate the amount of soil anisotropy, and the other parameters or factors that may play significant role in geotechnical design (number of loading cycles, stress history, soil types, Poisson's ratio, and friction angle) have not been utilized to determine the amount of soil anisotropy.

6.6. Materials and Methods

The procedures for the BP-CRS-BE testing on the laboratory prepared Kaolinite and Illite soil samples that were utilized were the same as those reported in Zhao and Coffman (2016). The procedures that were utilized for the triaixial testing on the aforementioned Kaolinite and Illite soil samples were the same as those reported in Zhao et al. (2016). Additionally, the procedures for obtaining small strain shear modulus [$G_{\max,BE}$] for the tests on Kaolinite and Illite soil

samples by using the BP-CRS-BE device were the same as those presented in Zhao et al. (2016). Unlike the BP-CRS-BE device that was utilized for Zhao and Coffman (2016) and Zhao et al. (2016), the device that was utilized to conduct the tests, that are described herein, included vertical BE (Figure 6.5). For this modification, a new pair of Polyoxymethylene slide bars were fabricated to house the new pair of bender elements. Utilizing these bars the vertically oriented bender elements were able to be horizontally inserted into the soil sample. This modification enabled horizontally propagated - horizontally polarized shear waves (HH shear wave) to be generated and received and thus measurement of $V_{s,HH}$.

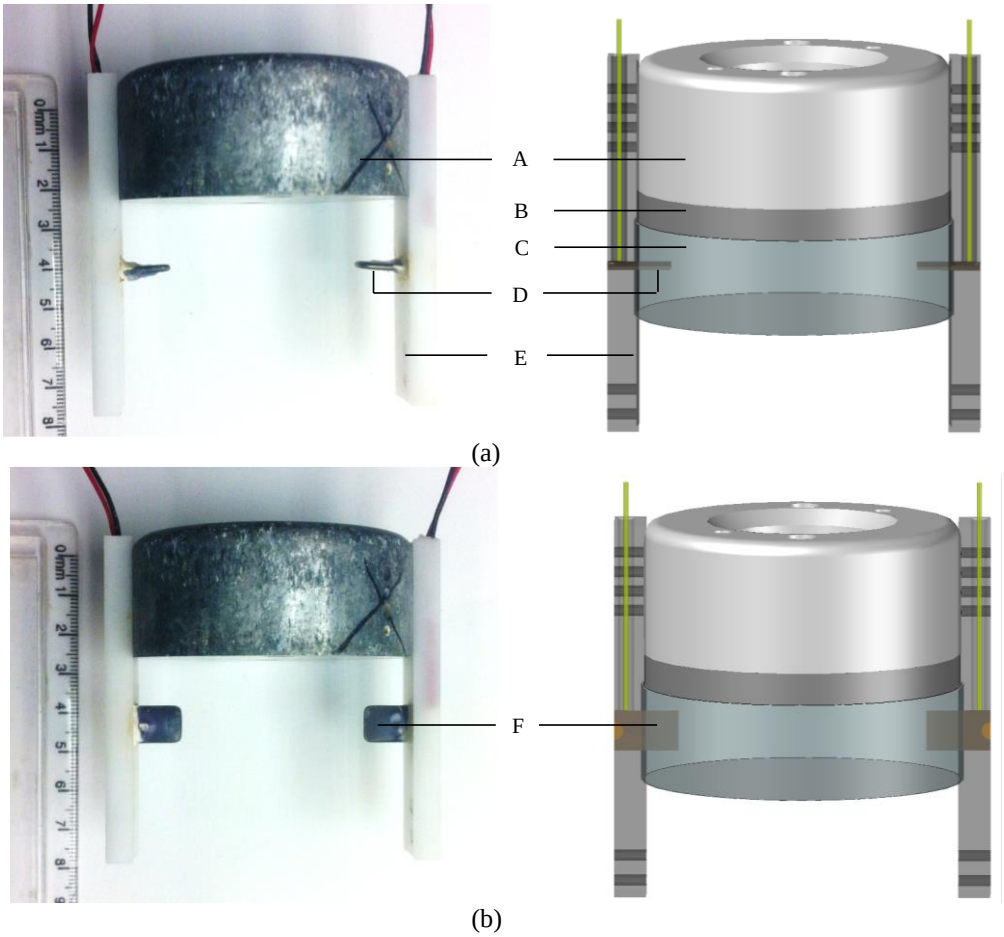

A. Alumimum loading cap. B. Porous stone. C. Soil sample. D. Horizontal bender element. E. Polyoxymethylene slide bar. F. Vertical bender element.

Figure 6.5. Photograph and schematic of BE within the fabricated Polyoxymethylene slide bars in the (a) horizontal orientation, and (b) vertical orientation.

Two types of soil, Kaolinite and Illite, were utilized in this study to investigate the effects of soil type on the soil anisotropy. The same Kaolinite soil (KaoWhite-S product), as reported in Garner and Coffman (2016), Zhao and Coffman (2016), and Zhao et al. (2016), that was obtained from Thiele Kaolin in Sandersville, Georgia, was utilized for this study. Following the same laboratory preparation method, as mentioned in Zhao and Coffman (2016), 400-grams of the Kaolinite soil was mixed with de-ionized, de-aired, water to form a 50-percent water content slurry. In addition, the Zhao and Coffman (2016) slurry consolidation soil preparation method was followed but additional water was added to produce a slurry with an initial water content 100-percent. The reason that the slurry was mixed to a higher water content was to ensure that the soil was reconstituted instead of remolded, based on the definition presented by Olson (1962) and Mahmood and Coffman (2016). The same Illite soil, as reported in Garner and Coffman (2016), which was obtained from the Knight Hawk Coal Company of Percy, Illinois, was utilized for this study; the soil was sieved to pass No. 200 prior to making the slurry. Following a similar laboratory preparation method as was utilized for the Kaolinite soil, 400-grams of the Illite soil was mixed with de-ionized, de-aired, water to form a slurry with an initial water content of 75-percent. Following preconsolidation of the slurried samples within the slurry consolidometer (preconsolidation to a stress of 138 kPa), four Kaolinite soil samples and two Illite soil samples were utilized within the BP-CRS-BE device to collect the required HV and HH shear wave measurement data. Also, three Kaolinite soil samples and three Illite soil samples were utilized within the triaxial device (preconsolidated to 207 kPa within a 3.81-cm diameter slurry consolidometer instead of within a 6.35-cm diameter slurry consolidometer). A summary of the soil samples that were utilized for this study is presented in Table 6.1.

Table 6.1. Summary of the soil samples utilized in BP-CRS-BE and triaxial tests.

Test	Material	σ'_p ,[kPa]	w_s, [%]	e_0	w_0, [%]	w_f, [%]	c_v, [m^2/s]	m_v, [Pa^{-1}]	k, [m/s]
BP-CRS-BE $V_{s, HV}$	Kaolinite	138	100	0.99	33.8	31.7	2.6E-08	1.9E-06	4.8E-10
BP-CRS-BE $V_{s, HH}$	Kaolinite	138	100	1.04	32.2	30.5	2.6E-08	1.9E-06	4.8E-10
BP-CRS-BE $V_{s, HV}$	Kaolinite	138	50	0.98	31.6	30.3	2.2E-08	7.5E-07	1.6E-10
BP-CRS-BE $V_{s, HV}$	Illite	138	75	1.56	43.6	38.4	2.0E-09	7.8E-07	1.6E-11
BP-CRS-BE $V_{s, HH}$	Illite	138	75	1.46	52.5	40.3	2.0E-09	7.8E-07	1.6E-11
Triaxial 310kPa	Kaolinite	207	50	0.93	31.3	31.0	2.1E-08	3.4E-07	7.0E-11
Triaxial 414kPa	Kaolinite	207	50	0.89	31.2	29.9	3.9E-08	4.5E-07	1.7E-10
Triaxial 828kPa	Kaolinite	207	50	0.90	31.7	28.7	2.1E-08	3.4E-07	7.0E-11
Triaxial 310kPa	Illite	207	75	1.02	33.2	31.8	1.4E-07	1.3E-06	1.8E-09
Triaxial 414kPa	Illite	207	75	1.02	36.6	29.5	1.4E-07	1.3E-06	1.8E-09
Triaxial 828kPa	Illite	207	75	1.07	36.0	26.3	1.7E-07	1.0E-06	1.7E-09

6.7. Results and Discussion

For simplicity, the Kaolinite samples, that were initially prepared to a water content of 50-percent or 100-percent, are hereinafter referred to as 50-percent and 100-percent, respectively, while the Illite sample, that was initially prepared to 75-percent, is hereinafter referred to as 75-percent. Based on the results that were obtained from the slurry consolidometer (Figure 6.6), for the Kaolinite and Illite samples, the Illite samples took longer to consolidate. The Illite took over an order of magnitude longer to consolidate than both of the Kaolinite samples, regardless of the initial water content of the Kaolinite samples. The Kaolinite samples, although mixed to different initial water contents, took approximately the same amount of time to consolidate but consolidated by different amounts. Moreover, the amount of consolidation, as a function of water content, was comparable for the 50-percent and 75-percent samples (2.29 cm for 50-percent sample and 2.66 cm for the 75-percent sample). The estimated values of c_v, m_v, and hydraulic conductivity (k), that were obtained from Figure 6.6, were presented previously in Table 6.1.

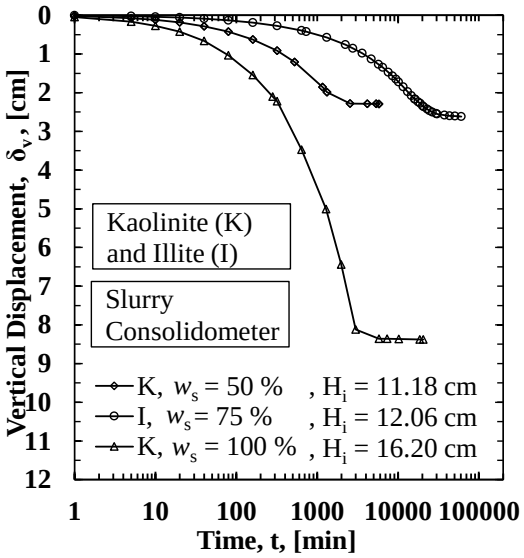

Figure 6.6. Vertical displacement as a function of elapsed time as collected during the sample preparation process, within the slurry-consolidometer, for the Kaolinite and Illite samples.

The 100-percent sample consolidated by approximately four times as much as the 50-percent sample. Albeit, the initial length of the 100-percent sample, within the slurry consolidometer, was also 1.5 times longer than the 50-percent sample, within the slurry consolidometer. These times and amounts of consolidation are indicative that the 50-percent sample should 1) have similar values for constrained modulus as the 100-percent sample because both took a similar amount of time to consolidate when subjected to the same amount of applied loading and should 2) have similar a structure as the 75-percent sample, because both samples consolidated by comparable amounts when subjected to the same amount of applied loading. By utilizing additional parameters, as obtained from the BP-CRS-BE device, these two aforementioned hypotheses are refuted herein.

6.7.1. *Similar Constrained Modulus*

As shown in Figures 6.6 and 6.7, even though the 100-percent sample deformed within the slurry consolidometer to a higher amount of axial strain than the 50-percent sample (51-percent and 20-percent, respectively), the initial void ratio after slurry consolidation for the 50-

percent sample was less than the initial void ratio of the 100-percent sample. Within the BP-CRS-BE, during the first unloading stage for the 50-percent sample and during the final unloading stage for the 100-percent sample, the void ratio values for both samples were similar, at corresponding levels of vertical effective stress, with the 100-percent sample void ratio values being slightly lower or equal to the 50-percent sample values. Although the void ratio values were similar for these unloading stages, the shear wave velocity values for these unloading stages, and the amount of axial strain within the BP-CRS-BE were different (Figures 6.8 and 6.9, respectively). This was attributed to the difference in the total amount of axial strain to which each sample was subjected. Even though the void ratio values of the samples were the same for these unloading cycles, due to the way in which the samples were prepared, the soil fabric of the 100-percent sample was dispersed whereas the soil fabric for the 50-percent sample was flocculated. Therefore, the ray path of the shear waves within the 100-percent sample was shorter, because of the edge-to-edge arrangement of the soil particles, but the ray path for the 50-percent sample was longer because of the edge-to-face orientation of the soil particles.

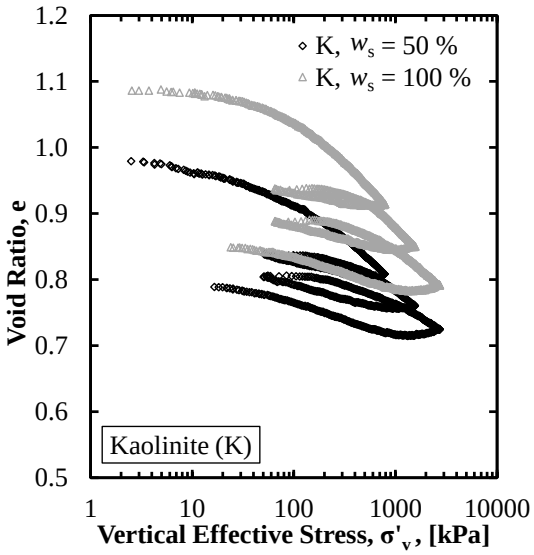

Figure 6.7. Void ratio as a function of vertical effective stress for the tests, as conducted using the BP-CRS-BE device, on Kaolinite specimens.

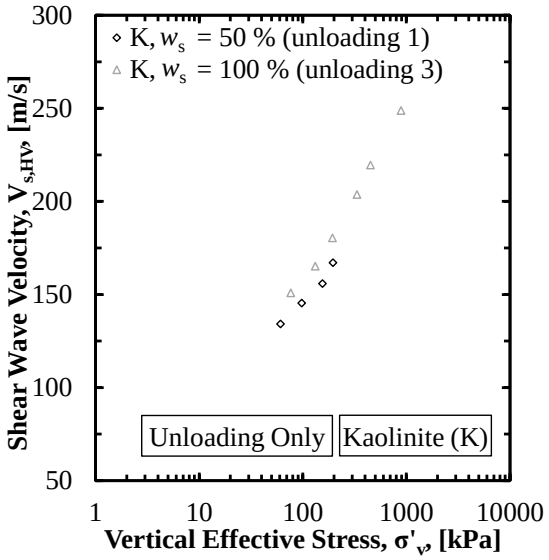

Figure 6.8. HV shear wave velocity as a function of vertical effective stress for the tests, as conducted using BP-CRS-BE device, on Kaolinite specimens.

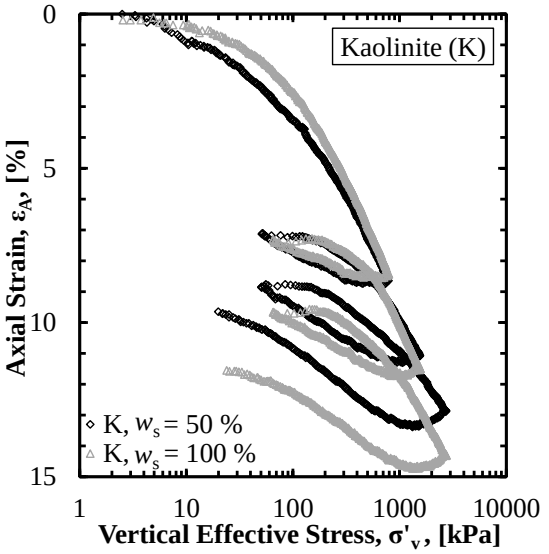

Figure 6.9. Axial strain as a function of vertical effective stress for the tests, as conducted using the BP-CRS-BE device, on Kaolinite specimens.

It appears that the amount of developed soil structure was also stress dependent. For the first loading-unloading cycle, for both the 50-percent sample and the 100-percent sample, the shear wave velocity values were similar (Figure 6.10a). However, as shown in Figure 6.10b, after a vertical effective stress of approximately 962kPa was reached, the shear wave velocity

within the 100-percent sample began to exceed the shear wave velocity within the 50-percent sample and the shear wave velocities for the 100-percent sample remained higher than the shear wave velocity values of the 50-percent sample thereafter (Figure 6.10c). The obtained effective stress value of approximately 962kPa corresponded to the value at which the virgin compression lines for the 100-percent and 50-percent samples crossed (Figure 6.11).

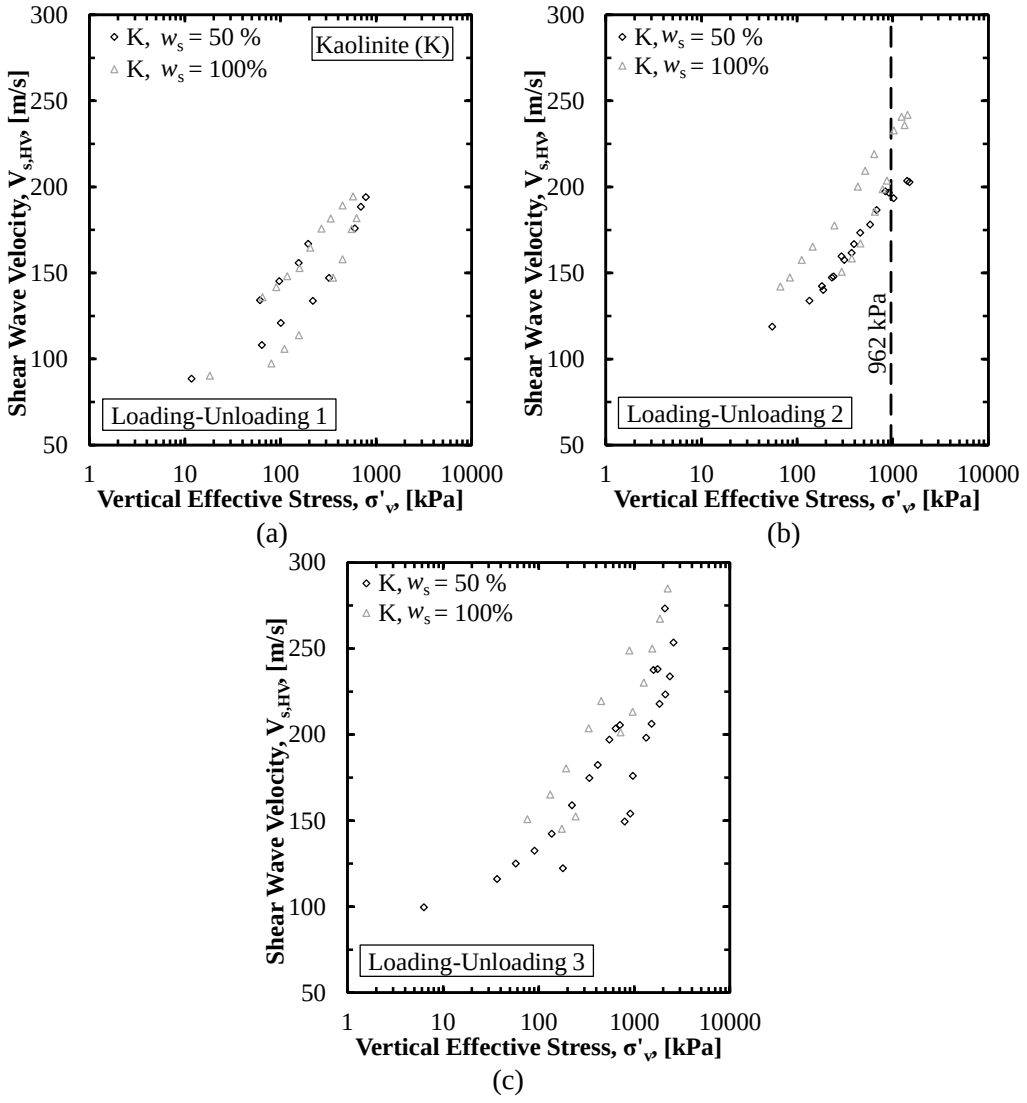

Figure 6.10. HV shear wave velocity as a function of vertical effective stress for the tests, as conducted using the BP-CRS-BE device, on Kaolinite specimens for: (a) loading-unloading Cycle 1, (b) loading-unloading Cycle 2, and (c) loading-unloading Cycle 3.

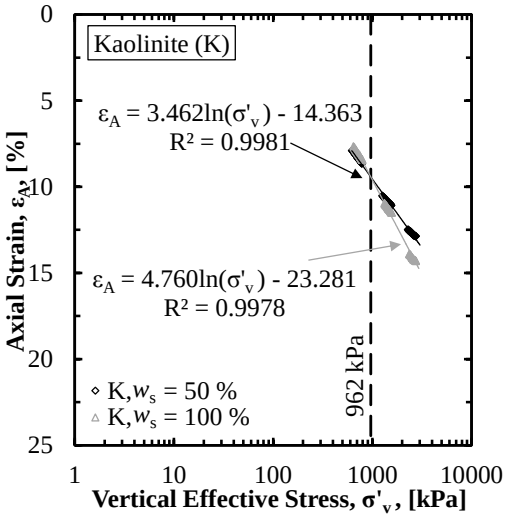

Figure 6.11. Comparison of the behavior of consolidation tests, as conducted using BP-CRS-BE device on Kaolinite specimens obtained from the 50-percent initial water content within the slurry consolidometer and the 100-percent initial water content within the slurry consolidometer.

Similar observations were drawn from the triaxial data. 1) The void ratio for the 100-percent sample was higher than the void ratio for the 50-percent sample (Figure 6.12a). 2) The 100-percent sample strained more than the 50-percent sample during Ko-consolidation (Figure 6.12b). 3) The secant Young's Modulus values that were observed during shearing (corollary to the shear modulus that was obtained from the BP-CRS-BE tests) were typically higher for the 100-percent sample than for the 50-percent sample (Figure 13a). Although the stress-strain diagram (Figure 6.13b) and p'-q plots (Figure 6.14) that were developed from the triaxial data also helped to prove that the 50-percent sample possessed a flocculated structure while the 100-percent sample possessed a dispersed structure (based on the post-peak residual behavior in triaxial tests and based on the direction of the effective stress path in Figure 6.14), the undrained shear strength value that was obtained from the 50-percent data was higher than the undrained shear strength value that was obtained from the 100-percent data. This goes against the rational that larger values of modulus will result in larger values of shear strength. Although the jigsaw

orientation of the particles in the flocculated structure reduced the travel time of the shear waves (and thereby reduced the shear modulus values), the interlocking nature of the flocculated particles assisted with the increase in the shear strength values.

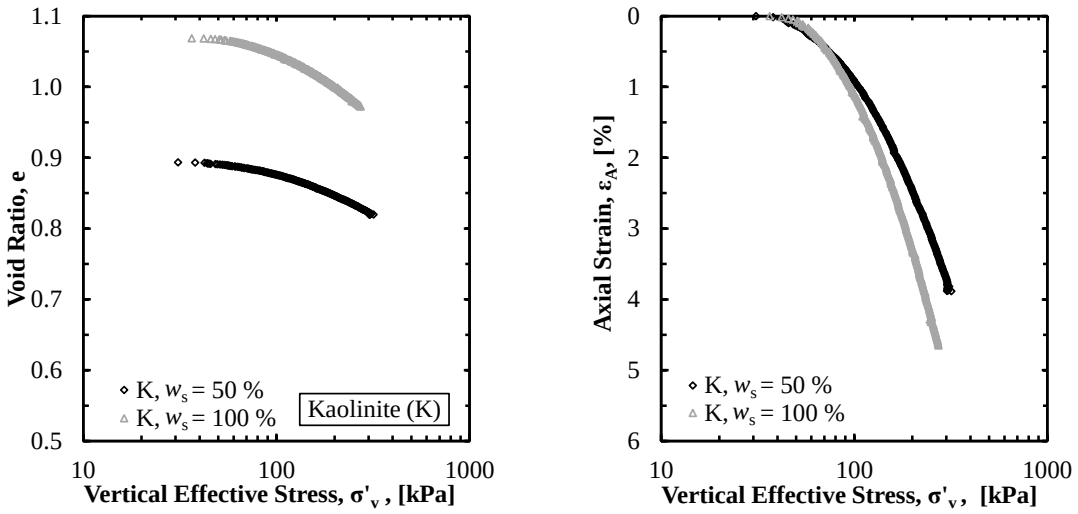

(a) (b)

Figure 6.12. Comparison of the behavior of the triaxial data, during K0-consolidation, for the 50-percent and 100-percent Kaolinite soil samples, in terms of: (a) void ratio as a function of vertical effective stress, and (b) axial strain as a function of vertical effective stress.

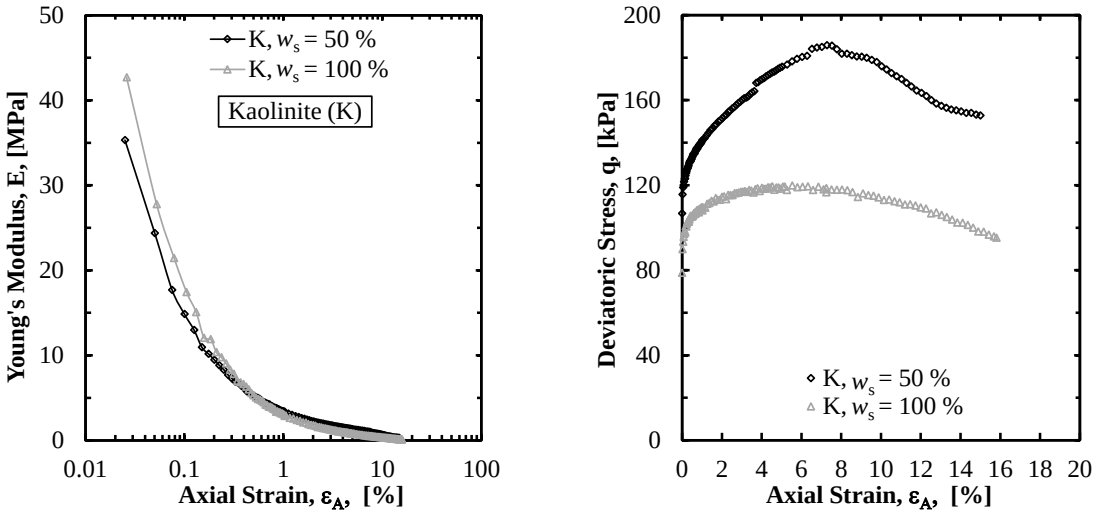

(a) (b)

Figure 6.13. Comparison of the behavior of the 50-percent and 100-percent Kaolinite soil samples in terms of: (a) Young's modulus as a function of axial strain, and (b) deviatoric stress as a function of axial strain.

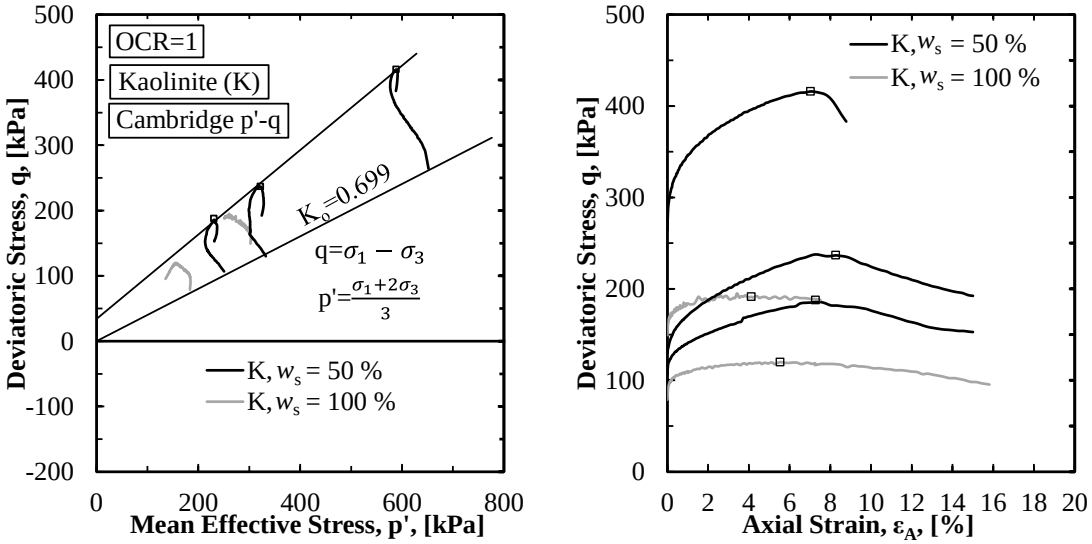

Figure 6.14. Comparison of the behavior of the 50-percent and 100-percent Kaolinite samples as conducted in triaxial tests in terms of: (a) deviatoric stress as a function of mean effective stress, and (b) deviatoric stress as a function of axial strain.

6.7.2. *Similar Structure*

As with the aforementioned results from the slurry consolidometer (as shown previously in Figure 6.6), the Kaolinite and Illite samples with an initial water content of 50-percent and 75-percent, respectively, displaced by similar amounts when subjected to the same amount of axial load within the slurry consolidometer. Therefore, the samples were believed to have a similar soil fabric. However, unlike the previous discussion about the kaolinite soil prepared at various water contents, where the Kaolinite sample that was slurry-consolidated with a higher water content had higher shear wave velocity values than the lower water content sample due to the structure that was formed, the 50-percent initial water content Kaolinite soil had higher shear wave velocity values than the 75-percent initial water content Illite soil at almost every comparable loading increment (Figure 6.15). Moreover, as shown in Figure 6.15, the amount of hysteresis within the shear wave velocity – vertical effective stress curves was larger for the Illite

soil than for the Kaolinite soil. This difference was attributed to the layering structure of the Illite mineral (2:1 sheet) as compared with the Kaolinite mineral (1:1 sheet).

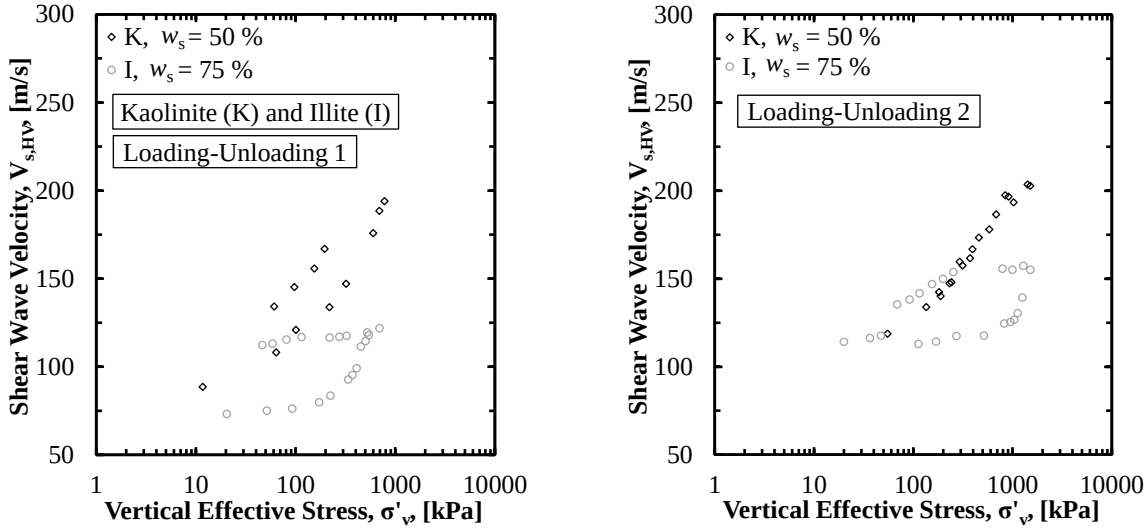

Figure 6.15. HV shear wave velocity as a function of vertical effective stress for the tests, as conducted using BP-CRS-BE device on Kaolinite and Illite during: (a) loading-unloading Cycle 1, and (b) loading-unloading Cycle 2.

Because shear waves do not travel through water, and because additional water was bound within the Illite mineral (or the Vermiculite mineral, depending upon the amount of weathering), the measured shear wave velocity values were slower within the Illite/Vermiculite sample. As shown in Figure 6.16, the slower shear wave velocity within the Illite soil also led to decreased soil modulus values when compared to both of the Kaolinite soil samples (w_s=50% and w_s=100%). Although both the 50-percent and 75-percent samples of the respective soil types displaced by the same amount within the slurry-consolidometer, the void ratio values were different and Illite soil deformed more than the Kaolinite when consolidated in both the BP-CRS-BE device and within the triaxial device (Figure 6.17). This increased amount of consolidation is indicative of a softer soil, as was shown previously based on modulus values in Figure 6.16.

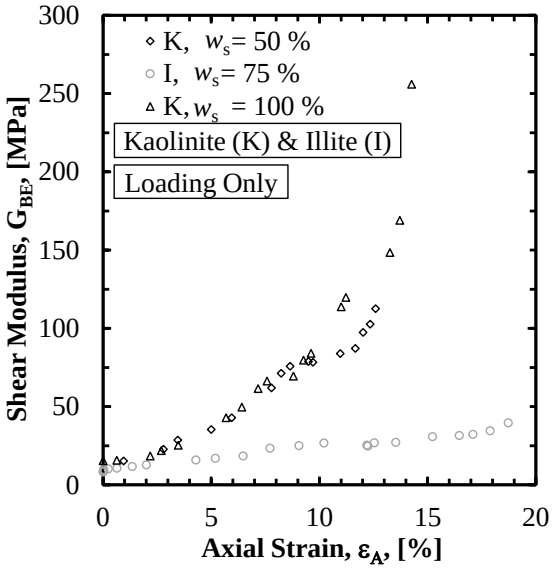

Figure 6.16. Shear modulus as a function of axial strain for the tests, as conducted using the BP-CRS-BE device, on Kaolinite and Illite.

In the opposite condition to that described in the "Similar Constrained Modulus" discussion, where the w_s=50% Kaolinite sample had a lower modulus but higher shear strength than the w_s=100% Kaolinite sample, the sample with the higher water content (w_s=75% Illite) had the lower shear modulus but higher shear strength (Figure 6.18a). Moreover, as was not expected from the aforementioned shear modulus results, the amount of strain that was required to reach failure for the w_s=50% Kaolinite sample was higher than the amount of strain that was required to reach failure for the w_s=75% Illite sample (Figure 6.18b). Specifically, based on the triaxial results, the Young's modulus was higher for the Illite soil than for the Kaolinite soil; this was not observed in the aforementioned shear modulus data.

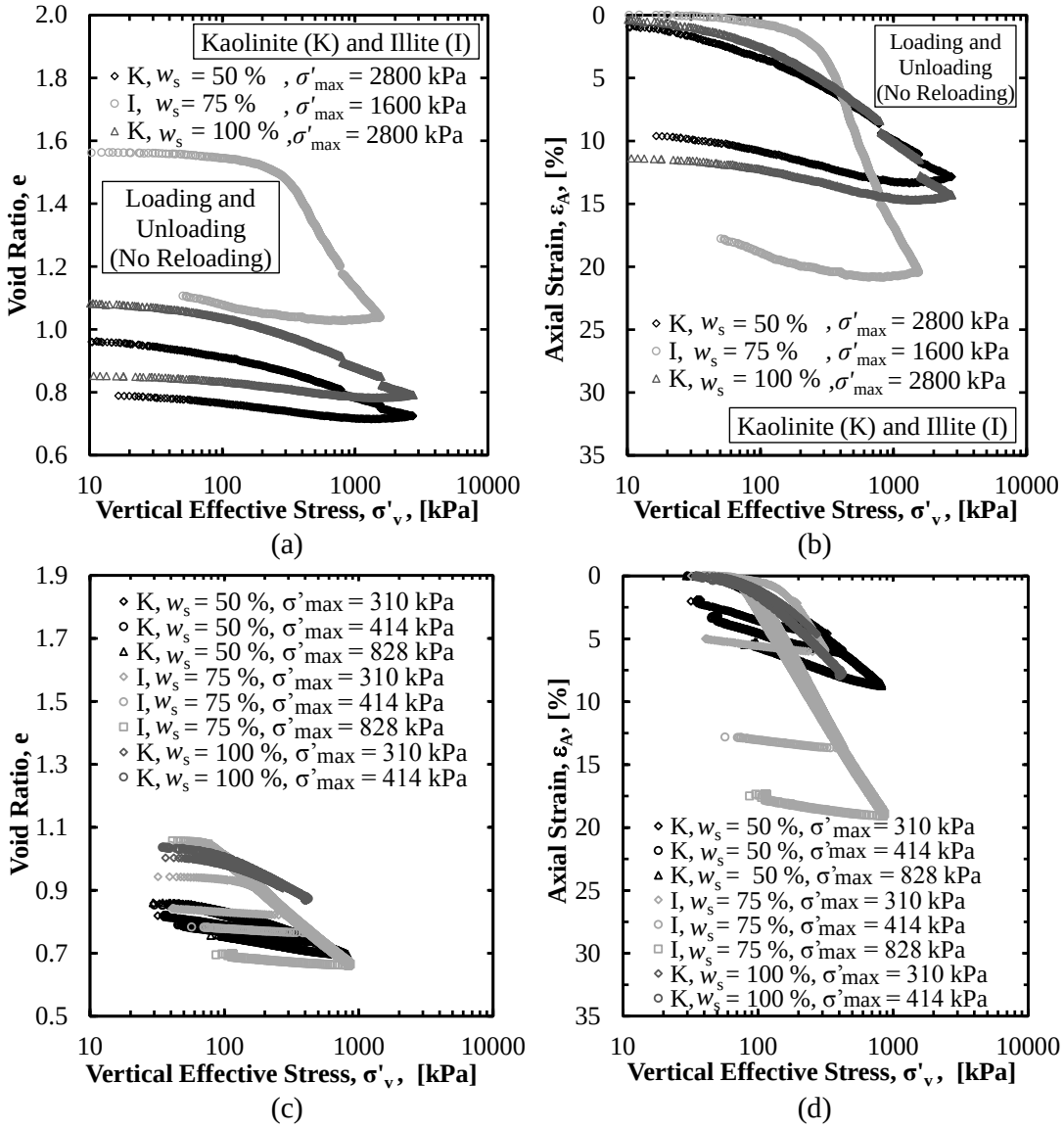

Figure 6.17. Comparison of the Kaolinite and Illite soil in terms of: (a) void ratio as a function of vertical effective stress as obtained from CRS tests, (b) axial strain as a function of vertical effective stress as obtained from CRS tests, (c) void ratio as a function of vertical effective stress as obtained from triaxial tests, and (d) axial strain as a function of vertical effective stress as obtained from triaxial tests.

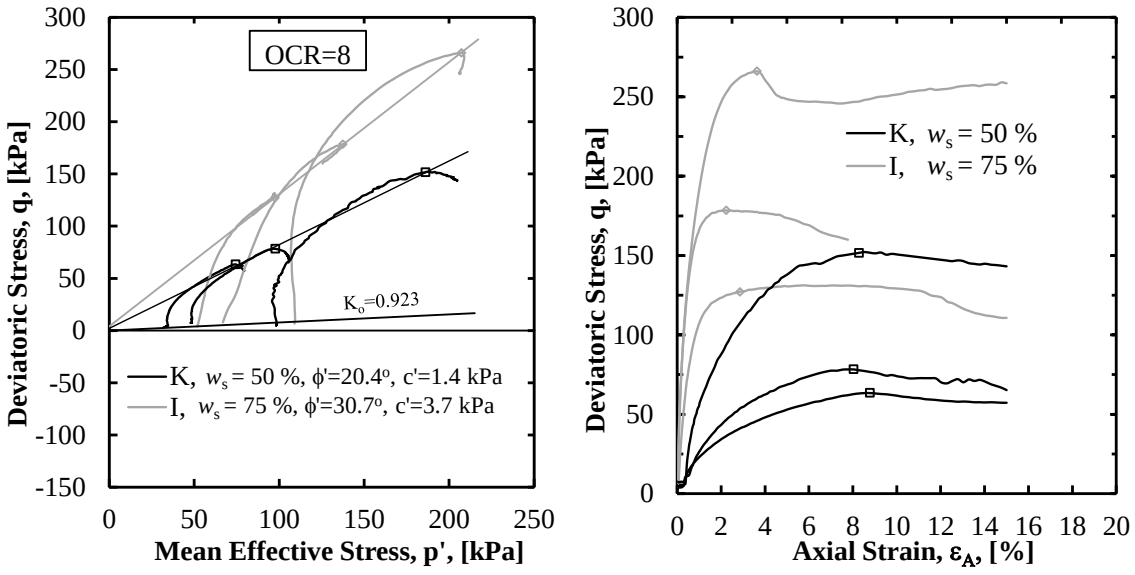

(a) (b)

Figure 6.18. Comparison of the behavior of the 50-percent Kaolinite and 75-percent Illite samples as conducted in triaxial tests in terms of: (a) deviatoric stress as a function of mean effective stress, and (b) deviatoric stress as a function of axial strain.

6.7.3. *Inherent Fabric Anisotropy*

For the Kaolinite and Illite samples, initially mixed at respective water content values of 100-percent and 75-percent, inherent fabric anisotropy was observed (Figure 6.19). The amount of inherent fabric anisotropy $(V_{s,HH}/V_{s,HV})$ for the Kaolinite sample ranged from 1.00 to 1.42, depending upon the stress level. The amount of inherent fabric anisotropy $(V_{s,HH}/V_{s,HV})$ for the Illite sample ranged from 1.00 to 1.56, depending upon the stress level. The stress dependence was associated with the plasticity of the soil. As previously mentioned, when the amount of strain-induced anisotropy was evaluated based on the $V_{S,HV}$ data, more strain-induced anisotropy was observed within the Illite soil than was observed within the Kaolinite soil. The same increased amount of strain-induced anisotropy for the Illite soil was also true when evaluated based on the $V_{S,HH}$ data.

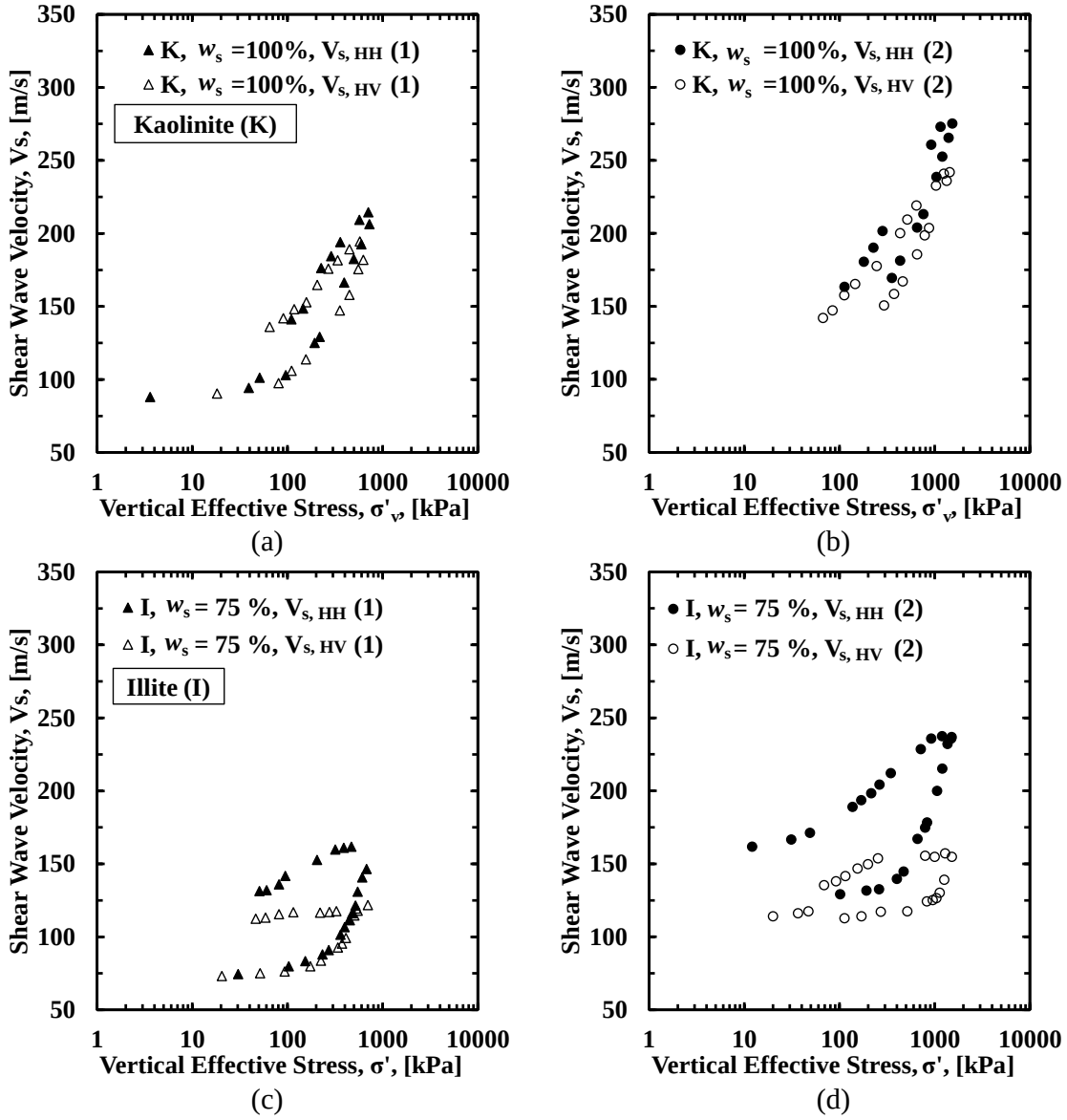

Figure 6.19. Shear wave velocity as a function of vertical effective stress for the tests conducted using BP-CRS-BE device on: (a) Kaolinite loading-unloading Cycle 1, (b) Kaolinite loading-unloading Cycle 2, (c) Illite loading-unloading Cycle 1, and (d) Illite loading-unloading Cycle 2.

Like with the BP-CRS-BE obtained axial strain – vertical effective stress plot that was presented in Figure 6.17b, in which the change in slope of the Illite curve following the preconsolidation pressure was greater than the change in slope of the Kaolinite curve following the preconsolidation pressure, the change in slope of shear wave velocity – vertical effective

stress curve following the preconsolidation pressure was greater than the change in slope of the Kaolinite curve following the preconsolidation pressure (Figure 6.19). As discussed by others (Ladd and Varallyay 1965, Ladd and Foott 1974, Landon 2007, DeGroot 2003, Ladd and DeGroot 2003, Poirier et al. 2005, Landon et al. 2007), the shapes of these curves are typically an indication of sample quality; rounder, flatter curves are usually symptomatic of disturbed soil samples. Based on the obtained results (Figure 6.19), in which the sample disturbance was negligible because the samples were created within the laboratory, the shape of these curves may also be attributed to the soil fabric that was created within the slurry consolidometer. Moreover, based on the shapes of the curves, the shape of the shear wave velocity curve may be indicative of the shape of the consolidation curve and vice-versa.

For the Illite soil, the slope of the virgin portion of the curve was significantly greater for the HH waves than for the HV waves (Figure 6.19). Therefore, if the shear wave velocity data are indicative of the consolidation curves, then the slope of the virgin portion of the consolidation curve for a reoriented soil specimen (horizontal bedding planes oriented to be loaded in the vertical direction) may also be greater. The use of the HH data should be utilized to assist in the determination of time-dependent consolidation. This type of behavior is typically taken into account when predicting the time-dependent nature of consolidation for large-scale projects by using radial time factors (Terzaghi 1943, Olson 1962); however, HH data may assist in the determination of these factors. Moreover, when considering the total amount of settlement, this behavior may also be able to be taken into account by using relationships between the shear wave velocity anisotropy and the radial consolidation properties (Sully and Campanella 1995, Pennington et al. 1997, Jovicic and Coop 1998, Lo Presti et al. 1999, Nash et al. 1999, Yamashita et al. 2005, Landon and DeGroot 2006, Kang et al. 2014).

For the Illite mineral, a more pronounced hysteresis was observed in the horizontally propagating – horizontally polarized waves than for the horizontally propagating – vertically polarized. The mechanical rearrangement of the soil particles when subjected to vertical pressure led to this behavior. However, because a greater amount of stress-induced anisotropy was observed for the Illite soil than was observed for the Kaolinite soil, the cause may have also been associated with decreased of thickness of actual soil particle layers. Regardless of the mechanism, the irreversible rearrangement of soil particles (plastic deformation) was witnessed through the irreversible increase in shear wave velocity when the soil returned to the same stress levels upon unloading. These results were in agreement with the results that were reported by Zeng and Ni (1999), Lee et al. (2008), and Kang et al. (2014).

6.8. Conclusions

Vertically and horizontally oriented bender elements were utilized, within a back-pressure saturated consolidation device, to measure the shear wave velocity during ongoing consolidation tests. From the results, as obtained from testing on Kaolinite and Illite samples, conclusions were drawn with respect to soil samples with similar constrained modulus, similar structure, and inherent fabric anisotropy. Specifically, the information was gained from the w_s=50% Kaolinite sample, the w_s=75% Illite sample, and the w_s=100% Kaolinite sample are summarized below.

Even when soils have the same constrained modulus, the structure of the soil samples (flocculated or dispersed) will cause differences in the measured shear wave velocity. For instance, the w_s=50% Kaolinite sample was flocculated while the w_s=100% Kaolinite sample was dispersed and the shear wave velocity (and therefore shear modulus) of the dispersed sample was

higher. These conclusions were also then validated utilizing triaxial testing data from samples mixed to the same initial water contents.

Different soils with a similar initial structure (initial void ratio) behaved very differently during consolidation and shearing. Although the w_s=50% Kaolinite sample and w_s=75% Illite samples were initially prepared with similar amounts of axial strain in the slurry consolidometer, the soil samples behaved very differently during consolidation and shearing. Utilizing the horizontally propagating - vertically polarized shear wave velocity measurements to gain insight into this difference, although this difference was water content related it was more attributed to the mineral structure of the Illite mineral (2:1 sheet) as compared with the Kaolinite mineral (1:1 sheet).

The sheet arrangement of the various minerals was also shown to affect the amount of inherent soil anisotropy. Again, the data collected from the Illite mineral (2:1 sheet) possessed more hysteresis in the shear wave velocity measurements than the data collected from the Kaolinite mineral (1:1 sheet). Moreover, the hysteresis was much more pronounced using the horizontally propagated – horizontally polarized waves. Although soil specific, the developed relationship between the virgin consolidation line within the axial strain – effective stress space and the virgin consolidation line within the axial shear wave velocity – effective stress space provides insight that multiple consolidation tests (tests with different orientations between the bedding planes and the loading direction) may need to be performed for soils identified to be highly anisotropic based on shear wave velocity testing.

For each of the items considered (constrained modulus, similar structure, and inherent fabric anisotropy), the amount of stress to which the sample was subjected played an integral role in the obtained results. For instance, and as is typical, 1) the patterns of the obtained data began

to change after the preconsolidation pressure was reached, and 2) the pattern of the obtained data began to change or become more exaggerated at high stress levels. Because of the way in which the BP-CRS-BE device was constructed, these patterns were able to be observed.

6.9. References

Arulnathan, R., Boulanger, R. W., and Riemer, M. F., "Analysis of Bender Element Tests," *Geotech. Test. J.*, Vol. 21, No. 2, 1998, pp. 120–131.

Abdoun, T. and Dobry, R., 2002, "Evaluation of Pile Foundation Response to Lateral Spreading." Soil Dynamics and Earthquake Engineering, Vol. 22, No. 9, pp.1051-1058.

Bauer, G. E., 1984, "Dewatering, Hydraulic Failure and Subsequent Analysis of a Sheeted Excavation," International Conference on Case Histories in Geotechnical Engineering. Paper 13.

Belardinelli, M. E., M. Cocco, O. Coutant, and F. Cotton, 1999, "Redistribution of Dynamic Stress during Coseismic Ruptures: Evidence for Fault Interaction and Earthquake Triggering." *Journal of Geophysics. Res.*, 104(B7), pp.14925–14945, doi:10.1029/1999JB900094.

Briaud, J.L., 2008, "Case Histories in Soil and Rock Erosion: Woodrow Wilson Bridge, Brazos River Meander, Normandy Cliffs, and New Orleans Levees." Journal of Geotechnical and Geoenvironmental Engineering, Vol. 134, No. 10, pp.1425-1447.

Briaud, J.L., Ting, F.C.K., Chen, H.C., Cao, Y., Han, S.W. and Kwak, K.W., 2001, "Erosion Function Apparatus for Scour Rate Predictions." Journal of geotechnical and geoenvironmental engineering, Vol. 127, No. 2, pp.105-113.

Brignoli, E.G.M., M. Gotti, and Stokoe, K.H., 1996, "Measurement of Shear Waves in Laboratory Specimens by Means of Piezoelectric Transducers", *Geotechnical Testing Journal*, Vol. 19, No. 4, pp. 384-397.

Coffman, R.A., Salazar, S.E., Zhao, Y., 2014, "Discussion of Measurement of Stiffness Anisotropy in Kaolinite Using Bender Element Tests in Floating Wall Consolidometer by X. Kang, G-C Kang, and B. Bate." *Geotechnical Testing Journal*. Vol. 37, No. 6, pp. 1-4.

DeGroot, D., 2003, "Laboratory Measurement and Interpretation of Soft Clay Mechanical Behavior." Soil Behavior and Soft Ground Construction. pp. 167-200.

Dyvik, R. and Olsen, T. S., 1989, "G_{max} Measured in Oedometer and DSS Tests Using Bender Elements," *Proceedings, Twelfth International Conference on Soil Mechanics and Foundation Engineering*, Rio de Janeiro, Vol. 1, pp. 39-42.

Garner, C.D., Coffman, R.A., 2016, "Visible and Near Infrared Diffuse Reflectance Properties of Geotechnical Reference Soils" *Geodurma*, Submitted for Review, Manuscript Number: GEODER-15-01244.

Ghayoomi, M., 2011, "Seismically Induced Settlement of Partially-saturated Sand," Ph.D. Dissertation, University of Colorado, Boulder, Boulder, CO.

Gray, D.H. and Al-Refeai, T., 1986, "Behavior of Fabric-versus Fiber-reinforced Sand." Journal of Geotechnical Engineering, Vol. 112, No. 8, pp. 804-820.

Gross, S. and Kisslinger, C., 1997, "Estimating Tectonic Stress Rate and State with Landers Aftershocks." *Journal of Geophysical Research*-all series-, 102, pp.7603-7612.

Holzer, T.L., 1981, "Preconsolidation Stress of Aquifer Systems." *Water Resources Research*, 17(3), pp.693-704.

Jovicic, V., Coop, M. R., and Simic, M., 1996, "Objective Criteria for Determining G_{max} from Bender Element Test," *Geotechnique*, Vol. 46, No. 2, pp. 357–362.

Jovicic, V., and Coop, M. R., 1998, "The Measurement of Stiffness Anisotropy in Clays with Bender Element Tests in the Triaxial Apparatus." *Geotechnical Testing Journal*, ASTM, 21(1), pp. 3-10.

Kaiser, P.K., Hewitt, K.J., 1982, "The Effect of Ground Water Flow on the Stability and Design of Retained Excavations." Canadian Geotechnical Journal, Vol. l9, pp. l39-153.

Kang, X., Kang, G.-C., and Bate, B., 2014, "Measurement of Stiffness Anisotropy of Kaolinite Using Bender Element Tests in a Floating Wall Consolidometer". *Geotechnical Testing Journal.* ASTM. Vol. 37, No. 5. pp. 1-16.

Kuwano, R., Connolly, T.M. and Kuwano, J., 1999, "Shear Stiffness Anisotropy Measured by Multi-directional Bender Element Transducers", Proceedings of the International Symposium on Pre-failure deformation characteristics of geomaterials, Torino, Balkema, pp. 205-212.

Ladd, C.C. and DeGroot, D.J., 2003, "Recommended Practice for Soft Ground Site Characterization: Arthur Casagrande Lecture." In 12th Panamerican Conference on Soil Mechanics and Geotechnical Engineering. Vol. 1, pp. 1-57.

Ladd, C. C, and Foott, R., 1974, "New Design Procedure for Stability of Soft Clays." Journal of Geotechnical Engineering Division," Vol. 100, No. 7, pp. 763-768.

Ladd, C. C., and Varallyay, J., 1965, "The Influence of Stress System on the Behavior of Saturated Clays during Undrained Shear." No. RR-R65-11. Massachusetts Inst of Tech, Cambridge Soil Mechanics Div.

Landon, M. M., and DeGroot, D. J., 2006, "Measurement of Small-strain Shear Modulus Anisotropy on Unconfined Clay Samples Using Bender Elements," *Proceedings of GeoCongress 2006,* ASCE.

Landon, M. M., 2007, "Development of a Non-destructive Sample Quality Assessment Method of Soft Clays," Ph.D. Dissertation, University of Massachusetts, Amherst, MA.

Landon, M.M., DeGroot, D.J. and Sheahan, T.C., 2007, "Nondestructive Sample Quality Assessment of a Soft Clay Using Shear Wave Velocity." Journal of geotechnical and geoenvironmental engineering, Vol. 133, No. 4, pp.424-432.

Lee, K.M. and Rowe, R.K., 1989, "Deformations Caused by Surface Loading and Tunnelling: the Role of Elastic Anisotropy." Geotechnique, Vol. 39, No. 1, pp.125-140.

Lee, J.-S., and Santamarina, J. C., 2005, "Bender Elements: Performance and Signal Interpretation," *Journal of Geotechnical and Geoenvironmental Engineering*, Vol. 131, No. 9, pp. 1063–1070.

Lee, C., Lee, J.-S., Lee, W., and Cho, T.-H., 2008, "Experiment Setup for Shear Wave and Electrical Resistance Measurements in an Oedometer," *Geotechnial Tesing Journal*, Vol. 31, No. 2, pp. 149–156.

Lings, M. L., Pennington, D. S., and Nash, D. F. T., 2000, "Anisotropic Stiffness Parameters and their Measurement in a Stiff Natural Clay," *Géotechnique,* Vol. 50, No. 2, pp. 109–125.

Lo Presti D.C.F., Jamiolkowski M., Lancellotta R. and Vercelli L., 1993. "Maximum Shear Modulus Measurement Using Bender Elements in Oedometer Tests", *Rivista Italiana de Geotechnica*, Vol.(XXVII), No. 1, pp. 5-9.

Lo Presti, D.C.F., Pallara, O., Jamiolkowski, M. and Cavallaro, A., 1999, "Anisotropy of Small Strain Stiffness of Undisturbed and Reconstituted Clays", Proceedings of the

International Symposium on Pre-failure deformation characteristics of geomaterials, Torino, Balkema,PP. 3-10.

Meade, R. H., 1964. "Removal of Water and Rearrangement of Particles during the Compaction of Clayey Sediments-Review (No. 497-B)."

Mahmood, N. S., and Coffman, R.A., 2016. "Investigation of the Effects of Stress Path on the Characterization of Remolded Clay." Journal of Testing and Evaluation. In preparation.

Mitchell, J.K. and Soga, K., 2005, "Fundamentals of Soil Behavior."

Montoya, B.M., Gerhard, R., DeJong, J.T., Weil, M.H., Martinez, B.C., and Pederson, L., 2011, "Fabrication, Operation, and Health Monitoring of Bender Elements in Aggressive Environments," *Geotechnical Testing Journal*, Vol.35, No. 5, pp. 1-15.

Nash .D.F.T., Lings, M.L., and Pennington, D.S., 1999, "The Dependence of Anisotropy G_0 Shear Moduli on Void Ratio and Stress State for Reconstituted Gault Clay." Proc., 2nd Int. Symp. on Pre-Failure Deformation Characteristics of Geomaterials, Torino, 229-238.

Olson, R. E., 1962, "The Shear Strength Properties of Calcium Illite." Geotechnique, Vol. 12, No. 1, pp.23-43.

Pennington, D. S., Nash, D. F. T., and Lings, L. L., 1997, "Anisotropy of G_0 Shear Stiffness in Gault Clay," *Geotechnique*, Vol. 47, No. 3, pp. 391–398.

Pennington, D.S., Nash, D.F.T., and Lings, M.L., 2001, "Horizontally Mounted Bender Elements for Measuring Anisotropic Shear Moduli in Triaxial Clay Specimens." *Geotechnical Testing Journal*, Vol. 24, No. 2, pp. 133-144.

Petroski, H., 1994, "Design paradigms: Case Histories of Error and Judgment in Engineering." Cambridge University Press.

Piriyakul, K., 2006. "Anisotropic Stress-Strain Behaviour of Belgian Boom Clay in the Small Strain Region." Ph.D., Ghent University.

Poirier, S.E., DeGroot, D.J. and Sheahan, T.C., 2005, "Measurement of Suction in a Marine Clay as an Indicator of Sample Disturbance." In Proc. GeoFrontiers Conference, ASCE, Austin.

Roesler, S. K., 1979. "Anisotropic Shear Modulus Due to Stress Anisotropy," *Journal of the Geotechnical Engineering Division*, 105(7), pp.871-880.

Salazar, S.E., Coffman, R.A., 2014, "Design and Fabrication of End Platens for Acquisition of Small-Strain Piezoelectric Measurements during Large-Strain Triaxial Extension and Triaxial Compression Testing." *Geotechnical Testing Journal*, Vol. 37, No. 6, pp. 1-12. doi:10.1520/GTJ20140057.

Santamarina, J.C., Klein, A. and Fam, M.A., 2001, "Soils and Waves: Particulate Materials Behavior, Characterization and Process Monitoring." Journal of Soils and Sediments, Vol. 1, No. 2, pp.130-130.

Sawangsuriya, A., Fratta, D., Bosscher, P., and Edil, T, 2007, S-Wave Velocity-Stress Power Relationship: Packing and Contact Behavior of Sand Specimens. Advances in Measurement and Modeling of Soil Behavior: pp. 1-10.

Seed, H.B. and Idriss, I.M., 1970, "Soil Moduli and Damping Factors for Dynamic Response Analyses." Report EERC-70-10, Earthquake Engineering Research Center, University of California, Berkeley, CA.

Shibuya, S., Hwang, S. C., and Mitachi, T., 1998, "Elastic Shear Modulus of Soft Clays from Shear Wave Velocity Measurement." *Geotechnique*, Vol. 47, No. 3, pp. 593-601.

Shirley, D. J. and Hampton, L. D., 1978, "Shear-Wave Measurement in Laboratory Sediments," *J. Acoust. Soc. Am.*, Vol. 63, No. 2, pp. 607–613.

Simpson, B., Atkinson, J. H., and Jovicˇic´, V., 1996, "The Influence of Anisotropy on Calculations of Ground Settlements above Tunnels," Proceedings, Geotechnical Aspects of Underground Construction in Soft Ground, The City University, London, pp.591–595.

Stark, T. and Eid, H., 1998, "Performance of Three-Dimensional Slope Stability Methods in Practice." J. Geotech. Geoenviron. Eng., 10.1061/(ASCE)1090-0241(1998)124:11(1049), 1049-1060.

Sully, J. P., Campanella, R. G., 1995, "Evaluation of In Situ Anisotropy from Crosshole and Downhole Shear Wave Velocity Measurements", Geotechnique, Vol. 45, No. 2, pp. 267-282.

Tanaka, T., Hirose, D., Kusaka, T. and Nagai, S., 2009, "Characteristics of Seepage Failure of Soil under Various Flow Conditions." In The Nineteenth International Offshore and Polar Engineering Conference. International Society of Offshore and Polar Engineers.

Terzaghi, K., 1943, "Theoretical Soil Mechanics." John Wiley & Sons, New York.

Terzaghi, K., Peck, R.B. & Mesri G. 1996. "Soil Mechanics in Engineering Practice." 3rd Edition, John Wiley & Sons, New York.

Vucetic, M. and Dobry, R., 1991, "Effect of Soil Plasticity on Cyclic Response." Journal of geotechnical engineering, Vol. 117, No. 1, pp.89-107.

Wheeler, S.J. and Sivakumar, V., 1995, "An Elasto-Plastic Critical State Framework for Unsaturated Soil." Géotechnique, Vol. 45, No. 1, pp.35-53.

Yamashita, S., Hori, T., and Suzuki, T., 2005. "Effects of Initial and Induced Anisotropy on Initial Stiffness of Sand by Triaxial and Bender Elements Tests." *Geomechanics*: pp. 350-369. doi: 10.1061/40797(172)20.

Yimsiri, S. and Soga, K., 2002, "A Review of Local Strain Measurement Systems for Triaxial Testing of Soils." Geotechnical Engineering, Vol. 33, pp.43-52.

Zeng, X. and Ni, B., 1999. "Stress-Induced Anisotropic G_{max} of Sands and Its Measurements." *ASCE Journal of Geotechnical and Geoenvironmental Engineering*, Vol. 125, No. 9, pp.741-749.

Zhao, Y., Coffman, R.A., 2016. "Back-Pressure Saturated Constant-Rate-of-Strain Consolidation Device with Bender Elements: Verification of System Compliance." *Journal of Testing and Evaluation*, Vol. 44, No. 6, pp. 1–12, doi:10.1520/JTE20140291.

Zhao, Y., Mahmood, N. S., Coffman, R.A., 2016. "Small-Strain and Large-Strain Modulus Measurements with a Consolidation Device." *Journal of Testing and Evaluation*. (Under review, Manuscript Number: JTE-2016-0331).

CHAPTER 7: Conclusions and Recommendations

7.1. Chapter Overview

Contained in this chapter is 1) a description of the conclusions drawn from the results of the research that is described in this manuscript, and 2) recommendations for further research for BP-CRS-BE testing. Specifically, the conclusions drawn from machine deflection tests performed within the BP-CRS-BE device, that was described in Chapter 4 are discussed in Section 7.2.1. The conclusions drawn from the system compliance for the newly fabricated consolidation device with shear wave measurements, which were described in Chapter 4, are discussed in Section 7.2.2. The conclusions drawn from the BP-CRS-BE tests on Kaolinite soil specimens, which were described in Chapter 5, are discussed in Section 7.2.3. The conclusions regarding the anisotropic soil properties, which were presented in Chapter 6, are discussed in Section 7.2.4. Finally, recommendations for future research are presented in Section 7.3.

7.2. Conclusions of Soil Modulus Measurements from a Consolidation Device

Contained in this section are the conclusions derived from 1) the results of research into the system compliance determination of a newly fabricated consolidation device that collects shear wave velocity measurements by using bender elements, and 2) the soil modulus determination by following the proposed procedures and methods. Conclusions related to machine deflection from the consolidation tests on Kaolinite soil specimens are discussed in Section 7.2.1. Conclusions related to the system compliance determination of the newly fabricated BP-CRS-BE device are documented in Section 7.2.2. Conclusions related to the procedures and methodology for small-strain soil modulus determination are presented in Section 7.2.3. The conclusions related to the obtained anisotropic soil properties are discussed in Section 7.2.4.

7.2.1. *Conclusions Related to Machine Deflection*

The amount of the machine deflection from the consolidation testing equipment was not included in the research of Kang et al. 2014. It was found that the amount of machine deflection must be taken into accounted. For the BP-CRS and BP-CRS-BE devices, the amount of machine deflection accounted for about 20 percent of the deformation of the soil samples. This amount of deformation was in agreement with Ladd and DeGroot 2003. To identify the amount of machine deflection of the consolidation testing equipment, a series tests were performed on an incompressible brass specimen and Kaolinite soil specimens by utilizing a back-pressure constant-rate-of-strain consolidation device with bender elements (BP-CRS-BE). The amounts of the machine deflection of the BP-CRS-BE equipment were found to cause a reduction in the consolidation indices: recompression index (c_r), compression index (C_c), and swell index (C_s) of up to 15, 20, and 26 percent, respectively. Thus, it is highly recommended that the machine deflection be taken into account. Recommendations were provided with the discussion paper that the amount of machine deflection for the floating wall consolidation device that was used by Kang et al. (2014) should be identified and the machine deflection be subtracted from the deformation of the tested soil sample to obtain more accurate values for the various soil parameters. Furthermore, it is recommended that the amount of machine deflection for any consolidation related tests should be identified and taken into accounted when determining soil consolidation parameters. Many researchers utilizing the GEOTAC testing devices are unaware that the amount of machine deflection has not been subtracted from their measurements.

7.2.2. *Conclusions Related to System Compliance Determination*

The newly fabricated BP-CRS-BE device incorporated the bender elements to obtain shear wave velocity measurements. The system compliance of the BP-CRS-BE was required to

be determined due to the modifications and material differences when compare with the traditional BP-CRS device. By performing a series of consolidation tests on a dummy brass specimen and Kaolinite soil specimens, with the BP-CRS and BP-CRS-BE devices, the amounts of machine deflection and the soil parameters were obtained for both the BP-CRS and BP-CRS-BE devices, respectively. The following conclusions were found from the system compliance tests. 1) The two approaches (quick and slow) that were utilized to determine the machine deflection of the consolidation device were identical. The "quick" approach was recommended for the determination of the machine deflection of the consolidation device for a test with one loading-unloading cycle test. However, the "slow" approach was recommended for the determination of the machine deflection for the consolidation device for a test with multiple loading-unloading cycles. 2) The machine deflection values obtained from the two devices were comparable. 3) The use of Delrin® material within the BP-CRS-BE resulted in an increase (11 percent for c_c, and three (3) percent for c_v) in the average values of compression index and coefficient of consolidation as compared to the BP-CRS device. The increase in the consolidation parameters such as the c_c values and the c_v values that were observed from the BP-CRS-BE device were more representative of the field conditions.

7.2.3. *Conclusions Related to Small-Strain Modulus Determination*

The BP-CRS-BE device was fabricated to incorporate bender elements. This fabrication was originally only aimed at obtaining the small-strain modulus values during a consolidation test. Through this fabrication, values of large-strain constrained modulus (M_{CRS}) and small-strain shear modulus ($G_{\max,BE}$) were respectively obtained from CRS consolidation testing and shear wave velocity measurements while the CRS tests were being performed. Within this

document, procedures were proposed to bridge the small-strain modulus to large –strain modulus gap (Chapter 5).

The output of the BP-CRS-BE tests included but was not limited to the following aspects. 1) Establishment of a shear modulus as a function of shear strain including small-strain and large-strain. 2) Determination the soil parameters such as constrained modulus (*M*), small-strain shear modulus ($G_{\max,BE}$), large-strain shear modulus (G), specific volume (v), horizontal effective stress ($\overline{\sigma_h}$), vertical effective stress ($\overline{\sigma_v}$), Poisson's ratio (ν), coefficient of lateral earth pressure (K_0), and drained friction angle (ϕ').

Five observations regarding the testing results on soil specimens were made from the research work that is described herein. 1) The G_{max} values increased with increasing values of vertical effective stress ($\overline{\sigma_v}$) and decreased with increasing values of OCR. 2) The $G_{\max,CRS,p'}$ values that were obtained by utilizing the large-strain BP-CRS-BE device, agreed with the $G_{\max,BE}$ values that were obtained from the bender element measurements within the BP-CRS-BE device. 3) The ν values increased with increasing $\overline{\sigma_v}$ values but decreased with the increasing void ratio (e) values. 4) The K_0 values increased with increasing OCR values. 5) The ϕ' values that were calculated for the soil that was tested within the BP-CRS-BE device, by using the K_0-OCR data that were obtained from the BP-CRS-BE device were in agreement with the ϕ' values that were obtained from modified Mohr-Coulomb diagrams from triaxial tests on the same soil type and stress conditions. Therefore, due to these positive results for the soil type, it is recommended that additional soils be analyzed within the BP-CRS-BE device to confirm that this device can be used for additional applications.

7.2.4. *Conclusions Related to Anisotropic Soil Properties*

The anisotropic soil properties were investigated by using the shear wave measurements from two directions: 1) horizontally propagated and vertically polarized shear waves (HV shear waves), and 2) horizontally propagated and horizontally polarized shear waves (HH shear waves). The HV shear wave velocity measurements and the HH shear wave velocity measurements were obtained from two sets of bender elements within BP-CRS-BE device, and the two sets of bender elements were obtained by placing the bender elements, in the horizontal and vertical directions.

The soil anisotropy properties were investigated from the tests conducted from the BP-CRS-BE device in terms of: 1) soil fabric / soil structure, 2) different soils with similar structure, and 3) sheet arrangement of the various minerals within soil material. The major conclusions are summarized below.

1) The soil fabric / soil structure attributed to soil anisotropy for the soil samples that were prepared by using the same soil material at different water content amounts was investigated. For example, the laboratory prepared kaolinite sample with the slurry water content (w_s) of 50% was flocculated in structure while the slurry with a w_s of 100% kaolinite sample was dispersed. It was observed that the dispersed (w_s=100%) soil sample had higher shear wave velocity than the flocculated (w_s=50%) soil sample. This was due to shorter travel distance for a shear wave in face-to-face contact (dispersed soil structure) structure than the edge-to-face contact (flocculated soil structures) structure.
2) The inherent mineral structure of the different soil types led to different amounts of soil anisotropy. For different soils with a similar initial structure (initial void ratio),

different amounts of anisotropy were observed. For instance, the w_s=50% Kaolinite soil sample and the w_s=75% Illite soil sample were prepared within laboratory to have similar initial void ratio, but the two types of soil samples behaved very differently during. This difference was observed by considering the HV shear wave measurements. The variation within the two types of soils was caused by the mineral structure of the Illite mineral (2:1 sheet) being different than that of the Kaolinite mineral (1:1 sheet).

3) The sheet arrangement of the various minerals when subjected to loading-unloading cycles led to the variation in the amount of hysteresis within the shear wave velocity measurements. For example, the data collected from the Illite mineral (2:1 sheet) possessed more hysteresis in the shear wave velocity measurements than the data collected from the kaolinite mineral (1:1 sheet). Furthermore, the hysteresis was much more significant by using the HH shear wave measurements than the HV shear wave measurements.

7.3. Recommendations for Future Research

Recommendations for Future Research on BP-CRS-BE Testing

The following areas of improvement have been identified to improve the performance of BP-CRS-BE testing.

1. Preparation of soil samples at various water content values, using the slurry consolidometer, is recommended. Further examination and validation of the findings from this research, specifically, that the consolidation behavior of soil is a function of soil fabric structure which is controlled by the water content of the soil can then be evaluated on these soils. Different soil consolidation behaviors, due to the differences in the water

content values are expected. The recommended water content values for Kaolinite soil slurry are 75 percent, 125 percent and 150 percent. These values of water content for the Kaolinite soil will offset the 50 percent and 100 percent water content values that were used in this research work. Moreover, the recommended water content values for Illite soil are 50 percent, 150 percent and 200 percent. These values of water content for the Illite soil will offset the 75 percent water content value that was used in this research work.

2. Image analysis including: X-ray absorption, laser diffraction, and / or electro-resistance particle counting methods are recommended to perform on the soil samples with various water content (Mustafa and Orhan 2015). This is to further examine the relationship between soil fabric structure and water content from a nanoparticle perspective.
3. It is recommended to perform the BP-CRS-BE test on other soil types to investigate the soil behavior variation, and thus to establish a testing database. The recommended soil types are not limited to Donna fill soil, Kaolinite soil with sodium solution, Illite soil with sodium solution, soil with mixed fly ash, and native Shelby tube obtained soil samples, and others.
4. Incorporation of a tactile sensor into CRS device is recommended to obtain the radial stress or horizontal stress from the tactile sensor measurement. This is an alternate method to acquire the coefficient of lateral earth pressure. The tactile obtained measurements can then be used to verify the triaxial/CRS methodology of obtaining the horizontal stress that was presented herein.

5. It is recommended that the BP-CRS-BE device be further modified so that it can house two sets of bender elements, at the same time, to perform HH and HV shear wave measurement within the same soil specimen.

7.4. References

Kang, X., Kang, G.-C., and Bate, B., "Measurement of Stiffness Anisotropy in Kaolinite Using Bender Element Tests in a Floating Wall Consolidometer," *Geotechnical Testing Journal*, Vol. 37, No. 5, 2014 pp. 1-15, doi:10.1520/GTJ20120205. ISSN 0149-6115.

Ladd, C.C., DeGroot, D.J., "Recommended Practice for Soft Ground Site Characterization: Arthur Casagrande Lecture." Proceedings of the 12th Pan American Conference on Soil Mechanics and Geotechnical Engineering, Massachusetts Institute of Technology, Cambridge, Massachusetts, 2003.

Mustafa ÖZ, ORHAN M. "Determination of an Appropriate Method for Dispersion of Soil Samples in Laser Diffraction Particle Size Analyses." *International Journal of Computational and Experimental Science and Engineering*. Vol. 1. No. 1, 2015.

CHAPTER 8: References

Abdoun, T. and Dobry, R., "Evaluation of Pile Foundation Response to Lateral Spreading." Soil Dynamics and Earthquake Engineering, Vol. 22, No. 9, 2002, pp.1051-1058.

American Society for Testing and Materials, "Standard Test Method for One-Dimensional Consolidation Properties of Soils Using Incremental Loading," *Annual Book of ASTM Standards*, Designation *D 2345*, ASTM, West Conshohocken, PA, 2014.

American Society for Testing and Materials, "Standard Test Method for One-Dimensional Consolidation Properties of Saturated Cohesive Soils Using Controlled-Strain Loading," *Annual Book of ASTM Standards, Designation D 4186*, ASTM, West Conshohocken, PA, 2014.

Arroyo, M., Muir Wood, D., and Greening, P. D., "Source Near-field Effects and Pulse Tests in Soil Samples," *Geotechnique*, Vol. 53, No. 3, 2003, pp. 337–345.

Arulnathan, R., Boulanger, R. W., and Riemer, M. F., "Analysis of Bender Element Tests," *Geotech. Test. J.*, Vol. 21, No. 2, 1998, pp. 120-131.

Atkinson, John, "The Mechanics of Soils and Foundations," Taylor & Francis, 2007.

Bauer, G. E., "Dewatering, Hydraulic Failure and Subsequent Analysis of a Sheeted Excavation," International Conference on Case Histories in Geotechnical Engineering. Paper 13, 1984.

Bate, B., Choo, H., Burns, S., "Dynamic Properties of Fine-grained Soils Engineering with a Controlled Organic Phase," Soil Dynamics Earthquake Engineering, Vol. 53, 2013, pp. 176-186.

Becker, D.E., Crooks, J.H.A., Been, K., Jefferies, M.G., "Work as a Criterion for Determining In situ and Yield Stresses in Clays". *Canadian Geotechnical Journal*, Volume 24, 1987, pp. 549-564.

Belardinelli, M. E., M. Cocco, O. Coutant, and F. Cotton, "Redistribution of Dynamic Stress during Coseismic Ruptures: Evidence for Fault Interaction and Earthquake Triggering." Journal of Geophysics. Res., 104(B7), 1999, pp.14925–14945, doi:10.1029/1999JB900094.

Briaud, J.L., "Case Histories in Soil and Rock Erosion: Woodrow Wilson Bridge, Brazos River Meander, Normandy Cliffs, and New Orleans Levees." Journal of Geotechnical and Geoenvironmental Engineering, Vol. 134, No. 10, 2008, pp.1425-1447.

Briaud, J.L., Ting, F.C.K., Chen, H.C., Cao, Y., Han, S.W. and Kwak, K.W., "Erosion Function Apparatus for Scour Rate Predictions." Journal of geotechnical and geoenvironmental engineering, Vol. 127, No. 2, 2001, pp.105-113.

Brignoli, E.G.M., M. Gotti, and K.H. Stokoe, "Measurement of Shear Waves in Laboratory Specimens by Means of Piezoelectric Transducers", *Geotechnical Testing Journal*, 19(4), 1996, pp.384-397.

Brocanelli, D. and Rinaldi, V., "Measurement of Lowstrain Material Damping and Wave Velocity with Bender Elements in the Frequency Domain," *Can. Geotech. J.*, Vol. 35, No. 6, 1998, pp. 1032-1040.

Casagrande, A., "The Determination of Pre-consolidation Load and its Practical Significance". *Proceedings Soil Mechanics and Foundation Engineering*, Volume 3, 1936, pp. 60-64.

Coffman, R.A., Bowders, J.J., Summary of Laboratory Testing Results, Grand Forks, ND. *University of Missouri Institute for Interdisciplinary Geotechnics Final Report*. Client: Burns and McDonnell Engineering, Inc., January, 2009.

Coffman, R.A., Salazar, S.E., Zhao, Y., "Discussion of Measurement of Stiffness Anisotropy in Kaolinite Using Bender Element Tests in Floating Wall Consolidometer by X. Kang, G-C Kang, and B. Bate." *Geotechnical Testing Journal*. Vol. 37, No. 6, 2014, pp. 1-4.

Darendeli, M.B., "Development of a New Family of Normalized Modulus Reduction and Material Damping Curves." *Doctoral Dissertation*, University of Texas, Austin, TX, 2001.

DeGroot, D., "Laboratory Measurement and Interpretation of Soft Clay Mechanical Behavior." Soil Behavior and Soft Ground Construction. 2003, pp. 167-200.

DeGroot, D.J., Poirier, S.E. and Landon, M.M., "Sample Disturbance—Soft Clays." Studia Geotechnica et Mechanica, 27(3-4), 2005, pp.91-105.

Drnevich, V.P., Hardin, B.O., and Shippy, D.J., "Modulus and Damping of Soils by the Resonant Column Method." *In Dynamic geotechnical testing*. Special Technical Publication 654, American Society for Testing and Materials (ASTM), West Conshohocken, Penn.1978, pp. 91–121.

Drnevich, V.P., "Recent Developments in Resonant Column Testing." Richart Commemorative Lectures, Proceedings, ASCE Specialty Session, Detroit, 1985, pp.79-107.

Duncan, J. and Bursey, A., "Soil Modulus Correlations." *Foundation Engineering in the Face of Uncertainty,* 2013, pp. 321-336. doi: 10.1061/9780784412763.026.

Dyvik, R., and Madshus, C., "Lab Measurements of G_{max} Using Bender Elements," Proceedings of the ASCE Convention on Advances in the Art of Testing Soils under Cyclic Conditions, 1986, pp. 186–196.

Dyvik, R. and Olsen, T. S., "G_{max} Measured in Oedometer and DSS Tests Using Bender Elements," *Proceedings, Twelfth International Conference on Soil Mechanics and Foundation Engineering, Rio de Janeiro*, Vol. 1, 1989, pp. 39-42.

El Mohtar, Chadi S., Drnevich, Vincent P., Santagata, Marika, and Bobet, Antonio, "Combined Resonant Column and Cyclic Triaxial Tests for Measuring Undrained Shear Modulus Reduction of Sand With Plastic Fines," *Geotechnical Testing Journal*, Vol. 36, No. 4, 2013, pp. 1-9.

Fam, M., and Santamarina, J. C., "Study of Geoprocesses with Complementary Mechanical and Electromagnetic Wave Measurements in an Oedometer," *Journal* of Geotechnical *Engineering*, Vol. 18, No. 3, 1995, pp. 307–314.

Fam, M., and Santamarina, J. C., "A Study of Consolidation Using Mechanical and Electromagnetic Waves," *Geotechnique*, Vol. 47, No. 2, 1997, pp. 203–219.

Fioravante, V. and Capoferri, R., "On the Use of Multidirectional Piezoelectric Transducers in Triaxial Testing," *Geotech. Test. J.*, Vol. 24, No. 3, 2001, pp. 243-255.

Garner, C.D., Coffman, R.A., "Visible and Near Infrared Diffuse Reflectance Properties of Geotechnical Reference Soils" Geodurma, 2016, Submitted for Review, Manuscript Number: GEODER-15-01244.

Georgiannou, V. N., Hight, D. W., and Burland, J. B., "Behavior of Clayey Sands under Undrained Cyclic Triaxial Loading," *Geotechnique*, Vol. 41, 1991, pp. 383-393.

Ghayoomi, M., "Seismically Induced Settlement of Partially-Saturated Sand," *Ph.D. Dissertation*, University of Colorado, Boulder, Boulder, CO, 2011.

Gray, D.H. and Al-Refeai, T., "Behavior of Fabric-versus Fiber-reinforced Sand." Journal of Geotechnical Engineering, Vol. 112, No. 8, 1986, pp. 804-820.

Gross, S. and Kisslinger, C., "Estimating Tectonic Stress Rate and State with Landers Aftershocks." Journal of Geophysical Research-all series-, 102, 1997, pp.7603-7612.

Hardin, B.O. and Black, W.L., "Vibration Modulus of Normally Consolidated Clay." *ASCE Journal of the Soil Mechanics and Foundation Division*, Vol. 94, No. 2, 1968, pp.353-369.

Hardin, B.O., and Drnervich, V. P., "Shear Modulus and Damping in Soils: Design Equations and Curves." *J. Soil Mech. And Found. Div*., ASCE, Vol. 98, No. 7, 1972a, pp.667-692.

Hardin, B. O., and Drnervich, V. P., "Shear Modulus and Damping in Soils: Measurement and Parameter Effects." *J. Soil Mech. And Found*. Div., ASCE, Vol. 98, No. 6,1972b, pp. 603-624.

Hardin, B.O., "The Nature of Stress Stain Behavior of Soils." *Earthquake Engineering and Soil Dynamics*. ASCE, Vol.1, 1978, pp. 3–90.

Hardin, B.O. and Blandford, G.E., "Elasticity of Particulate Material." *Journal* of Geotechnical *Engineering*, Vol. 115, No. 6, 1989, pp.788–805.

Holzer, T.L., "Preconsolidation Stress of Aquifer Systems." Water Resources Research, 17(3), 1981, pp.693-704.

Isenhower W. M. and Stokoe K. H., "Strain-Rate Dependent Shear Modulus of San Francisco Bay Mud." *International Conferences on Recent Advances in Geotechnical Earthquake Engineering and Soil Dynamics*. Paper 15, 1979.

Ishibashi, I., "Effect of Soil Plasticity on Cyclic Response (Discussion)." *Journal* of *Geotechnical Engineering*, Vol. 118, No. 5, 1992, pp.830-832.

Iwasaki, T., Tatsuoka, F., and Takagi, Y., "Shear Moduli of Sands Under Cyclic Torsional Shear Loading." *Soils and Foundations*, Vol. 18, No. 1, 1978, pp. 39–56.

Jaky, J., "The Coefficient of Earth Pressure at Rest," *J. Soc. Hung. Architects Engineers*, Vol. 7, 1944, pp. 355-358.

Johnson, S. M., "Modeling a Bender Element Test Using Abaqus Finite Element Program." Master's thesis, Massachusetts Institute of Technology, Cambridge, MA, 2001.

Jovicic, V., Coop, M. R., and Simic, M., "Objective Criteria for Determining G_{max} from Bender Element Test," *Geotechnique*, Vol. 46, No. 2, 1996, pp. 357–362.

Jovicic, V., and Coop, M. R. (1998). "The Measurement of Stiffness Anisotropy in Clays with Bender Element Tests in the Triaxial Apparatus." *Geotechnical Testing Journal*, ASTM, Vol. 21, No.1, 1998, pp. 3-10.

Kaiser, P.K., Hewitt, K.J., "The Effect of Ground Water Flow on the Stability and Design of Retained Excavations." Canadian Geotechnical Journal, Vol. l9, 1982, pp. l39-153.

Kang, X., Kang, G.-C., and Bate, B., "Measurement of Stiffness Anisotropy of Kaolinite Using Bender Element Tests in a Floating Wall Consolidometer". *Geotechnical Testing Journal*. ASTM. Vol. 37, No.5. 2014, pp. 1-16.

Kawaguchi, T., Mitachi, T., and Shibuya, S., "Evaluation of Shear Wave Travel Time in Laboratory Bender Element Test," *Proceedings of the 15th International Conference on Soil Mechanics and Geotechanics Engineering*, CRC Press, Boca Raton, FL, 2001, pp. 155-158.

Kokusho, T., "Cyclic Triaxial Test on Dynamic Soil Properties For Wide Strain Range." *Soils Found.*, Vol. 20, No.2, 1980, pp.45–60.

Kuwano, R., Connolly, T.M. and Kuwano, J., "Shear Stiffness Anisotropy Measured by Multi-directional Bender Element Transducers", Proceedings of the International Symposium on Pre-failure deformation characteristics of geomaterials, Torino, Balkema, 1999, pp. 205-212.

Ladd, C.C. and DeGroot, D.J., Invited Paper: "Recommended Practice for Soft Ground Site Characterization," The Arthur Casagrande Lecture, *Proceedings of the 12th Panamerican*

Conference on Soil Mechanics and Geotechnical Engineering, Boston, MA, 2003, pp.3-57.

Ladd, C. C, and Foott, R., "New Design Procedure for Stability of Soft Clays." Journal of Geotechnical Engineering Division," Vol. 100, No. 7, 1974, pp. 763-768.

Ladd, C. C., and Varallyay, J., "The Influence of Stress System on the Behavior of Saturated Clays during Undrained Shear." No. RR-R65-11. Massachusetts Inst of Tech, Cambridge Soil Mechanics Div, 1965.

Landon, M. M., and DeGroot, D. J., "Measurement of Small Strain Shear Modulus Anisotropy on Unconfined Clay Samples Using Bender Elements," Proceedings of GeoCongress 2006, ASCE, 2006.

Landon, M. M., DeGroot, D. J., and Sheahan, T. C., "Nondestructive Sample Quality Assessment of a Soft Clay Using Shear Wave Velocity," *J. Geotech. Geoenviron. Eng.,* Vol. 133, No. 4, 2007, pp. 424–432.

Landon, M. M., "Development of a Non-destructive Sample Quality Assessment Method of Soft Clays," Ph.D. dissertation, University of Massachusetts, Amherst, MA, 2007.

Lee, K.M. and Rowe, R.K., "Deformations Caused by Surface Loading and Tunnelling: the Role of Elastic Anisotropy." Geotechnique, Vol. 39, No. 1, 1989, pp.125-140.

Lee, J.-S., and Santamarina, J. C., "Bender Elements: Performance and Signal Interpretation," *J. Geotech. Geoenviron. Eng*., 2005, pp. 1063–1070.

Lee, C., Lee, J.-S., Lee, W., and Cho, T.-H., "Experiment Setup for Shear Wave and Electrical Resistance Measurements in an Oedometer," *Geotech. Test. J.*, Vol. 31, No. 2, 2008, pp. 149–156.

Liner, Christopher, "Elements of 3-D Seismology," Pennwell, 2nd edition, 2004.

Lings, M. L., Pennington, D. S., and Nash, D. F. T., "Anisotropic Stiffness Parameters and their Measurement in a Stiff Natural Clay," *Géotechnique*, Vol. 50, No. 2, 2000, pp. 109–125.

Lo Presti D.C.F., Jamiolkowski M., Lancellotta R. and Vercelli L., "Maximum Shear Modulus Measurement using Bender Elements in Oedometer Tests", *Rivista Italiana de Geotechnica*, Vol.(XXVII), No. 1, 1993, pp. 5-9.

Lo Presti, D.C.F., Pallara, O., Jamiolkowski, M. and Cavallaro, A., "Anisotropy of Small Strain Stiffness of Undisturbed and Reconstituted Clays", Proceedings of the International Symposium on Pre-failure deformation characteristics of geomaterials, Torino, Balkema, 1999, pp. 3-10.

Mahmood, N. S., and Coffman, R.A., "Investigation of the Effects of Stress Path on the Characterization of Remolded Clay." Journal of Testing and Evaluation. 2016, In preparation.

Marjanovic, J., and Germaine, J.T., "Experimental Study Investigating the Effects of Setup Conditions on Bender Element Velocity Results." *Geotechnical Testing Journal*, Vol. 36, 2013, p. 11, doi: DOI: 10.1520/GTJ20120131.

Mathworks, "MATLAB Programing Environment and Documentation, Version r.14b." The MathWorks, Inc. Natick, MA, 2014.

Mayne, P. W. and Kulhawy, F. H., "K_0-OCR Relationships in Soil," *Journal of the Geotechnical Engineering Division*, Vol. 108, No. GT6, 1982, pp. 851-872.

Meade, R. H., "Removal of Water and Rearrangement of Particles during the Compaction of Clayey Sediments-Review (No. 497-B)." 1964.

Menzies, B.K., "A Computer Controlled Hydraulic Triaxial Testing System." *Advanced Triaxial Testing of Soil and Rock*, ASTM STP 977, Robert T. Donaghe, Ronald C. Chaney, and Marshall L. Silver, Eds., American Society for Testing Materials, Philadelphia, 1988, pp. 82-94.

Mitchell, J.K. and Soga, K., "Fundamentals of Soil Behavior." 2005.

Mohsin, A. K. M. and Airey, D. W., "Automating G_{max} Measurement in Triaxial Tests," *Proceedings of the 3rd International Symposium on the Deformation Characteristics of Geomaterials*, Lyon, France, Sept. 22–24, 2003, pp. 73-80.

Montoya, B.M., Gerhard, R., DeJong, J.T., Weil, M.H., Martinez, B.C., and Pederson, L., "Fabrication, Operation, and Health Monitoring of Bender Elements in Aggressive Environments," *Geotechnical Testing Journal*, Vol.35, No. 5, 2011, pp. 1-15.

Mustafa ÖZ, ORHAN M. "Determination of an Appropriate Method for Dispersion of Soil Samples in Laser Diffraction Particle Size Analyses." *International Journal of Computational and Experimental Science and Engineering*. Vol. 1. No. 1, 2015.

Nash, D.F.T., Lings, M.L., and Pennington, D.S., "The Dependence of Anisotropy G0 Shear Moduli on Void Ratio and Stress State for Reconstituted Gault Clay." Proc., 2nd Int. Symp. on Pre-Failure Deformation Characteristics of Geomaterials, Torino, 1999, pp. 229-238.

Newcomb, D. E., and Birgisson B., "Measuring in Situ Mechanical Properties of Pavement Subgrade Soils." *Transportation Research Record*, Washington, DC: National Academy Press, 1999.

Olson, R. E., "The Shear Strength Properties of Calcium Illite." Geotechnique, Vol. 12, No. 1, 1662, pp.23-43.

Pennington, D. S., Nash, D. F. T., and Lings, M. L., "Anisotropy of G_0 Shear Stiffness in Gault Clay," *Geotechnique*, ol. 47, No. 3, 1997, pp. 391–398.

Pennington, D.S., Nash, D.F.T., and Lings, M.L., "Horizontally Mounted Bender Elements for Measuring Anisotropic Shear Moduli in Triaxial Clay Specimens." *Geotechnical Testing Journal*, Vol. 24, No. 2, 2001, pp.133-144.

Petroski, H., "Design paradigms: Case Histories of Error and Judgment in Engineering." Cambridge University Press, 1994.

Piriyakul, K., "Anisotropic Stress-Strain Behavior of Belgian Boom Clay in the Small Strain Region." Ph.D., Ghent University, 2006.

Poirier, S.E., DeGroot, D.J. and Sheahan, T.C., "Measurement of Suction in a Marine Clay as an Indicator of Sample Disturbance." In Proc. GeoFrontiers Conference, ASCE, Austin, 2005.

Race, M.L., Coffman, R.A., "Effects of Piston Uplift, Piston Friction, and Machine Deflection in Reduced Triaxial Extension Testing." *ASCE Geotechnical Special Publication No. 211, Proc. GeoFrontie*rs 2011: Advances in Geotechnical Engineering, Dallas, Texas, March, 2011, pp. 2649-2658.

Roesler, S. K., "Anisotropic Shear Modulus due to Stress Anisotropy," *J. Geotech. Eng. Div.*, Vol. 105, No. 7, 1979, pp. 871–880.

Roscoe, K. H., Schofield, A., & Wroth, C. P., "On the Yielding of Soils." *Geotechnique*, Vol. 8, No. 1, 1958, pp.22-53.

Sadda, A. S., "Hollow Cylinder Torsional Devices: Their Advantages and Limitation," Advanced Triaxial Testing of Soil and Rock, ASTM STP 997, Philadelphia, PA. 1988, pp.766-779.

Salazar, S.E., Coffman, R.A., "Design and Fabrication of End Platens for Acquisition of Small-Strain Piezoelectric Measurements during Large-Strain Triaxial Extension and Triaxial Compression Testing." *Geotechnical Testing Journal*, Vol. 37, No. 6, 2014, pp. 1-12. doi:10.1520/GTJ20140057.

Salem, M. A., "Stiffness of Unsaturated Compacted Clays at Small Strains," *Ph.D. Dissertation*, Univeristy of Texas at Austin, Austin, TX, 2006.

Sanchez-Salinero, I., Roesset, J. M., and Stokoe, K. H., II, "Analytical Studies of Body Wave Propagation and Attenuation," *Geotechnical Engineering GR86-15*, University of Texas at Austin, September, 1986.

Santamarina, J.C., Klein, A. and Fam, M.A., "Soils and Waves: Particulate Materials Behavior, Characterization and Process Monitoring." Journal of Soils and Sediments, Vol. 1, No. 2, 2001, pp.130-130.

Sawangsuriya, A., Fratta, D., Bosscher, P., and Edil, T, S-Wave Velocity-Stress Power Relationship: Packing and Contact Behavior of Sand Specimens. Advances in Measurement and Modeling of Soil Behavior. 2007, pp. 1-10.

Sasanakul, I., "Development Of An Electromagnetic And Mechanical Model For A Resonant Column And Torsional Testing Device For Soils." Ph.D. Dissertation, The Utah State University, Logan, Utah. 2005.

Schanz, T., Vermeer, P.A. and Bonnier, P.G., "The hardening soil model: formulation and verification." *Beyond 2000 in computational geotechnics*, 1999, pp.281-296.

Schmentmann, J.H., "The Undisturbed Consolidation Behavior of Clay". *ASCE Transactions*, Volume 120, 1955, pp. 1201-1227.

Seed, H.B. & Idriss, I.M., "Soil Moduli and Damping Factors for Dynamic Response Analyses." Report EERC-70-10, Earthquake Engineering Research Center, University of California, Berkeley, CA, 1970.

Seed, H.B., Wong, R.T., Idriss, I.M. & Tokimatsu, K., "Moduli and Damping Factors for Dynamic Analyses of Cohesionless Soils". *Journal of Geotechnical Engineering*, ASCE. Vol. 112, No. 11, 1986, pp.1016-1032.

Sharma, S. and Fahey, M., "Degradation of Stiffness of Cemented Calcareous Soil in Cyclic Triaxial Tests." *J. Geotech. Geoenviron. Eng.*, Vol. 129, No. 7, 2003, pp. 619-629.

Shibuya, S., Hwang, S. C., & Mitachi, T., "Elastic Shear Modulus of Soft Clays from Shear Wave Velocity Measurement." *Geotechnique*, Vol. 47, No. 3, 1998, pp: 593-601.

Shirley, D. J. and Hampton, L. D., "Shear-Wave Measurement in Laboratory Sediments," *J. Acoust. Soc. Am.*, Vol. 63, No. 2, 1978, pp. 607–613.

Simpson, B., Atkinson, J. H., and Jovicˇic´, V., "The Influence of Anisotropy on Calculations of Ground Settlements above Tunnels," Proceedings, Geotechnical Aspects of Underground Construction in Soft Ground, The City University, London, 1996, pp.591–595.

Smith, R., and Wahls, H., "Consolidation under Constant Rates of Strain," *Journal of the Soil Mechanics and Foundations Division*, Vol. 95, No. SM2, 1969, pp. 519–539.

Stark, T. and Eid, H., "Performance of Three-Dimensional Slope Stability Methods in Practice." J. Geotech. Geoenviron. Eng., 10.1061/(ASCE)1090-0241(1998)124:11(1049), 1998, pp. 1049-1060.

Stokoe, K.H., II, Joh, S.H. & Woods, R.D., "Some Contributions of In Situ Geophysical Measurements to Solving Geotechnical Engineering Problems." *2nd International Conference on Site Characterization (ISC-2*), Porto, Portugal, September, 2004.

Strassburger, E., "Use of Piezoelectric Transducers for Stiffness and Density Measurements of Soils," *M.S. Report*, University of Texas at Austin, Austin, TX, 1982.

Sully, J. P., Campanella, R. G., "Evaluation of In Situ Anisotropy from Crosshole and Downhole Shear Wave Velocity Measurements", Geotechnique, Vol. 45, No. 2, 1995, pp. 267-282.

Tanaka, T., Hirose, D., Kusaka, T. and Nagai, S., "Characteristics of Seepage Failure of Soil under Various Flow Conditions." In The Nineteenth International Offshore and Polar Engineering Conference. International Society of Offshore and Polar Engineers, 2009.

Terzaghi, K. T. and O. K. Frohlich, "Theorie der Setzung von Tonschichten," FranzDeuticke, Leipzig, 1936.

Terzaghi, K., "Theoretical soil mechanics." New York: J. Wiley and Sons, Inc, 1943.

Terzaghi, K., Peck, R.B. & Mesri G., "Soil Mechanics in Engineering Practice." 3rd Edition, John Wiley & Sons, New York, 1996.

Trautwein, S., "FW: True Path," Personal Communication, July 3, 2014.

Valle-Molina, C., "Measurements of V_p and V_s in Dry, Unsaturated, and Saturated Sand Specimens with Piezoelectric Transducers," *Ph.D. Dissertation*, University of Texas at Austin, Austin, TX, 2006.

Valle-Molina, C. and Stokoe, K. H., II, "Seismic Measurements in Sand Specimens with Varying Degrees of Saturation Using Piezoelectric Transducers," *Canadian Geotechnical Journal,* Vol. 49, No. 6, 2012, pp. 671–685.

Vecchio, F.J. and Collins, M.P., "The Modified Compression-field Theory for Reinforced Concrete Elements Subjected to Shear." *ACI J.*, Vol. 83, No. 2, 1986, pp.219-231.

Viana da Fonseca, A., Ferreira, C., and Fahey, M., "A Framework Interpreting Bender Element Tests, Combining Time-domain and Frequency-domain Methods," *Geotech. Test. J.*, Vol. 32, No. 2, 2009.

Viggiani, G. and Atkinson, J. H., "Interpretation of Bender Element Tests." *Geotechnique*, Vol. 45, No. 1, 1995, pp. 149-154.

Vucetic, M. & Dobry, R., "Effect of Soil Plasticity on Cyclic Response." *J. Geotech. Eng*., Vol. 117, No. 1, 1991, pp.89-107.

Wheeler, S.J. and Sivakumar, V., "An Elasto-Plastic Critical State Framework for Unsaturated Soil." Géotechnique, Vol. 45, No. 1, 1995, pp.35-53.

Wissa, A., Christain, J., Davis, H., and Heiberg, S., "Consolidation at Constant Rate of Strain," *Journal of the Soil Mechanics and Foundations Division*, Vol. 97, No. SM10, 1971, pp. 1391–1413.

Yamashita,S., Jamiolkowski,M., and Presti,D.C.F., "Stiffness Nonlinearity of Three Sands". *Journal of Geotechnical and Geoenvironmental Engineering*, Vol. 126, No.10, 2001, pp. 929-938.

Yamashita, S., Hori, T., and Suzuki, T., "Effects of Initial and Induced Anisotropy on Initial Stiffness of Sand by Triaxial and Bender Elements Tests." *Geomechanics*: 2005, pp. 350-369. doi: 10.1061/40797(172)20

Yasuhara, K., Murakami, S., Song, B., Yokokawa, S., and Hyde, A., "Postcyclic Degradation of Strength and Stiffness for Low Plasticity Silt." *J. Geotech. Geoenviron. Eng*., 10.1061/(ASCE)1090-0241(2003)129:8(756), 2003, pp. 756-769.

Yimsiri, S., Soga, K., "Application of Micromechanics Model to Study Anisotropy of Soils at Small Strain." *Soil and Foundations*, Vol. 42, 2002, pp. 15-26.

Youn, J. U., Choo, Y. W., & Kim, D. S., "Measurement of Small-Strain Shear Modulus G_{max} of Dry and Saturated Sands By Bender Element, Resonant Column, and Torsional Shear Tests." *Canadian Geotechnical Journal*, Vol. 45, No. 10, 2008, pp.1426-1438.

Zekkos, D., Bray, J. D., & Riemer, M. F., "Shear Modulus and Material Damping of Municipal Solid Waste Based on Large-Scale Cyclic Triaxial Testing." *Canadian Geotechnical Journal*, Vol. 45, No.1, 2008, pp. 45-58.

Zeng, X. and Ni, B., "Stress-Induced Anisotropic G_{max} of Sands and Its Measurements." ASCE *Journal of Geotechnical and Geoenvironmental Engineering*, Vol. 125, No. 9, 1999, pp.741-749.

Zhao, Y. and Coffman, R. A., "Back-Pressure Saturated Constant-Rate-of-Strain Consolidation Device With Bender Elements: Verification of System Compliance," *Journal of Testing and Evaluation*, Vol. 44, No. 6, 2016, pp. 1–12, doi:10.1520/JTE20140291. ISSN 0090-3973.

Zhao, Y., Mahmood, N., and Coffman, R. A., "Small-Strain and Large-Strain Modulus Measurements with a Consolidation Device," *Journal of Testing and Evaluation*, Under Review, Manuscript Number: JTE-2016-0331, 2016.

Zhao, Y. and Coffman, R. A., "Soil Anisotropy Observed During Consolidation Using Bender Elements," *Clay and Clay Minerals*, Under Review, Manuscript Number: CCM-1143, 2016.

APPENDIX A: Consolidation Data

A.1. Chapter Overview

A summary of all the BP-CRS-BE tests is presented in Table A.1. Contained in this appendix are the consolidation curves from CRS tests that were performed by using BP-CRS-BE tests. These consolidation curves are presented as void ratio as a function of vertical effective stress.

Table A.1. A summary of all the BP-CRS-BE tests performed in this research.

Test No.	Soil Type	Testing Date	w_s, [%]	w_i, [%]	CRS Test	BE Testing Type	Comments
T1	Kaolinite	1/15/2015	50	31.04	Loading-unloading	HV shear wave	Good quality of BE testing, slight interference
T2	Kaolinite	2/18/2015	50	31.68	Loading-unloading	HV shear wave	Good quality of BE testing, slight interference
T4	Kaolinite	3/26/2015	50	33.12	Loading-unloading	HV shear wave	Good quality of BE testing, no interference
T3	Kaolinite	5/13/2015	50	32.17	Loading-unloading	HV shear wave	Good quality of BE testing, slight interference
T5	Kaolinite	9/1/2015	50	31.63	Loading-unloading-loading-unloading-loading-unloading	HV shear wave	Good quality of BE testing, slight interference
T6	Kaolinite	9/14/2015	50	30.51	Loading-unloading-loading-unloading-loading-unloading	HV shear wave	Good quality of BE testing, slight interference
T7	Kaolinite	9/29/2015	50	32.63	Loading-unloading-loading-unloading-loading-unloading	HV shear wave	Bad quality of BE testing,strong interference, missing signal for the first loading-unloading cycle
T8	Kaolinite	10/27/2015	50	32.18	Loading-unloading-loading-unloading-loading-unloading	HV shear wave	The quality of BE testing was OK, strong interference
T9	Kaolinite	11/13/2015	100	34.01	Loading-unloading-loading-unloading-loading-unloading	HV shear wave	Bad quality of BE testing,strong interference in third loading-unloading cycle, missing signal for the third loading-unloading cycle
T10	Kaolinite	12/7/2015	100	33.77	Loading-unloading-loading-unloading-loading-unloading	HH shear wave	Perfect quality of BE testing, no interference
T11	Kaolinite	1/24/2016	100	32.16	Loading-unloading-loading-unloading-loading-unloading	HV shear wave	Perfect quality of BE testing, no interference
T12	Illite	1/5/2016	75	43.59	Loading-unloading-loading-unloading	HH shear wave	Perfect quality of BE testing, no interference
T13	Illite	2/24/2016	75	52.47	Loading-unloading-loading-unloading	HV shear wave	Good quality of BE testing, negligible interference
Shelby Tube		4/1/2015	-	34.51	Loading-unloading	HV shear wave	The quality of BE testing was OK, slight to strong interference

Note: w_s and w_i are the water content of slurry consolidometer and the initial water content of soil specimen.

A.2. BP-CRS-BE Consolidation Tests

Included in this section are the consolidation of CRS consolidation curves and data reduction from the BP-CRS-BE tests on Kaolinite soil specimens and Illite soil specimens.

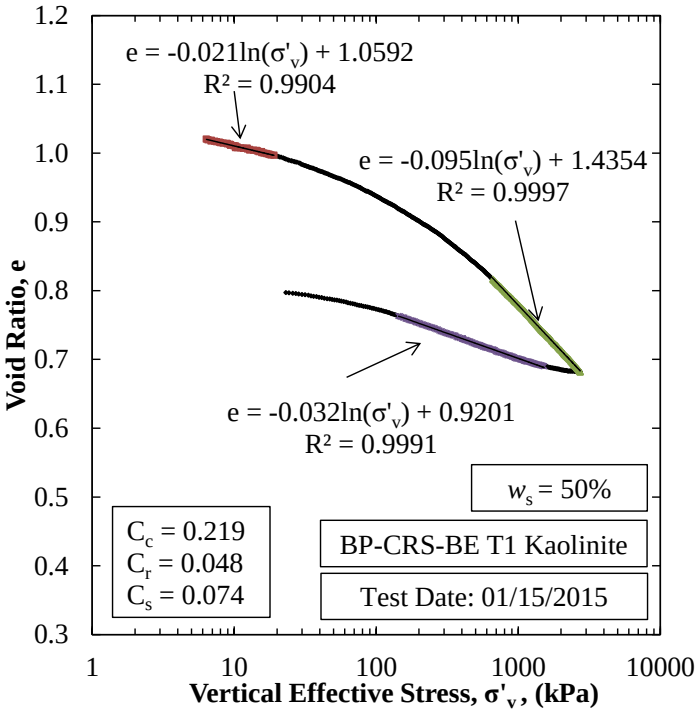

Figure A.1. Void ratio as a function of vertical effective stress for BP-CRS-BE T1 on Kaolinite soil specimen.

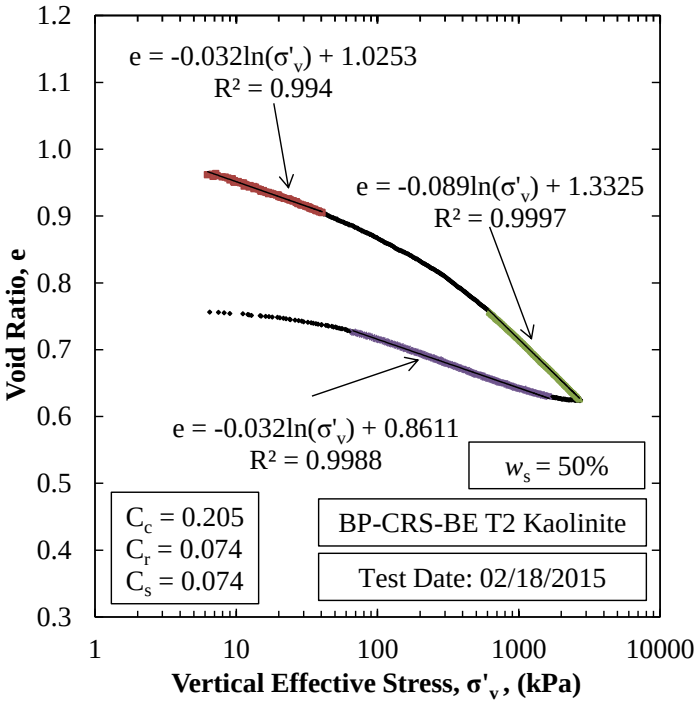

Figure A.2. Void ratio as a function of vertical effective stress for BP-CRS-BE T2 on Kaolinite soil specimen.

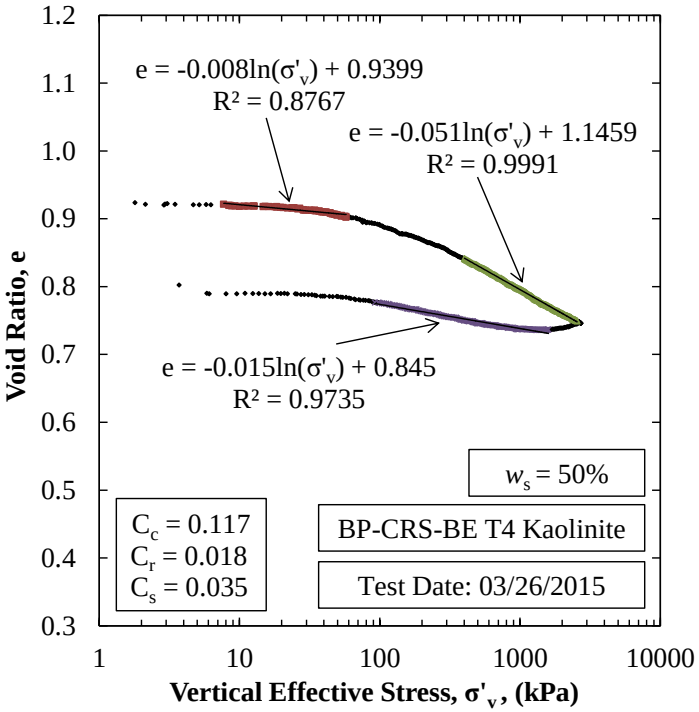

Figure A.3. Void ratio as a function of vertical effective stress for BP-CRS-BE T4 on Kaolinite soil specimen tested on 03/26/2015.

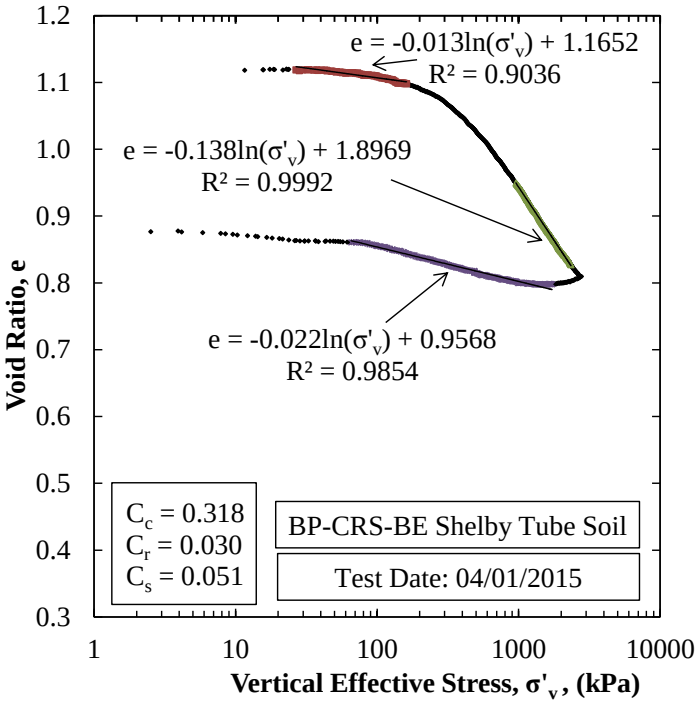

Figure A.4. Void ratio as a function of vertical effective stress for BP-CRS-BE on Shelby tube soil specimen.

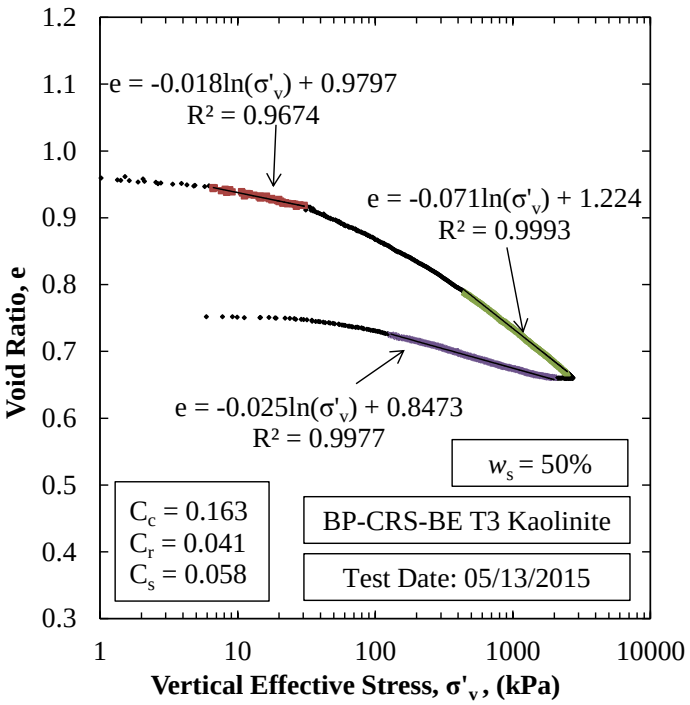

Figure A.5. Void ratio as a function of vertical effective stress for BP-CRS-BE T3 on Kaolinite soil specimen.

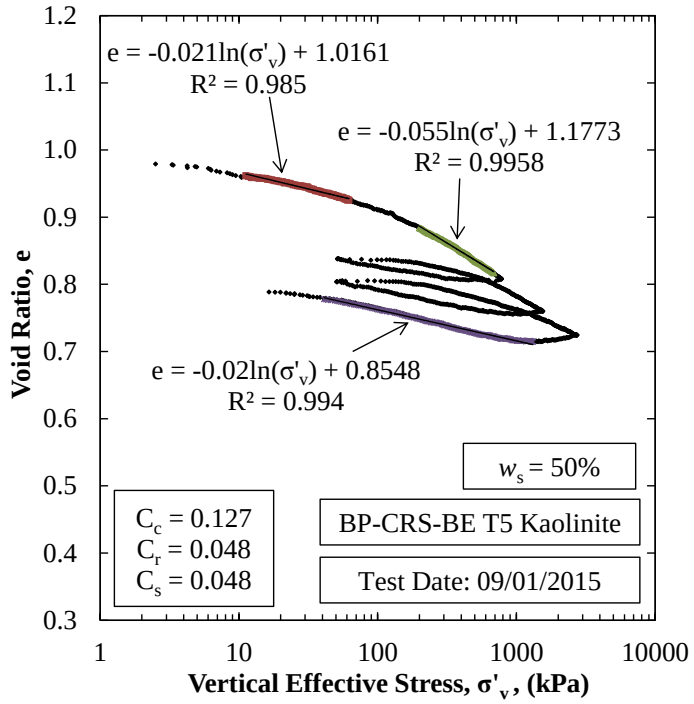

Figure A.6. Void ratio as a function of vertical effective stress for BP-CRS-BE T5 on Kaolinite soil specimen.

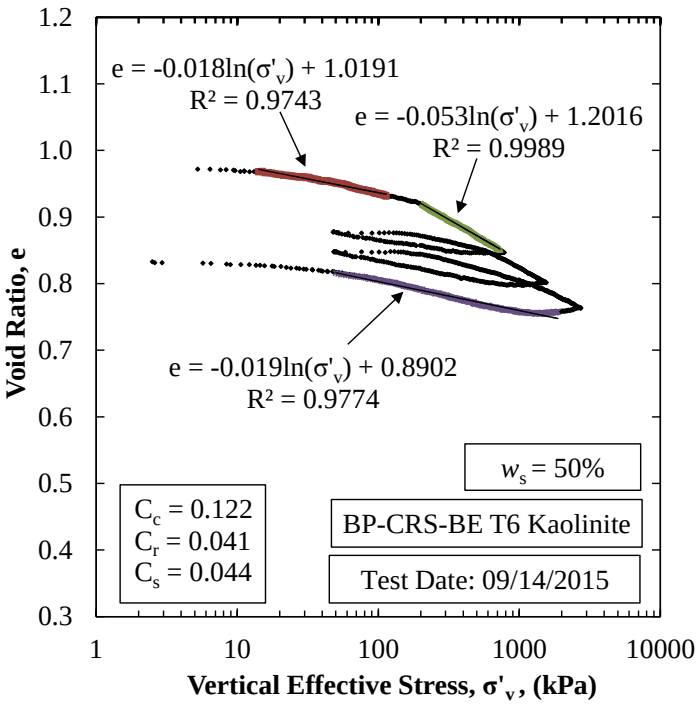

Figure A.7. Void ratio as a function of vertical effective stress for BP-CRS-BE T6 on Kaolinite soil specimen.

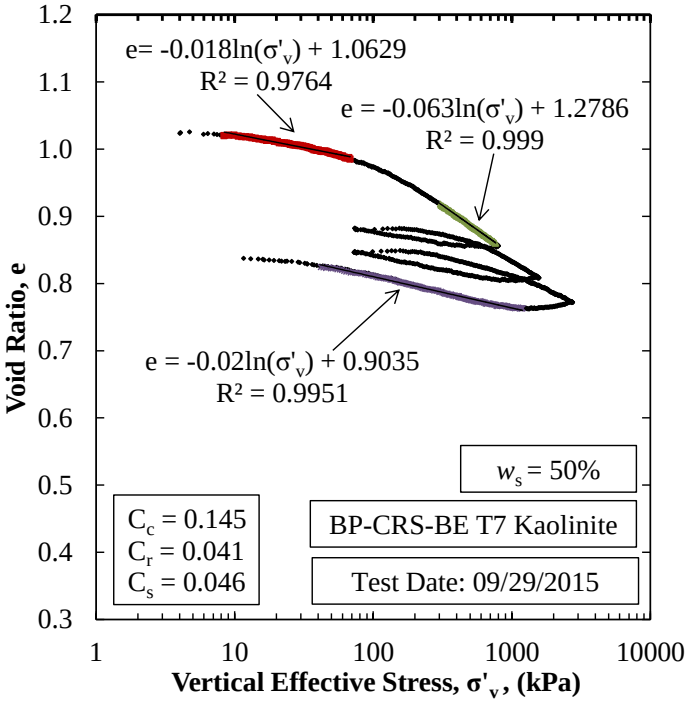

Figure A.8. Void ratio as a function of vertical effective stress for BP-CRS-BE T7 on Kaolinite soil specimen.

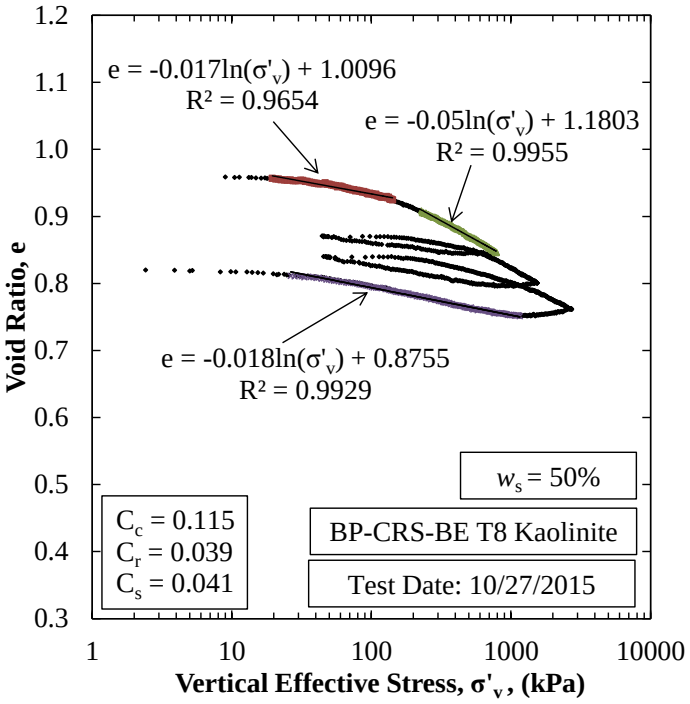

Figure A.9. Void ratio as a function of vertical effective stress for BP-CRS-BE T8 on Kaolinite soil specimen.

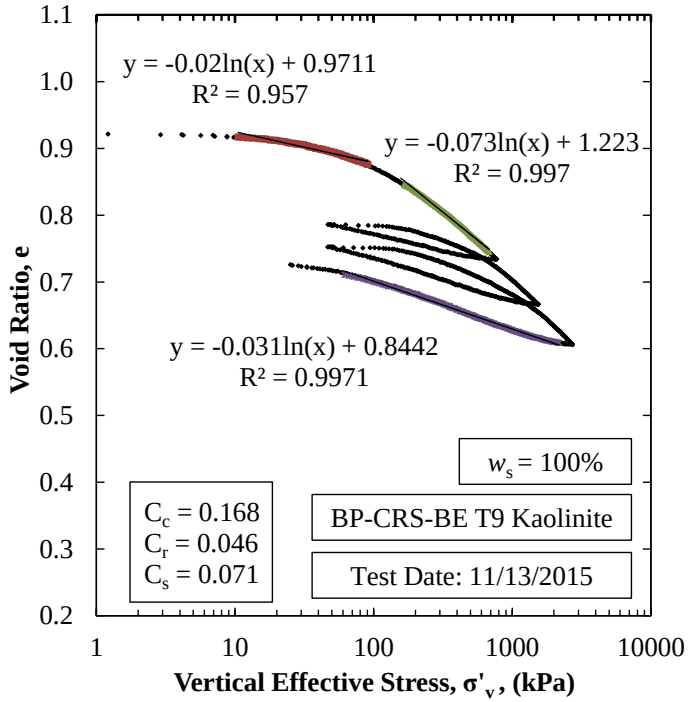

Figure A.10. Void ratio as a function of vertical effective stress for BP-CRS-BE T9 on Kaolinite soil specimen.

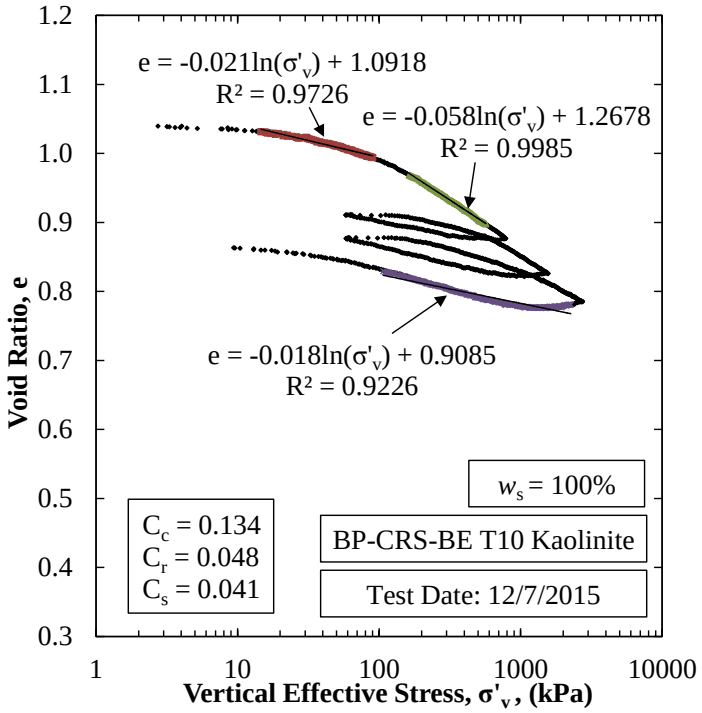

Figure A.11. Void ratio as a function of vertical effective stress for BP-CRS-BE T10 on Kaolinite soil specimen.

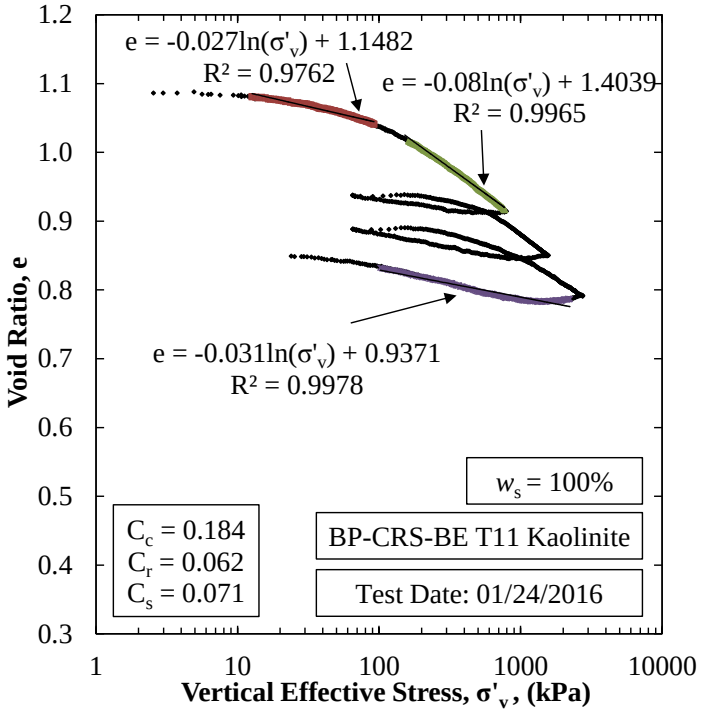

Figure A.12. Void ratio as a function of vertical effective stress for BP-CRS-BE T11 on Kaolinite soil specimen.

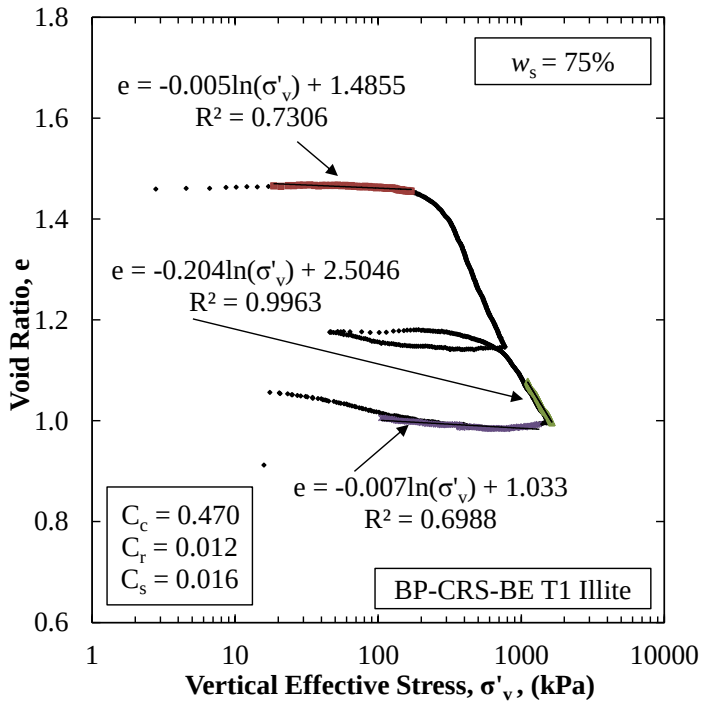

Figure A.13. Void ratio as a function of vertical effective stress for BP-CRS-BE T1 on Illite soil specimen.

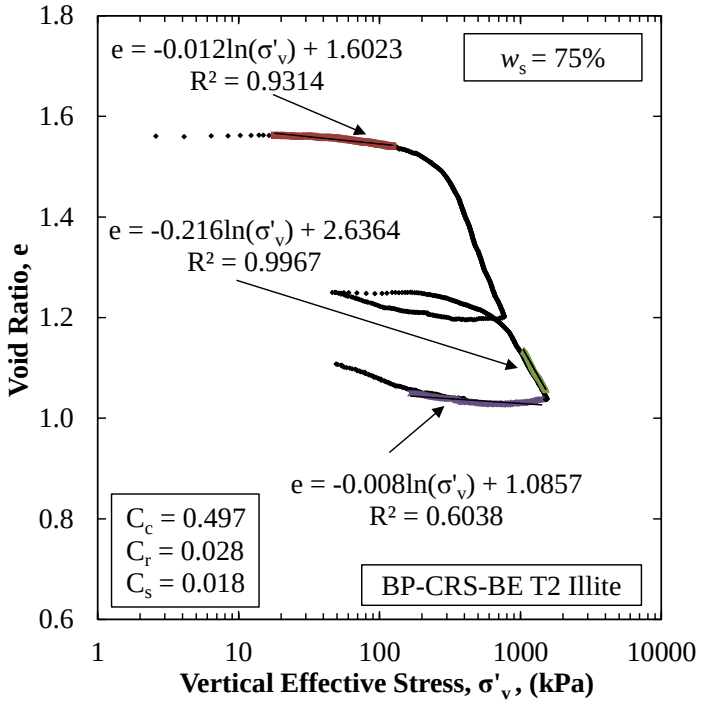

Figure A.14. Void ratio as a function of vertical effective stress for BP-CRS-BE T2 on Illite soil specimen.

Figure A.15. Laboratory prepared Kaolinite sample from a slurry consolidometer at the University of Arkansas.

A.3. References

Casagrande, A., "The Determination of Pre-consolidation Load and its Practical Significance". *Proceedings Soil Mechanics and Foundation Engineering*, Volume 3, 1936, pp. 60-64.

Schmentmann, J.H., "The Undisturbed Consolidation Behavior of Clay". *ASCE Transactions*, Volume 120, 1955, pp. 1201-1227.

APPENDIX B: BE Data

B.1. Chapter Overview

Contained in this appendix are the waterfall plots for the shear wave measurements from the bender element tests performed within BP-CRS-BE device (Appendix B.2). Examples of MATLAB code that was developed to generate the waterfall plots are attached in Appendix B.3.

B.2. BP-CRS-BE Shear Wave Measurements

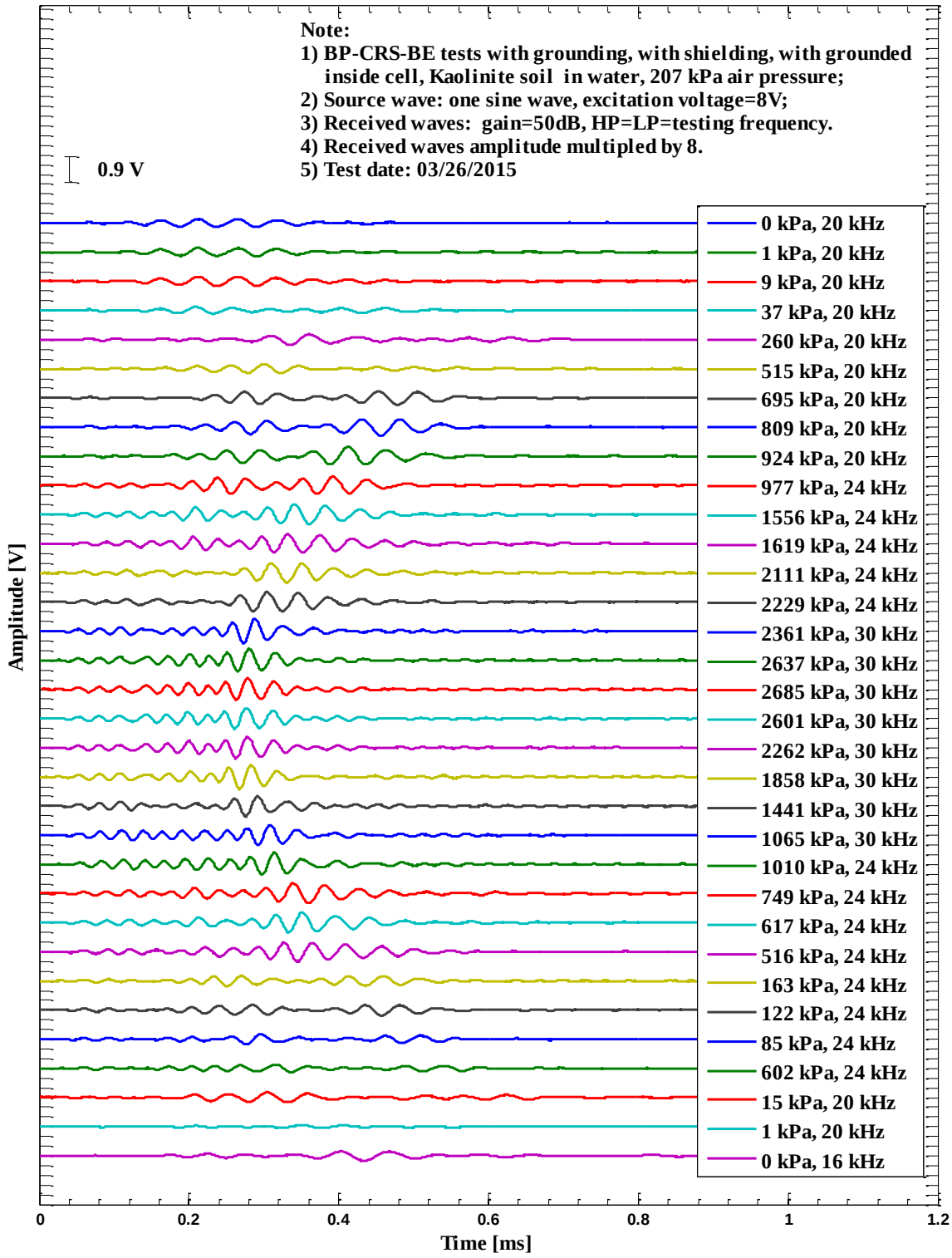

Figure B.1. Waterfall plot of collected shear wave signals of BP-CRS-BE tests on kaolinite soil for determination of Vs (HV) during consolidation tests (oscilloscope collected shear wave signals, test date: 03/26/2015).

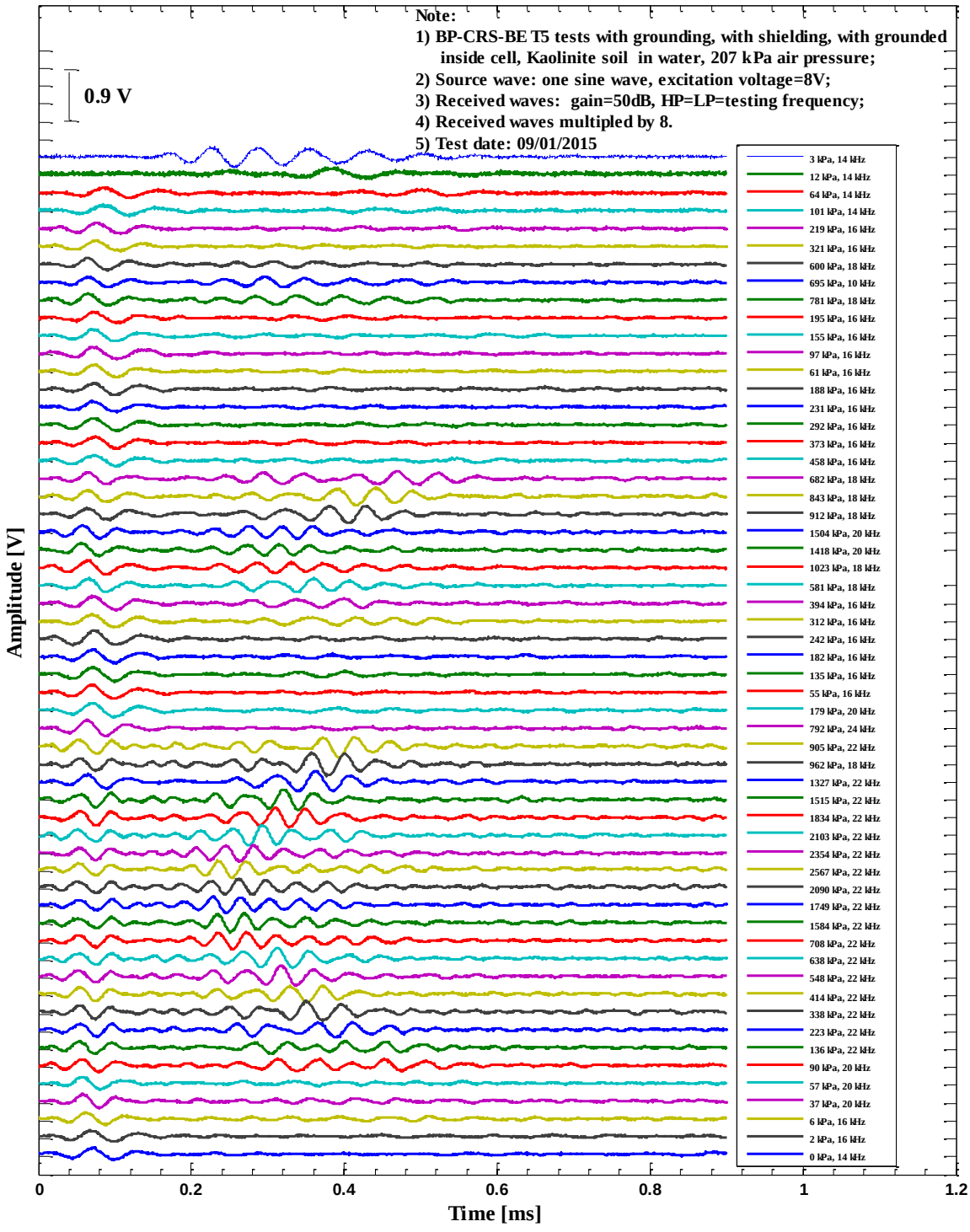

Figure B.2. Waterfall plot of collected shear wave signals of BP-CRS-BE T5 tests on kaolinite soil for determination of Vs (HV) during consolidation tests (oscilloscope collected shear wave signals, test date: 09/01/2015).

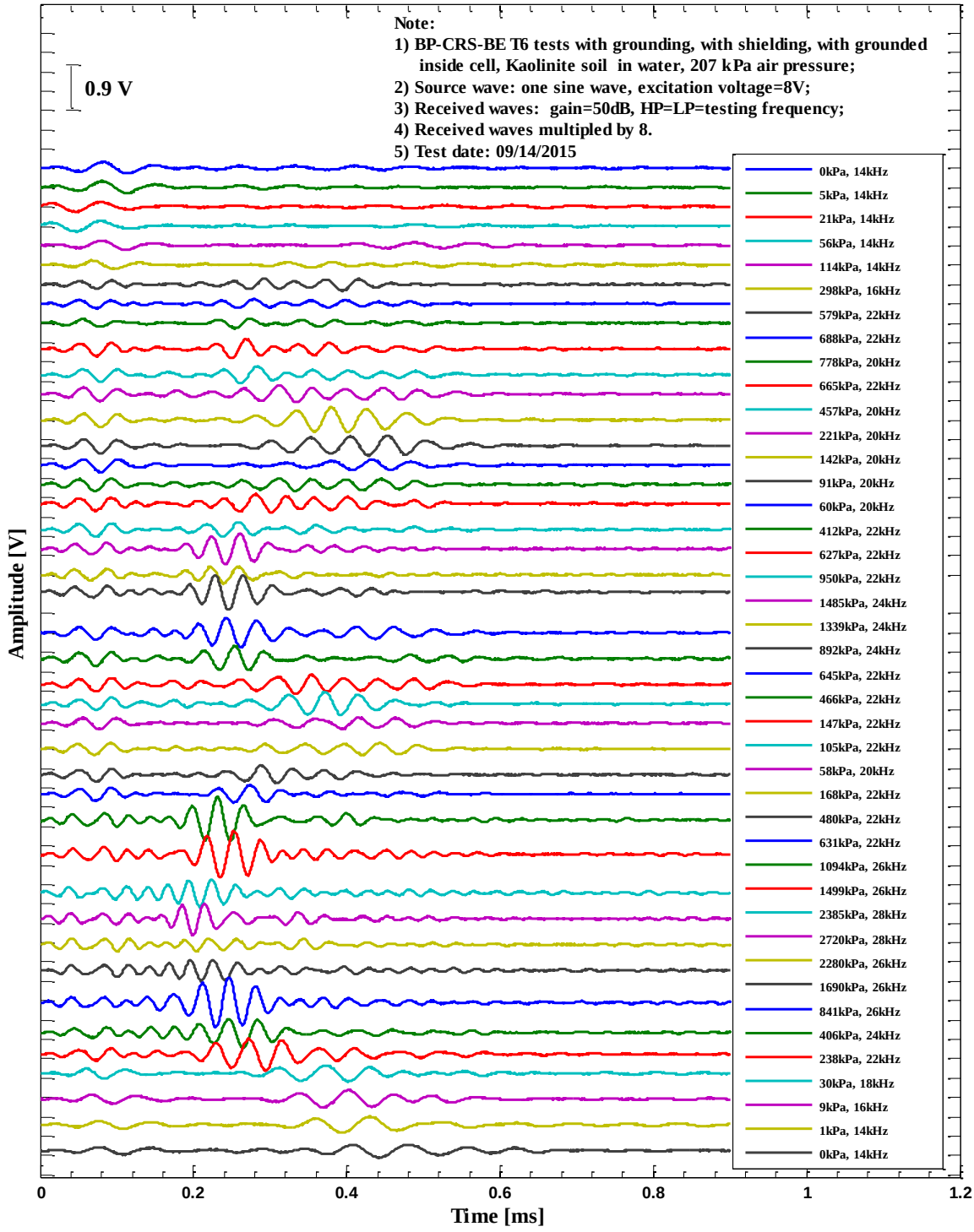

Figure B.3. Waterfall plot of collected shear wave signals of BP-CRS-BE T6 tests on kaolinite soil for determination of Vs (HV) during consolidation tests (oscilloscope collected shear wave signals, test date: 09/14/2015).

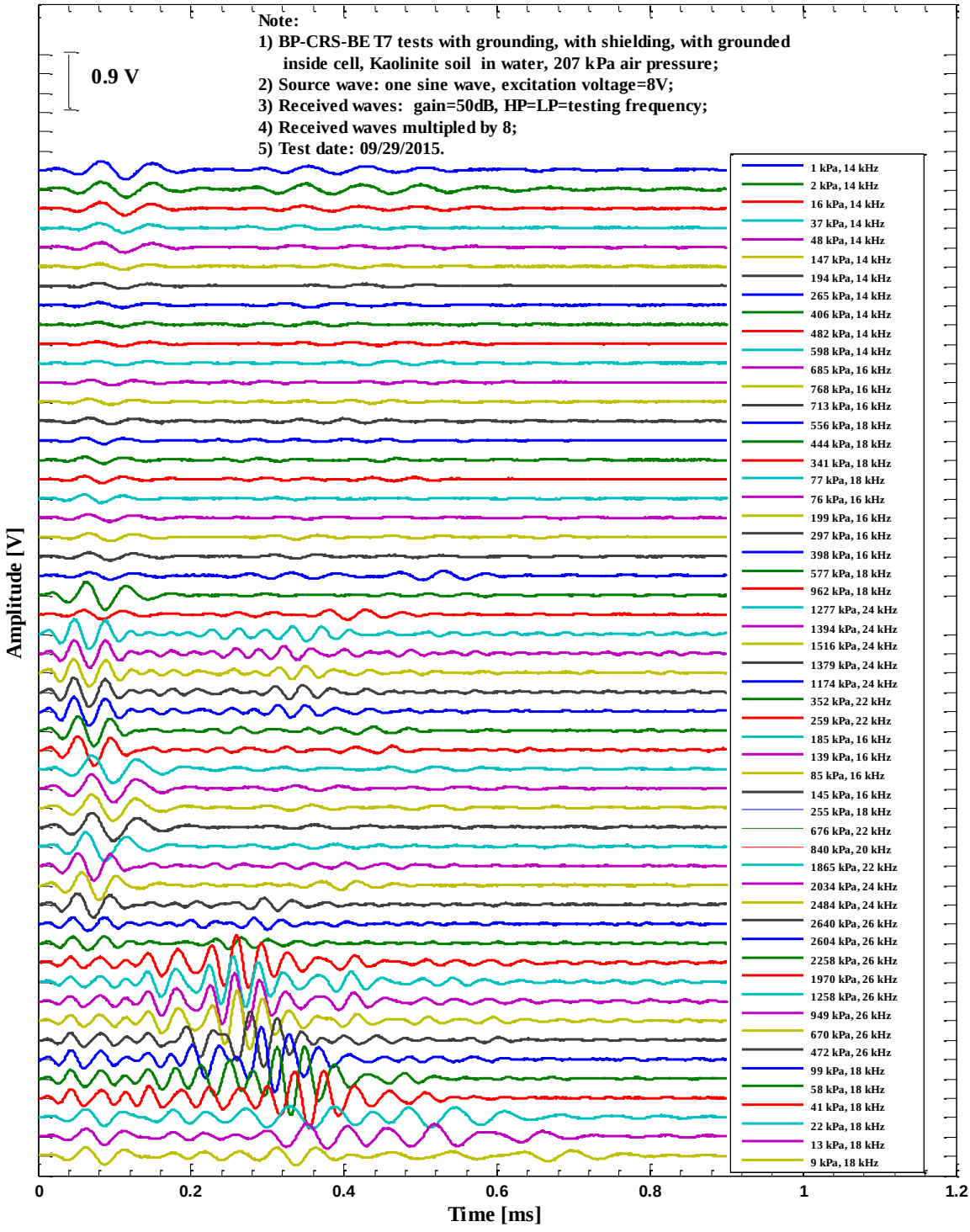

Figure B.4. Waterfall plot of collected shear wave signals of BP-CRS-BE T7 tests on kaolinite soil for determination of Vs (HV) during consolidation tests (oscilloscope collected shear wave signals, test date: 09/29/2015).

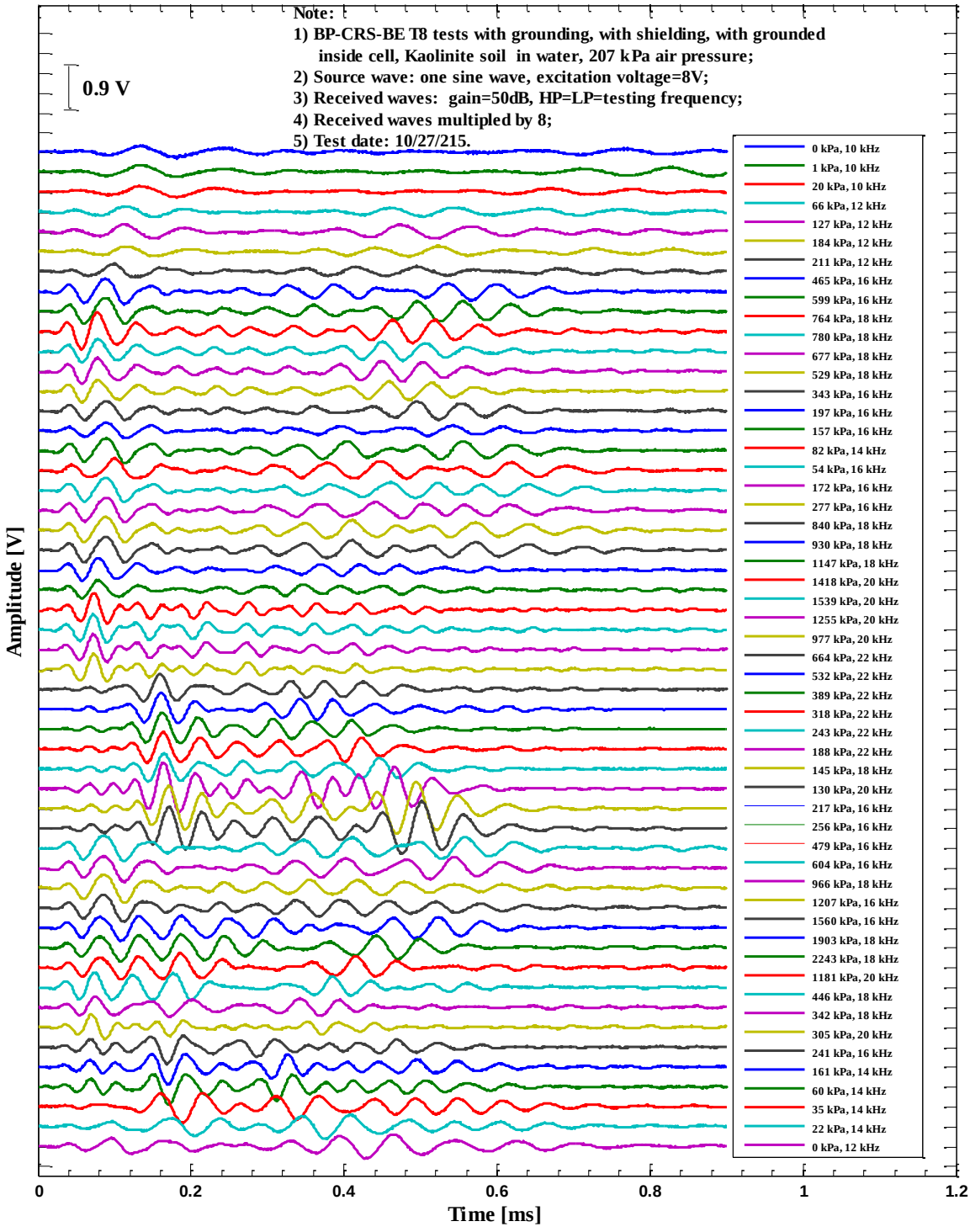

Figure B.5. Waterfall plot of collected shear wave signals of BP-CRS-BE T8 tests on kaolinite soil for determination of Vs (HV) during consolidation tests (oscilloscope collected shear wave signals, test date: 10/27/2015).

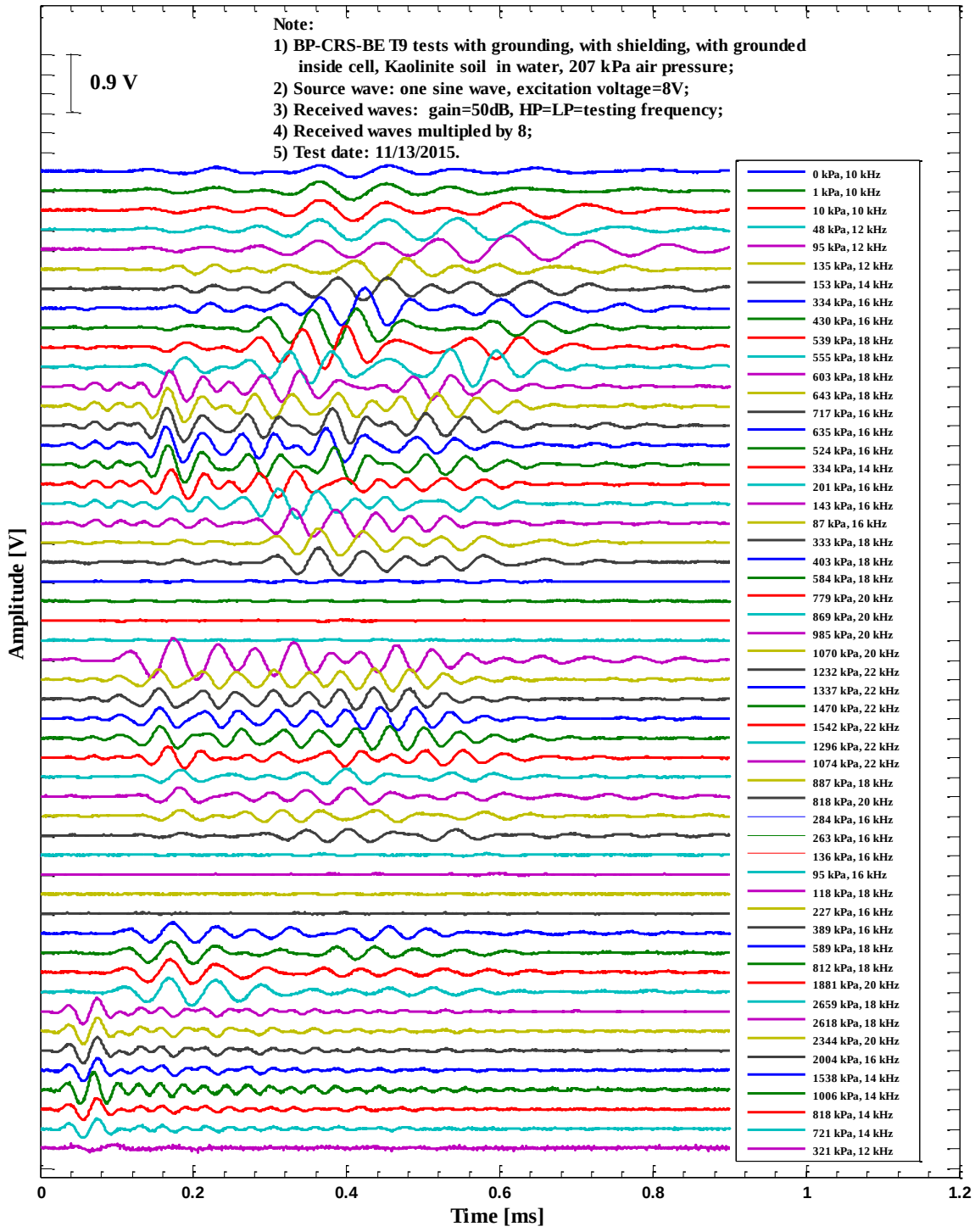

Figure B.6. Waterfall plot of collected shear wave signals of BP-CRS-BE T9 tests on kaolinite soil for determination of Vs (HV) during consolidation tests (oscilloscope collected shear wave signals, test date: 11/13/2015).

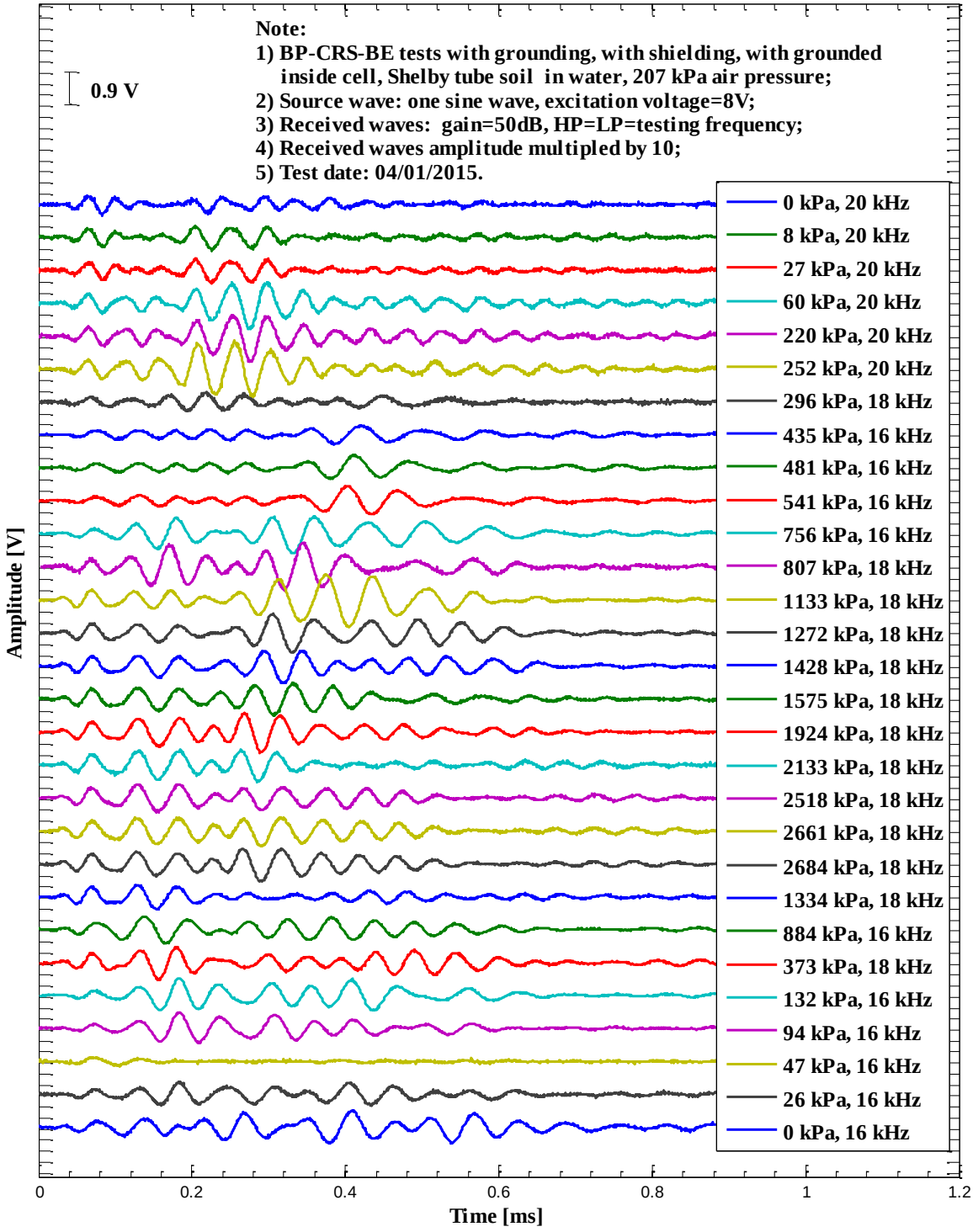

Figure B.7. Waterfall plot of collected shear wave signals of BP-CRS-BE tests on Shelby tube soil for determination of Vs (HV) during consolidation tests (oscilloscope collected shear wave signals, test date: 04/01/2015).

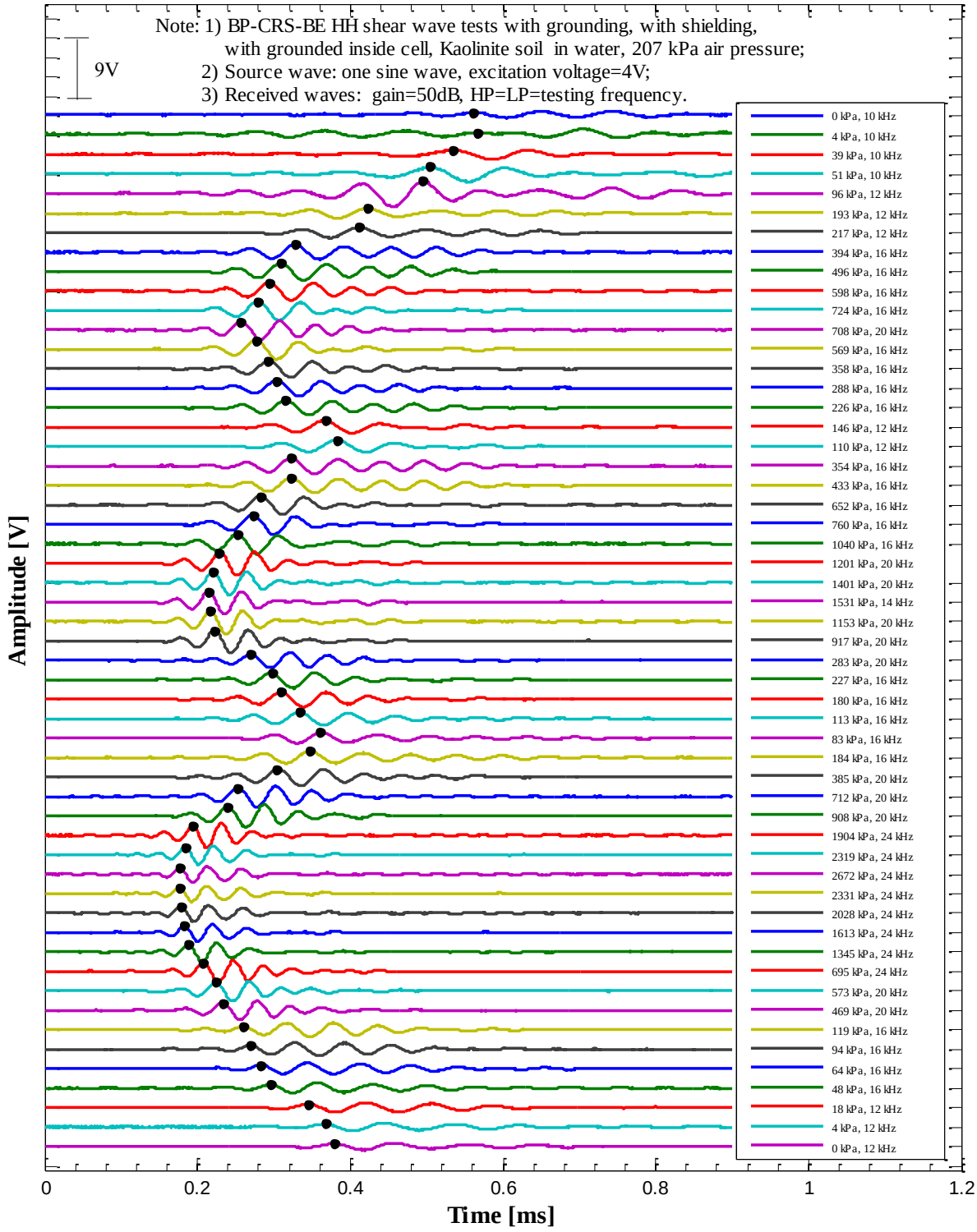

Figure B.8. Waterfall plot of collected shear wave signals of BP-CRS-BE T10 tests on kaolinite soil for determination of Vs (HH) during consolidation tests (oscilloscope collected shear wave signals, test date: 12/07/2015).

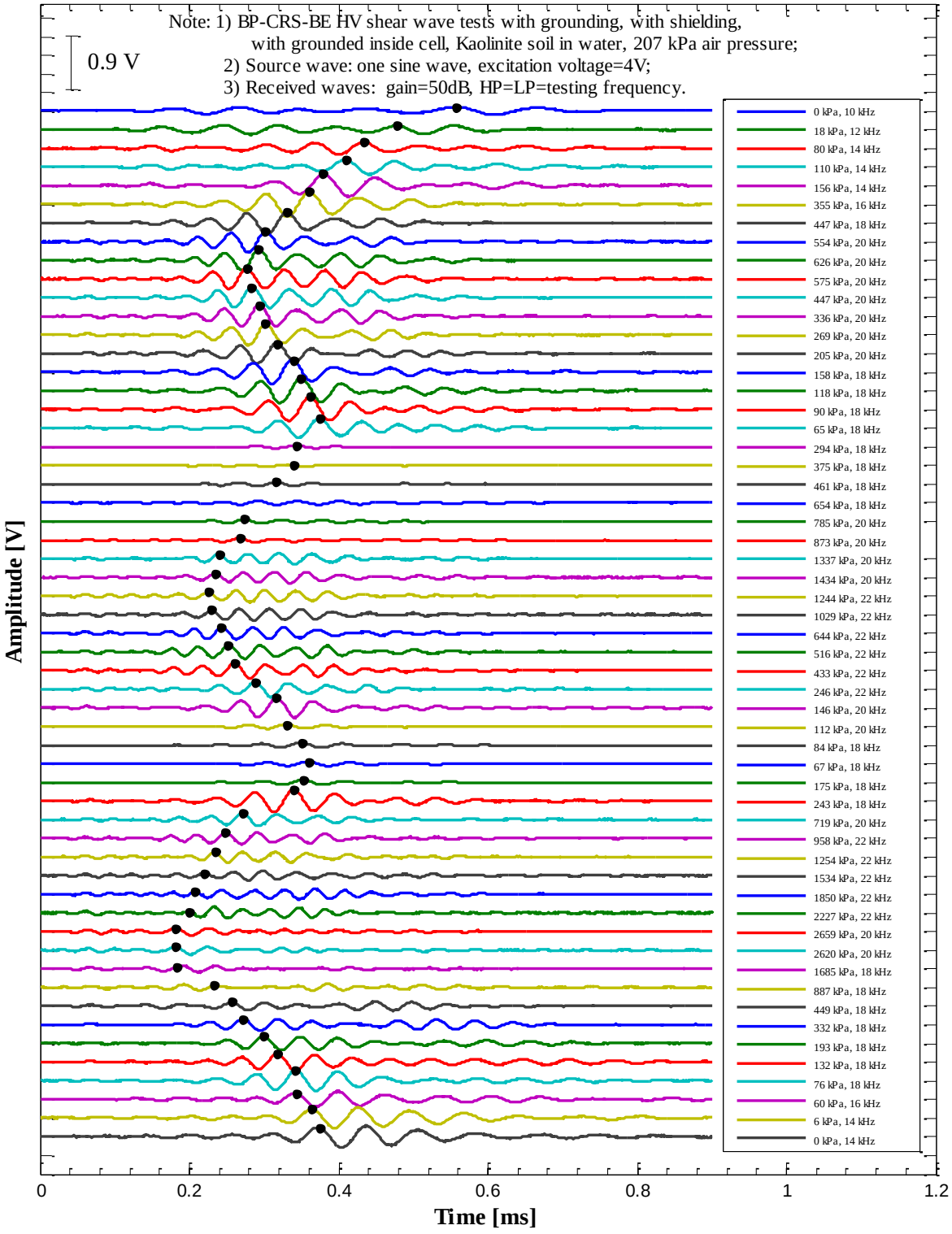

Figure B.9. Waterfall plot of collected shear wave signals of BP-CRS-BE T11 tests on kaolinite soil for determination of Vs (HV) during consolidation tests (oscilloscope collected shear wave signals, test date: 01/24/2016).

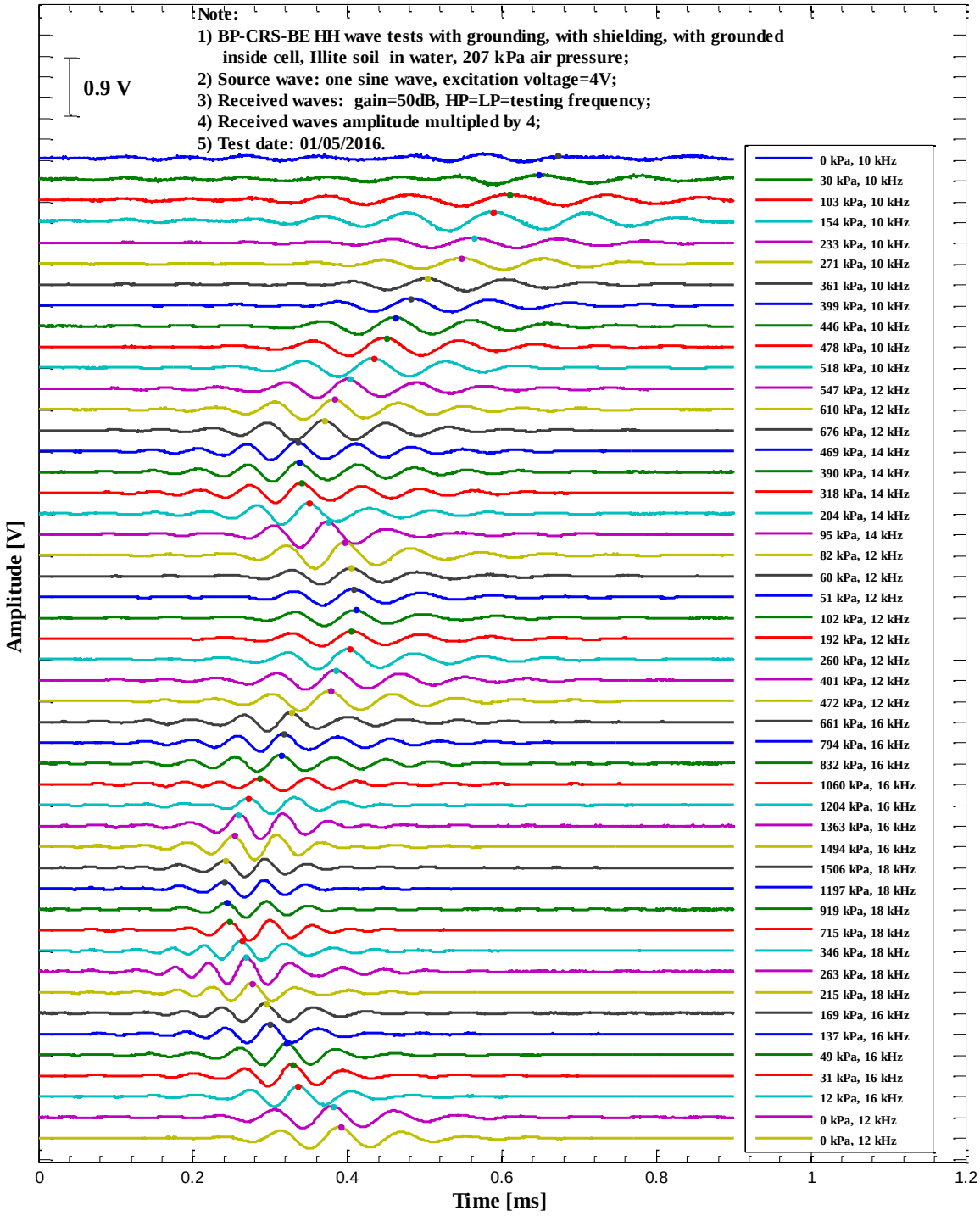

Figure B.10. Waterfall plot of collected shear wave signals of BP-CRS-BE T1 tests on Illite soil for determination of Vs (HH) during consolidation tests (oscilloscope collected shear wave signals, test date: 01/05/2016).

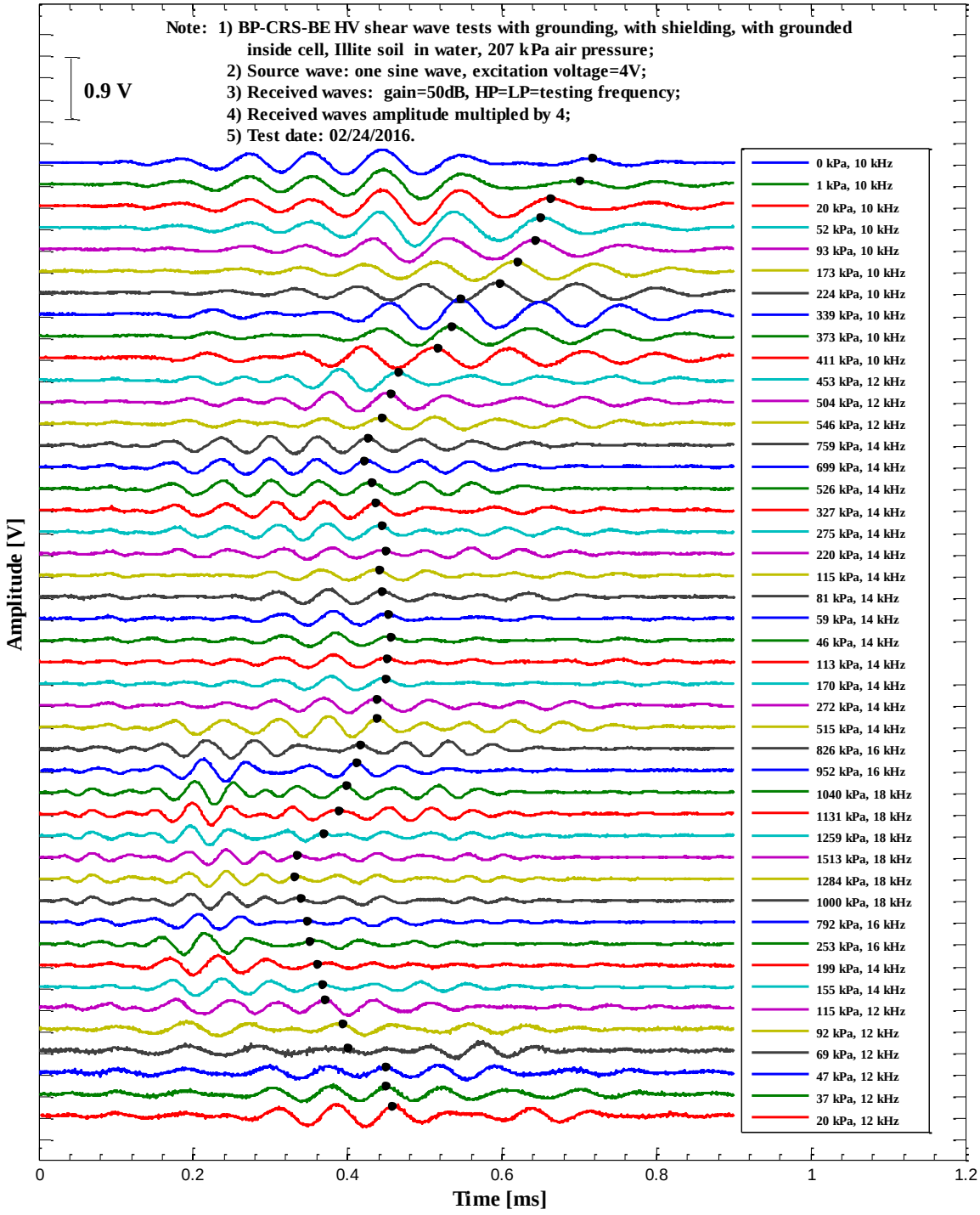

Figure B.11. Waterfall plot of collected shear wave signals of BP-CRS-BE T2 tests on Illite soil for determination of Vs (HV) during consolidation tests (oscilloscope collected shear wave signals, test date: 02/24/2016).

B.3. Example MATLAB Code for Waterfall Plots

```
%%%
```

```
data = xlsread('T1(4).CSV');

data_raw5_4 = data(:,3:4);

data = xlsread('T1(5).CSV');

data_raw5_5 = data(:,3:4);

data_raw2 = (data_raw5_1+data_raw5_2+data_raw5_3+data_raw5_4+data_raw5_5)/5;

% Stress=1795 psf, strain=0.79%

data = xlsread('T1(19).CSV');

data_raw7_1 = data(:,3:4);

data = xlsread('T1(20).CSV');

data_raw7_2 = data(:,3:4);

data = xlsread('T1(21).CSV');

data_raw7_3 = data(:,3:4);

data = xlsread('T1(22).CSV');

data_raw7_4 = data(:,3:4);

data = xlsread('T1(23).CSV');

data_raw7_5 = data(:,3:4);

data_raw3 = (data_raw7_1+data_raw7_2+data_raw7_3+data_raw7_4+data_raw7_5)/5;

% Stress=3331 psf, strain=2.01%

data = xlsread('T1(42).CSV');

data_raw8_1 = data(:,3:4);

data = xlsread('T1(43).CSV');

data_raw8_2 = data(:,3:4);

data = xlsread('T1(44).CSV');
```

```
data_raw8_3 = data(:,3:4);

data = xlsread('T1(45).CSV');

data_raw8_4 = data(:,3:4);

data = xlsread('T1(46).CSV');

data_raw8_5 = data(:,3:4);

data_raw4 = (data_raw8_1+data_raw8_2+data_raw8_3+data_raw8_4+data_raw8_5)/5;

% Stress=4394 psf, strain=2.76%

data = xlsread('T1(61).CSV');

data_raw9_1 = data(:,3:4);

data = xlsread('T1(62).CSV');

data_raw9_2 = data(:,3:4);

data = xlsread('T1(63).CSV');

data_raw9_3 = data(:,3:4);

data = xlsread('T1(64).CSV');

data_raw9_4 = data(:,3:4);

data = xlsread('T1(65).CSV');

data_raw9_5 = data(:,3:4);

data_raw5 = (data_raw9_1+data_raw9_2+data_raw9_3+data_raw9_4+data_raw9_5)/5;

% Stress=6053 psf, strain=4.26%

data = xlsread('T1(73).CSV');

data_raw11_1 = data(:,3:4);

data = xlsread('T1(74).CSV');

data_raw11_2 = data(:,3:4);
```

```
data = xlsread('T1(75).CSV');
data_raw11_3 = data(:,3:4);
data = xlsread('T1(76).CSV');
data_raw11_4 = data(:,3:4);
data = xlsread('T1(77).CSV');
data_raw11_5 = data(:,3:4);
data_raw6 = (data_raw11_1+data_raw11_2+data_raw11_3+data_raw11_4+data_raw11_5)/5;
% Stress=6877 psf, strain=5.22%
data = xlsread('T1(85).CSV');
data_raw12_1 = data(:,3:4);
data = xlsread('T1(86).CSV');
data_raw12_2 = data(:,3:4);
data = xlsread('T1(87).CSV');
data_raw12_3 = data(:,3:4);
data = xlsread('T1(88).CSV');
data_raw12_4 = data(:,3:4);
data = xlsread('T1(89).CSV');
data_raw12_5 = data(:,3:4);
data_raw7 = (data_raw12_1+data_raw12_2+data_raw12_3+data_raw12_4+data_raw12_5)/5;
% Stress=8777 psf, strain=8.28%
data = xlsread('T2(1).CSV');
data_raw13_1 = data(:,3:4);
data = xlsread('T2(2).CSV');
```

```
data_raw13_2 = data(:,3:4);

data = xlsread('T2(3).CSV');

data_raw13_3 = data(:,3:4);

data = xlsread('T2(4).CSV');

data_raw13_4 = data(:,3:4);

data = xlsread('T2(5).CSV');

data_raw13_5 = data(:,3:4);

data_raw8 = (data_raw13_1+data_raw13_2+data_raw13_3+data_raw13_4+data_raw13_5)/5;

% Stress=9549 psf, strain=9.6%----------

data = xlsread('T2(19).CSV');

data_raw14_1 = data(:,3:4);

data = xlsread('T2(20).CSV');

data_raw14_2 = data(:,3:4);

data = xlsread('T2(21).CSV');

data_raw14_3 = data(:,3:4);

data = xlsread('T2(22).CSV');

data_raw14_4 = data(:,3:4);

data = xlsread('T2(23).CSV');

data_raw14_5 = data(:,3:4);

data_raw9 = (data_raw14_1+data_raw14_2+data_raw14_3+data_raw14_4+data_raw14_5)/5;

% Stress=10508 psf, strain=11.23%

data = xlsread('T2(37).CSV');

data_raw15_1 = data(:,3:4);
```

```
data = xlsread('T2(38).CSV');

data_raw15_2 = data(:,3:4);

data = xlsread('T2(39).CSV');

data_raw15_3 = data(:,3:4);

data = xlsread('T2(40).CSV');

data_raw15_4 = data(:,3:4);

data = xlsread('T2(41).CSV');

data_raw15_5 = data(:,3:4);

data_raw10 = (data_raw15_1+data_raw15_2+data_raw15_3+data_raw15_4+data_raw15_5)/5;

% Stress=11177 psf, strain=12.34%

data = xlsread('T2(49).CSV');

data_raw17_1 = data(:,3:4);

data = xlsread('T2(50).CSV');

data_raw17_2 = data(:,3:4);

data = xlsread('T2(51).CSV');

data_raw17_3 = data(:,3:4);

data = xlsread('T2(52).CSV');

data_raw17_4 = data(:,3:4);

data = xlsread('T2(53).CSV');

data_raw17_5 = data(:,3:4);

data_raw11 = (data_raw17_1+data_raw17_2+data_raw17_3+data_raw17_4+data_raw17_5)/5;


% Stress=12033 psf, strain=13.54%
```

```
data = xlsread('T2(67).CSV');
data_raw18_1 = data(:,3:4);
data = xlsread('T2(68).CSV');
data_raw18_2 = data(:,3:4);
data = xlsread('T2(69).CSV');
data_raw18_3 = data(:,3:4);
data = xlsread('T2(70).CSV');
data_raw18_4 = data(:,3:4);
data = xlsread('T2(71).CSV');
data_raw18_5 = data(:,3:4);
data_raw12 = (data_raw18_1+data_raw18_2+data_raw18_3+data_raw18_4+data_raw18_5)/5;
% Stress=12626 psf, strain=14.24%
data = xlsread('T2(85).CSV');
data_raw20_1 = data(:,3:4);
data = xlsread('T2(86).CSV');
data_raw20_2 = data(:,3:4);
data = xlsread('T2(87).CSV');
data_raw20_3 = data(:,3:4);
data = xlsread('T2(88).CSV');
data_raw20_4 = data(:,3:4);
data = xlsread('T2(89).CSV');
data_raw20_5 = data(:,3:4);
data_raw14 = (data_raw20_1+data_raw20_2+data_raw20_3+data_raw20_4+data_raw20_5)/5;
```

```
% Stress=13928 psf, strain=15.81%
data = xlsread('T3(7).CSV');
data_raw21_1 = data(:,3:4);
data = xlsread('T3(8).CSV');
data_raw21_2 = data(:,3:4);
data = xlsread('T3(9).CSV');
data_raw21_3 = data(:,3:4);
data = xlsread('T3(10).CSV');
data_raw21_4 = data(:,3:4);
data = xlsread('T3(11).CSV');
data_raw21_5 = data(:,3:4);
data_raw15 = (data_raw21_1+data_raw21_2+data_raw21_3+data_raw21_4+data_raw21_5)/5;
% Stress=15281 psf, strain=17.13%
data = xlsread('T3(19).CSV');
data_raw22_1 = data(:,3:4);
data = xlsread('T3(20).CSV');
data_raw22_2 = data(:,3:4);
data = xlsread('T3(21).CSV');
data_raw22_3 = data(:,3:4);
data = xlsread('T3(22).CSV');
data_raw22_4 = data(:,3:4);
data = xlsread('T3(23).CSV');
data_raw22_5 = data(:,3:4);
```

```
data_raw16 = (data_raw22_1+data_raw22_2+data_raw22_3+data_raw22_4+data_raw22_5)/5;
% Stress=11257 psf, strain=18.43%
data = xlsread('T3(43).CSV');
data_raw23_1 = data(:,3:4);
data = xlsread('T3(44).CSV');
data_raw23_2 = data(:,3:4);
data = xlsread('T3(45).CSV');
data_raw23_3 = data(:,3:4);
data = xlsread('T3(46).CSV');
data_raw23_4 = data(:,3:4);
data = xlsread('T3(47).CSV');
data_raw23_5 = data(:,3:4);
data_raw17 = (data_raw23_1+data_raw23_2+data_raw23_3+data_raw23_4+data_raw23_5)/5;
% Stress=9639 psf, strain=18.24%
data = xlsread('T3(55).CSV');
data_raw24_1 = data(:,3:4);
data = xlsread('T3(56).CSV');
data_raw24_2 = data(:,3:4);
data = xlsread('T3(57).CSV');
data_raw24_3 = data(:,3:4);
data = xlsread('T3(58).CSV');
data_raw24_4 = data(:,3:4);
data = xlsread('T3(59).CSV');
```

```
data_raw24_5 = data(:,3:4);

data_raw18 = (data_raw24_1+data_raw24_2+data_raw24_3+data_raw24_4+data_raw24_5)/5;

% Stress=7868 psf, strain=17.95%

data = xlsread('T3(73).CSV');

data_raw25_1 = data(:,3:4);

data = xlsread('T3(74).CSV');

data_raw25_2 = data(:,3:4);

data = xlsread('T3(75).CSV');

data_raw25_3 = data(:,3:4);

data = xlsread('T3(76).CSV');

data_raw25_4 = data(:,3:4);

data = xlsread('T3(77).CSV');

data_raw25_5 = data(:,3:4);

data_raw19 = (data_raw25_1+data_raw25_2+data_raw25_3+data_raw25_4+data_raw25_5)/5;

% Stress=5579 psf, strain=17.39%

data = xlsread('T3(85).CSV');

data_raw26_1 = data(:,3:4);

data = xlsread('T3(86).CSV');

data_raw26_2 = data(:,3:4);

data = xlsread('T3(87).CSV');

data_raw26_3 = data(:,3:4);

data = xlsread('T3(88).CSV');

data_raw26_4 = data(:,3:4);
```

```
data = xlsread('T3(89).CSV');

data_raw26_5 = data(:,3:4);

data_raw20 = (data_raw26_1+data_raw26_2+data_raw26_3+data_raw26_4+data_raw26_5)/5;

% Stress=4052 psf, strain=16.82%

data = xlsread('T4(7).CSV');

data_raw27_1 = data(:,3:4);

data = xlsread('T4(8).CSV');

data_raw27_2 = data(:,3:4);

data = xlsread('T4(9).CSV');

data_raw27_3 = data(:,3:4);

data = xlsread('T4(10).CSV');

data_raw27_4 = data(:,3:4);

data = xlsread('T4(11).CSV');

data_raw27_5 = data(:,3:4);

data_raw21 = (data_raw27_1+data_raw27_2+data_raw27_3+data_raw27_4+data_raw27_5)/5;

% Stress=2959 psf, strain=16.16%

data = xlsread('T4(13).CSV');

data_raw28_1 = data(:,3:4);

data = xlsread('T4(14).CSV');

data_raw28_2 = data(:,3:4);

data = xlsread('T4(15).CSV');

data_raw28_3 = data(:,3:4);

data = xlsread('T4(16).CSV');
```

```
data_raw28_4 = data(:,3:4);

data = xlsread('T4(17).CSV');

data_raw28_5 = data(:,3:4);

data_raw22 = (data_raw28_1+data_raw28_2+data_raw28_3+data_raw28_4+data_raw28_5)/5;

% Stress=2468 psf, strain=15.77%

data = xlsread('T4(24).CSV');

data_raw29_1 = data(:,3:4);

data = xlsread('T4(25).CSV');

data_raw29_2 = data(:,3:4);

data = xlsread('T4(26).CSV');

data_raw29_3 = data(:,3:4);

data = xlsread('T4(27).CSV');

data_raw29_4 = data(:,3:4);

data = xlsread('T4(28).CSV');

data_raw29_5 = data(:,3:4);

data_raw23 = (data_raw29_1+data_raw29_2+data_raw29_3+data_raw29_4+data_raw29_5)/5;

% Stress=2288 psf, strain=15.62%

data = xlsread('T4(37).CSV');

data_raw30_1 = data(:,3:4);

data = xlsread('T4(38).CSV');

data_raw30_2 = data(:,3:4);

data = xlsread('T4(39).CSV');

data_raw30_3 = data(:,3:4);
```

```
data = xlsread('T4(40).CSV');

data_raw30_4 = data(:,3:4);

data = xlsread('T4(41).CSV');

data_raw30_5 = data(:,3:4);

data_raw24 = (data_raw30_1+data_raw30_2+data_raw30_3+data_raw30_4+data_raw30_5)/5;

% Stress=3170 psf, strain=15.5%

data = xlsread('T4(49).CSV');

data_raw31_1 = data(:,3:4);

data = xlsread('T4(50).CSV');

data_raw31_2 = data(:,3:4);

data = xlsread('T4(51).CSV');

data_raw31_3 = data(:,3:4);

data = xlsread('T4(52).CSV');

data_raw31_4 = data(:,3:4);

data = xlsread('T4(53).CSV');

data_raw31_5 = data(:,3:4);

data_raw25 = (data_raw31_1+data_raw31_2+data_raw31_3+data_raw31_4+data_raw31_5)/5;

% Stress=5170 psf, strain=15.75%

data = xlsread('T4(61).CSV');

data_raw32_1 = data(:,3:4);

data = xlsread('T4(62).CSV');

data_raw32_2 = data(:,3:4);

data = xlsread('T4(63).CSV');
```

```
data_raw32_3 = data(:,3:4);

data = xlsread('T4(64).CSV');

data_raw32_4 = data(:,3:4);

data = xlsread('T4(65).CSV');

data_raw32_5 = data(:,3:4);

data_raw26 = (data_raw32_1+data_raw32_2+data_raw32_3+data_raw32_4+data_raw32_5)/5;

% Stress=6629 psf, strain=16.16%

data = xlsread('T4(73).CSV');

data_raw33_1 = data(:,3:4);

data = xlsread('T4(74).CSV');

data_raw33_2 = data(:,3:4);

data = xlsread('T4(75).CSV');

data_raw33_3 = data(:,3:4);

data = xlsread('T4(76).CSV');

data_raw33_4 = data(:,3:4);

data = xlsread('T4(77).CSV');

data_raw33_5 = data(:,3:4);

data_raw27 = (data_raw33_1+data_raw33_2+data_raw33_3+data_raw33_4+data_raw33_5)/5;

% Stress=9543 psf, strain=17.06%

data = xlsread('T4(85).CSV');

data_raw34_1 = data(:,3:4);

data = xlsread('T4(86).CSV');

data_raw34_2 = data(:,3:4);
```

```
data = xlsread('T4(87).CSV');

data_raw34_3 = data(:,3:4);

data = xlsread('T4(88).CSV');

data_raw34_4 = data(:,3:4);

data = xlsread('T4(89).CSV');

data_raw34_5 = data(:,3:4);

data_raw28 = (data_raw34_1+data_raw34_2+data_raw34_3+data_raw34_4+data_raw34_5)/5;

% Stress=10944 psf, strain=17.52%

data = xlsread('T5(1).CSV');

data_raw35_1 = data(:,3:4);

data = xlsread('T5(2).CSV');

data_raw35_2 = data(:,3:4);

data = xlsread('T5(3).CSV');

data_raw35_3 = data(:,3:4);

data = xlsread('T5(4).CSV');

data_raw35_4 = data(:,3:4);

data = xlsread('T5(5).CSV');

data_raw35_5 = data(:,3:4);

data_raw29 = (data_raw35_1+data_raw35_2+data_raw35_3+data_raw35_4+data_raw35_5)/5;

% Stress=14865 psf, strain=18.73%

data = xlsread('T5(31).CSV');

data_raw36_1 = data(:,3:4);

data = xlsread('T5(32).CSV');
```

```
data_raw36_2 = data(:,3:4);

data = xlsread('T5(33).CSV');

data_raw36_3 = data(:,3:4);

data = xlsread('T5(34).CSV');

data_raw36_4 = data(:,3:4);

data = xlsread('T5(35).CSV');

data_raw36_5 = data(:,3:4);

data_raw30 = (data_raw36_1+data_raw36_2+data_raw36_3+data_raw36_4+data_raw36_5)/5;

% Stress=17700 psf, strain=19.8%

data = xlsread('T5(49).CSV');

data_raw37_1 = data(:,3:4);

data = xlsread('T5(50).CSV');

data_raw37_2 = data(:,3:4);

data = xlsread('T5(51).CSV');

data_raw37_3 = data(:,3:4);

data = xlsread('T5(52).CSV');

data_raw37_4 = data(:,3:4);

data = xlsread('T5(53).CSV');

data_raw37_5 = data(:,3:4);

data_raw31 = (data_raw37_1+data_raw37_2+data_raw37_3+data_raw37_4+data_raw37_5)/5;

% Stress=18526 psf, strain=20.22%

data = xlsread('T5(61).CSV');

data_raw38_1 = data(:,3:4);
```

```
data = xlsread('T5(62).CSV');

data_raw38_2 = data(:,3:4);

data = xlsread('T5(63).CSV');

data_raw38_3 = data(:,3:4);

data = xlsread('T5(64).CSV');

data_raw38_4 = data(:,3:4);

data = xlsread('T5(65).CSV');

data_raw38_5 = data(:,3:4);

data_raw32 = (data_raw38_1+data_raw38_2+data_raw38_3+data_raw38_4+data_raw38_5)/5;

% Stress=23318 psf, strain=22.87%

data = xlsread('T5(79).CSV');

data_raw39_1 = data(:,3:4);

data = xlsread('T5(80).CSV');

data_raw39_2 = data(:,3:4);

data = xlsread('T5(81).CSV');

data_raw39_3 = data(:,3:4);

data = xlsread('T5(82).CSV');

data_raw39_4 = data(:,3:4);

data = xlsread('T5(83).CSV');

data_raw39_5 = data(:,3:4);

data_raw33 = (data_raw39_1+data_raw39_2+data_raw39_3+data_raw39_4+data_raw39_5)/5;

% Stress=26292 psf, strain=14.23%

data = xlsread('T6(7).CSV');
```

```
data_raw40_1 = data(:,3:4);

data = xlsread('T6(8).CSV');

data_raw40_2 = data(:,3:4);

data = xlsread('T6(9).CSV');

data_raw40_3 = data(:,3:4);

data = xlsread('T6(10).CSV');

data_raw40_4 = data(:,3:4);

data = xlsread('T6(11).CSV');

data_raw40_5 = data(:,3:4);

data_raw34 = (data_raw40_1+data_raw40_2+data_raw40_3+data_raw40_4+data_raw40_5)/5;

% Stress=29625 psf, strain=25.78%

data = xlsread('T6(25).CSV');

data_raw42_1 = data(:,3:4);

data = xlsread('T6(26).CSV');

data_raw42_2 = data(:,3:4);

data = xlsread('T6(27).CSV');

data_raw42_3 = data(:,3:4);

data = xlsread('T6(28).CSV');

data_raw42_4 = data(:,3:4);

data = xlsread('T6(29).CSV');

data_raw42_5 = data(:,3:4);

data_raw36 = (data_raw42_1+data_raw42_2+data_raw42_3+data_raw42_4+data_raw42_5)/5;
```

```
% Stress=32274 psf, strain=26.69%
data = xlsread('T6(43).CSV');
data_raw43_1 = data(:,3:4);
data = xlsread('T6(44).CSV');
data_raw43_2 = data(:,3:4);
data = xlsread('T6(45).CSV');
data_raw43_3 = data(:,3:4);
data = xlsread('T6(46).CSV');
data_raw43_4 = data(:,3:4);
data = xlsread('T6(47).CSV');
data_raw43_5 = data(:,3:4);
data_raw37 = (data_raw43_1+data_raw43_2+data_raw43_3+data_raw43_4+data_raw43_5)/5;
% Stress=33373 psf, strain=27.08%
data = xlsread('T6(61).CSV');
data_raw44_1 = data(:,3:4);
data = xlsread('T6(62).CSV');
data_raw44_2 = data(:,3:4);
data = xlsread('T6(63).CSV');
data_raw44_3 = data(:,3:4);
data = xlsread('T6(64).CSV');
data_raw44_4 = data(:,3:4);
data = xlsread('T6(65).CSV');
data_raw44_5 = data(:,3:4);
```

```
data_raw38 = (data_raw44_1+data_raw44_2+data_raw44_3+data_raw44_4+data_raw44_5)/5;
% Stress=27074 psf, strain=26.85%
data = xlsread('T6(79).CSV');
data_raw45_1 = data(:,3:4);
data = xlsread('T6(80).CSV');
data_raw45_2 = data(:,3:4);
data = xlsread('T6(81).CSV');
data_raw45_3 = data(:,3:4);
data = xlsread('T6(82).CSV');
data_raw45_4 = data(:,3:4);
data = xlsread('T6(83).CSV');
data_raw45_5 = data(:,3:4);
data_raw39 = (data_raw45_1+data_raw45_2+data_raw45_3+data_raw45_4+data_raw45_5)/5;
% Stress=20719 psf, strain=26.47%
data = xlsread('T6(85).CSV');
data_raw46_1 = data(:,3:4);
data = xlsread('T6(86).CSV');
data_raw46_2 = data(:,3:4);
data = xlsread('T6(87).CSV');
data_raw46_3 = data(:,3:4);
data = xlsread('T6(88).CSV');
data_raw46_4 = data(:,3:4);
data = xlsread('T6(89).CSV');
```

```
data_raw46_5 = data(:,3:4);

data_raw40 = (data_raw46_1+data_raw46_2+data_raw46_3+data_raw46_4+data_raw46_5)/5;

% Stress=10362 psf, strain=26.15%

data = xlsread('T7(1).CSV');

data_raw47_1 = data(:,3:4);

data = xlsread('T7(2).CSV');

data_raw47_2 = data(:,3:4);

data = xlsread('T7(3).CSV');

data_raw47_3 = data(:,3:4);

data = xlsread('T7(4).CSV');

data_raw47_4 = data(:,3:4);

data = xlsread('T7(5).CSV');

data_raw47_5 = data(:,3:4);

data_raw41 = (data_raw47_1+data_raw47_2+data_raw47_3+data_raw47_4+data_raw47_5)/5;

% Stress=8619 psf, strain=24.88%

data = xlsread('T7(19).CSV');

data_raw48_1 = data(:,3:4);

data = xlsread('T7(20).CSV');

data_raw48_2 = data(:,3:4);

data = xlsread('T7(21).CSV');

data_raw48_3 = data(:,3:4);

data = xlsread('T7(22).CSV');

data_raw48_4 = data(:,3:4);
```

```
data = xlsread('T7(23).CSV');

data_raw48_5 = data(:,3:4);

data_raw42 = (data_raw48_1+data_raw48_2+data_raw48_3+data_raw48_4+data_raw48_5)/5;

% Stress=6835 psf, strain=24.4%

data = xlsread('T7(37).CSV');

data_raw49_1 = data(:,3:4);

data = xlsread('T7(38).CSV');

data_raw49_2 = data(:,3:4);

data = xlsread('T7(39).CSV');

data_raw49_3 = data(:,3:4);

data = xlsread('T7(40).CSV');

data_raw49_4 = data(:,3:4);

data = xlsread('T7(41).CSV');

data_raw49_5 = data(:,3:4);

data_raw43 = (data_raw49_1+data_raw49_2+data_raw49_3+data_raw49_4+data_raw49_5)/5;

% Stress=5735 psf, strain=24.01%

data = xlsread('T7(49).CSV');

data_raw50_1 = data(:,3:4);

data = xlsread('T7(50).CSV');

data_raw50_2 = data(:,3:4);

data = xlsread('T7(51).CSV');

data_raw50_3 = data(:,3:4);

data = xlsread('T7(52).CSV');
```

```
data_raw50_4 = data(:,3:4);

data = xlsread('T7(53).CSV');

data_raw50_5 = data(:,3:4);

data_raw44 = (data_raw50_1+data_raw50_2+data_raw50_3+data_raw50_4+data_raw50_5)/5;

% Stress=4764 psf, strain=23.56%

data = xlsread('T7(73).CSV');

data_raw51_1 = data(:,3:4);

data = xlsread('T7(74).CSV');

data_raw51_2 = data(:,3:4);

data = xlsread('T7(75).CSV');

data_raw51_3 = data(:,3:4);

data = xlsread('T7(76).CSV');

data_raw51_4 = data(:,3:4);

data = xlsread('T7(77).CSV');

data_raw51_5 = data(:,3:4);

data_raw45 = (data_raw51_1+data_raw51_2+data_raw51_3+data_raw51_4+data_raw51_5)/5;

% Stress=4136 psf, strain=23.23%

data = xlsread('T7(91).CSV');

data_raw52_1 = data(:,3:4);

data = xlsread('T7(92).CSV');

data_raw52_2 = data(:,3:4);

data = xlsread('T7(93).CSV');

data_raw52_3 = data(:,3:4);
```

```
data = xlsread('T7(94).CSV');

data_raw52_4 = data(:,3:4);

data = xlsread('T7(95).CSV');

data_raw52_5 = data(:,3:4);

data_raw46 = (data_raw52_1+data_raw52_2+data_raw52_3+data_raw52_4+data_raw52_5)/5;

% Stress=2187 psf, strain=21.79%

data = xlsread('T8(1).CSV');

data_raw53_1 = data(:,3:4);

data = xlsread('T8(2).CSV');

data_raw53_2 = data(:,3:4);

data = xlsread('T8(3).CSV');

data_raw53_3 = data(:,3:4);

data = xlsread('T8(4).CSV');

data_raw53_4 = data(:,3:4);

data = xlsread('T8(5).CSV');

data_raw53_5 = data(:,3:4);

data_raw47 = (data_raw53_1+data_raw53_2+data_raw53_3+data_raw53_4+data_raw53_5)/5;

% Stress=1781 psf, strain=21.33%

data = xlsread('T8(25).CSV');

data_raw54_1 = data(:,3:4);

data = xlsread('T8(26).CSV');

data_raw54_2 = data(:,3:4);

data = xlsread('T8(27).CSV');
```

```
data_raw54_3 = data(:,3:4);

data = xlsread('T8(28).CSV');

data_raw54_4 = data(:,3:4);

data = xlsread('T8(29).CSV');

data_raw54_5 = data(:,3:4);

data_raw48 = (data_raw54_1+data_raw54_2+data_raw54_3+data_raw54_4+data_raw54_5)/5;

% Stress=1382 psf, strain=20.81%

data = xlsread('T8(43).CSV');

data_raw55_1 = data(:,3:4);

data = xlsread('T8(44).CSV');

data_raw55_2 = data(:,3:4);

data = xlsread('T8(45).CSV');

data_raw55_3 = data(:,3:4);

data = xlsread('T8(46).CSV');

data_raw55_4 = data(:,3:4);

data = xlsread('T8(47).CSV');

data_raw55_5 = data(:,3:4);

data_raw49 = (data_raw55_1+data_raw55_2+data_raw55_3+data_raw55_4+data_raw55_5)/5;

% Stress=834 psf, strain=20.14%

data = xlsread('T8(49).CSV');

data_raw56_1 = data(:,3:4);

data = xlsread('T8(50).CSV');

data_raw56_2 = data(:,3:4);
```

```
data = xlsread('T8(51).CSV');

data_raw56_3 = data(:,3:4);

data = xlsread('T8(52).CSV');

data_raw56_4 = data(:,3:4);

data = xlsread('T8(53).CSV');

data_raw56_5 = data(:,3:4);

data_raw50 = (data_raw56_1+data_raw56_2+data_raw56_3+data_raw56_4+data_raw56_5)/5;

% Stress=502 psf, strain=19.67%

data = xlsread('T8(67).CSV');

data_raw57_1 = data(:,3:4);

data = xlsread('T8(68).CSV');

data_raw57_2 = data(:,3:4);

data = xlsread('T8(69).CSV');

data_raw57_3 = data(:,3:4);

data = xlsread('T8(70).CSV');

data_raw57_4 = data(:,3:4);

data = xlsread('T8(71).CSV');

data_raw57_5 = data(:,3:4);

data_raw51 = (data_raw57_1+data_raw57_2+data_raw57_3+data_raw57_4+data_raw57_5)/5;

%%%%%%%%%%%%%%%%%% Make waterfall plots

clear data


figure1 = figure('units','inches','pos',[0 0 6.5 3.5]);
```

```
set(gcf,'color','w');
%%%----------------------------------Source wave
%subplot1=subplot(5,1,1,'Parent',figure1,'YMinorTick','on',...
%    'XMinorTick','on');
%box(subplot1,'on');
%hold(subplot1,'all');
%plot(data_raw1(:,1)*1000,data_raw1(:,2),'-g')
% Create plot
%ylim([-3 3]);
%xlim([-0.2 1.2]);
%hleg = legend('Source');
%set([hleg],'FontName','Times New Roman','FontSize',12);
% set legend position
%set(hleg,...
%    'Position',[0.771705840455833 0.86216759431045 0.113194444444445
0.0368298368298368]);
%---------------------------------- plot separate components
%%%%%%%%%%%%%%%%%%%%----------tick for figure----------------------
% %subplot(3,1,2);
% subplot1=subplot(5,1,2,'Parent',figure1,'YMinorTick','off','YTickLabel','',...
%     'YTick',[-24 -23.7 -23.4 -23.1 -22.8 -22.5 -22.2 -21.9 -21.6 -21.3 -21 -20.7 -20.4 -20.1 -19.8
-19.5 -19.2 -18.9 -18.6 -18.3 -18 -17.7 -17.4 -17.1 -16.8 -16.5 -16.2 -15.9 -15.6 -15.3 -15 -14.7 -
14.4 -14.1 -13.8 -13.5 -13.2 -12.9 -12.6 -12.3 -12.0 -11.7 -11.4 -11.1 -10.8 -10.5 -10.2 -9.9 -9.6 -
```

9.3 -9 -8.7 -8.4 -8.1 -7.8 -7.5 -7.2 -6.9 -6.6 -6.3 -6 -5.7 -5.4 -5.1 -4.8 -4.5 -4.2 -3.9 -3.6 -3.3 -3 -
2.7 -2.4 -2.1 -1.8 -1.5 -1.2 -0.9 -0.6 -0.3 0 0.3 0.6 0.9 1.2 1.5 1.8 2.1],...

% 'YMinorTick','off',...

% 'XMinorTick','on',...

% 'Position',[0.13 0.0713286713286713 0.775 0.912907781873299]);

% box(subplot1,'on');

% hold(subplot1,'all');

subplot1=subplot(5,1,2,'Parent',figure1,'YMinorTick','off','YTickLabel','',...

  'YTick',[-60.3 -59.4 -58.5 -57.6 -56.7 -55.8 -54.9 -54 -53.1 -52.2 -51.3 -50.4 -49.5 -48.6 -47.7
-46.8 -45.9 -45 -44.1 -43.2 -42.3 -41.4 -40.5 -39.6 -38.7 -37.8 -36.9 -36 -35.1 -34.2 -33.3 -32.4 -
31.5 -30.6 -29.7 -28.8 -27.9 -27 -26.1 -25.2 -24.3 -22.5 -21.6 -20.7 -19.8 -18.9 -18 -17.1 -16.2 -
15.3 -14.4 -13.5 -12.6 -11.7 -10.8 -9.9 -9 -8.1 -7.2 -6.3 -5.4 -4.5 -3.6 -2.7 -1.8 -0.9 0 0.9 1.8
2.7],...

 'YMinorTick','off',...

  'XMinorTick','on',...

  'Position',[0.13 0.0713286713286713 0.775 0.912907781873299]);

box(subplot1,'on');

hold(subplot1,'all');

% plot(data_raw2(:,1)*1000,data_raw2(:,2)*8-2.7,data_raw3(:,1)*1000,data_raw3(:,2)*8-
3.6,data_raw4(:,1)*1000,data_raw4(:,2)*8-4.5,data_raw5(:,1)*1000,data_raw5(:,2)*8-
5.4,data_raw6(:,1)*1000,data_raw6(:,2)*8-6.3,data_raw7(:,1)*1000,data_raw7(:,2)*8-
7.2,data_raw8(:,1)*1000,data_raw8(:,2)*8-8.1,data_raw9(:,1)*1000,data_raw9(:,2)*8-
9.0,data_raw10(:,1)*1000,data_raw10(:,2)*8-9.9,data_raw11(:,1)*1000,data_raw11(:,2)*8-

10.8,data_raw12(:,1)*1000,data_raw12(:,2)*8-11.7,data_raw13(:,1)*1000,data_raw13(:,2)*8-12.6,data_raw14(:,1)*1000,data_raw14(:,2)*8-13.5,data_raw15(:,1)*1000,data_raw15(:,2)*8-14.4,data_raw16(:,1)*1000,data_raw16(:,2)*8-15.3,data_raw17(:,1)*1000,data_raw17(:,2)*8-16.2,data_raw18(:,1)*1000,data_raw18(:,2)*8-17.1,data_raw19(:,1)*1000,data_raw19(:,2)*8-18,data_raw20(:,1)*1000,data_raw20(:,2)*8-18.9,data_raw21(:,1)*1000,data_raw21(:,2)*8-19.8,data_raw21(:,1)*1000,data_raw21(:,2)*8-20.7,data_raw23(:,1)*1000,data_raw23(:,2)*8-21.6,data_raw24(:,1)*1000,data_raw24(:,2)*8-22.5,data_raw25(:,1)*1000,data_raw25(:,2)*8-23.4,data_raw26(:,1)*1000,data_raw26(:,2)*8-24.3,data_raw27(:,1)*1000,data_raw27(:,2)*8-25.2,data_raw28(:,1)*1000,data_raw28(:,2)*8-26.1,data_raw29(:,1)*1000,data_raw29(:,2)*8-27,data_raw30(:,1)*1000,data_raw30(:,2)*8-27.9,data_raw31(:,1)*1000,data_raw31(:,2)*8-28.8,data_raw32(:,1)*1000,data_raw32(:,2)*8-29.7,data_raw33(:,1)*1000,data_raw33(:,2)*8-30.6,data_raw34(:,1)*1000,data_raw34(:,2)*8-31.5,data_raw35(:,1)*1000,data_raw35(:,2)*8-32.4,data_raw36(:,1)*1000,data_raw36(:,2)*8-33.3,data_raw37(:,1)*1000,data_raw37(:,2)*8-34.2,data_raw38(:,1)*1000,data_raw38(:,2)*8-35.1,data_raw39(:,1)*1000,data_raw39(:,2)*8-36,data_raw37(:,1)*1000,data_raw37(:,2)*8-34.2,data_raw38(:,1)*1000,data_raw38(:,2)*8-35.1,data_raw39(:,1)*1000,data_raw39(:,2)*8-36,data_raw40(:,1)*1000,data_raw40(:,2)*8-36.9,data_raw41(:,1)*1000,data_raw41(:,2)*8-37.8,data_raw42(:,1)*1000,data_raw42(:,2)*8-38.7,data_raw43(:,1)*1000,data_raw43(:,2)*8-39.6,data_raw44(:,1)*1000,data_raw44(:,2)*8-40.5,data_raw45(:,1)*1000,data_raw45(:,2)*8-41.4,data_raw46(:,1)*1000,data_raw46(:,2)*8-42.3,data_raw47(:,1)*1000,data_raw47(:,2)*8-43.2,data_raw48(:,1)*1000,data_raw48(:,2)*8-44.1,data_raw49(:,1)*1000,data_raw49(:,2)*8-45,data_raw50(:,1)*1000,data_raw50(:,2)*8-45.9,data_raw51(:,1)*1000,data_raw51(:,2)*8-46.8,data_raw52(:,1)*1000,data_raw52(:,2)*8-47.7,data_raw53(:,1)*1000,data_raw53(:,2)*8-48.6,data_raw54(:,1)*1000,data_raw54(:,2)*8-

```
49.5,data_raw55(:,1)*1000,data_raw55(:,2)*8-50.4,data_raw56(:,1)*1000,data_raw56(:,2)*8-
51.3,data_raw57(:,1)*1000,data_raw57(:,2)*8-52.2,data_raw58(:,1)*1000,data_raw58(:,2)*8-
53.1,data_raw59(:,1)*1000,data_raw59(:,2)*8-54)
a=4;     % Multipled by the strong signal,   01/10/2016
b=1;     % Multipled by the weak signal.
c=3;     % Only for the first FOUR curves. Modified and added on 01/10/2016
d=1;     % Only for the 3-5 curves. Modified and added on 01/10/2016
e=3;     % Only for data of 19,20,21,22,23,  33,34,35,36.  Modified on 01/10/2016
f=0.4;   % Only for data of 19,20,  33.  Modified on 01/10/2016
g=3;     % Only for data of 26,  37,40,43.  Modified on 01/11/2016
h=0.5;   % Only for data of  37,43.  Modified on 01/11/2016
hh=plot(data_raw2(:,1)*1000,data_raw2(:,2)*a*c-2.7,data_raw3(:,1)*1000,data_raw3(:,2)*a*c-
3.6,data_raw4(:,1)*1000,data_raw4(:,2)*a*c*d-4.5,data_raw5(:,1)*1000,data_raw5(:,2)*a*c*d-
5.4,data_raw6(:,1)*1000,data_raw6(:,2)*a*d-6.3,data_raw7(:,1)*1000,data_raw7(:,2)*a-
7.2,data_raw8(:,1)*1000,data_raw8(:,2)*a-8.1,data_raw9(:,1)*1000,data_raw9(:,2)*a-
9.0,data_raw10(:,1)*1000,data_raw10(:,2)*a-9.9,data_raw11(:,1)*1000,data_raw11(:,2)*a-
10.8,data_raw12(:,1)*1000,data_raw12(:,2)*a-11.7,data_raw14(:,1)*1000,data_raw14(:,2)*a-
12.6,data_raw15(:,1)*1000,data_raw15(:,2)*a-13.5,data_raw16(:,1)*1000,data_raw16(:,2)*a-
14.4,data_raw17(:,1)*1000,data_raw17(:,2)*a-15.3,data_raw18(:,1)*1000,data_raw18(:,2)*a-
16.2,data_raw19(:,1)*1000,data_raw19(:,2)*a-17.1,data_raw20(:,1)*1000,data_raw20(:,2)*a-
18,data_raw21(:,1)*1000,data_raw21(:,2)*a*e*f/10-
18.9,data_raw22(:,1)*1000,(data_raw22(:,2)/10)*a*e*f-
19.8,data_raw23(:,1)*1000,data_raw23(:,2)*b*e-
```

```
20.7,data_raw24(:,1)*1000,data_raw24(:,2)*b*e-
21.6,data_raw25(:,1)*1000,data_raw25(:,2)*b*e-
22.5,data_raw26(:,1)*1000,data_raw26(:,2)*b*g-23.4,data_raw27(:,1)*1000,data_raw27(:,2)*a-
24.3,data_raw28(:,1)*1000,data_raw28(:,2)*a-25.2,data_raw29(:,1)*1000,data_raw29(:,2)*a-
26.1,data_raw30(:,1)*1000,data_raw30(:,2)*a-27,data_raw31(:,1)*1000,data_raw31(:,2)*a-
27.9,data_raw32(:,1)*1000,data_raw32(:,2)*a-28.8,data_raw33(:,1)*1000,data_raw33(:,2)*a-
29.7,data_raw34(:,1)*1000,data_raw34(:,2)*a-
30.6,data_raw36(:,1)*1000,data_raw36(:,2)*a*e*f-
31.5,data_raw37(:,1)*1000,data_raw37(:,2)*b*e*g*h-
32.4,data_raw38(:,1)*1000,data_raw38(:,2)*b*e-
33.3,data_raw39(:,1)*1000,data_raw39(:,2)*b*e-
34.2,data_raw40(:,1)*1000,data_raw40(:,2)*b*g-35.1,data_raw41(:,1)*1000,data_raw41(:,2)*a-
36,data_raw42(:,1)*1000,data_raw42(:,2)*a-36.9,data_raw43(:,1)*1000,data_raw43(:,2)*a*g*h-
37.8,data_raw44(:,1)*1000,data_raw44(:,2)*a-38.7,data_raw45(:,1)*1000,data_raw45(:,2)*a-
39.6,data_raw46(:,1)*1000,data_raw46(:,2)*a-40.5,data_raw47(:,1)*1000,data_raw47(:,2)*a-
41.4,data_raw48(:,1)*1000,data_raw48(:,2)*a-42.3,data_raw49(:,1)*1000,data_raw49(:,2)*a-
43.2,data_raw50(:,1)*1000,data_raw50(:,2)*a-44.1,data_raw51(:,1)*1000,data_raw51(:,2)*a-
45);
ylim([-46 2.5]);
xlim([0 1.2]);
%set(gca,'XMinorTick','on','YMinorTick','on')
set(hh,'LineWidth',1.5)
```

```
hleg = legend('0 kPa, 10 kHz','30 kPa, 10 kHz','103 kPa, 10 kHz','154 kPa, 10 kHz','233 kPa, 10
kHz','271 kPa, 10 kHz','361 kPa, 10 kHz','399 kPa, 10 kHz','446 kPa, 10 kHz','478 kPa, 10
kHz','518 kPa, 10 kHz','547 kPa, 12 kHz','610 kPa, 12 kHz','676 kPa, 12 kHz','469 kPa, 14
kHz','390 kPa, 14 kHz','318 kPa, 14 kHz','204 kPa, 14 kHz','95 kPa, 14 kHz','82 kPa, 12 kHz','60
kPa, 12 kHz','51 kPa, 12 kHz','102 kPa, 12 kHz','192 kPa, 12 kHz','260 kPa, 12 kHz','401 kPa, 12
kHz','472 kPa, 12 kHz','661 kPa, 16 kHz','794 kPa, 16 kHz','832 kPa, 16 kHz','1060 kPa, 16
kHz','1204 kPa, 16 kHz','1363 kPa, 16 kHz','1494 kPa, 16 kHz','1506 kPa, 18 kHz','1197 kPa, 18
kHz','919 kPa, 18 kHz','715 kPa, 18 kHz','346 kPa, 18 kHz','263 kPa, 18 kHz','215 kPa, 18
kHz','169 kPa, 16 kHz','137 kPa, 16 kHz','49 kPa, 16 kHz','31 kPa, 16 kHz','12 kPa, 16 kHz','0
kPa, 12 kHz','0 kPa, 12 kHz');
set([hleg],'FontName','Times New Roman','FontSize',7.5);
% set legend position
set(hleg,...
    'Position',[0.714358885112275 0.0896708286038593 0.161842105263158
0.707150964812713],...
    'FontSize',7.5,...
   'FontName','Times New Roman');
% Create ylabel and xlabel
% Create xlabel
xlabel('Time [ms]','FontWeight','bold','FontSize',12,...
   'FontName','Times New Roman');
% Create ylabel
ylabel('Amplitude [V]','FontWeight','bold','FontSize',12,...
```

```
    'FontName','Times New Roman');
% Below is the code from MATLAB to be used to create dashed lines
% Create line
annotation(figure1,'line',[0.151966173996635 0.162382840663302],...
    [0.902905569208222 0.902905569208222],'LineWidth',1);
% Create textbox
annotation(figure1,'textbox',...
    [0.223926619915686 0.867286684273214 0.552304894792054 0.117350966764192],...
    'String',{'Note:','1) BP-CRS-BE tests with grounding, with shielding, with grounded','     inside
cell, Illite soil  in water, 207 kPa air pressure;','2) Source wave: one sine wave, excitation
voltage=4V;','3) Received waves:  gain=50dB, HP=LP=testing frequency;'},...
    'FontName','Times New Roman',...
    'FitBoxToText','off',...
    'LineStyle','none');
% Create line
annotation(figure1,'line',[0.151966173996635 0.162382840663302],...
    [0.937727355055925 0.937727355055925],'LineWidth',1);
% Create line
annotation(figure1,'line',[0.156679140889674 0.155720338983051],...
    [0.936997327631588 0.904904904904905],'LineWidth',1);
% Create textbox
annotation(figure1,'textbox',...
    [0.160561556023884 0.902855136843817 0.138700825430278 0.0301075268817204],...
```

```
    'String',{'0.9 V'},...
    'FontSize',12,...
    'FontName','Times New Roman',...
    'FitBoxToText','off',...
    'LineStyle','none');
% Plot the dots on the curves to IDENTIFY the 'First Arrival Time'
% Coordinates were read from the figure with SHOWING Cursor Coordinate
% % create plot
% plot(0.4892,-4.481,'.',0.3868,-5.408,'.',0.3356,-6.363,'.',0.266,-7.201,'.',0.242,-8.193,'.',0.23,-
9.081,'.',0.2364,-9.873,'.',0.222,-10.86,'.',0.202,-11.81,'.',0.192,-12.83,'.',0.1856,-13.75,'.',0.1736,-
14.61,'.',0.1404,-15.35,'.',0.1364,-16.35,'.',0.1364,-17.27,'.',0.1676,-18.08,'.',0.172,-
19.09,'.',0.1772,-20.06,'.',0.19,-20.87,'.',0.1944,-21.79,'.',0.1904,-22.72,'.',0.1928,-
23.51,'.',0.2324,-24.34,'.',0.2696,-26.81,'.',0.3984,-26.97,'.',0.4324,-27.83,'.',0.2484,-
25.25,'.',0.2644,-26.17,'.');
```

B.4. References

Mathworks, “MATLAB Programing Environment and Documentation, Version r.14b.” The MathWorks, Inc. Natick, MA, 2014.

APPENDIX C: Shear Modulus and Shear Wave Velocity Results

C.1. Chapter Overview

Contained in this appendix are the shear modulus and shear wave velocity obtained from the BP-CRS-BE tests and their relationships with axial strain, vertical effective stress, specific volume, overconsolidation ratio and other parameters of interest.

C.2. Shear Modulus and Shear Wave Velocity

Included in this section are the results obtained from BP-CRS-BE tests on Kaolinite soil specimens and Illite soil specimens. These results include but are not limited to: 1) shear wave velocity as a function of axial stress, 2) shear wave velocity as a function of specific volume, 3) measured shear modulus as a function of axial strain, 4) measured shear modulus as a function of specific volume, 5) constrained modulus as a function of axial strain, 6) Poisson's ratio as a function of normalized specific volume, 7) predicted shear modulus as a function of over-consolidation ratio, and 8) comparison of the predicted shear modulus with the measured shear modulus.

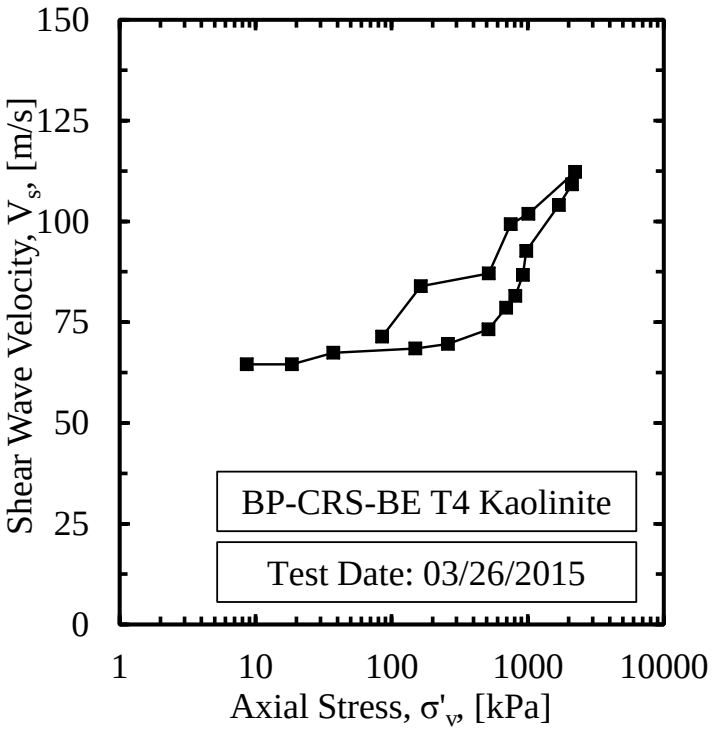

Figure C.1. Shear wave velocity as a function of vertical effective stress for BP-CRS-BE on Kaolinite soil specimen (tested on 03/26/2015).

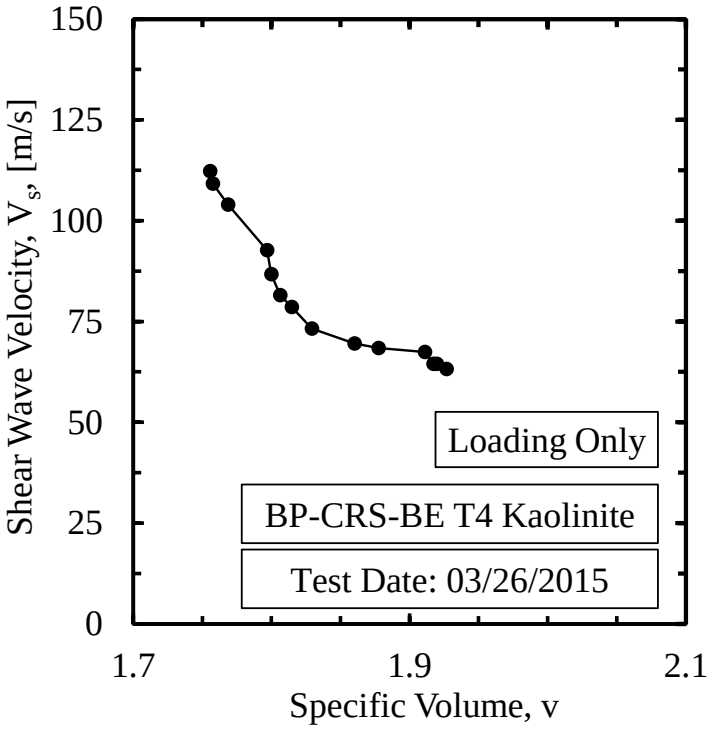

Figure C.2. Shear wave velocity as a function of specific volume for BP-CRS-BE on Kaolinite soil specimen (tested on 03/26/2015).

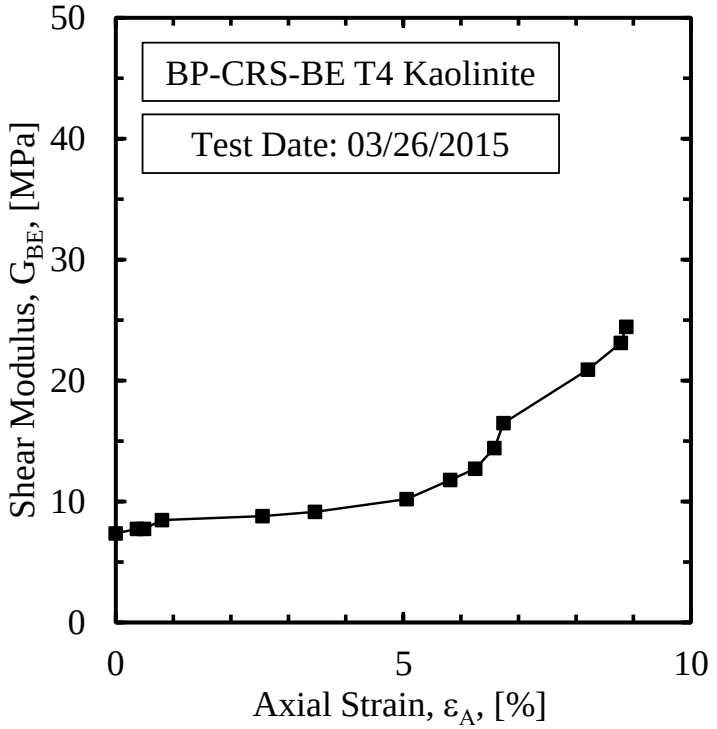

Figure C.3. Shear modulus as a function of axial strain for BP-CRS-BE on Kaolinite soil specimen (tested on 03/26/2015).

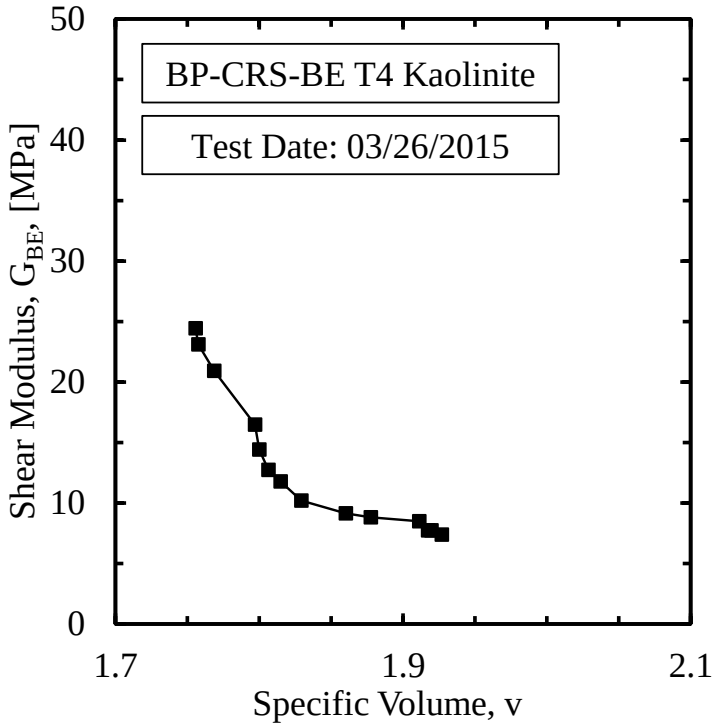

Figure C.4. Shear modulus as a function of specific volume for BP-CRS-BE on Kaolinite soil specimen (tested on 03/26/2015).

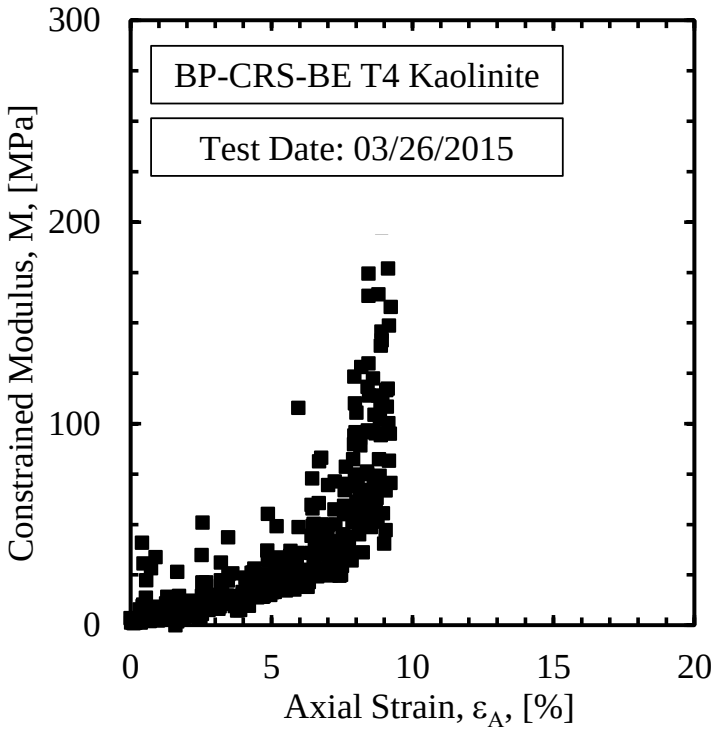

Figure C.5. Constrained modulus as a function of axial strain for BP-CRS-BE on Kaolinite soil specimen (tested on 03/26/2015).

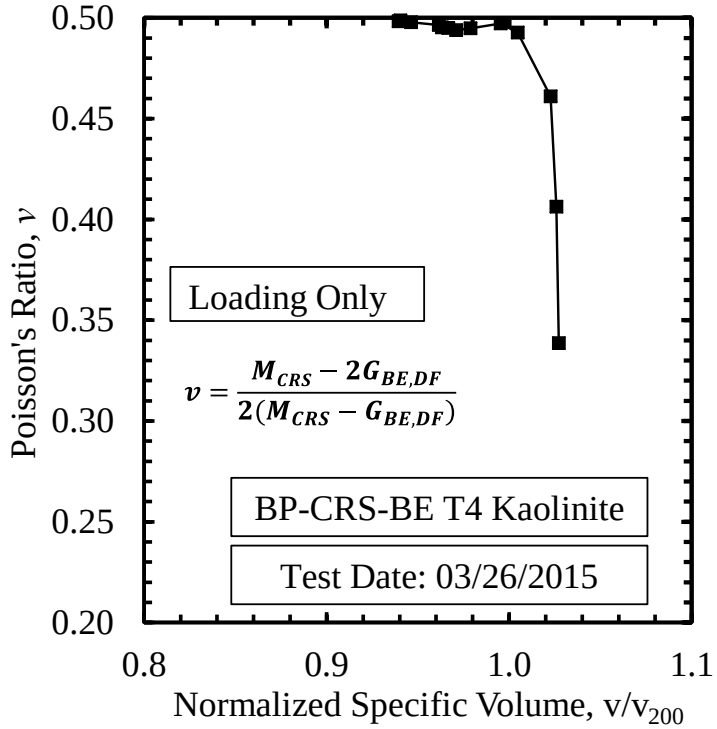

Figure C.6. Poisson's ratio as a function of normalized specific volume for BP-CRS-BE on Kaolinite soil specimen (tested on 03/26/2015).

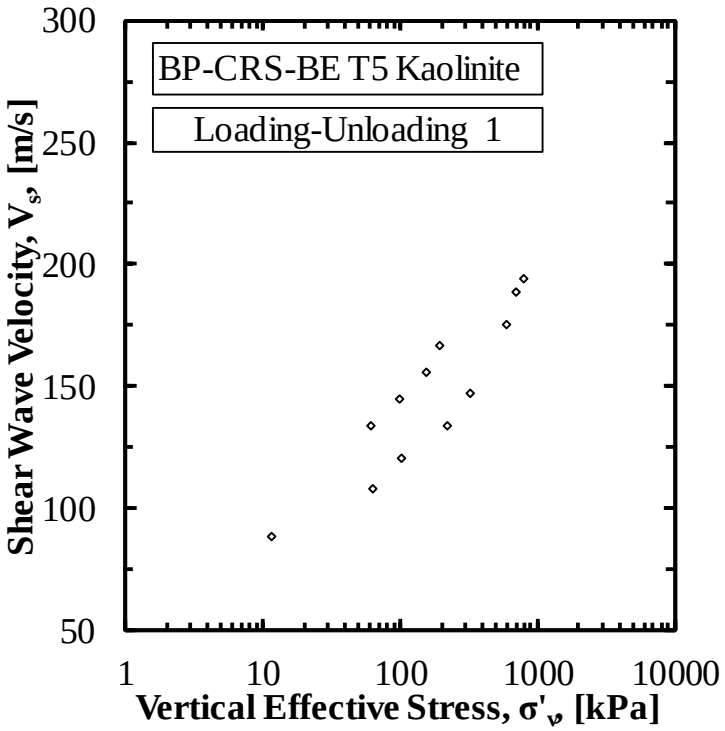

Figure C.7. Shear wave velocity as a function of vertical effective stress for BP-CRS-BE T5 on Kaolinite soil specimen (loading-unloading 1).

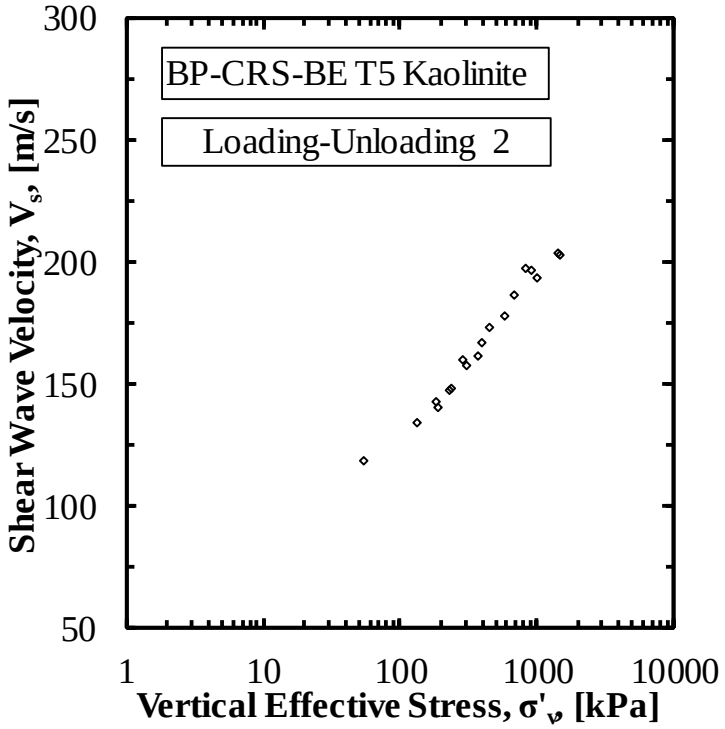

Figure C.8. Shear wave velocity as a function of vertical effective stress for BP-CRS-BE T5 on Kaolinite soil specimen (loading-unloading 2).

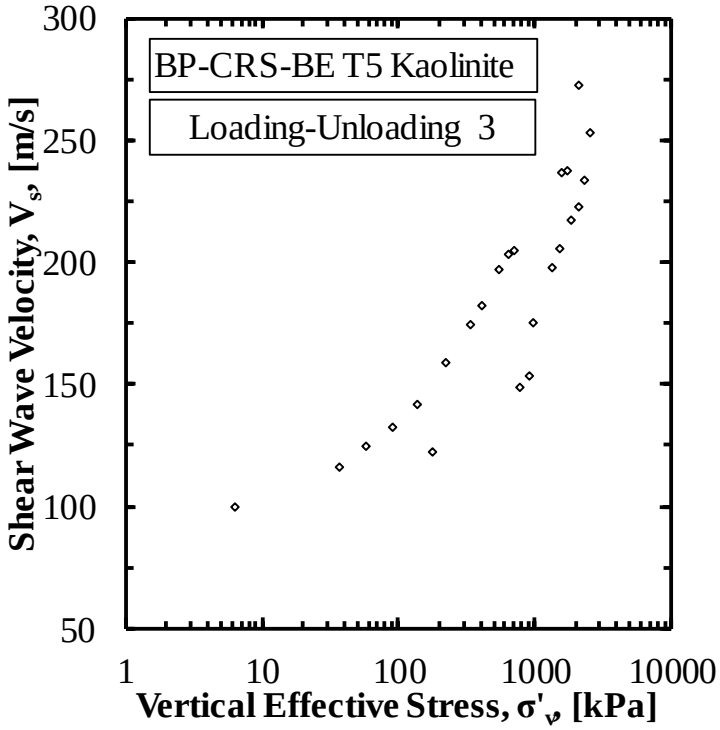

Figure C.9. Shear wave velocity as a function of vertical effective stress for BP-CRS-BE T5 on Kaolinite soil specimen (loading-unloading 3).

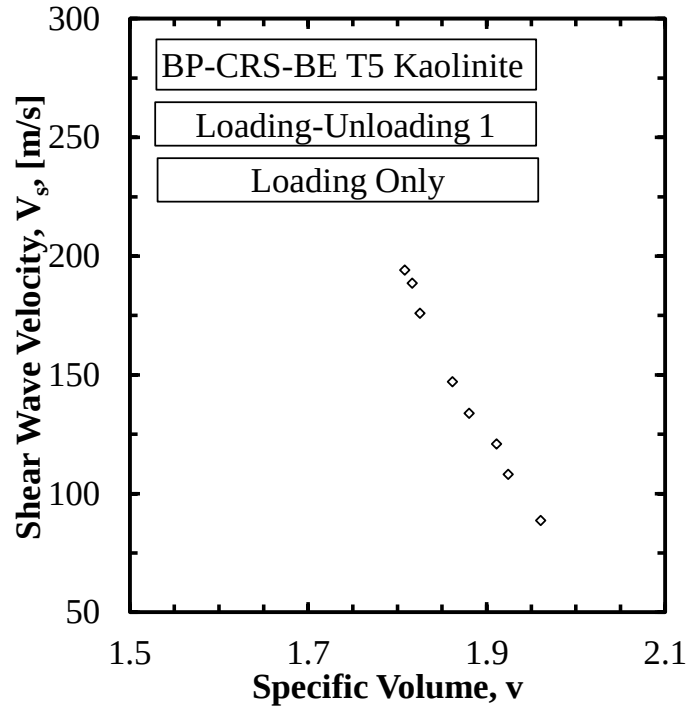

Figure C.10. Shear wave velocity as a function of vertical effective stress for BP-CRS-BE T5 on Kaolinite soil specimen (loading-unloading 1).

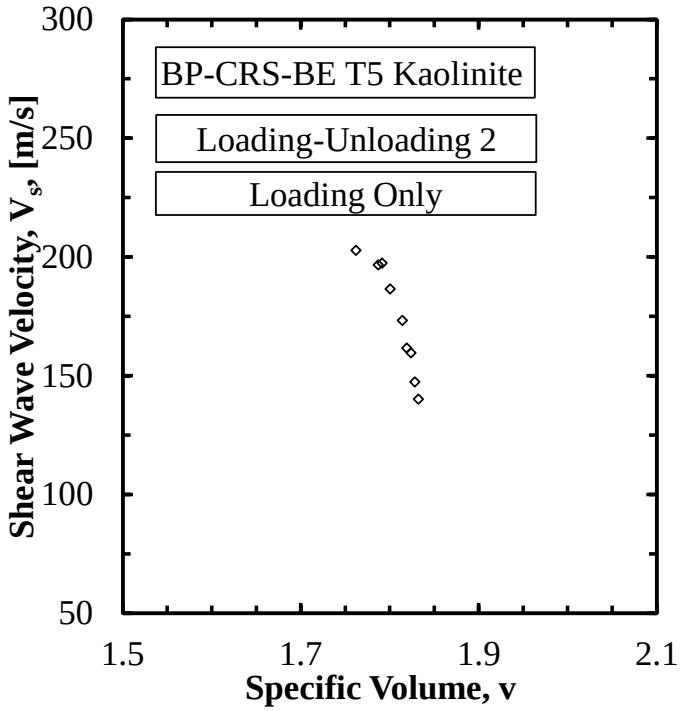

Figure C.11. Shear wave velocity as a function of vertical effective stress for BP-CRS-BE T5 on Kaolinite soil specimen (loading-unloading 2).

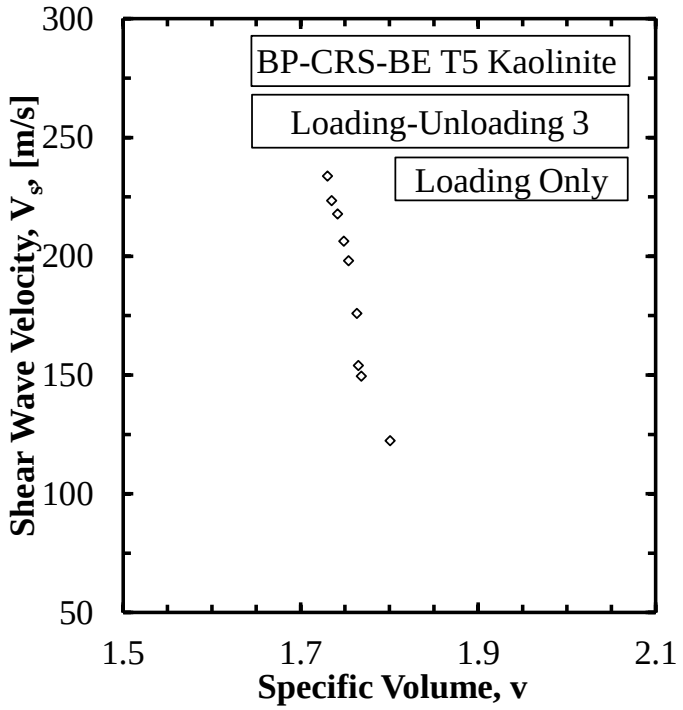

Figure C.12. Shear wave velocity as a function of vertical effective stress for BP-CRS-BE T5 on Kaolinite soil specimen (loading-unloading 3).

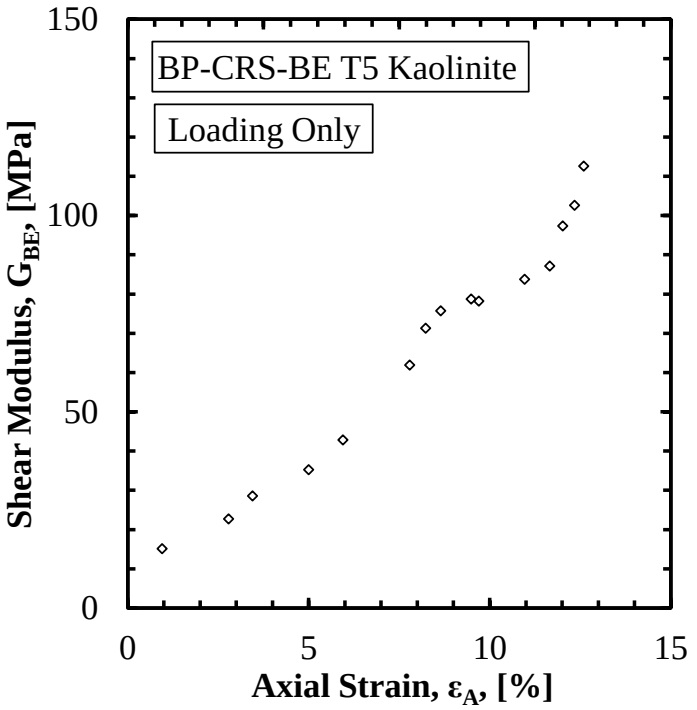

Figure C.13. Shear modulus as a function of axial strain for BP-CRS-BE T5 on Kaolinite soil specimen.

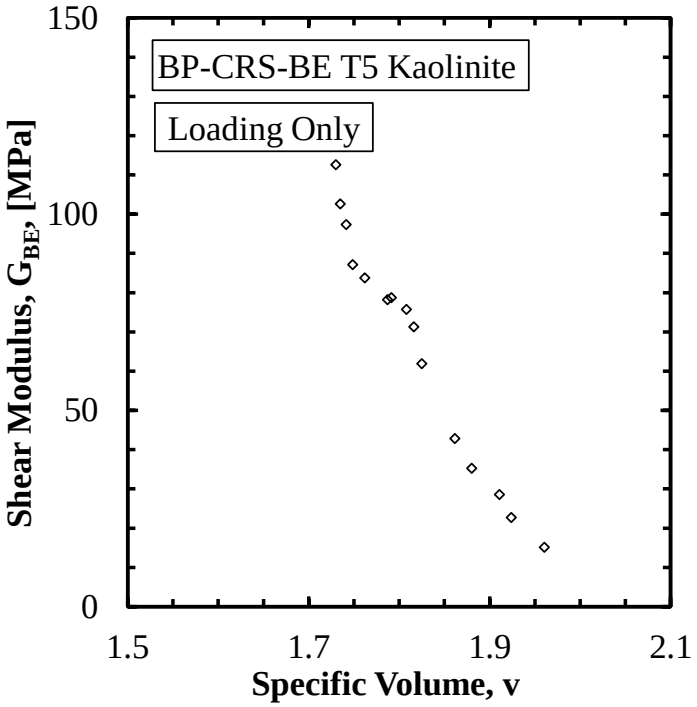

Figure C.14. Shear modulus as a function of specific volume for BP-CRS-BE T5 on Kaolinite soil specimen.

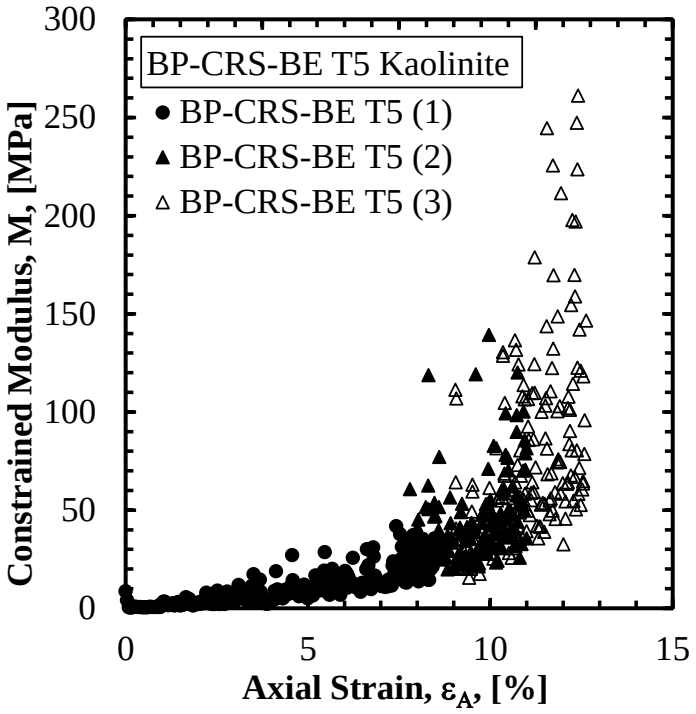

Figure C.15. Constrained modulus as a function of axial strain for BP-CRS-BE T5 on Kaolinite soil specimen.

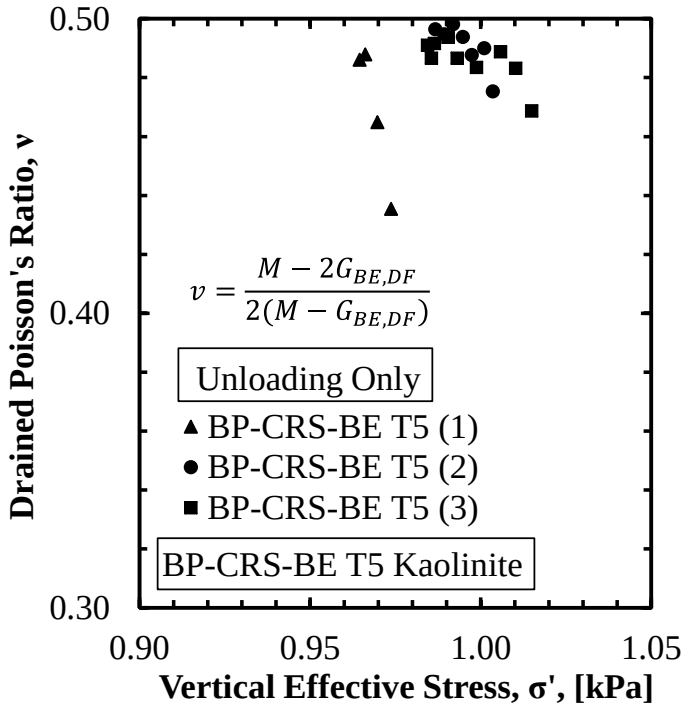

Figure C.16. Poisson's ratio as a function of vertical effective stress for BP-CRS-BE T5 on Kaolinite soil specimen.

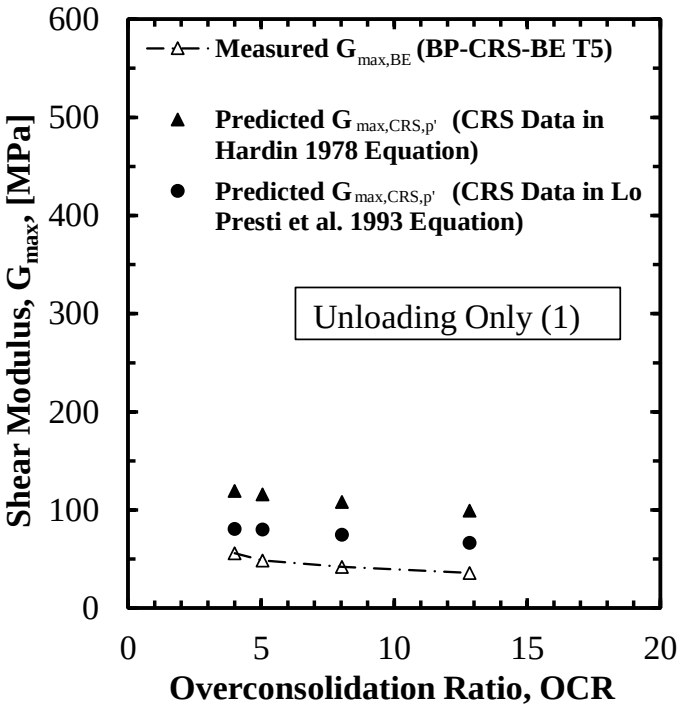

Figure C.17. Shear modulus as a function of overconsolidation ratio for BP-CRS-BE T5 on Kaolinite soil specimen (unloading 1).

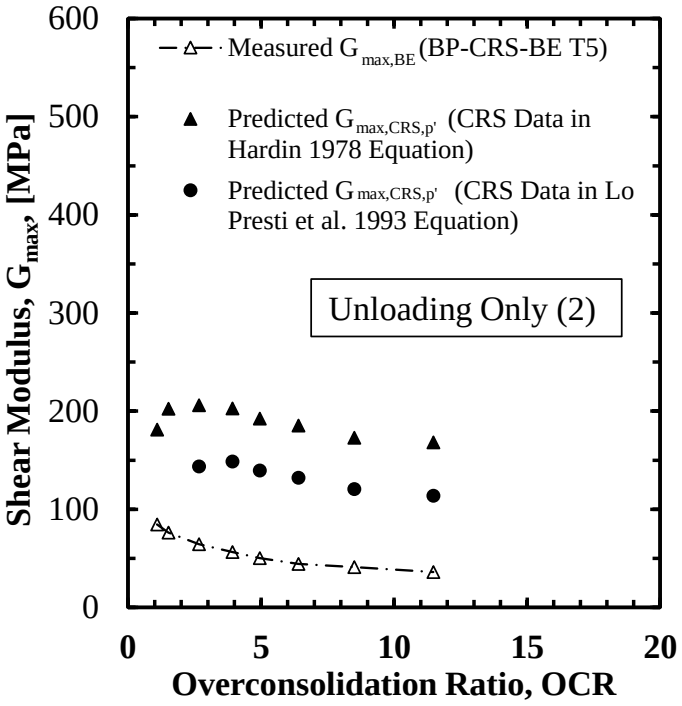

Figure C.18. Shear modulus as a function of overconsolidation ratio for BP-CRS-BE T5 on Kaolinite soil specimen (unloading 2).

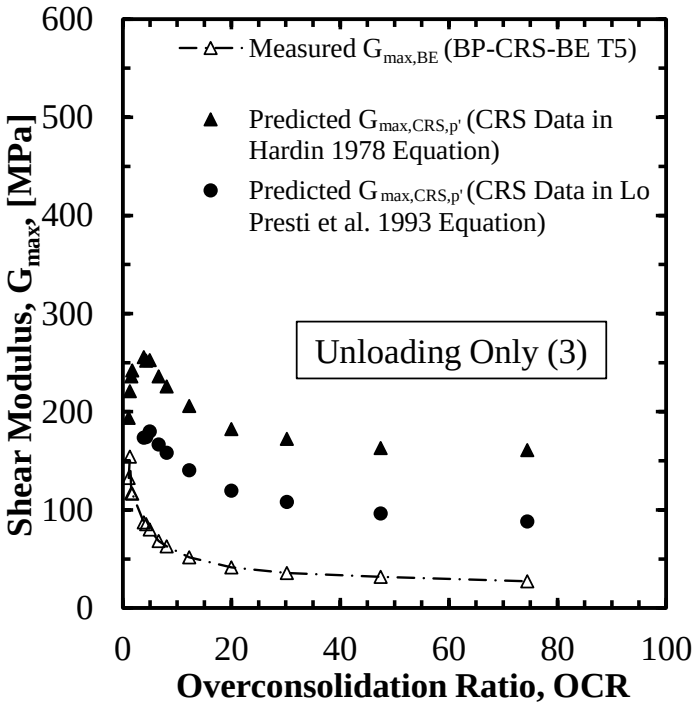

Figure C.19. Shear modulus as a function of overconsolidation ratio for BP-CRS-BE T5 on Kaolinite soil specimen (unloading 3).

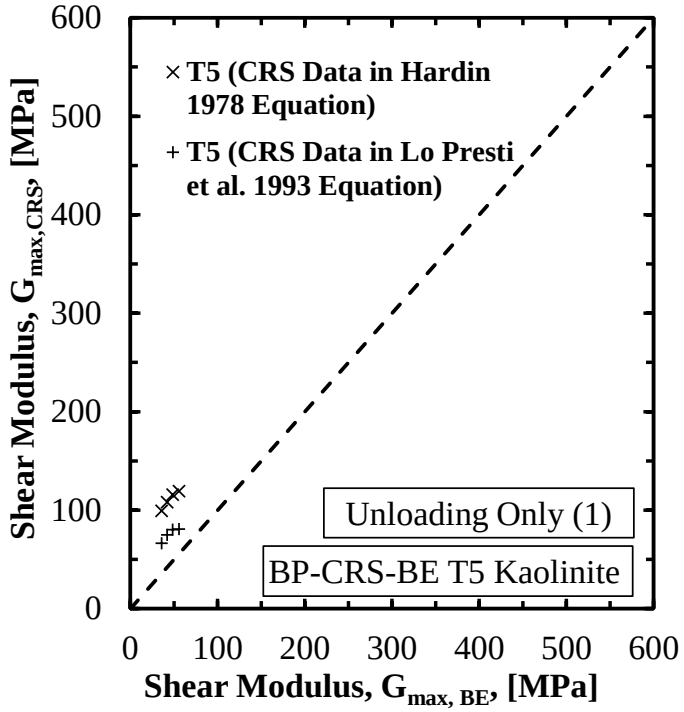

Figure C.20. Comparison of the predicted shear modulus with the measured shear modulus for BP-CRS-BE T5 on Kaolinite soil specimen (unloading 1).

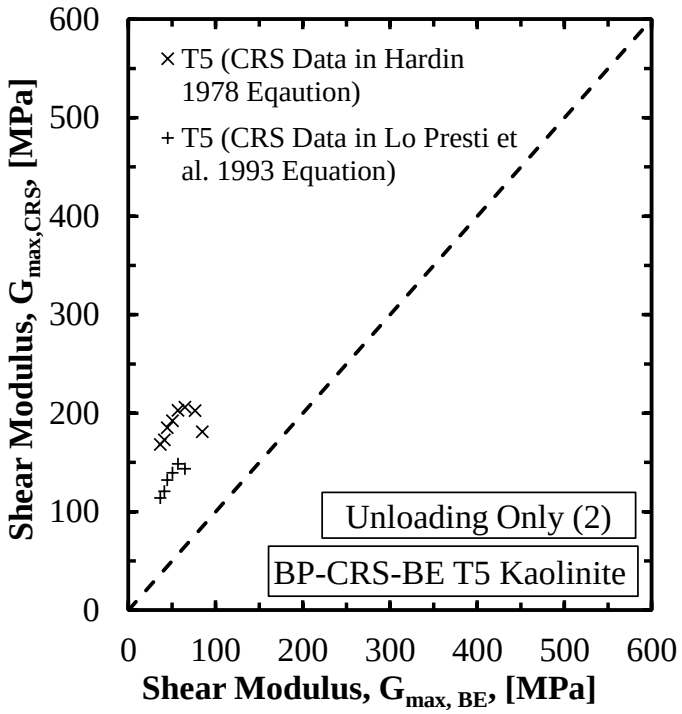

Figure C.21. Comparison of the predicted shear modulus with the measured shear modulus for BP-CRS-BE T5 on Kaolinite soil specimen (unloading 2).

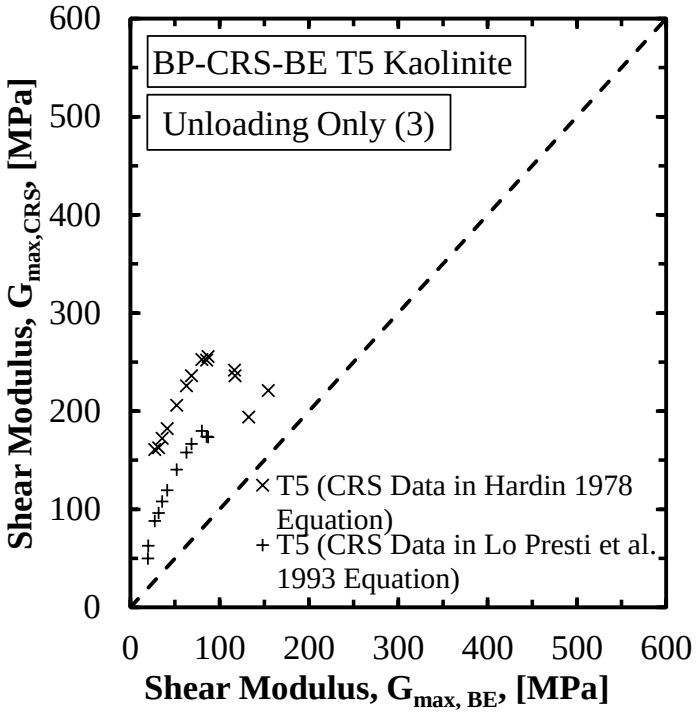

Figure C.22. Comparison of the predicted shear modulus with the measured shear modulus for BP-CRS-BE T5 on Kaolinite soil specimen (unloading 3).

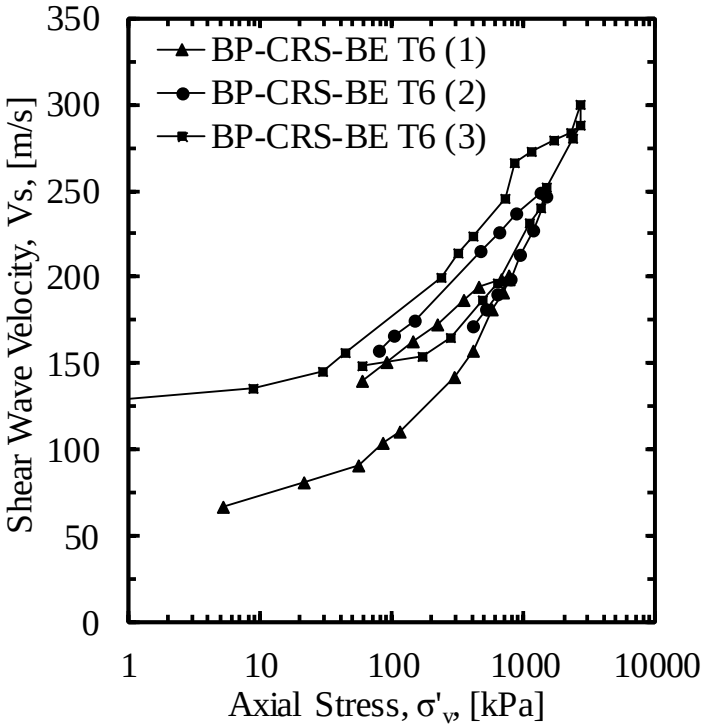

Figure C.23. Shear wave velocity as a function of vertical effective stress for BP-CRS-BE T6 on Kaolinite soil specimen.

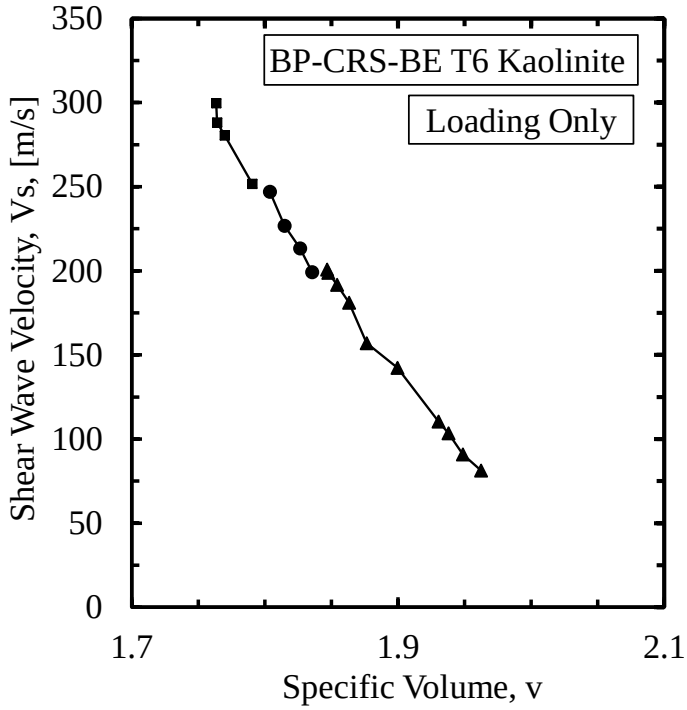

Figure C.24. Shear wave velocity as a function of specific volume for BP-CRS-BE T6 on Kaolinite soil specimen.

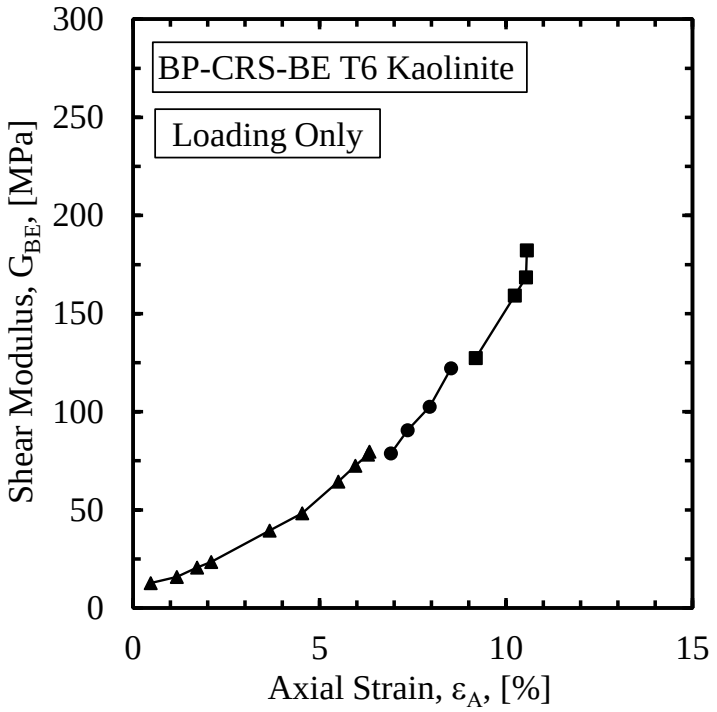

Figure C.25. Shear modulus as a function of axial strain for BP-CRS-BE T6 on Kaolinite soil specimen.

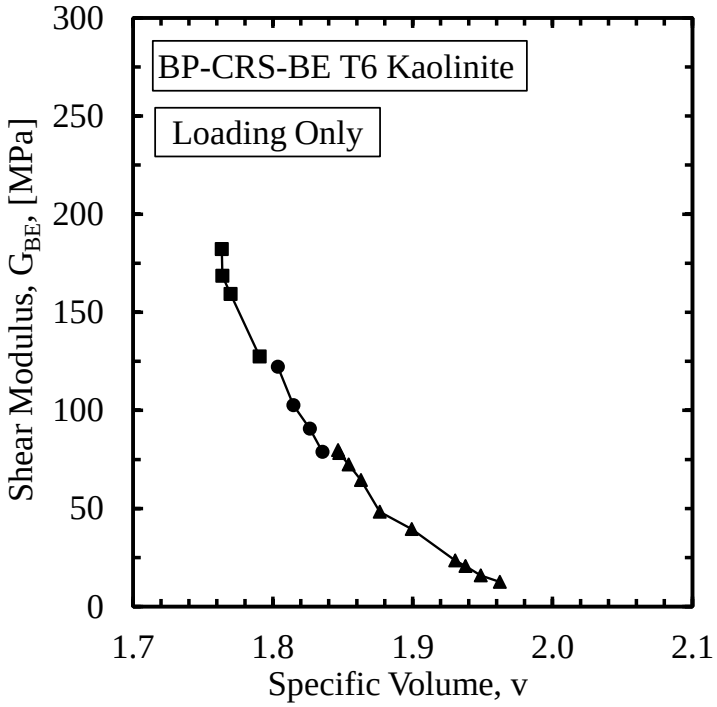

Figure C.26. Shear modulus as a function of specific volume for BP-CRS-BE T6 on Kaolinite soil specimen.

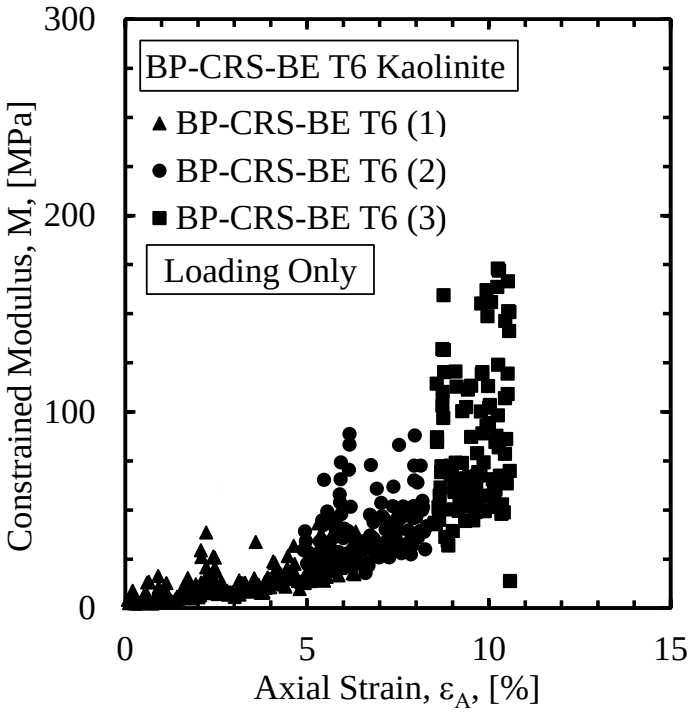

Figure C.27. Constrained modulus as a function of axial strain for BP-CRS-BE T6 on Kaolinite soil specimen.

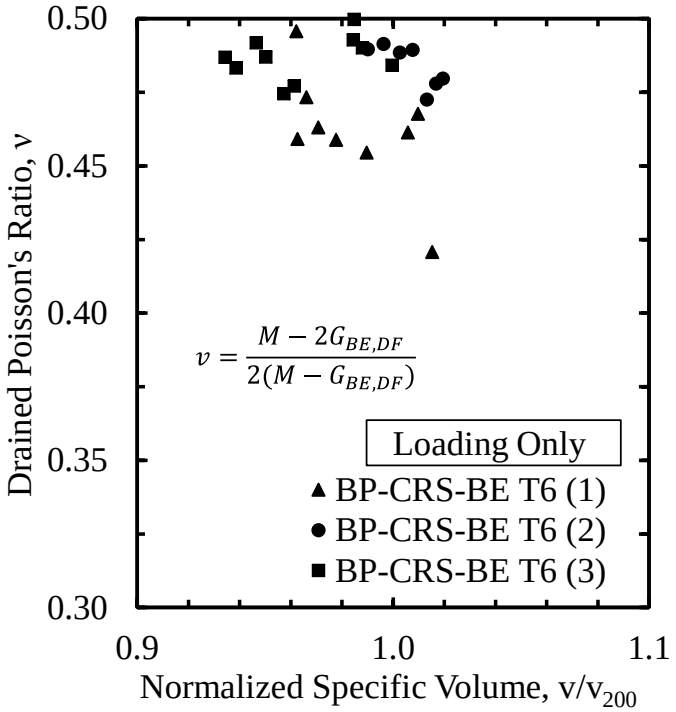

Figure C.28. Poisson's ratio as a function of normalized specific volume for BP-CRS-BE T6 on Kaolinite soil specimen.

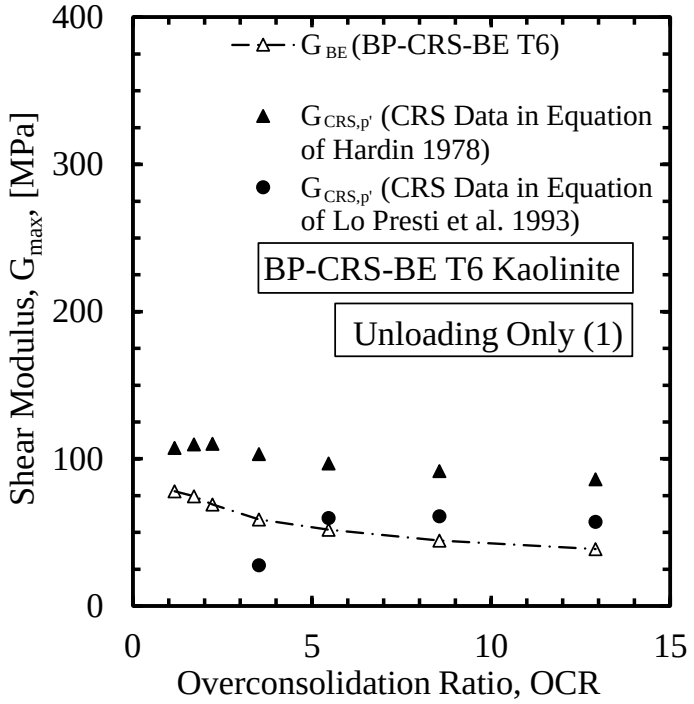

Figure C.29. Shear wave velocity as a function of overconsolidation ratio for BP-CRS-BE T6 on Kaolinite soil specimen (unloading 1).

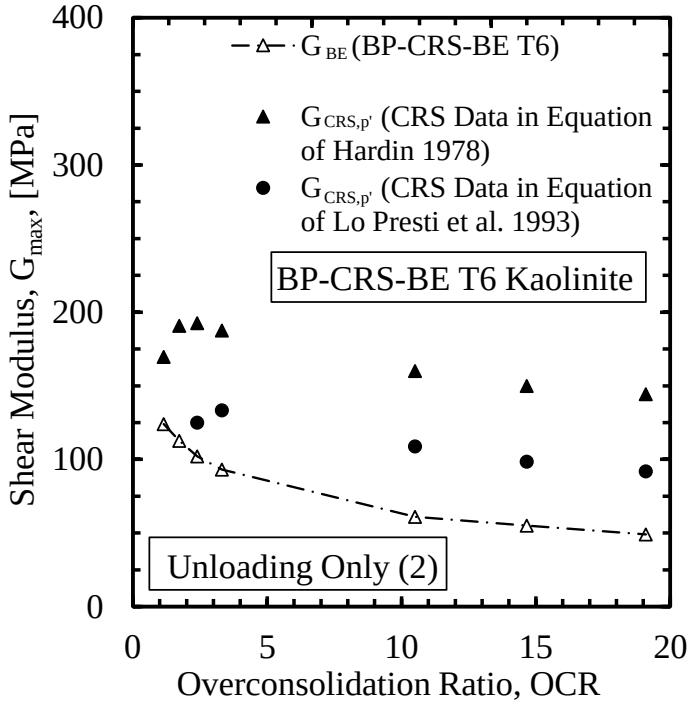

Figure C.30. Shear wave velocity as a function of overconsolidation ratio for BP-CRS-BE T6 on Kaolinite soil specimen (unloading 2).

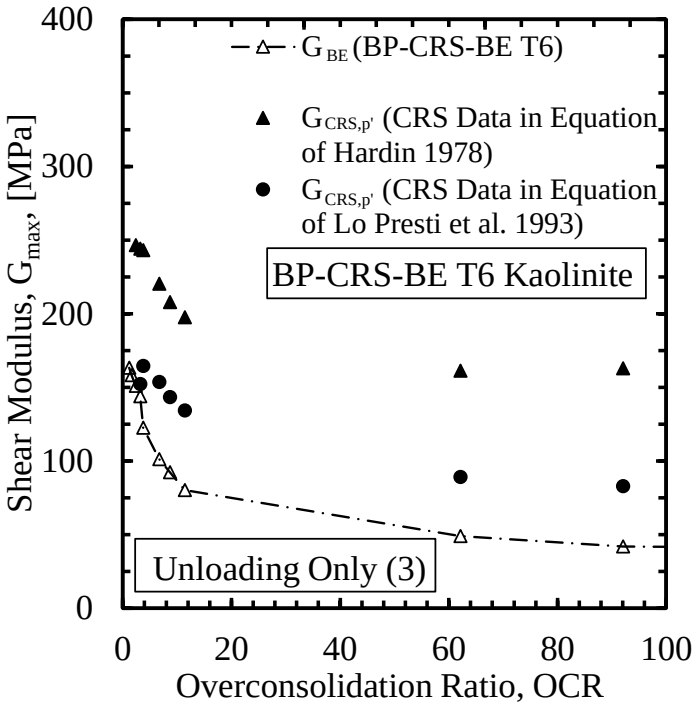

Figure C.31. Shear wave velocity as a function of overconsolidation ratio for BP-CRS-BE T6 on Kaolinite soil specimen (unloading 3).

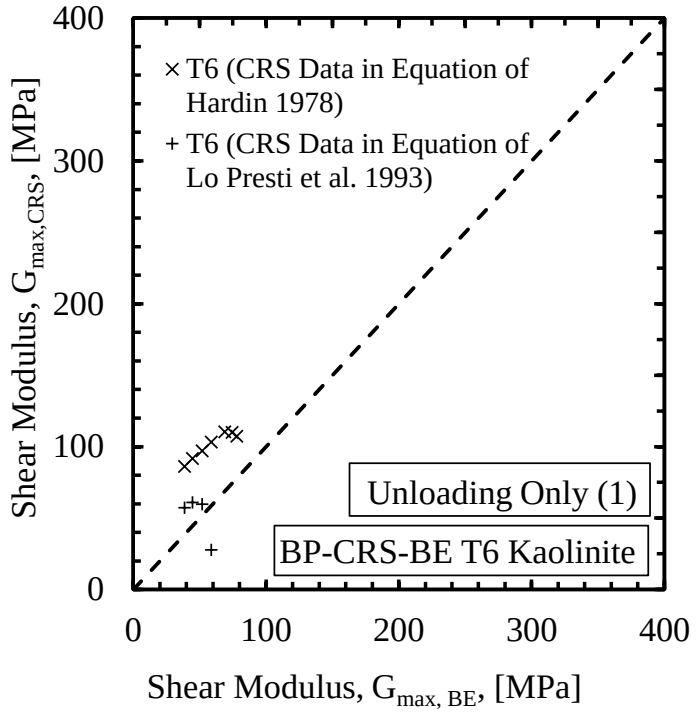

Figure C.32. Comparison of the predicted shear modulus with the measured shear modulus for BP-CRS-BE T6 on Kaolinite soil specimen (unloading 1).

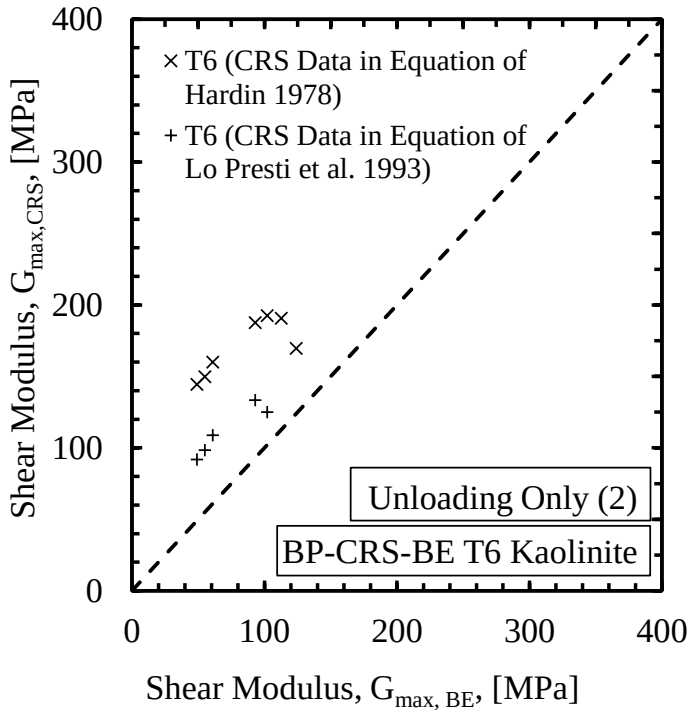

Figure C.33. Comparison of the predicted shear modulus with the measured shear modulus for BP-CRS-BE T6 on Kaolinite soil specimen (unloading 2).

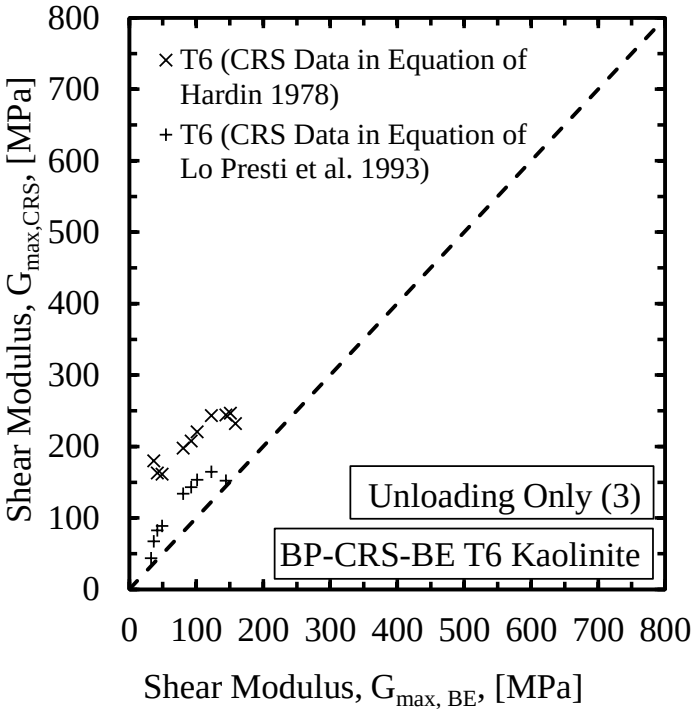

Figure C.34. Comparison of the predicted shear modulus with the measured shear modulus for BP-CRS-BE T6 on Kaolinite soil specimen (unloading 3).

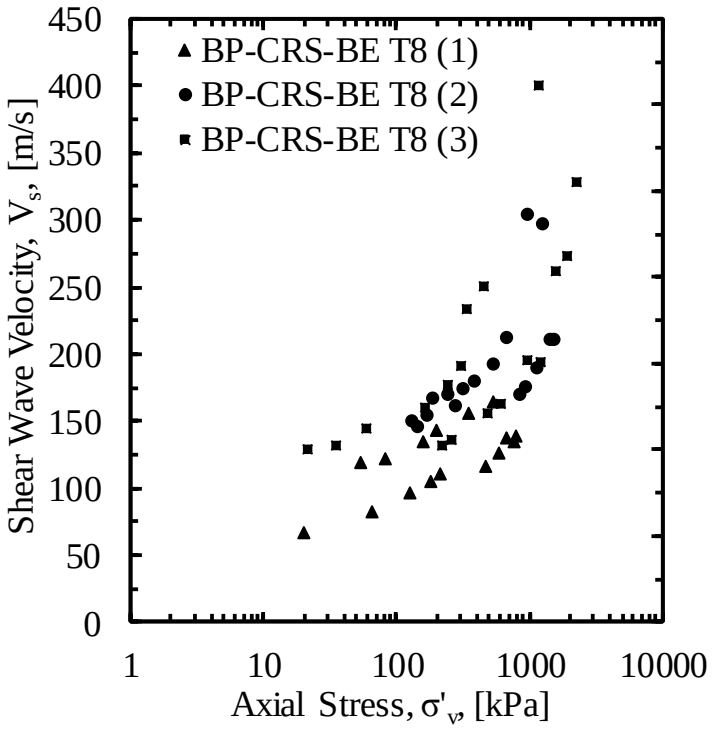

Figure C.35. Shear wave velocity as a function of vertical effective stress for BP-CRS-BE T8 on Kaolinite soil specimen.

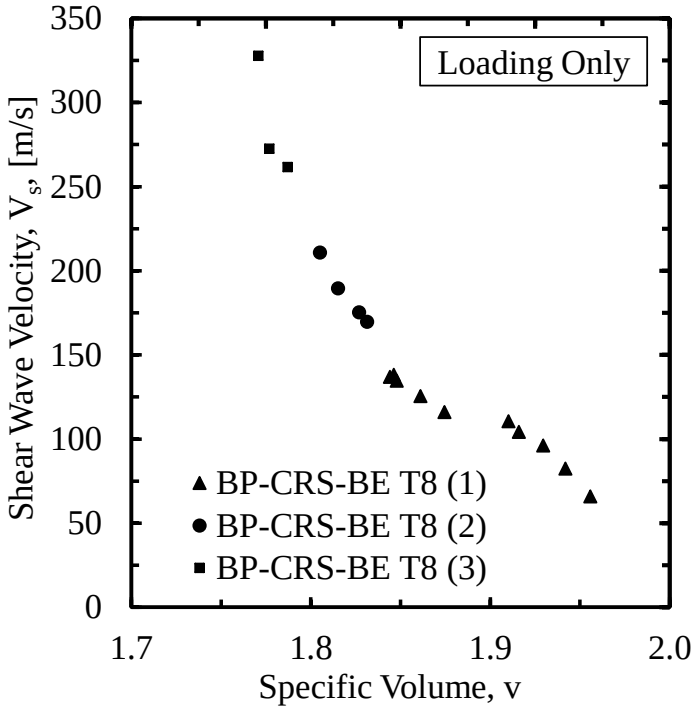

Figure C.36. Shear wave velocity as a function of specific volume for BP-CRS-BE T8 on Kaolinite soil specimen.

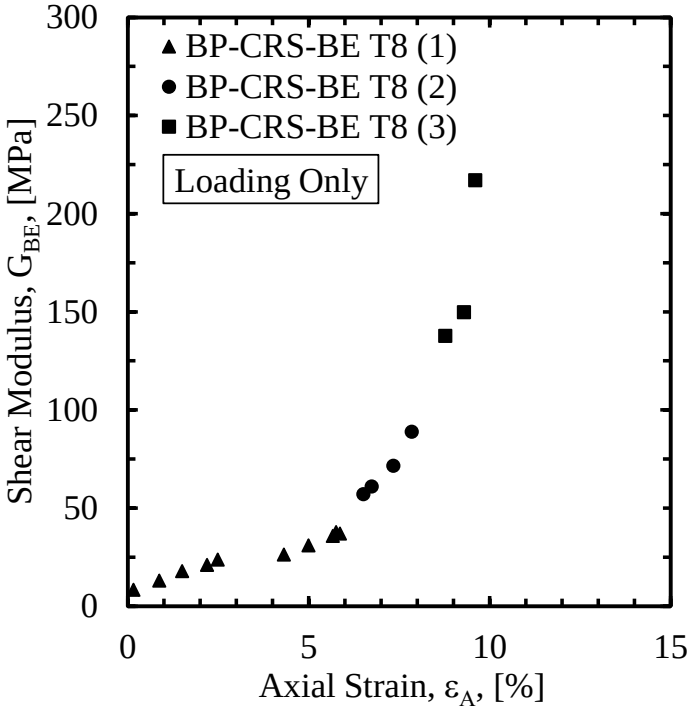

Figure C.37. Shear modulus as a function of axial strain for BP-CRS-BE T8 on Kaolinite soil specimen.

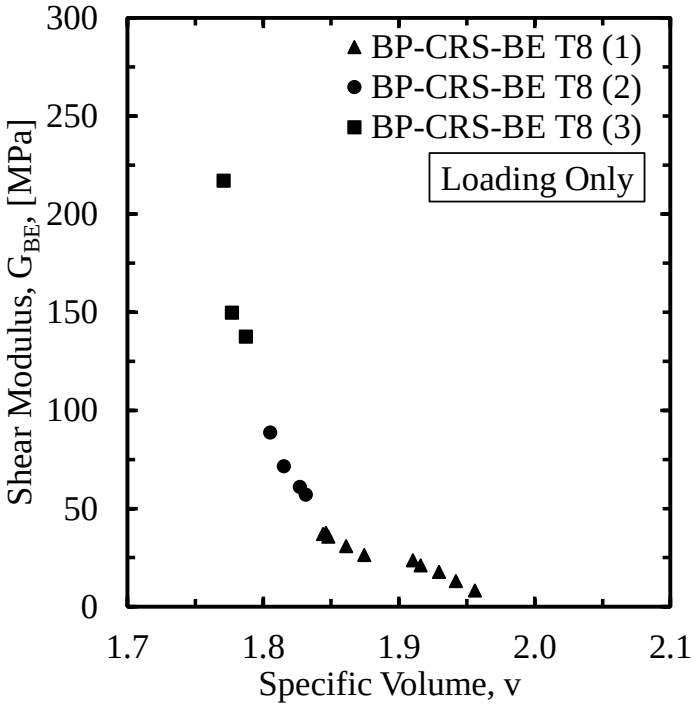

Figure C.38. Shear modulus as a function of specific volume for BP-CRS-BE T8 on Kaolinite soil specimen.

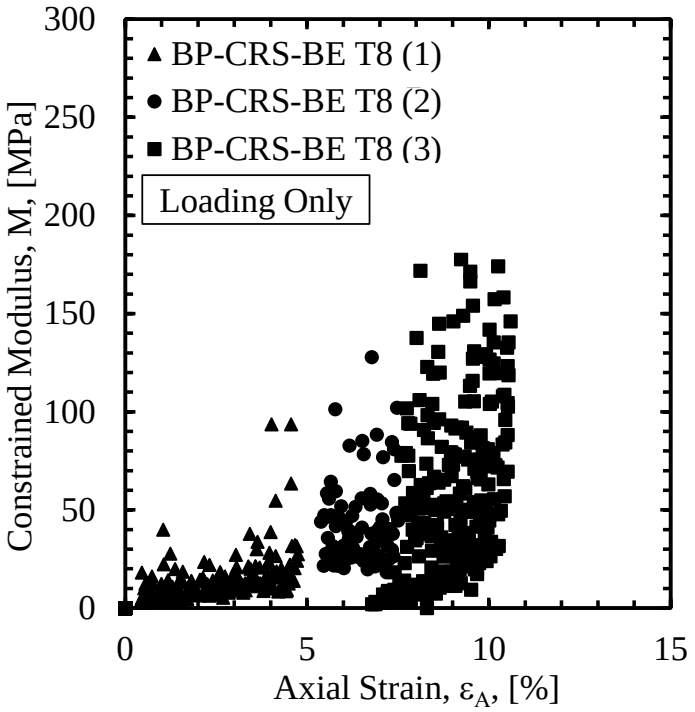

Figure C.39. Constrained modulus as a function of axial strain for BP-CRS-BE T8 on Kaolinite soil specimen.

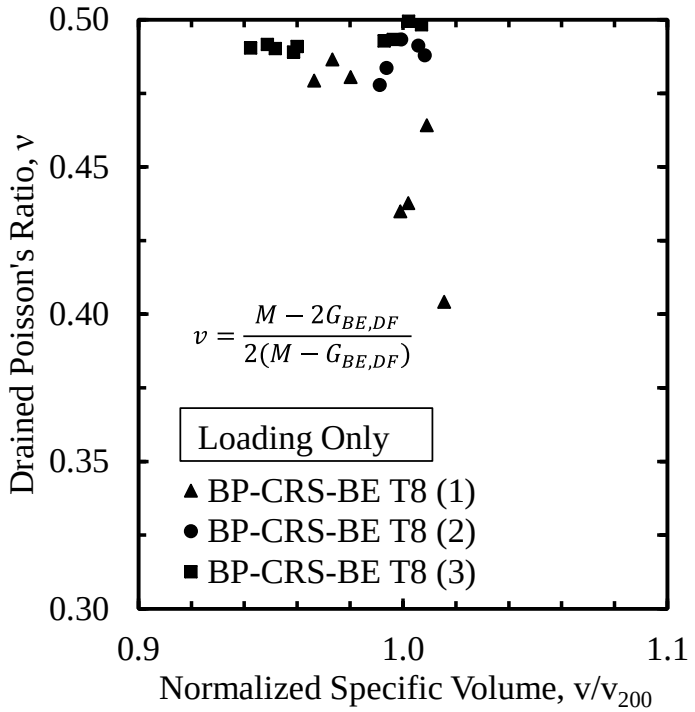

Figure C.40. Poisson's ratio as a function of normalized specific volume for BP-CRS-BE T8 on Kaolinite soil specimen.

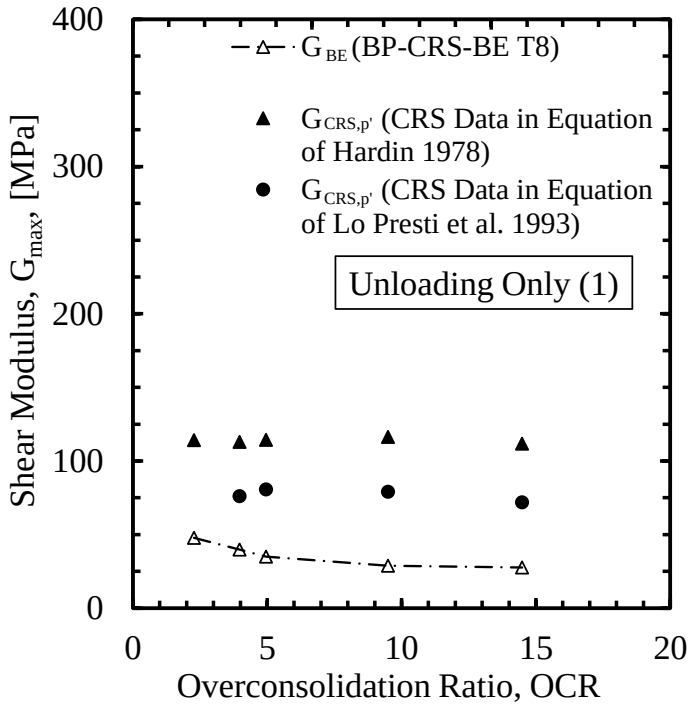

Figure C.41. Shear wave velocity as a function of overconsolidation ratio for BP-CRS-BE T8 on Kaolinite soil specimen (unloading 1).

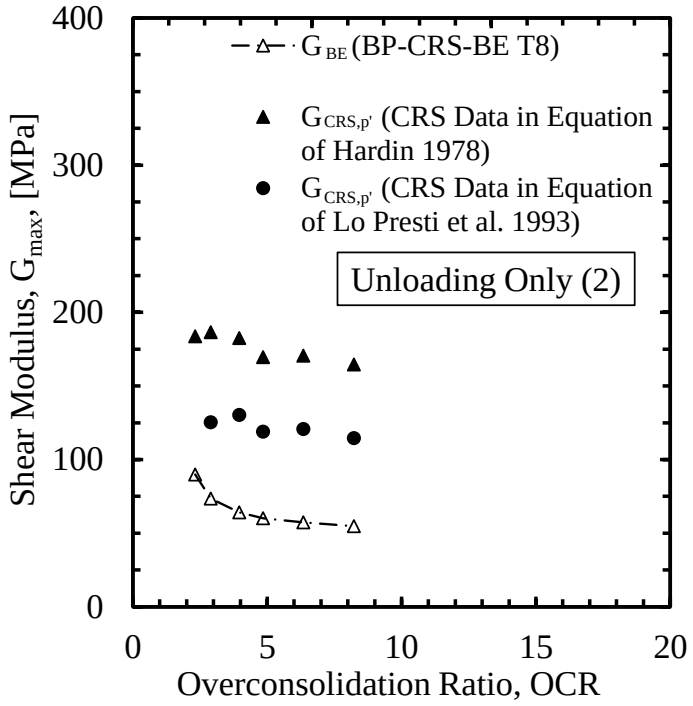

Figure C.42. Shear wave velocity as a function of overconsolidation ratio for BP-CRS-BE T8 on Kaolinite soil specimen (unloading 2).

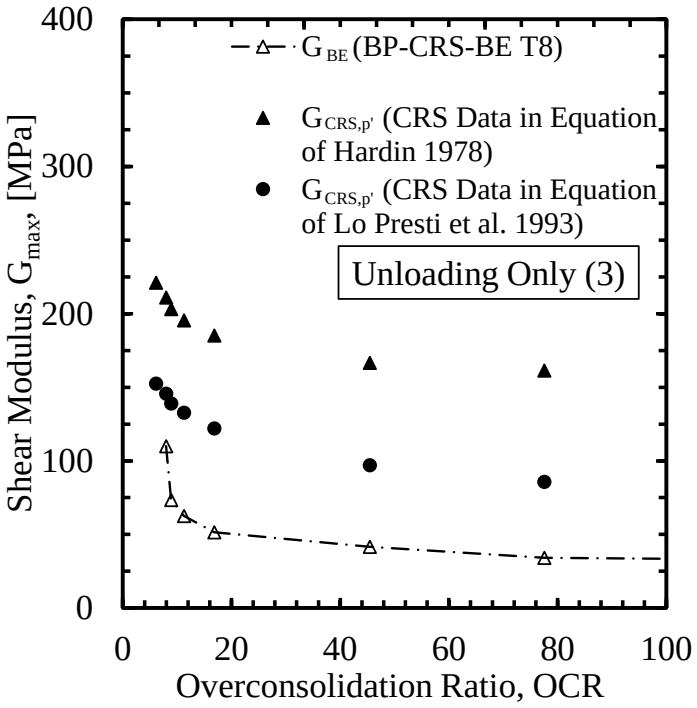

Figure C.43. Shear wave velocity as a function of overconsolidation ratio for BP-CRS-BE T8 on Kaolinite soil specimen (unloading 3).

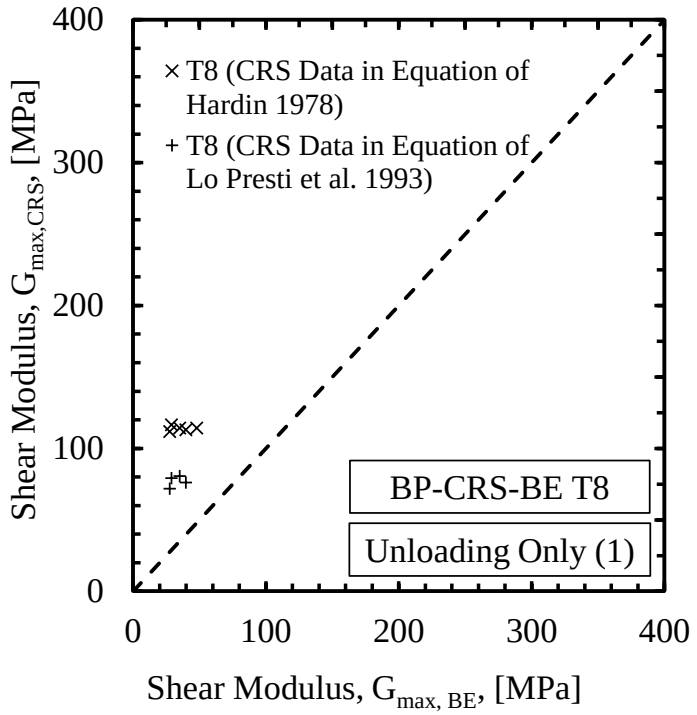

Figure C.44. Comparison of the predicted shear modulus with the measured shear modulus for BP-CRS-BE T8 on Kaolinite soil specimen (unloading 1).

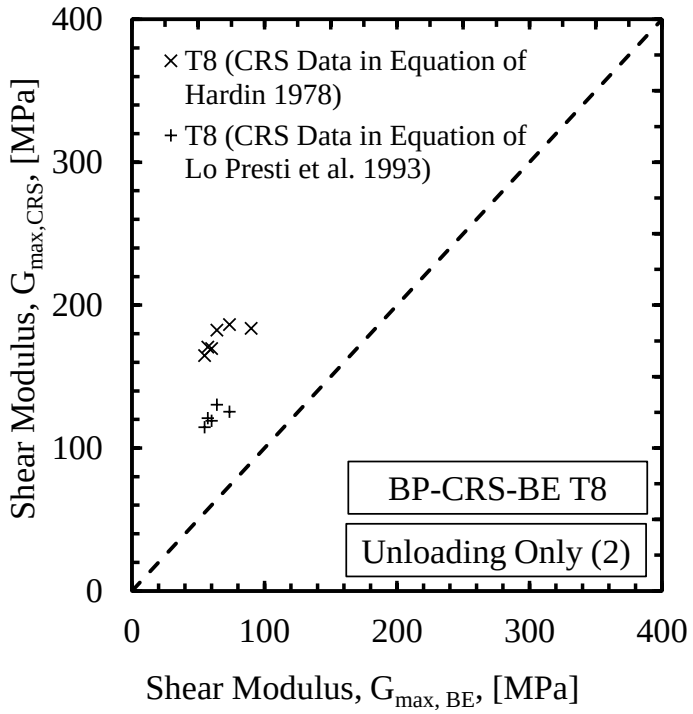

Figure C.45. Comparison of the predicted shear modulus with the measured shear modulus for BP-CRS-BE T8 on Kaolinite soil specimen (unloading 2).

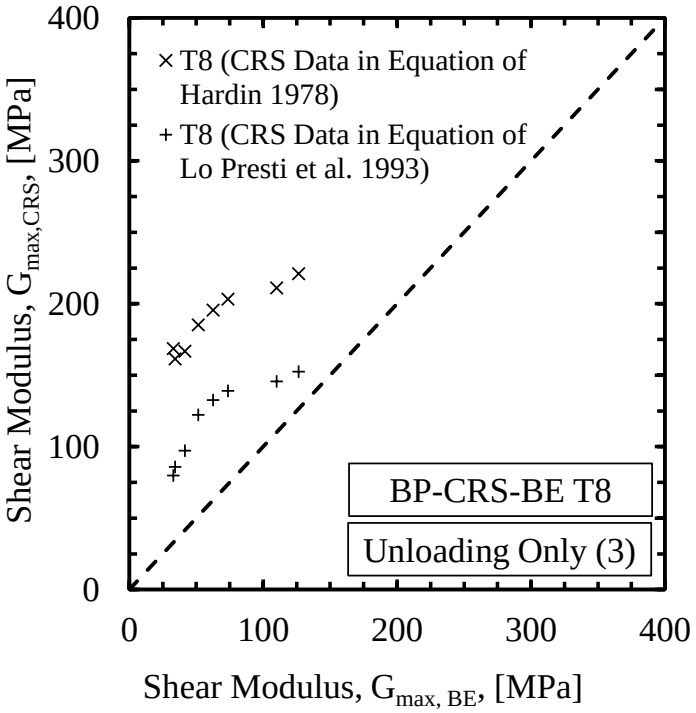

Figure C.46. Comparison of the predicted shear modulus with the measured shear modulus for BP-CRS-BE T8 on Kaolinite soil specimen (unloading 3).

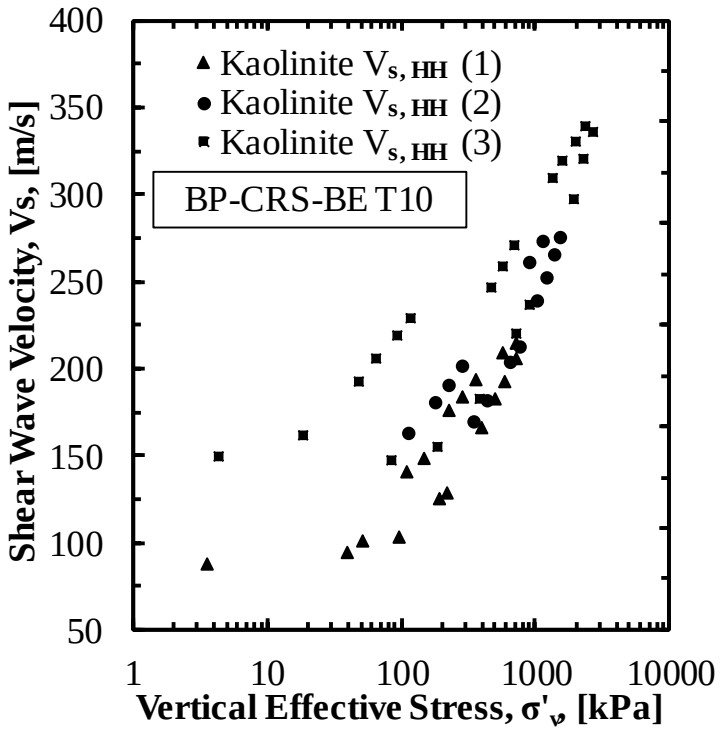

Figure C.47. Shear wave velocity as a function of vertical effective stress for BP-CRS-BE T10 on Kaolinite soil specimen.

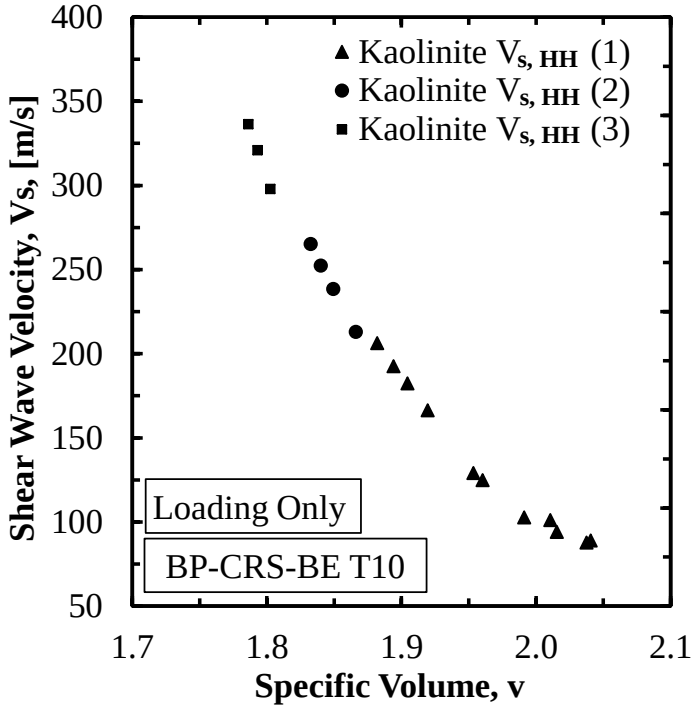

Figure C.48. Shear wave velocity as a function of specific volume for BP-CRS-BE T10 on Kaolinite soil specimen.

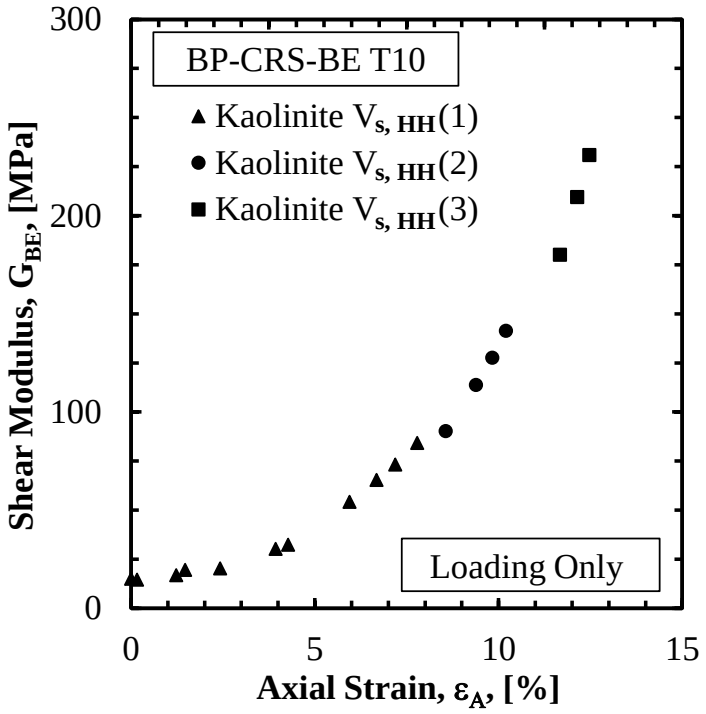

Figure C.49. Shear modulus as a function of axial strain for BP-CRS-BE T10 on Kaolinite soil specimen.

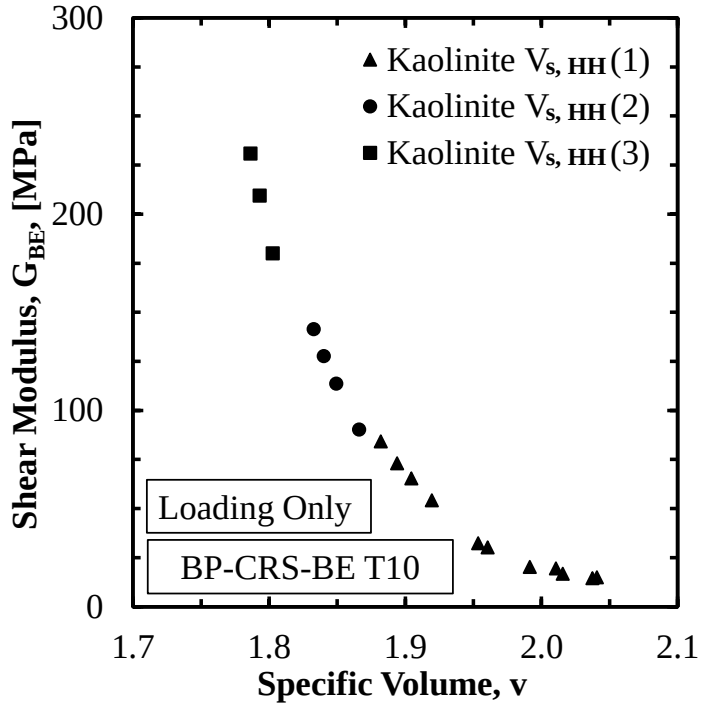

Figure C.50. Shear modulus as a function of specific volume for BP-CRS-BE T10 on Kaolinite soil specimen.

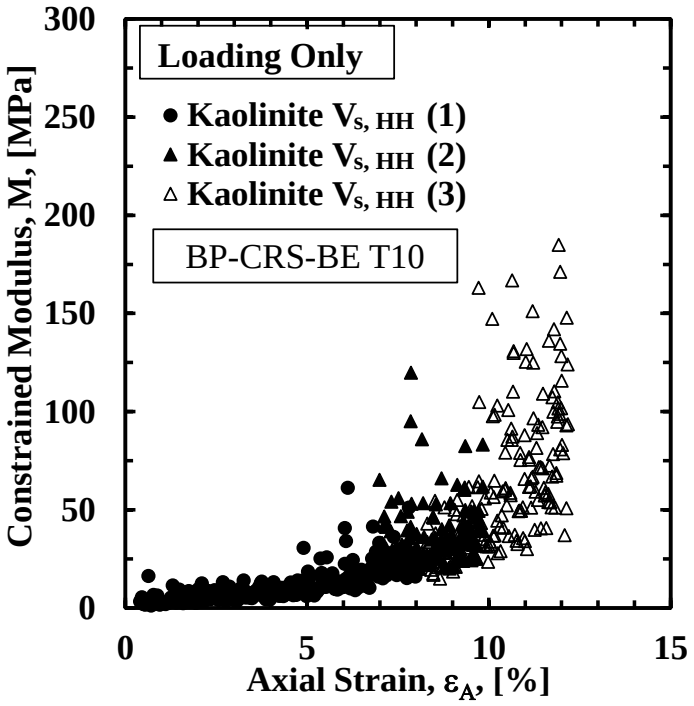

Figure C.51. Constrained modulus as a function of axial strain for BP-CRS-BE T10 on Kaolinite soil specimen.

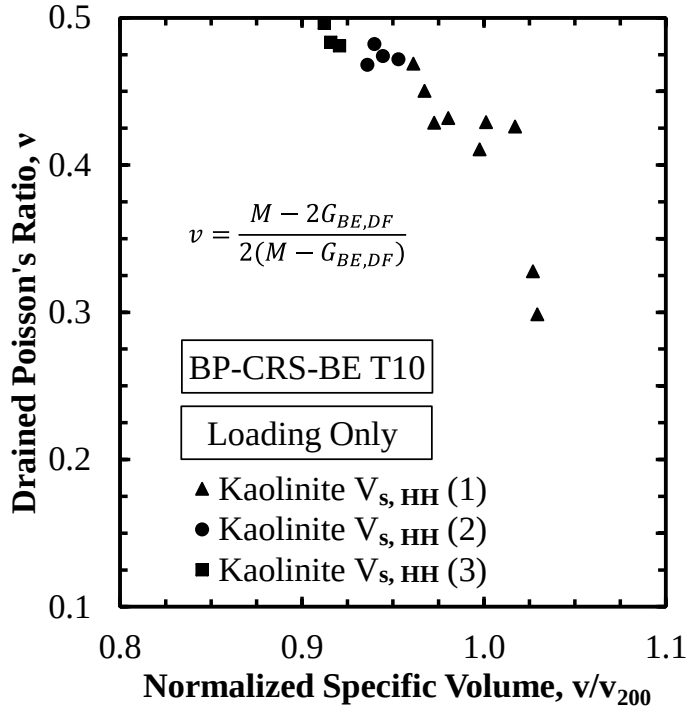

Figure C.52. Poisson's ratio as a function of normalized specific volume for BP-CRS-BE T10 on Kaolinite soil specimen (loading only).

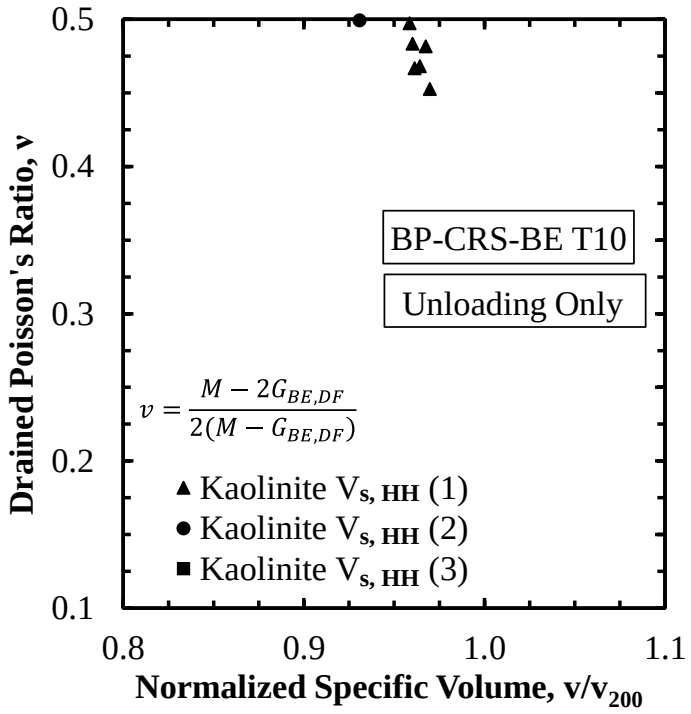

Figure C.53. Poisson's ratio as a function of normalized specific volume for BP-CRS-BE T10 on Kaolinite soil specimen (unloading only).

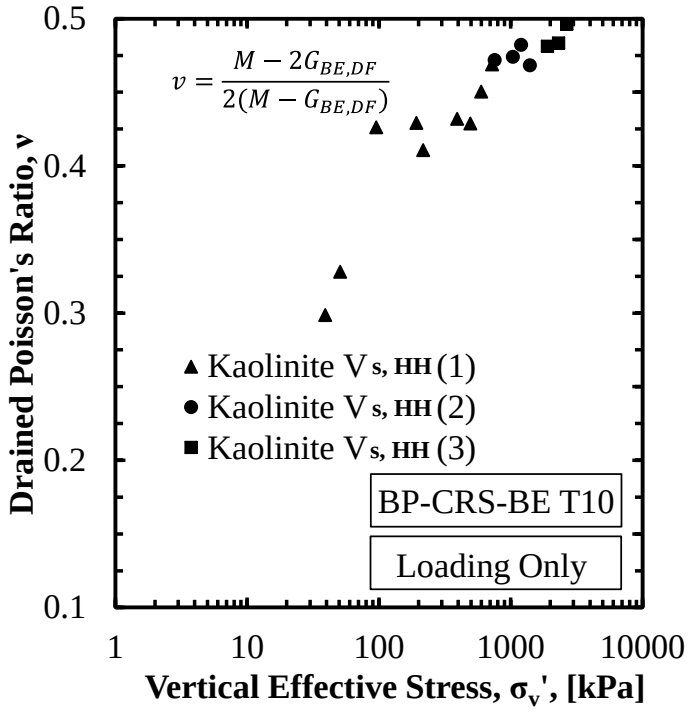

Figure C.54. Poisson's ratio as a function of vertical effective stress for BP-CRS-BE T10 on Kaolinite soil specimen (loading only).

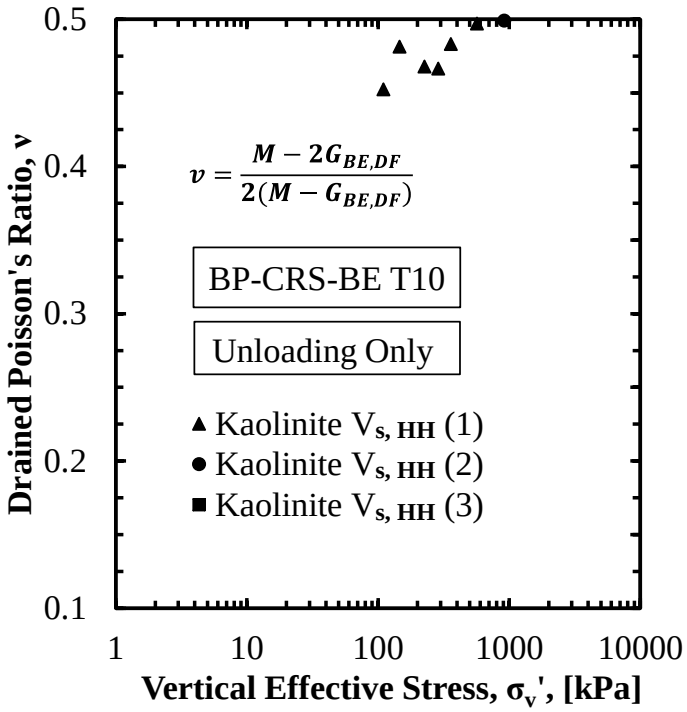

Figure C.55. Poisson's ratio as a function of vertical effective stress for BP-CRS-BE T10 on Kaolinite soil specimen (unloading only).

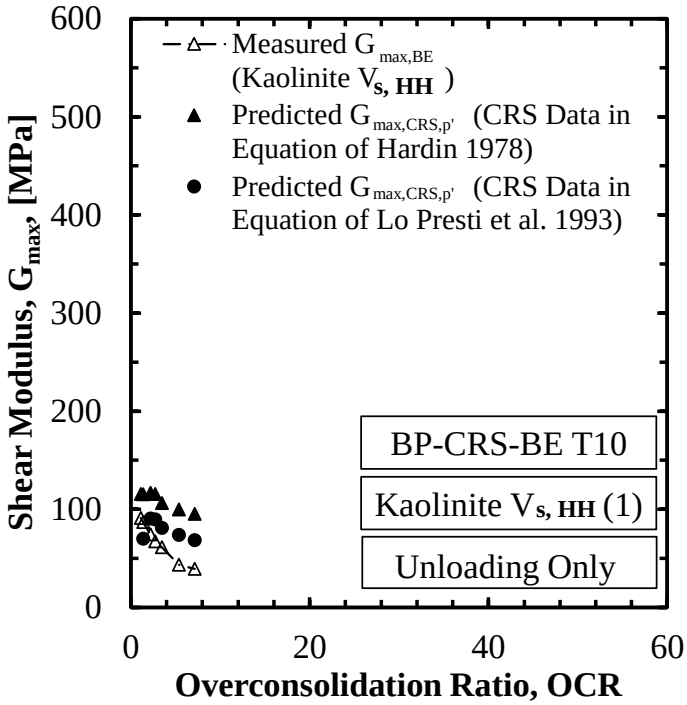

Figure C.56. Shear wave velocity as a function of overconsolidation ratio for BP-CRS-BE T10 on Kaolinite soil specimen (unloading 1).

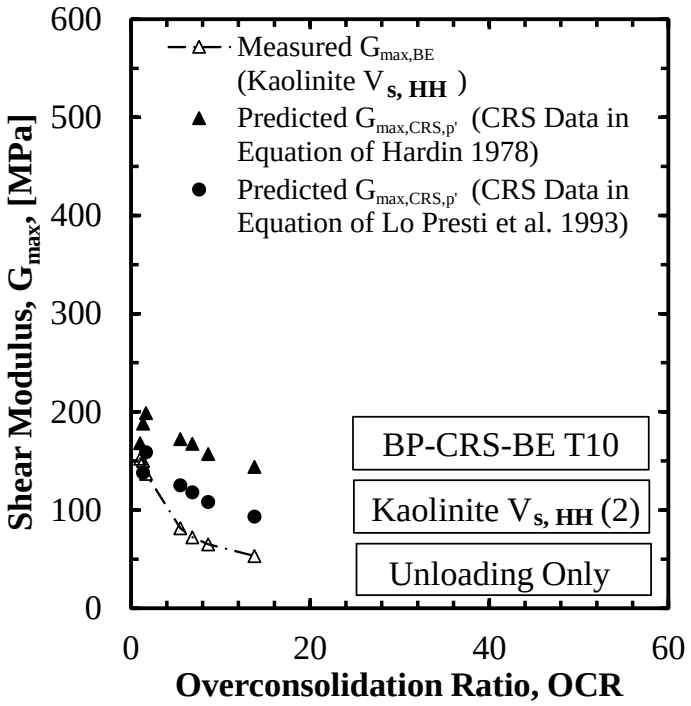

Figure C.57. Shear wave velocity as a function of overconsolidation ratio for BP-CRS-BE T10 on Kaolinite soil specimen (unloading 2).

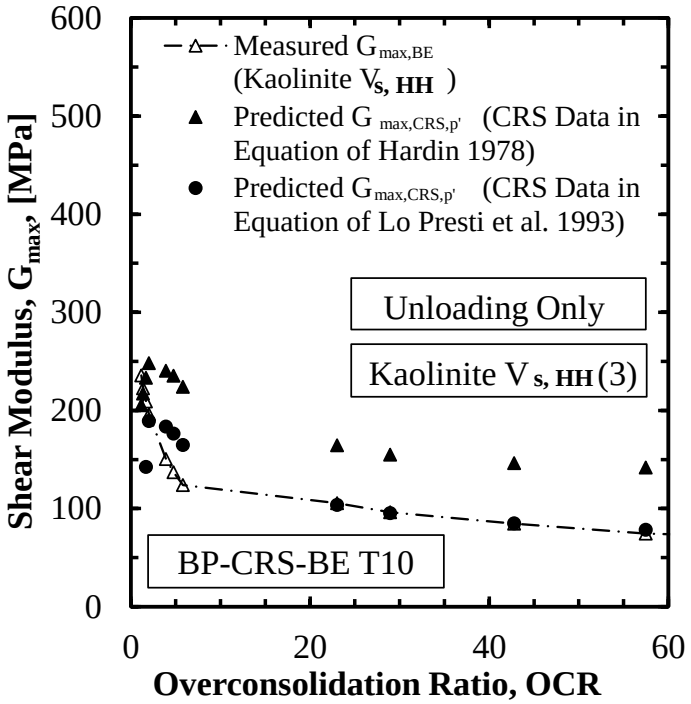

Figure C.58. Shear wave velocity as a function of overconsolidation ratio for BP-CRS-BE T10 on Kaolinite soil specimen (unloading 3).

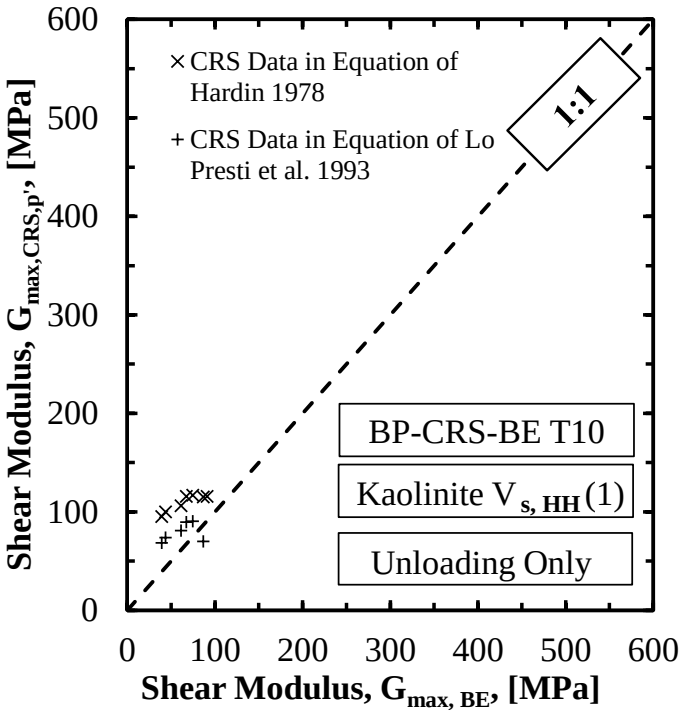

Figure C.59. Comparison of the predicted shear modulus with the measured shear modulus for BP-CRS-BE T10 on Kaolinite soil specimen (unloading 1).

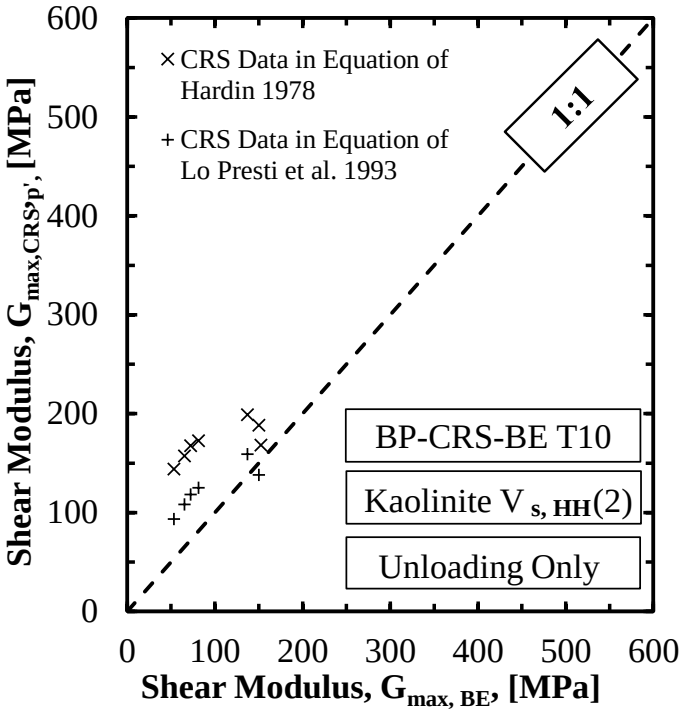

Figure C.60. Comparison of the predicted shear modulus with the measured shear modulus for BP-CRS-BE T10 on Kaolinite soil specimen (unloading 2).

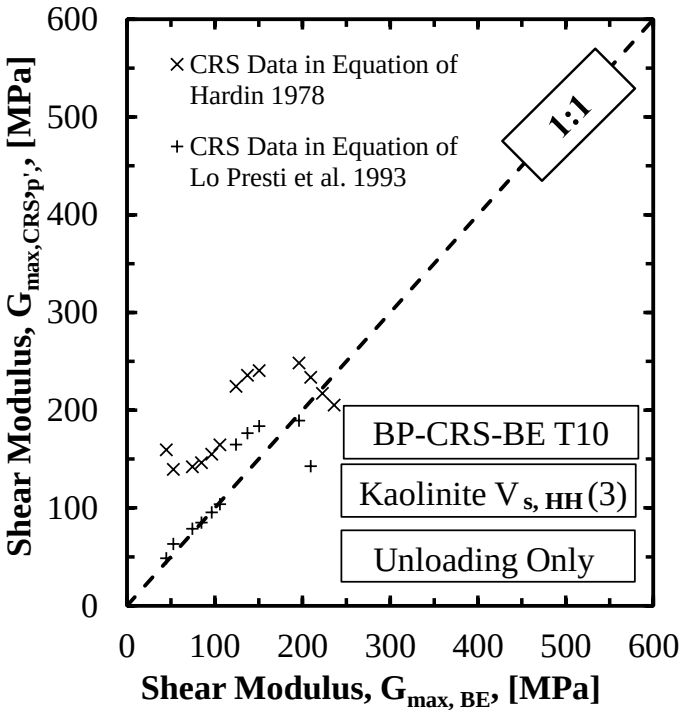

Figure C.61. Comparison of the predicted shear modulus with the measured shear modulus for BP-CRS-BE T10 on Kaolinite soil specimen (unloading 3).

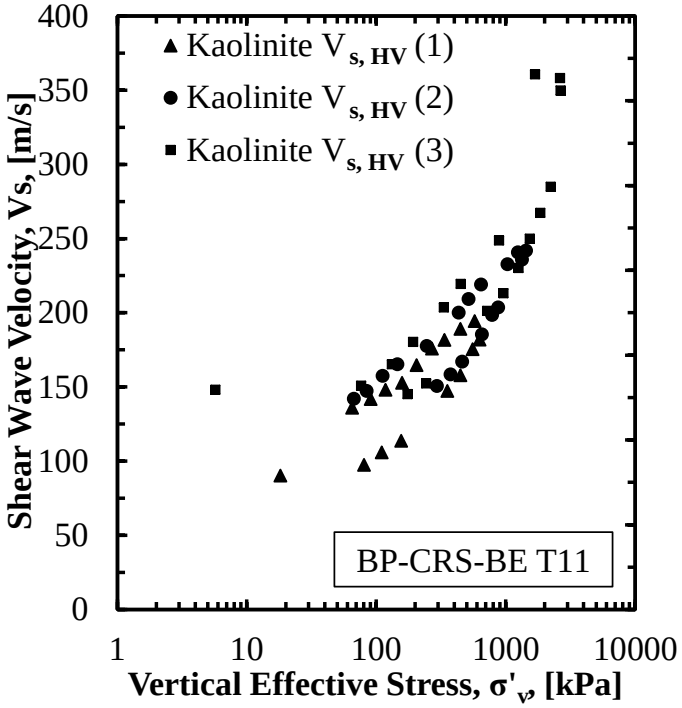

Figure C.62. Shear wave velocity as a function of vertical effective stress for BP-CRS-BE T11 on Kaolinite soil specimen.

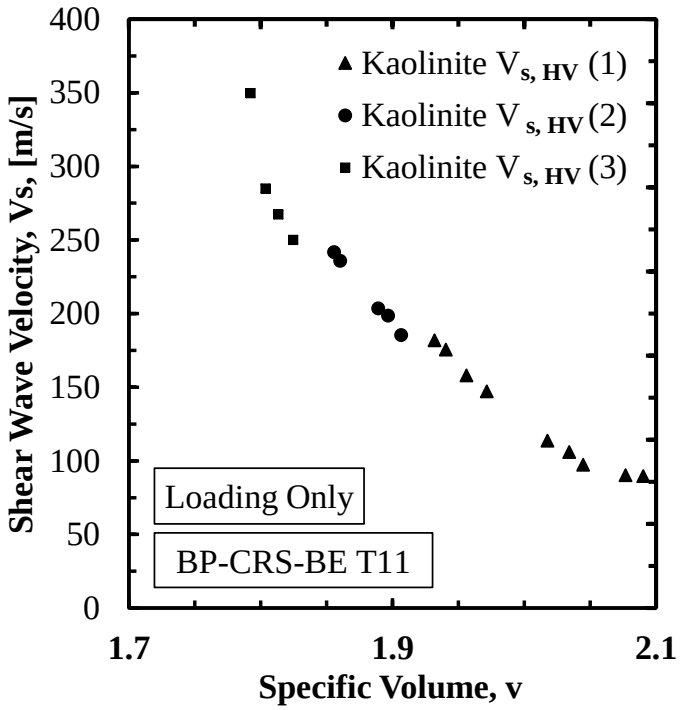

Figure C.63. Shear wave velocity as a function of specific volume for BP-CRS-BE T11 on Kaolinite soil specimen.

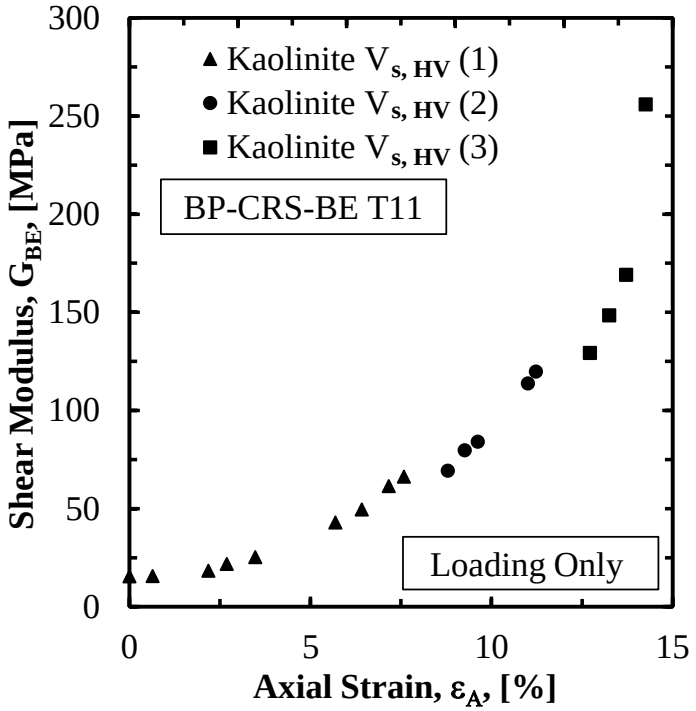

Figure C.64. Shear modulus as a function of axial strain for BP-CRS-BE T11 on Kaolinite soil specimen.

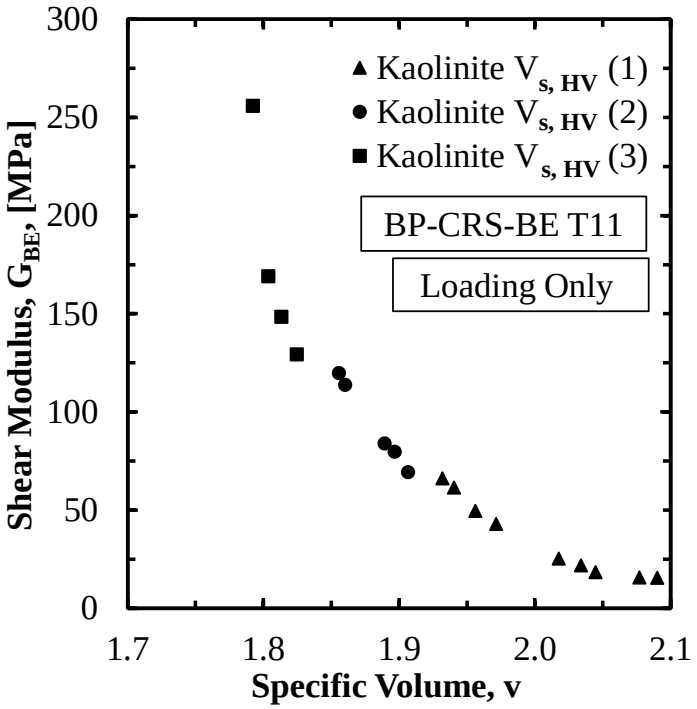

Figure C.65. Shear modulus as a function of specific volume for BP-CRS-BE T11 on Kaolinite soil specimen.

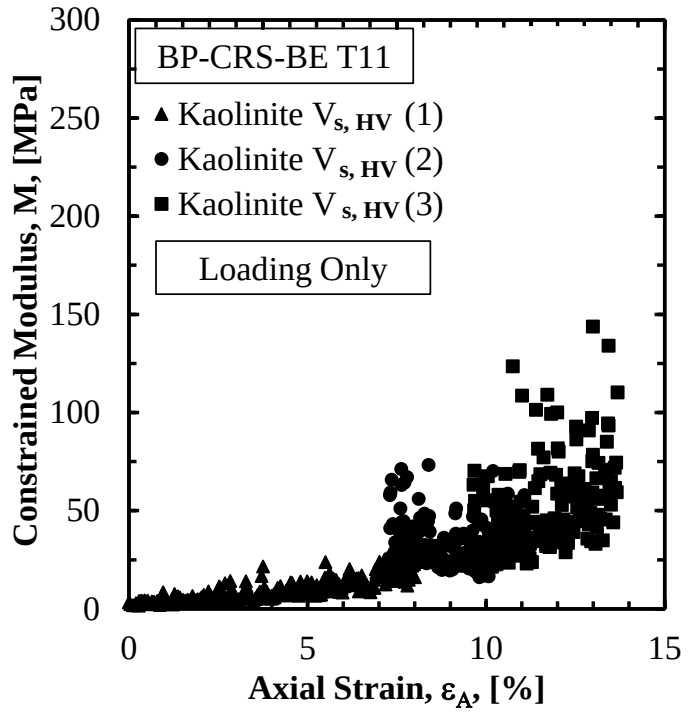

Figure C.66. Constrained modulus as a function of axial strain for BP-CRS-BE T11 on Kaolinite soil specimen.

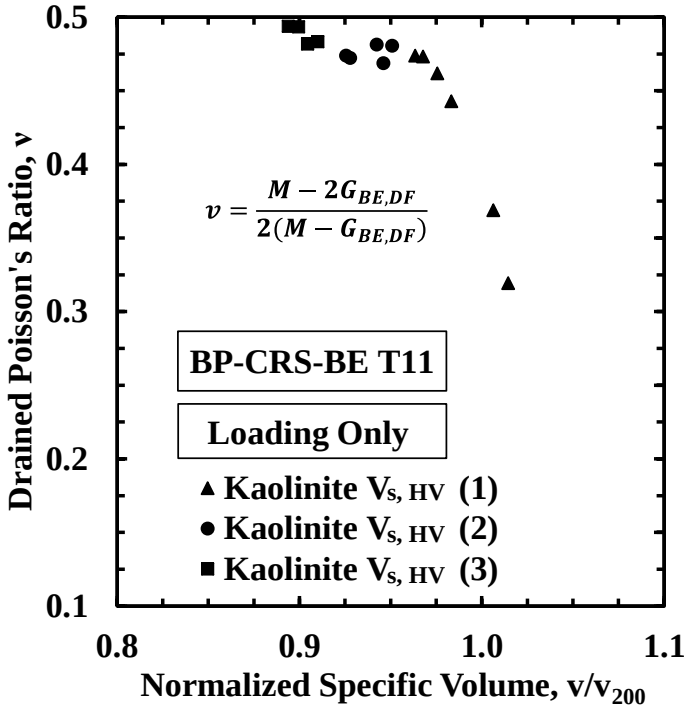

Figure C.67. Poisson's ratio as a function of normalized specific volume for BP-CRS-BE T11 on Kaolinite soil specimen (loading only).

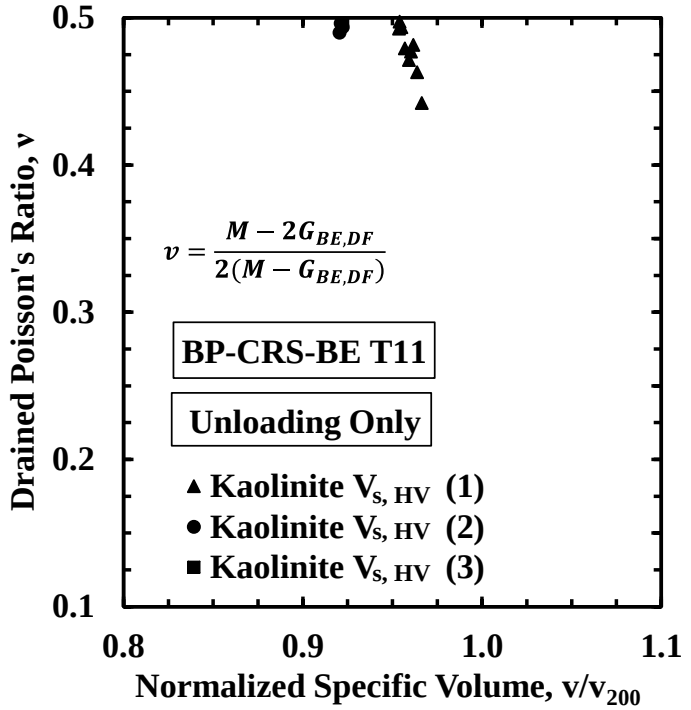

Figure C.68. Poisson's ratio as a function of normalized specific volume for BP-CRS-BE T11 on Kaolinite soil specimen (unloading only).

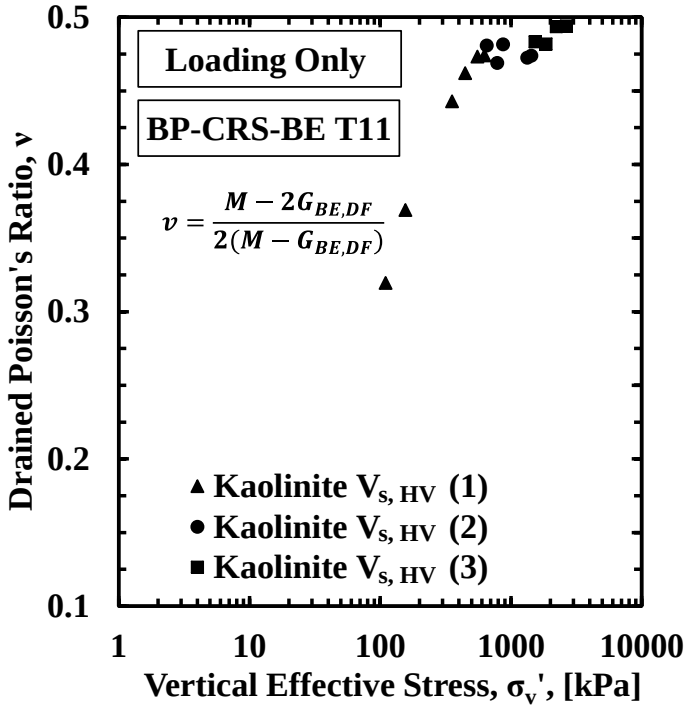

Figure C.69. Poisson's ratio as a function of vertical effective stress for BP-CRS-BE T11 on Kaolinite soil specimen (loading only).

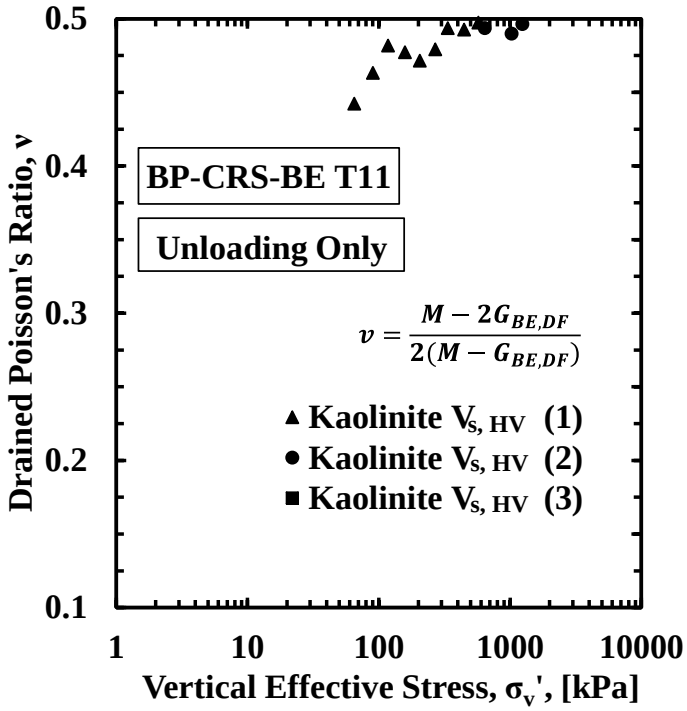

Figure C.70. Poisson's ratio as a function of vertical effective stress for BP-CRS-BE T11 on Kaolinite soil specimen (unloading only).

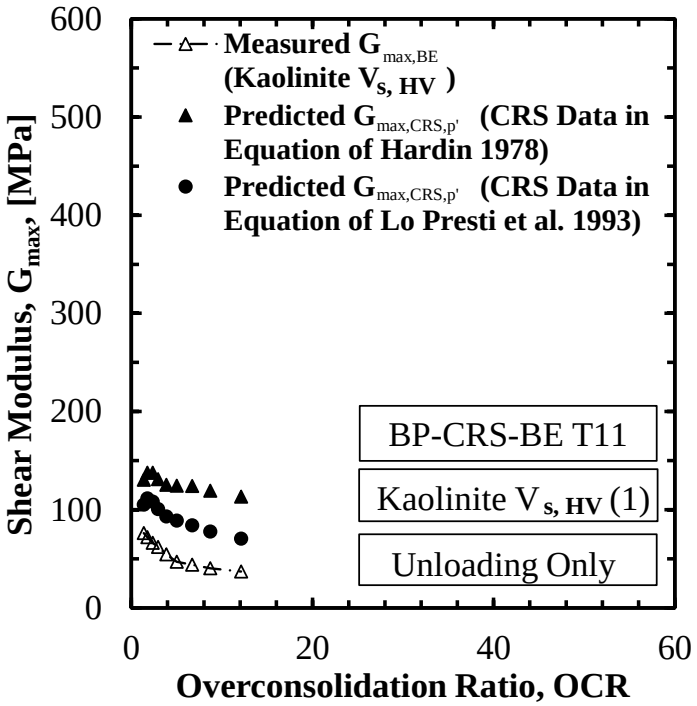

Figure C.71. Shear wave velocity as a function of overconsolidation ratio for BP-CRS-BE T11 on Kaolinite soil specimen (unloading 1).

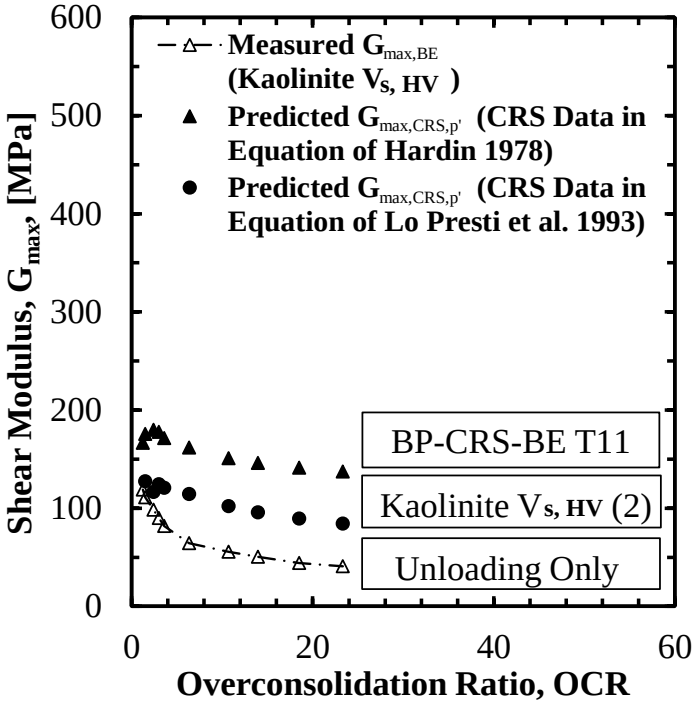

Figure C.72. Shear wave velocity as a function of overconsolidation ratio for BP-CRS-BE T11 on Kaolinite soil specimen (unloading 2).

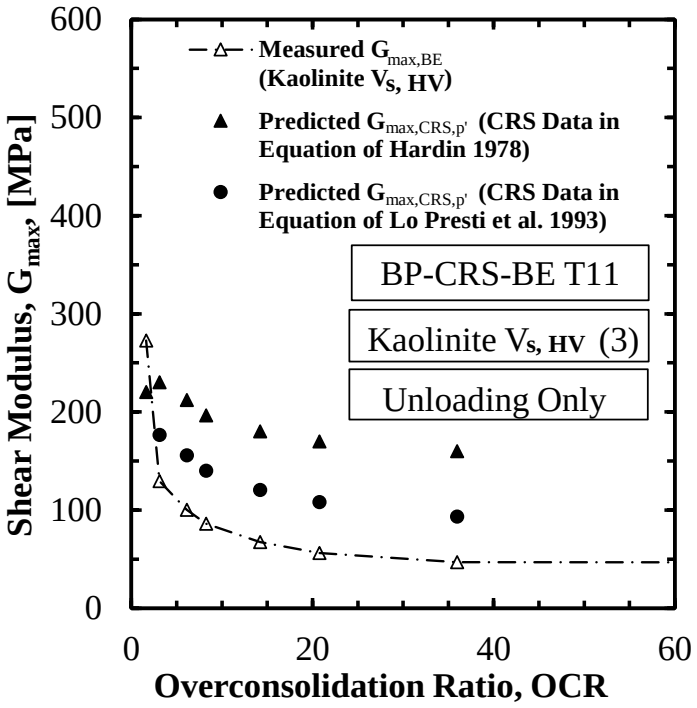

Figure C.73. Shear wave velocity as a function of overconsolidation ratio for BP-CRS-BE T11 on Kaolinite soil specimen (unloading 3).

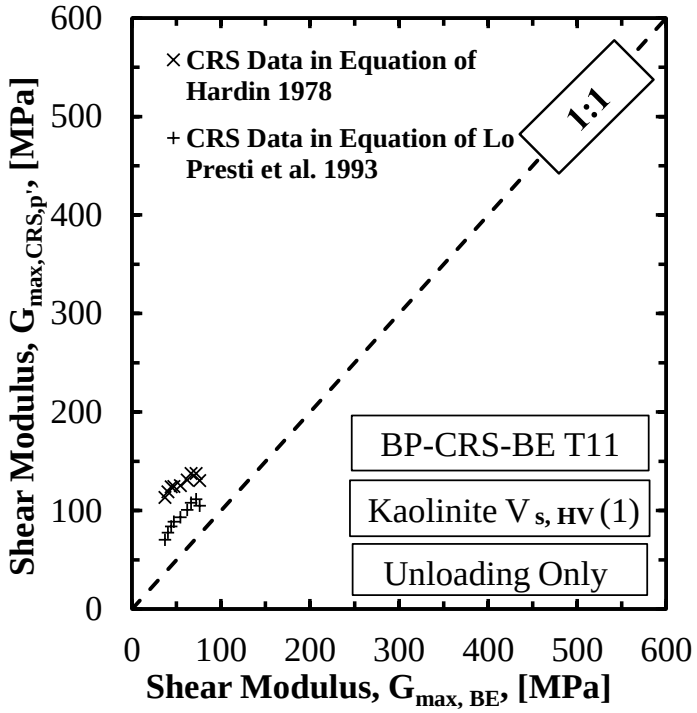

Figure C.74. Comparison of the predicted shear modulus with the measured shear modulus for BP-CRS-BE T11 on Kaolinite soil specimen (unloading 1).

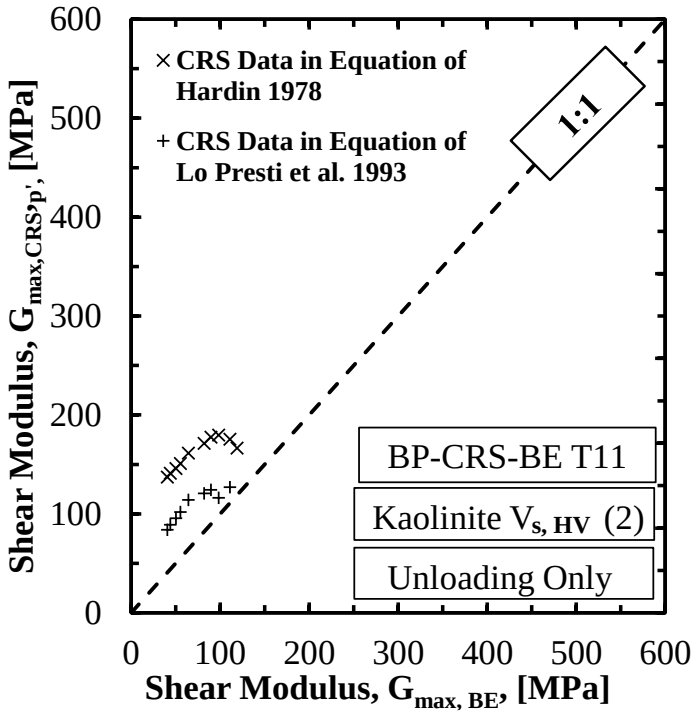

Figure C.75. Comparison of the predicted shear modulus with the measured shear modulus for BP-CRS-BE T11 on Kaolinite soil specimen (unloading 2).

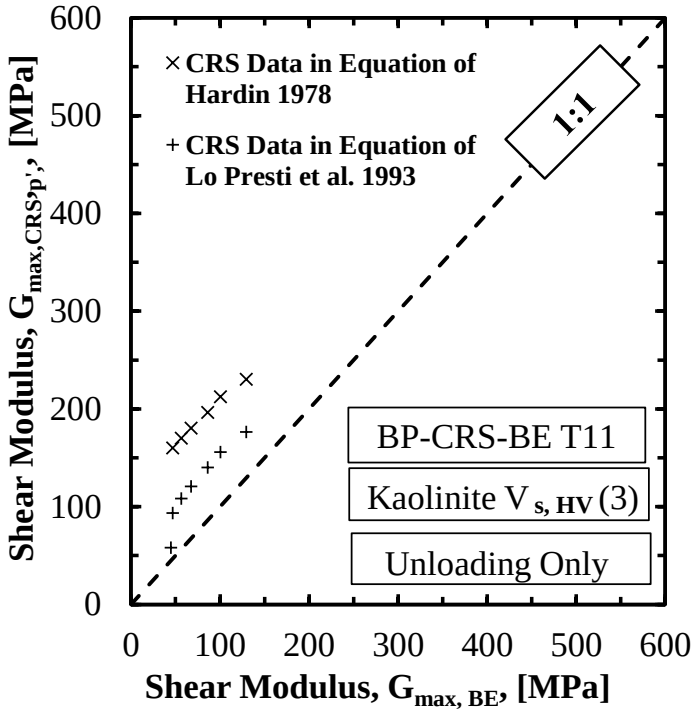

Figure C.76. Comparison of the predicted shear modulus with the measured shear modulus for BP-CRS-BE T11 on Kaolinite soil specimen (unloading 3).

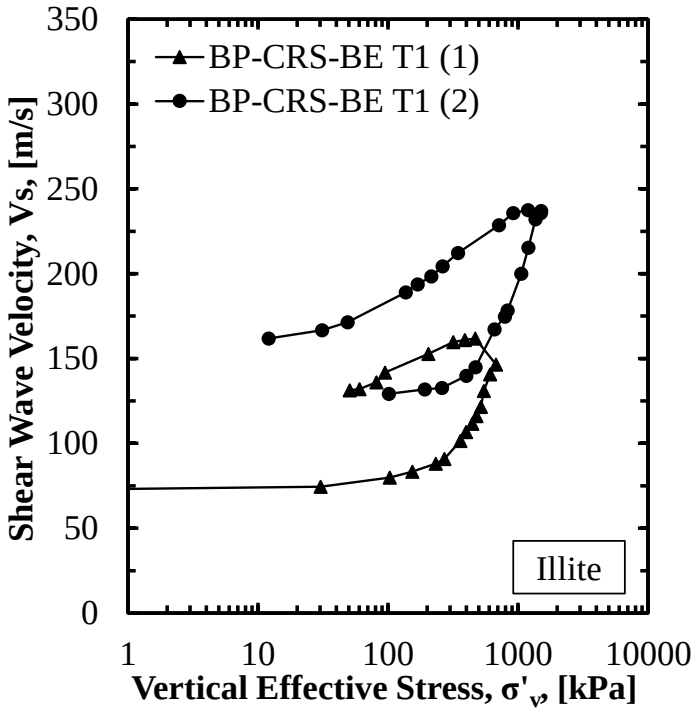

Figure C.77. Shear wave velocity as a function of vertical effective stress for BP-CRS-BE T1 on Illite soil specimen.

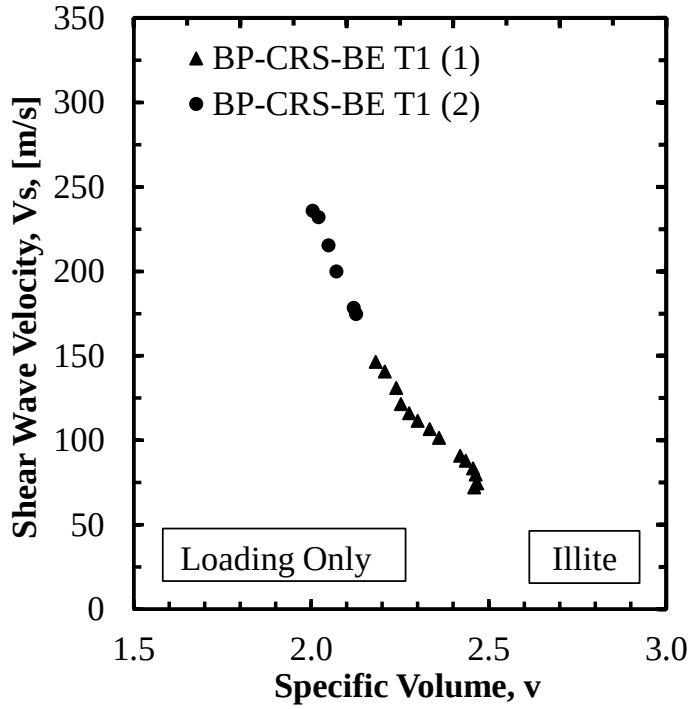

Figure C.78. Shear wave velocity as a function of specific volume for BP-CRS-BE T1 on Illite soil specimen.

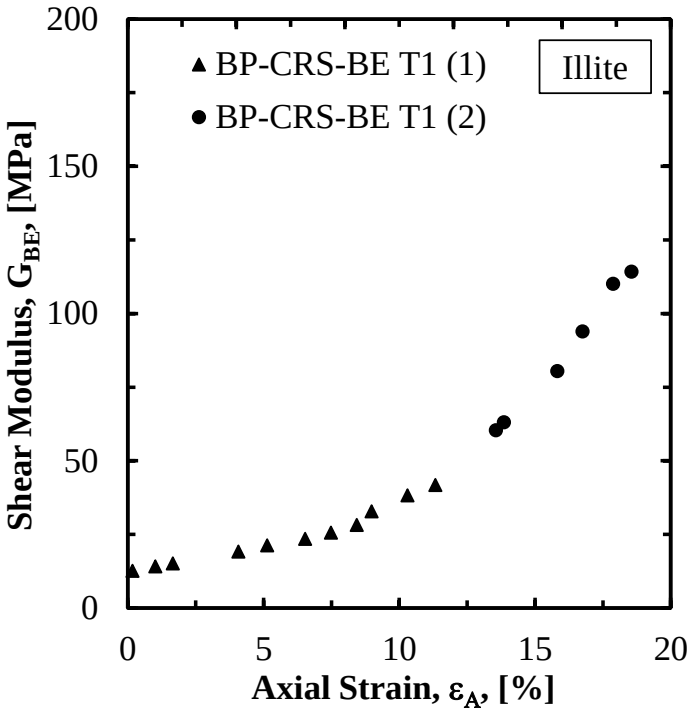

Figure C.79. Shear modulus as a function of axial strain for BP-CRS-BE T1 on Illite soil specimen.

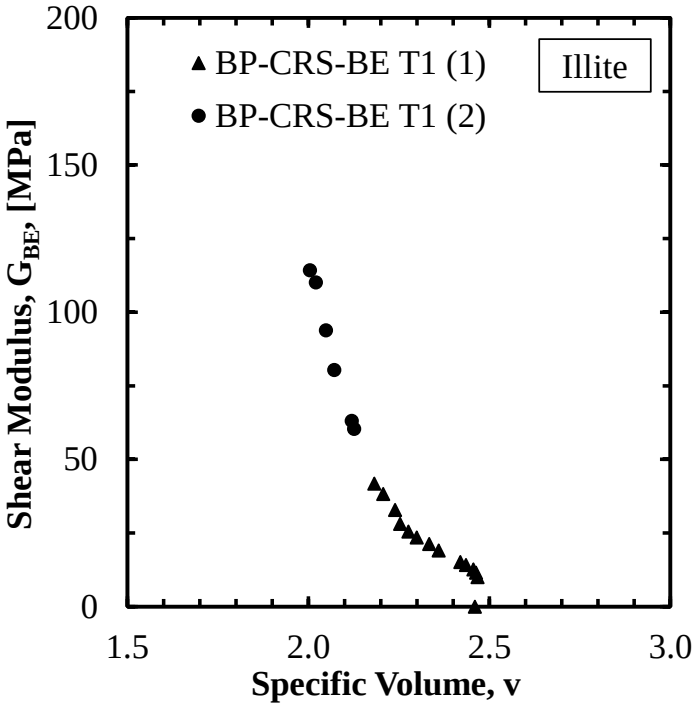

Figure C.80. Shear modulus as a function of specific volume for BP-CRS-BE T1 on Illite soil specimen.

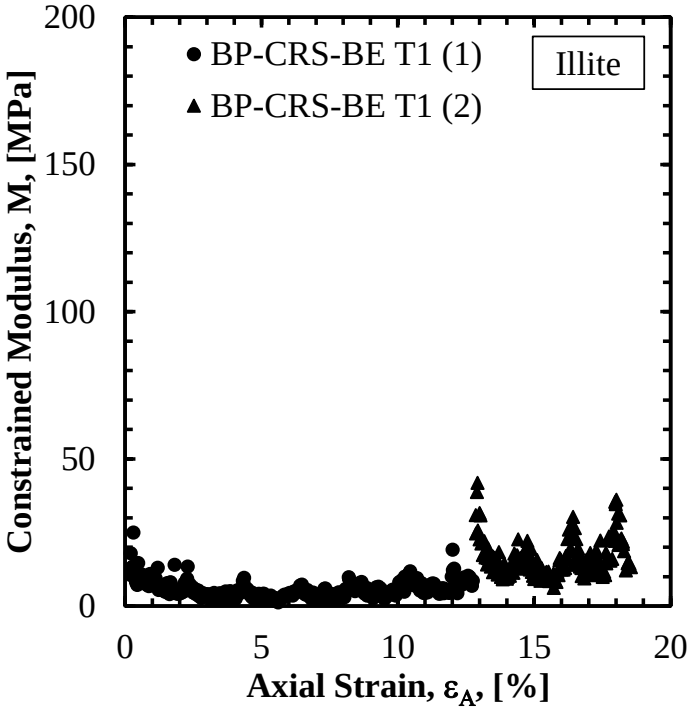

Figure C.81. Constrained modulus as a function of axial strain for BP-CRS-BE T1 on Illite soil specimen.

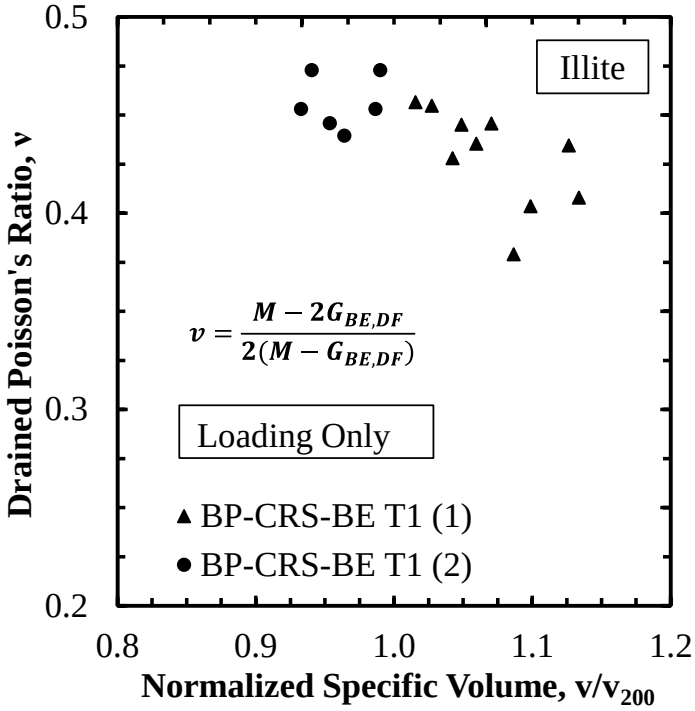

Figure C.82. Poisson's ratio as a function of normalized specific volume for BP-CRS-BE T1 on Illite soil specimen.

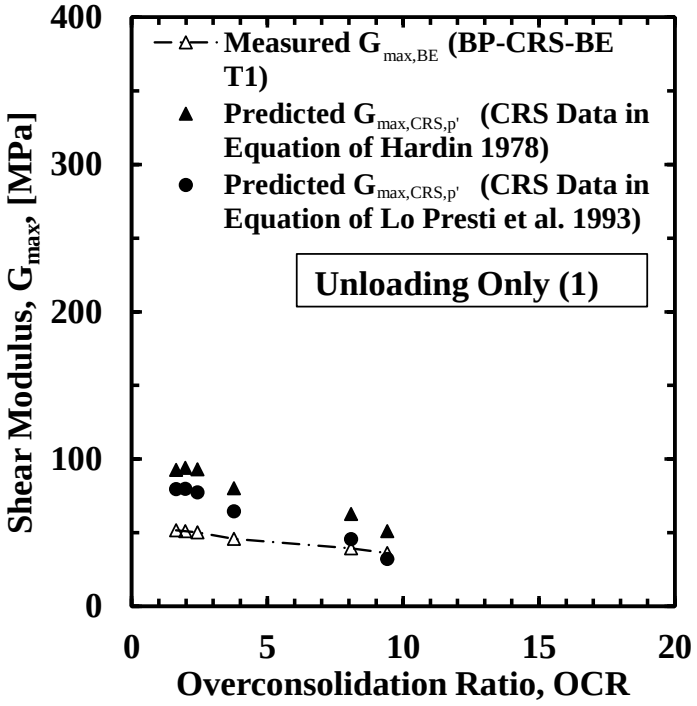

Figure C.83. Shear wave velocity as a function of overconsolidation ratio for BP-CRS-BE T1 on Illite soil specimen (unloading 1).

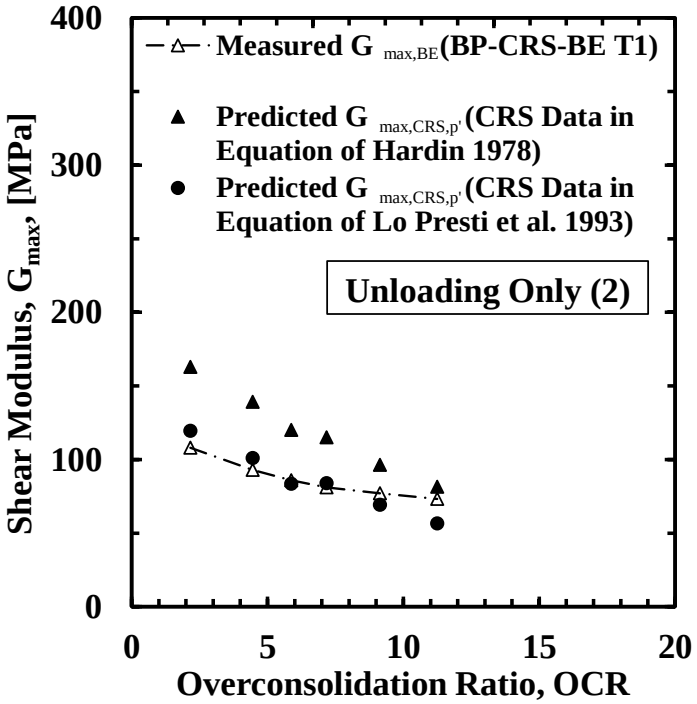

Figure C.84. Shear wave velocity as a function of overconsolidation ratio for BP-CRS-BE T1 on Illite soil specimen (unloading 2).

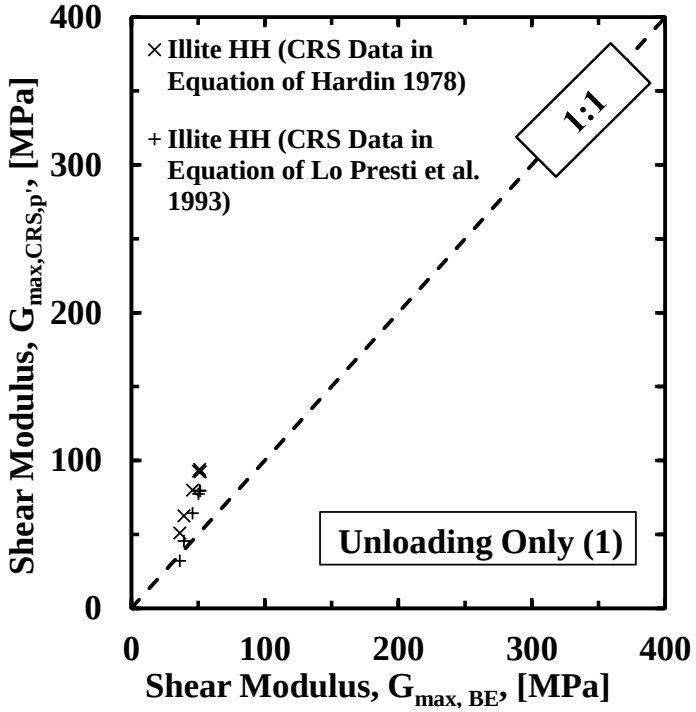

Figure C.85. Comparison of the predicted shear modulus with the measured shear modulus for BP-CRS-BE T1 on Illite soil specimen (unloading 1).

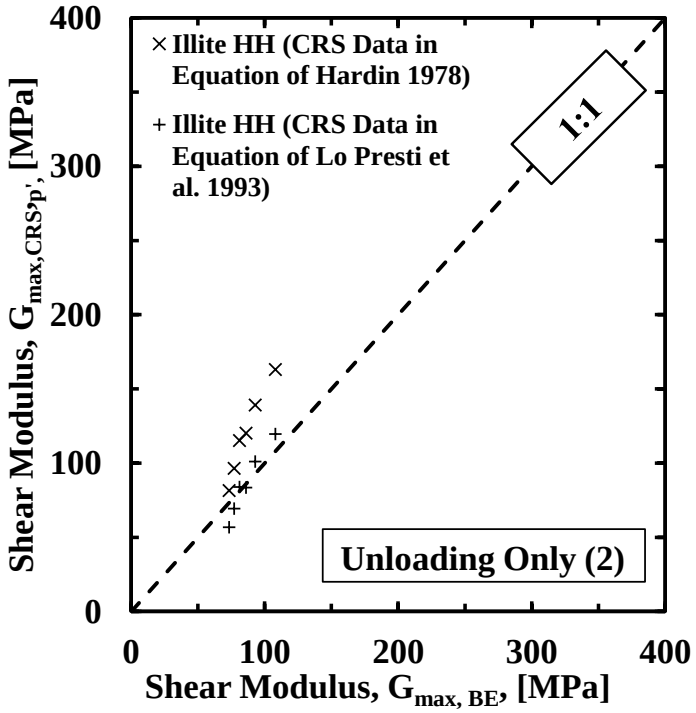

Figure C.86. Comparison of the predicted shear modulus with the measured shear modulus for BP-CRS-BE T1 on Illite soil specimen (unloading 2).

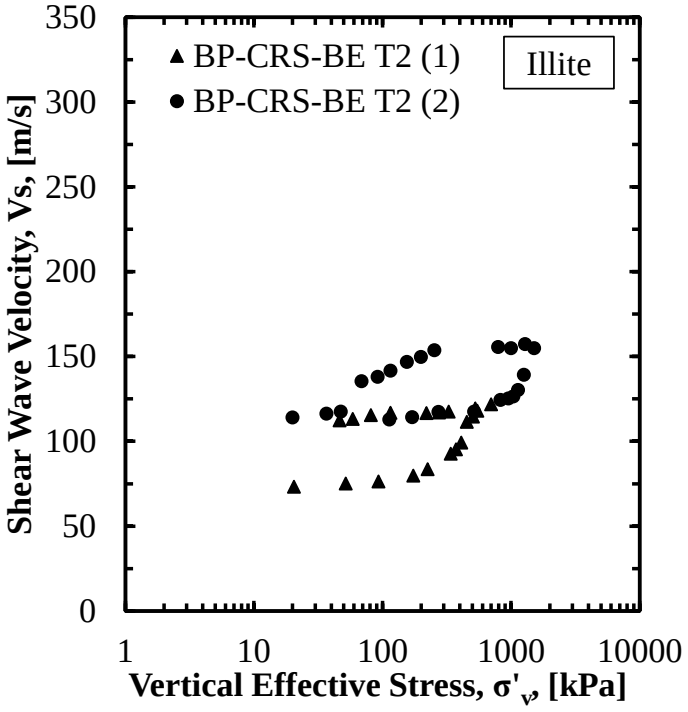

Figure C.87. Shear wave velocity as a function of vertical effective stress for BP-CRS-BE T2 on Illite soil specimen.

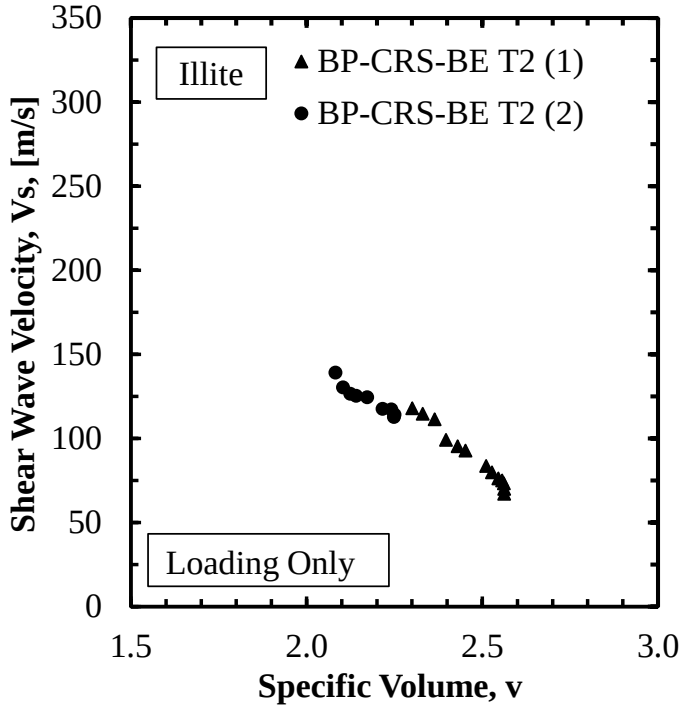

Figure C.88. Shear wave velocity as a function of specific volume for BP-CRS-BE T2 on Illite soil specimen.

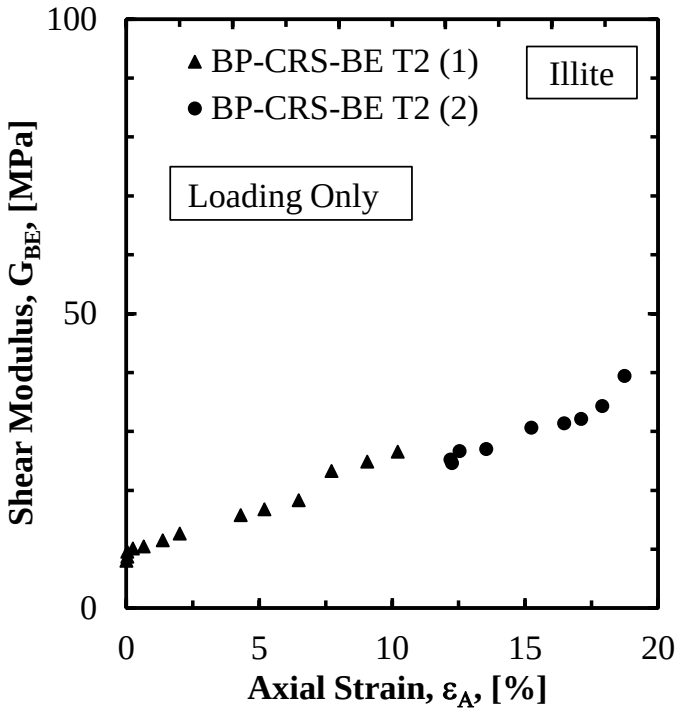

Figure C.89. Shear modulus as a function of axial strain for BP-CRS-BE T2 on Illite soil specimen.

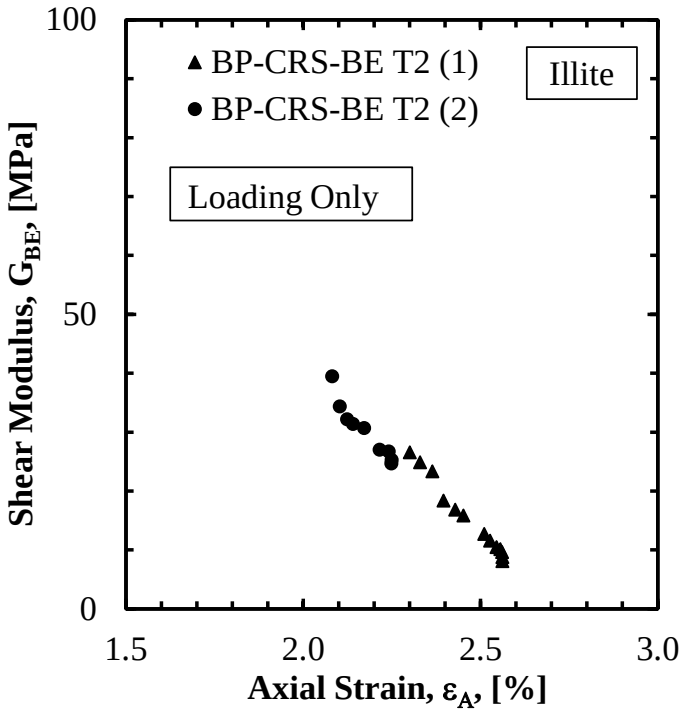

Figure C.90. Shear modulus as a function of specific volume for BP-CRS-BE T2 on Illite soil specimen.

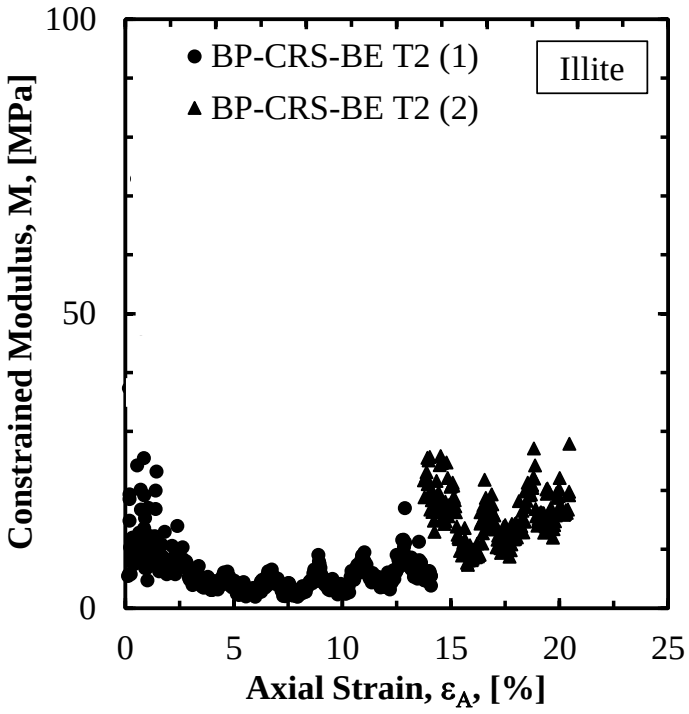

Figure C.91. Constrained modulus as a function of axial strain for BP-CRS-BE T2 on Illite soil specimen.

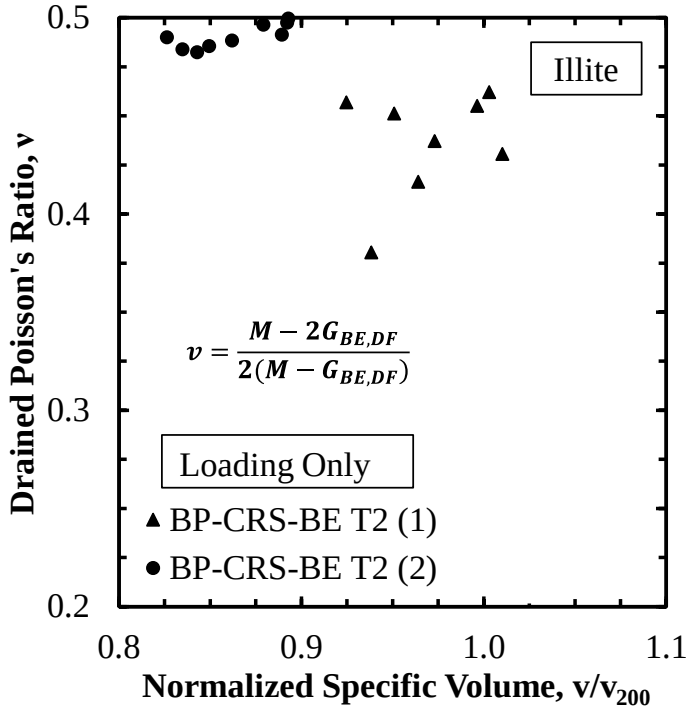

Figure C.92. Poisson's ratio as a function of normalized specific volume for BP-CRS-BE T2 on Illite soil specimen.

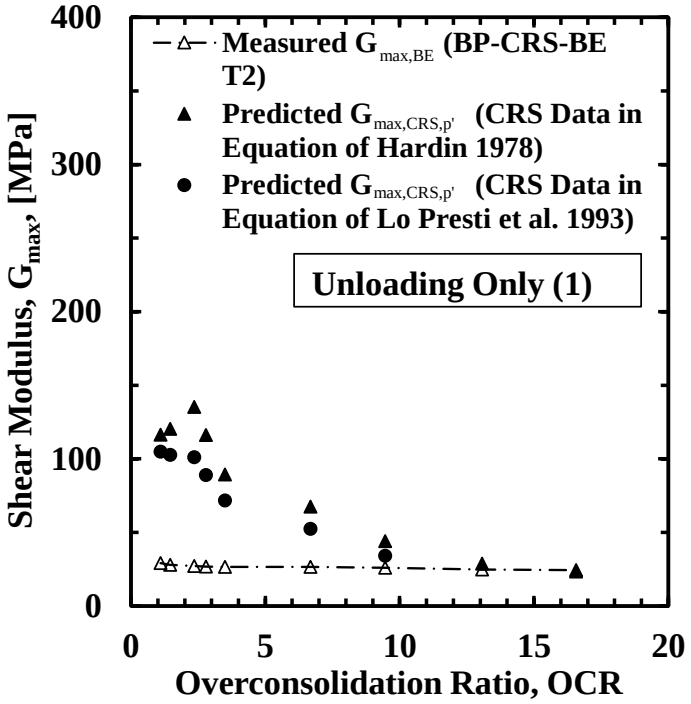

Figure C.93. Shear wave velocity as a function of overconsolidation ratio for BP-CRS-BE T2 on Illite soil specimen (unloading 1).

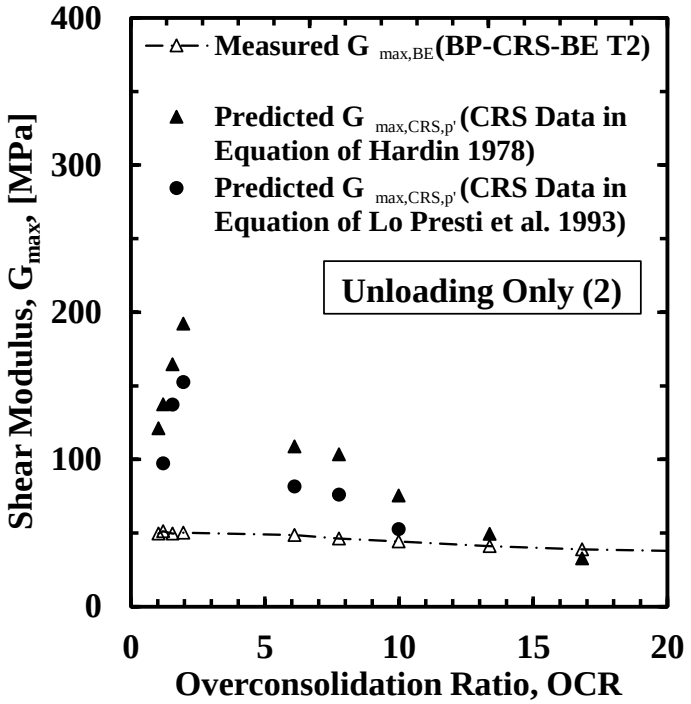

Figure C.94. Shear wave velocity as a function of overconsolidation ratio for BP-CRS-BE T2 on Illite soil specimen (unloading 2).

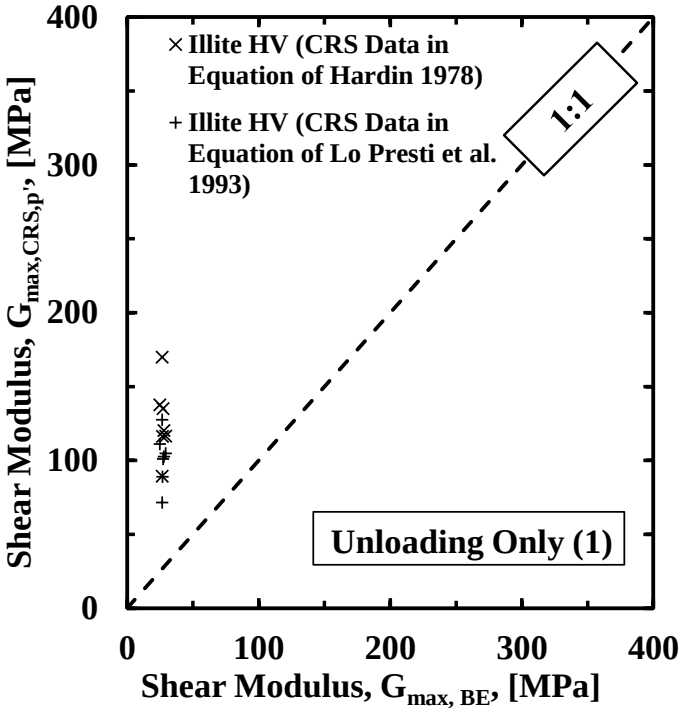

Figure C.95. Comparison of the predicted shear modulus with the measured shear modulus for BP-CRS-BE T2 on Illite soil specimen (unloading 1).

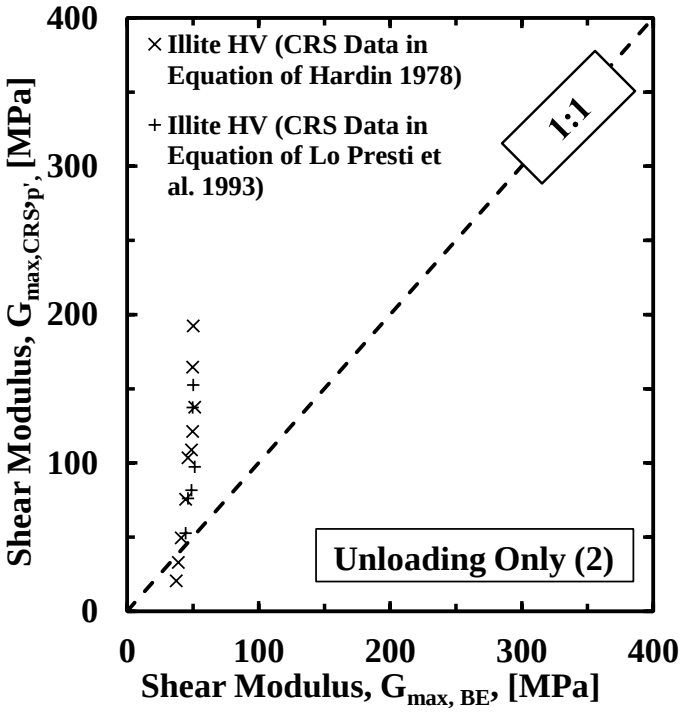

Figure C.96. Comparison of the predicted shear modulus with the measured shear modulus for BP-CRS-BE T2 on Illite soil specimen (unloading 2).

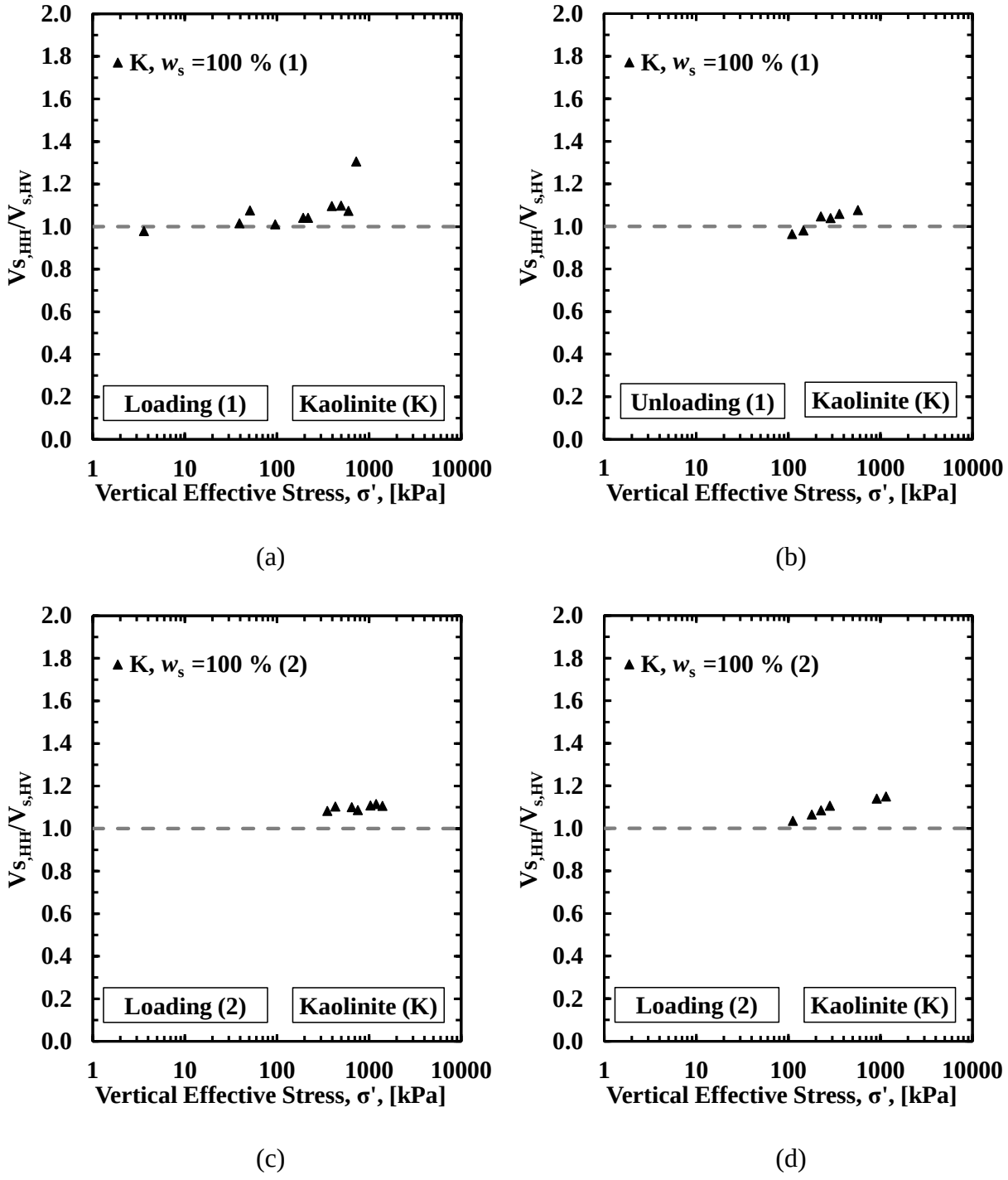

Figure C.97. The ratio of $V_{s,HH}$ to $V_{s,HV}$ as a function of vertical effective stress for BP-CRS-BE tests on Kaolinite soil for: (a) loading 1, (b) unloading 1, (c) loading 2, and (d) unloading 2.

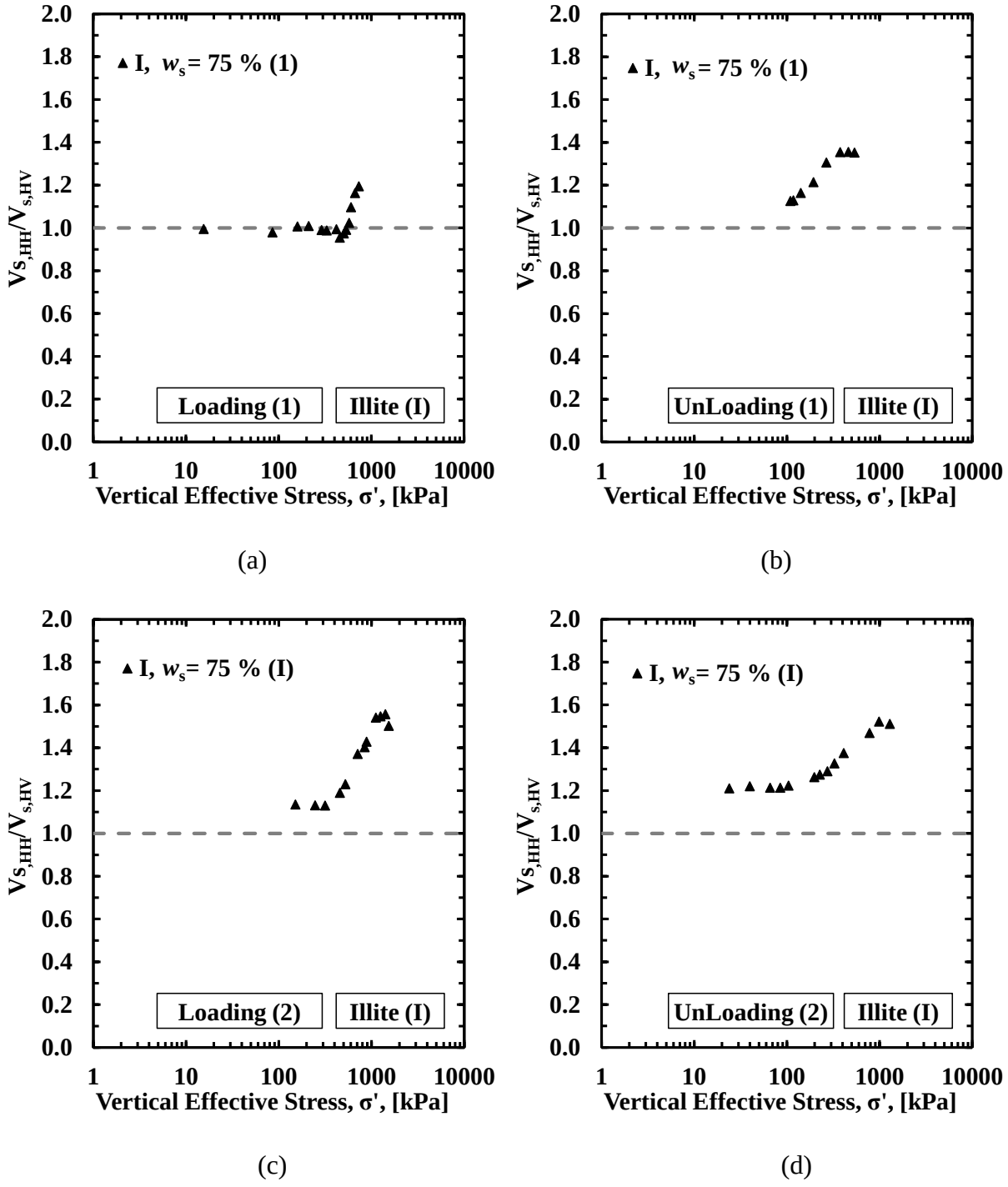

Figure C.98. The ratio of $V_{s,HH}$ to $V_{s,HV}$ as a function of vertical effective stress for BP-CRS-BE tests on Illite soil for: (a) loading 1, (b) unloading 1, (c) loading 2, and (d) unloading 2.

C.3. References

Hardin, B.O., "The Nature of Stress Stain Behavior of Soils." *Earthquake Engineering and Soil Dynamics*. ASCE, Vol.1, 1978, pp. 3–90.

Lo Presti D.C.F., Jamiolkowski M., Lancellotta R. and Vercelli L., "Maximum shear modulus measurement using bender elements in oedometer tests", *Rivista Italiana de Geotechnica*, Vol.(XXVII), No. 1, 1993, pp. 5-9.